

Re-designing EX-CORE for large
scale automotive manufacturing
Reducing cure cycle times of EX-CORE
K.J.M. Mattheus



Re-designing EX-CORE for large scale automotive manufacturing

Reducing cure cycle times of EX-CORE

by

K.J.M. Mattheus

Master of Science Thesis

Department of Aerospace Structures & Materials

Faculty of Aerospace Engineering - Delft University of Technology

In cooperation with Donkervoort Automobielen B.V.



December 11, 2018

Student number: 4197585
Project duration: January 2, 2018 – December 11, 2018
Thesis committee: Dr. ir. J.M.J.F. van Campen, Supervisor, TU Delft, Aerospace Structures and Computational Mechanics
Dr. J.C. Bijleveld, TU Delft, Novel Aerospace Materials
Ir. J. Sinke, TU Delft, Structural Integrity and Composites
J. Wiersma, MSc Company supervisor, Donkervoort Automobielen B.V.

This report is subject to the cooperation agreement between the Delft University of Technology & Donkervoort Automobielen B.V.

It may not be published or redistributed without agreement of both parties.

Embargo date: December 11, 2023

Preface

In front of you lies a Master's thesis, which is the synthesis of the work performed to obtain the degree of Master of Science in Aerospace Engineering at the Delft University of Technology. Performing research at Donkervoort Automobielen B.V. on their EX-CORE technology has been a challenging but nonetheless highly rewarding experience. I have been engaged in the development of EX-CORE since July 2017, when I first started my internship at Donkervoort. During this internship I obtained valuable insights and hands-on experience which prepared me well for the subsequent thesis project. It was exiting to be part of the development of this innovative core material offering large potential to re-shape the manufacturing process of composite sandwich structure.

The function of this report is twofold; next to the fact that it serves as a means to obtain the degree of Master of Science, it functions as a detailed reference document to be used by new interns/graduates in future research at Donkervoort. For the quick reader; at the end of most chapters a summary of important chapter conclusions and/or discussion of results is given.

I would like to express my sincerest gratitude to my former and current supervisors at Donkervoort, Roel and Jordi, who where always open for discussion and dedicated their time, knowledge and humor to guide my through this project. I also would like to thank Julien for providing me with valuable feedback. Special thanks also goes to Matthijs and Dennis for introducing me to the world of EX-CORE and for laying the foundation of my research. Furthermore, I would like to thank my colleagues at Donkervoort for borrowing their tools and sharing their insights to help me solve my problems. The technical staff at the DASML lab is also thanked for their help in performing experiments. Finally, many thanks to my friends and boyfriend Tom with whom I could share the struggle of completing a MSc thesis and my family for their unconditional support.

*K. J. M. Mattheus
Lelystad, November 2018*

Abstract

EX-CORE, an innovative foam core material developed by Donkervoort Automobielen B.V. enables the one-shot manufacturing of complexly shaped sandwich structures. The syntactic foam consists of three types of microspheres embedded in an epoxy binder. Through the incorporation of the thermo-expandable microspheres Expancel[®] DU, the pressure to consolidate the laminate is generated by the core itself during curing. This eliminates the need for an autoclave or vacuum bag and allows to obtain small tolerances and a high surface finish on all sides of the product. The EX-CORE technology has achieved its intended goal at Donkervoort of saving cost and time for the production of sandwich structures for their cars. Now, Donkervoort has the ambition to commercialize EX-CORE for larger scale automotive manufacturing. To achieve this, the cycle times of several hours should be reduced to several minutes. The present research contributes to this development by re-engineering the EX-CORE foam composition such that the cure cycle times are reduced.

Three new types of fast curing epoxy curing agents and one new epoxy resin were selected that could replace the original epoxy matrix which formed a major limitation to obtain short cure cycle times. The cure kinetics of these epoxies were experimentally determined using Differential Scanning Calorimetry (DSC) and fitted to a modified autocatalytic cure-kinetic model. The required time to obtain 98% cure (at 110°C) was reduced from 46min to 7.2min for the new SR 1280/Ancamine[®] 2442 epoxy system. This system has been later selected as most suitable candidate matrix based on its promising test sample results, relatively low exothermic reaction and because Ancamine[®] 2442 has a physical thermal block which prevents the mixture from reacting at room temperature.

To predict the temperature and degree of cure distribution for various EX-CORE compositions during curing, an existing numerical thermal model had been improved. The cure kinetics of the epoxies are incorporated to simulate the heat release of the exothermic reaction, while theoretical models are implemented to predict the thermal conductivity and specific heat capacity of the chosen EX-CORE composition. Due to the limited time frame, only temperature measurements from samples produced with a 270kg/m³ "270-opt" mix composition using the SR 1280/Ancamine[®] 2442 epoxy have been generated to validate the numerical model predictions.

In the end, the model could only be validated for isothermally cured samples not thicker than 30mm, since results of thicker samples fell outside the acceptable discrepancy bounds. The discrepancies are most probably related to the following assumptions made for the numerical model: First of all, the assumption of constant mold temperature and secondly the assumption of constant onset reaction temperature (T_{onset}) of the Ancamine[®] 2442 curing agent. It was verified with DSC tests that the heat-up rate influences the measured value of T_{onset} , which in turn has a major effect on the model predictions. Additionally, temperature measurements indicated that the heat-up rate varies through the thickness of the core. This effect is more pronounced for samples thicker than 30mm.

During the research, the Expancel[®] 031 DU 40 grade was replaced with the more solvent resistant 043 DU 80 grade, which has a higher T_{onset} (95-115°C) and higher maximum temperature (147-167°C). Several compression tests were performed on various EX-CORE samples containing the new DU grade and the SR 1280/Ancamine[®] 2442 matrix to investigate the effect of cure temperature, cure time and epoxy mix ratio on compressive strength. The tests revealed that the compressive strength of EX-CORE samples became 4 times higher when using a 100:20 epoxy ratio instead of 100:60. However, the consequence was that the required cure time more than doubled.

It was verified that the mold cannot be opened before the maximum core temperature is allowed to drop below T_{onset} of DU (95°C). This to ensure dimensionally stable EX-CORE products without cracks. From the numerical model predictions it became clear that it is not possible to obtain cure cycle times below 10 minutes with the re-engineered EX-CORE foam. The poor conductive properties of the microspheres form a major limitation to obtain shorter cure- and cool-down times. Interestingly, higher cure temperatures do not necessarily imply shorter in-mold cycle times because the resulting higher temperature peaks increase the required cool-down time.

Finally, promising sandwich panels with good surface quality were created with the re-designed EX-CORE foam and TenCate E732 snap-cure prepreg. It was measured that the CFRP prepreg facings mainly near the prepreg facings influenced the temperature in the core, allowing the numerical model to be used for sandwich panel predictions. Next, using the model, a case study was performed for the 8mm thick floor panels of the Donkervoort D8-GTO-RS. The shortest in-mold cycle times can be achieved when cured at 110°C (with conservative 1°C/min mold cool down rate). More specifically, with the new EX-CORE formulation the cure time can be reduced from 3hours to 19min and the total in-mold cycle time can be reduced from 4hours to 35min; a reduction of 85.4%.

With the knowledge gained during the research, the EX-CORE technology is now one step closer to commercialization.

Contents

Preface	iii
Abstract	v
List of Symbols	xi
1 Introduction	1
2 Relevant literature and background	3
2.1 Principles of sandwich structures	3
2.1.1 Concept of sandwich structures	3
2.1.2 Fiber-reinforced polymer laminate facings.	4
2.1.3 Polymeric foam core materials.	6
2.1.4 Manufacturing aspects of foam cored sandwich structures	7
2.2 Syntactic foams	8
2.3 Cure process aspects and thermal modeling of thermoset composites	9
2.3.1 Cure process principles of thermosetting composites	9
2.3.2 Finite difference thermal models for thick thermosetting composites	10
2.3.3 Thermoset cure kinetic theory and models	11
3 The EX-CORE concept and its development	13
3.1 The concept of EX-CORE	13
3.2 Previous research and developments	14
3.2.1 Houwers 2013: Pure Expancel [®] DU/DE core and addition of thermoset binder	15
3.2.2 Minde 2014: Manufacturing process & Approaches for density decrease and improvement of surface porosity	16
3.2.3 Santos & Boegem 2015: Material testing	17
3.2.4 Berckmoes 2016: Integrally heated tooling.	17
3.2.5 Vial 2016: Relating constituents to EX-CORE material properties	18
3.2.6 Berckmoes 2017: Effect of EX-CORE foam processing on surface defects in carbon fiber-epoxy sandwich composites	20
3.2.7 Eversdijk 2017: Relating process parameters to EX-CORE properties through experimental testing and modeling	22
3.2.8 Mattheus 2017: Exploration with reinforcing fillers and diluents & Proof of concept for EX-CORE component dosing and mixing automation	24
3.2.9 Ten Hoeve 2018: EX-CORE production machine	24
3.3 EX-CORE constituents (at the start of the current research)	25
3.3.1 Thermoplastic expandable microspheres: Expancel [®] DU	25
3.3.2 Thermoplastic expanded microspheres: Expancel [®] DE	26
3.3.3 Hollow glass microspheres: Q-Cel [®]	26
3.3.4 Epoxy matrix; Ancarez [®] RZ4010/ Ancamide [™] 3399	26
3.4 Typical manufacturing process of EX-CORE products.	27
3.5 Drivers for EX-CORE development towards large series automotive manufacturing	27
3.5.1 Evolution of CFRP composites in the automotive industry.	27
3.5.2 Advantages of EX-CORE w.r.t. other CFRP composite technologies	28
3.5.3 EX-CORE's closest competitors	29
3.5.4 Main drivers for the future development of EX-CORE	29

4	Defining cure kinetics of new candidate epoxy resins by DSC	31
4.1	Selection of new candidate snap-cure epoxy resins	31
4.1.1	Resin selection criteria	31
4.1.2	Acquiring new candidate "fast curing" epoxy resins	33
4.2	Theory on resin cure kinetics and Differential Scanning Calorimetry	34
4.2.1	Resin cure kinetics	34
4.2.2	Differential Scanning Calorimetry (DSC).	35
4.3	Resin cure kinetics determination with DSC	36
4.3.1	Experimental setup and isothermal DSC test methodology	36
4.3.2	Data processing part 1) Experimental results from isothermal DSC scans	37
4.3.3	Data processing part 2) Computing cure kinetic parameters from experimental DSC results	39
4.4	Autocatalytic cure kinetic model results.	42
4.4.1	Cure kinetic parameter results	42
4.4.2	Autocatalytic model results and comparison with isothermal DCS measurements.	43
5	Numerical EX-CORE thermal model	45
5.1	Finite difference method	45
5.1.1	Assumptions.	46
5.1.2	Governing equations.	48
5.1.3	Solution methodology and stability criteria	50
5.2	Mesh	50
5.2.1	Central nodes	51
5.2.2	Boundary nodes	51
5.2.3	Boundary conditions.	53
5.2.4	Initial conditions.	53
5.3	Thermal properties of EX-CORE components.	54
5.4	Thermal conductivity of EX-CORE	55
5.4.1	Theoretical models for effective thermal conductivity of particle filled composites	55
5.4.2	Effective thermal conductivity of microspheres	57
5.4.3	Effective thermal conductivity of EX-CORE	59
5.4.4	Note on validation of the effective thermal conductivity of EX-CORE	60
5.5	Specific heat capacity of EX-CORE	61
5.5.1	Specific heat capacity of epoxy-amine resins.	61
5.5.2	Effective specific heat capacity of microspheres	61
5.5.3	Effective specific heat of EX-CORE.	62
5.5.4	Note on validation of the effective specific heat capacity of EX-CORE	63
5.6	Implementation of cure kinetics into the numerical thermal model	63
5.7	Updates and alterations w.r.t. previous numerical thermal model by Eversdijk	64
5.7.1	Overview model updates.	64
5.7.2	Comparison output data original vs updated numerical thermal model	66
5.8	Verification of numerical thermal model	67
5.8.1	Graphic-analytical one-dimensional solution using Heisler charts.	67
5.8.2	Convergence of numerical model solution.	68
5.9	Numerical model sensitivity on thermal conductivity and specific heat capacity	70
5.10	Flow chart of the numerical model and output example	71
5.11	Conclusions.	72
6	Test phase 1: Exploratory isothermal EX-CORE curing with new epoxies	73
6.1	Methodology and experimental set-up	73
6.1.1	EX-CORE base mix selection: "270-optimal" mix	73
6.1.2	Tooling for sample production.	74
6.1.3	Manufacturing of samples in the tile mold.	77
6.2	First two series of EX-CORE samples produced with new epoxy matrices (R1 & R2).	77
6.2.1	Test series R1: Initial exploration.	78
6.2.2	Test series R2: Reduced sample thickness of 10mm	81
6.2.3	Conclusions test series R1 & R2	82

7	Test phase 2: A new Expancel® DU grade	83
7.1	Selecting the new Expancel® 043 DU 80 grade	83
7.2	Methodology and experimental set-up	85
7.2.1	Temperature monitoring with NTC sensor grid	85
7.2.2	Data processing using new Arduino® Mega setup	87
7.3	Test series R3: EX-CORE samples with new 043 DU 80 grade	87
7.4	Conclusion: final selection of most promising epoxy system	90
8	Test phase 3: Compression strength tests & epoxy mix ratio update	93
8.1	Test series R4: EX-CORE samples with various resin mix ratios cured at different temperatures.	93
8.2	Determination of the lower boundary of SR 1280/Ancamine® 2442 epoxy mix ratio	96
8.3	Compressive strength determination using Donkervoort's pressure jack	97
8.3.1	Compression test procedure and data processing	97
8.3.2	Compressive strength results R3 & R4 samples.	98
8.4	DSC tests of SR 1280/Ancamine® 2442 epoxy at 100:20 mix ratio	102
8.4.1	Experimental DSC results from isothermal DSC scans	102
8.4.2	Modified-autocatalytic model cure kinetic parameters	104
8.5	Test series R5: Different EX-CORE mix formulation & increased DU content	105
8.6	Discussion on crack initiation.	107
8.7	Summary & chapter conclusions	107
9	Validation of numerical EX-CORE thermal model	111
9.1	Validation methodology.	111
9.2	Phase 1: Validation of numerical EX-CORE model using metal NTC sensor grid	112
9.2.1	Comparison of numerical model simulation with experimental results (phase 1)	113
9.3	Phase 2: Updating the reaction onset temperature of Ancamine® 2442 in the numerical model	114
9.3.1	Determining the reaction onset temperature of Ancamine® 2442 with DSC	114
9.3.2	Comparison of numerical model simulation with experimental results (phase 2)	115
9.3.3	Effect of tuning onset reaction temperature on numerical model results.	117
9.4	Phase 3: Validation of numerical EX-CORE model using bamboo NTC sensor grid	117
9.4.1	Poorly-conductive bamboo NTC sensor grid set-up	118
9.4.2	Test series R6: EX-CORE samples monitored with non-conducting NTC sensor grid	118
9.4.3	Comparison of numerical model simulation with experimental results (phase 3)	119
9.4.4	Visualization of temperature distribution	121
9.5	Summary & chapter conclusions	122
10	Discussion on achievable cure & cycle times of EX-CORE prepreg sandwich panels	125
10.1	Investigating required EX-CORE cool-down.	125
10.1.1	Test series R7: EX-CORE samples cooled before mold opening.	125
10.1.2	Discussion on maximum allowable core temperature before mold opening	127
10.2	EX-CORE samples with prepreg facings and their effect on core temperature	127
10.2.1	Selection of snap-cure prepreg.	127
10.2.2	Test series R8: EX-CORE samples with CFRP prepreg facings.	128
10.2.3	Effect of CFRP prepreg facings on EX-CORE foam core temperature distribution	130
10.3	Exploring achievable cure and in-mold cycle times of EX-CORE products with a range of core thicknesses and cure temperatures	131
10.4	Case study: cycle time reduction of floor panels	133
10.5	Remaining questions and challenges w.r.t. EX-CORE development towards large scale automotive manufacturing	135
10.6	Summary & chapter conclusions	135
11	Conclusion	137
12	Recommendations	141
12.1	EX-CORE	141
12.2	Prepreg	143
12.3	Further improvement and validation of numerical model.	143
12.4	EX-CORE commercialization and further development towards large scale applications	145

Bibliography	147
A Procedure isothermal DSC	155
B Experimental DSC & autocatalytic model cure kinetic results	157
B.1 Former resin: Ancarez [®] RZ4010 & hardener: Ancamide [™] 3399	157
B.1.1 Previous results by Eversdijk ; May 2017 (Ref. nr: 0a)	157
B.1.2 Re-do by Mattheus; April 2018 (Ref. nr.: 0b)	159
B.2 Resin: SR 1280 & Hardener: SZ 8525 (Ref. nr.: 1)	161
B.3 Resin: Ancarez [®] RZ4010 & hardener: Ancamine [™] 2337s (Ref. nr.: 2)	162
B.4 Resin: Ancarez [®] RZ4010 & hardener: Ancamine [™] 2442 (Ref. nr.: 3)	164
B.5 Resin: SR 1280 & hardener: Ancamine [®] 2337s (Ref. nr.: 4)	166
B.6 Resin: SR 1280 & hardener: Ancamine [®] 2442	167
B.6.1 Test series 1: epoxy mix ratio: 100/60 (Ref. nr.: 5).	167
B.6.2 Test series 2: epoxy mix ratio: 100/20 at temperatures 90°C to 110°C (Ref. nr.: 5.2).	169
B.6.3 Test series 3: epoxy mix ratio: 100/20 at temperatures 140°C to 160°C (Ref. nr.: 5.2- HighTemp)	171
B.6.4 Test series 4: epoxy mix ratio: 100/20 at temperatures 115°C to 135°C (Ref. nr.: 5.2- MidTemp)	171
B.6.5 Combined test series 2, 3 and 4: epoxy mix ratio: 100/20. Temperatures 90°C to 160°C (Ref. nr.: 5.2-AllTemp)	172
C Effect of isothermal aluminum edge assumption in numerical model	173
D Verification Heisler charts	175
E EX-CORE sample manufacturing procedures	177
E.1 Steps for EX-CORE sample preparation	177
E.2 Sample naming convention	180
F Flexiforce[®] HT201 FSR calibration	181
G NTC calibration	183
H Pressure and temperature measurements	185
H.1 Measurements of samples R1-TM1-1 to R1-TM1-7	185
H.2 Measurements of samples R2-TM1-1 to R2-TM1-2	188
H.3 Measurements of samples R3-TM1-1 to R3-TM1-7	188
H.4 Measurements of sample R4-TM1-1 to R4-TM1-6	191
H.5 Measurements of sample R5-TM1-1 to R5-TM1-3	194
H.6 Measurements of sample R6-TM1-1 to R6-TM1-2	195
H.7 Measurements of sample R7-TM1-1 to R7-TM1-4	196
H.8 Measurements of sample R8-TM1-1 to R8-TM1-2	197
I Compression test results	199

List of Symbols

Symbol	Unit	Property
α	-	Degree of cure
α	m^2/s	Thermal diffusivity
Δt_{crit}	s	Largest allowable critical time step
$\Delta E_{element}$	J/m	Internal energy change per unit length
θ	-	Temperature ratio
ρ	kg/m^3	Density
ρ_{bulk}	kg/m^3	Bulk density of microspheres
ρ_g	kg/m^3	Density of gas inside microsphere
ρ_w	kg/m^3	Density of microsphere wall
ρ_{true}	kg/m^3	True density (single microsphere)
ϕ	mW	Heat flow
ϕ_{DU}	-	Volume fraction of Expancel [®] DU
a	m	Sample thickness/height
A	1/s	Pre-exponential constant; Arrhenius frequency factor
b	m	Sample width
Bi	-	Biot number
C	$\text{J}/\text{m}^3\text{K}$	Volumetric heat capacity
C_p	J/kgK	Specific heat capacity
$C_{p_{microsphere}}$	J/kgK	Specific heat capacity of a single microsphere
$C_{p_{eff}}$	J/kgK	Effective specific heat capacity of EX-CORE
$C_{p_{gas}}$	J/kgK	Specific heat capacity of gas inside microsphere
$C_{p_{wall}}$	J/kgK	Specific heat capacity of microsphere wall
E	kJ/mol	Activation energy
E	J	Internal energy
Fo	-	Fourier number
h	m	Sample height
h	$\text{W}/\text{m}^2\text{K}$	Convection coefficient
H_c	mJ	Cumulative liberated heat up to time t
H_T	mJ	Reaction enthalpy; total heat of reaction
$H_{T_{spec}}$	J/kg	Specific total heat of reaction
k	s^{-1}	Reaction Rate constant
$k_{1microsphere}$	W/mK	Thermal conductivity of a single microsphere
k_b	W/mK	Thermal conductivity of binder
k_{eff}	W/mK	Effective thermal conductivity of EX-CORE
k_f	W/mK	Thermal conductivity of fillers
k_g	W/mK	Thermal conductivity of gas inside microsphere
k_w	W/mK	Thermal conductivity of microsphere wall material
K	W/mK	Thermal conductance
K_{int}	W/mK	Interface thermal conductance
L	m	Half wall thickness

m	kg	Mass
m	-	Reaction order
m_f	-	Mass fraction
m_{fb}	-	Mass fraction binder
m_{filler}	-	Mass fraction fillers
m_{gas}	-	Mass fraction of gas inside microsphere
m_{wall}	-	Mass fraction of microsphere wall
n	-	Reaction order
P	bar	Pressure
q_{int}	W/m ³	Volumetric internal heat generation term
\dot{Q}	W/m	Rate of heat transfer
r	-	Epoxy mix ratio
R	J/molK	Universal gas constant
R_{int}	m ² K/W	Interface resistance
t	s	Time
$t_{center@95C}$	s	Time to reach 95°C in the center
t_{peak}	s	Time to peak temperature
$t_{top@95C}$	s	Time to reach 95°C at the top (90% sample height)
T	K	Temperature
T_{bottom}	°C	Maximum temperature at bottom (10% sample height)
T_{center}	°C	Maximum temperature at center
T_{cure}	°C	Isothermal cure temperature
T_{onset}	°C	Onset reaction temperature
T_{top}	°C	Maximum temperature at top (90% sample height)
T_{trans}	°C	Transition temperature
v_f	-	Volume fraction of fillers
v_g	-	Volume fraction of gas inside microsphere
v_r	-	Relative volume fraction microsphere w.r.t. v_f
V	m ³	Volume
V_{fepoxy}	-	Volume fraction of epoxy



Introduction

Donkervoort Automobielen B.V. is a Dutch sports car manufacturer that was founded by Joop Donkervoort in 1978. They specialize in designing and producing exclusive, hand-built, road legal sports cars with ultra-low weight. All Donkervoort cars are built according to their "no compromise" philosophy, meaning that any function or part that might impair the on-track performance of the car is simply left out or reduced to a minimum. This makes it possible to keep the weight of the car as low as possible. Also, since a pure driving experience is of paramount importance practically no electronic assists are implemented. Since carbon fiber reinforced polymer (CFRP) composites can offer superior strength- and stiffness to weight ratios, they started using CFRP for load bearing components in 2007 for the D8 model. The latest Donkervoort D8 GTO-RS and 40 year anniversary D8 GTO-40 models which currently roll out of the factory in Lelystad have a body that consists for 90% out of CFRP composites.

In the high-end sports and race car industry the use of fiber reinforced polymers (FRP) has been well established for structural components. Here it is also driven by the desire to increase performance through reducing vehicle weight [1]. When compared to the current steel and aluminum alloys, especially CFRP can offer superior specific properties. Next to this FRP offer unique advantages such as anisotropy, tailor-ability, fatigue- and corrosion resistance etc. [2]. Despite those advantage FRP have not been widely used for structural parts in high volume automotive applications. There are multiple reasons for this but the main issue remains their high cost compared to metals, which prevented a major breakthrough in the medium- to large-series automotive industry [3–5]. However, it is expected that the implementation of CFRP for high volume automotive applications will rapidly increase in the next two decades [6, 7]. The key drivers for this change are the stringent CO₂ emission reduction regulations being implemented in different parts of the world [8]. Car manufacturers are therefore challenged to look for new types of power trains and ways to reduce vehicle weight [5]. Due to their high potential for weight reduction there is a strong incentive to implement CFRP for structural automotive parts. Hence the automotive industry is challenged to develop more cost-effective CFRP manufacturing technologies that allow the production of CFRP parts within short cycle times [1, 9].

Also at Donkervoort, the high cost related to CFRP part manufacturing resulted in research towards a more cost effective production method. This eventually led to the development of a novel expanding foam core material, named EX-CORE. It is revolutionary since it allows to manufacture complex-shaped sandwich structures with mold defined features all-around in a one shot process without the need of an autoclave or vacuum bag. EX-CORE can be classified as a syntactic foam but is unique in the sense that it contains thermo-expandable microspheres, named Expancel[®] DU. When enclosed in a heated mold, EX-CORE delivers the required pressure to consolidate the CFRP facings from the inside out. Since its first implementation in the D8 GTO-RS, which was launched in 2016, the EX-CORE technology has demonstrated to be capable of achieving its intended goal of saving cost and time for the manufacturing of CFRP sandwich structures at Donkervoort such as floor panels and door window frames. EX-CORE has the potential to offer several advantages compared to other CFRP technologies, not only from a material point of view, but also from a production point of view. Unsurprisingly, EX-CORE has caught the attention of several automotive OEMs. Furthermore, Donkervoort's EX-CORE technology has recently been awarded the "European Innovation Grant in High-Tech Materials and Advanced Manufacturing Technologies" within the scope of the Horizon 2020 EU program.

The development of EX-CORE has not come to an end. Donkervoort has the ambition to further develop and commercialize the EX-CORE technology for larger series automotive manufacturing. To make EX-CORE competitive with other high volume composite production processes such as High-Pressure Resin Transfer Molding (HP-RTM) and Wet Compression Molding (WCM), the cycle time of several hours should be drastically reduced to several minutes. To facilitate this, not only should the production process be re-designed and automated but also the EX-CORE material itself has to be re-engineered. This resulted in the following research objective:

Contribute to the development of the one-shot manufacturing of EX-CORE CFRP sandwich structures suitable for large scale automotive production by re-engineering the EX-CORE material and/or production process.

From the literature study performed during the first two months of the Master's Thesis research, it became clear that a major restriction to obtain short cycle times are the long times required for curing the EX-CORE foam (over 3 hours) [10]. Therefore and due to the limited 9 month time frame of the Master's Thesis it was decided to focus on researching the possibilities of re-designing the EX-CORE foam in such a way that major cure cycle time reductions can be achieved. The thesis report is split into several topics of interest and experimental test phases, discussed upon in the separate chapters:

The report starts off with a brief review of relevant literature and background information in Chapter 2. Chapter 3 covers the concept of EX-CORE, previous developments, the current level of technology and drivers for its future development towards large scale automotive manufacturing. An important step in reducing the cure time of EX-CORE is to replace the current epoxy binder with a fast curing epoxy system. The selection procedure of new candidate epoxy resins is covered in Chapter 4 along with the determination of their cure kinetic parameters using Differential Scanning Calorimetry (DSC). The resulting cure kinetic model, together with theoretical models which predict the effective thermal conductivity and specific heat capacity of EX-CORE, are then implemented in a transient numerical EX-CORE thermal model discussed in Chapter 5. This model allows simulating the temperature and degree of cure distribution inside EX-CORE over time during a cure cycle. Chapter 6 covers the first test phase in which EX-CORE samples are produced with the new epoxy matrices to explore their compatibility. In this chapter the general test methodology, mold tooling and used sensors are discussed. During the second test phase, which is presented in Chapter 7, a different grade of Expancel[®] DU is selected and used for the production of additional EX-CORE samples. Ultimately one epoxy system is chosen as most promising candidate to continue the research with. During the third experimental phase discussed in Chapter 8, compression strength tests are performed on various EX-CORE samples to investigate the effect of cure temperature, cure time and epoxy mix ratio. Based on these results it became clear that the epoxy mix ratio had to be updated and so new DSC experiments had to be performed to determine the corresponding cure kinetics. In Chapter 9 the numerical model is validated with experimental temperature data obtained from various EX-CORE samples produced throughout the research. Afterwards, in Chapter 10, the required sample cool down to prevent crack formation is investigated. Additionally, EX-CORE prepreg samples are produced to investigate the effect of CFRP facings on the temperature distribution in EX-CORE. Eventually the achievable cure and in-mold cycle times of EX-CORE sandwich panels for a range of core thicknesses and cure temperatures are explored using the numerical model. Additionally, a case study for the floor panels of the D8-GTO-RS is performed. Finally, conclusions on the presented work are given in Chapter 11, followed by recommendations for future research in Chapter 12.

2

Relevant literature and background


Before delving into the research performed in this master thesis, it is beneficial to first review the relevant literature and background on topics covered in this report. EX-CORE is a foam core material that is used in a special category of composites, namely sandwich structures. Therefore the basic principles of sandwich structures are covered in Section 2.1. Several types of constituent materials are used in sandwich structures, however as is the case with EX-CORE, polymer foam cores are mainly of interest. Epoxy is used as a binder matrix in both the foam itself as well as in the carbon fiber prepreg facings, it is therefore relevant to discuss epoxies, carbon fiber and prepreg materials in more detail as well. EX-CORE can be further categorized as a syntactic foam core material, this group is elaborated upon in Section 2.2. Finally, in Section 2.3, relevant cure process aspects and literature found on thermal modeling of thermosetting composites, including the theory of cure kinetics is addressed.

2.1. Principles of sandwich structures

A sandwich structure is a special type of composite laminate generally build up out of two relatively stiff and strong thin facesheets separated by and attached to a thicker lightweight and less stiff and strong core material. The core material can be made out of polymer foam, honeycomb, (balsa-) wood or even trusses, while the facesheets (or facings) are generally made from metals or composite laminates. They are commonly used in applications such as aerospace, automotive and sporting goods that require lightweight materials. Structural- and manufacturing aspects as well as relevant constituent materials of sandwich structures are discussed in the next paragraphs.

2.1.1. Concept of sandwich structures

The main design idea behind a sandwich structure is to obtain a relatively lightweight structure with a high bending- stiffness and strength by increasing the moment of inertia with the minimal added weight. More specifically, by separating the two facings with a lightweight core material (and so moving them away from the neutral axis) the bending stiffness increases with only a small addition in weight. The effect of increasing the core thickness on the relative bending stiffness and strength is illustrated in Figure 2.1.



Relative Bending Stiffness	1	7.0	37
Relative Bending Strength	1	3.5	9.2
Relative Weight	1	1.03	1.06

Figure 2.1: Relative- bending stiffness, bending strength and weight of sandwich panels compared to solid laminate. [11]

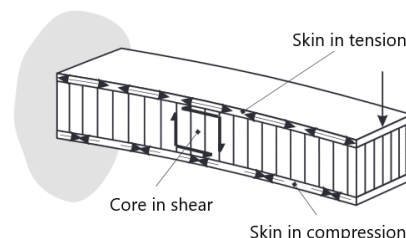


Figure 2.2: Schematic of sandwich panel with load applied at free end, resulting in top skin in tension, bottom skin in compression and core carrying shear forces. [12]

Under loading, the high strength facesheets carry most of the normal tensile- and compressive stresses, while the core absorbs shear stresses due to the transverse load. This is schematically visualized in Figure 2.2. The core material defines the out-of plane behavior of the sandwich structure, supports the facings and prevents them from buckling. Additionally, the core could also function as acoustic or thermal insulation.

2.1.2. Fiber-reinforced polymer laminate facings

The EX-CORE foam investigated in this research is used in combination with fiber-reinforced polymer (FRP) laminate facesheets to obtain a sandwich structure. A FRP is by definition already a composite material; it is composed out of strong reinforcing fibers that are embedded in a polymer matrix. The fibers are the main load carrying members, while the matrix keeps them in the correct position & orientation, protects them and transfers the load between the fibers. When compared to traditional monolithic metals and polymers, FRP can offer unique advantages such as high specific strength & stiffness, anisotropy, design freedom and long fatigue life. The design freedom not only refers to the anisotropic nature of the FRP, but also to the wide variety of reinforcing fibers and polymer matrices available. With EX-CORE the FRP facesheets are made from carbon fibers embedded in an epoxy matrix, which can be purchased as pre-impregnated fabrics, known as prepregs. In the following paragraphs background information is therefore restricted to carbon fibres, prepregs and epoxies due to their relevance with EX-CORE. Note that the binder matrix used in EX-CORE is also an epoxy resin. The microspheric fillers embedded in this matrix will be discussed in Chapter 3.

Epoxy

Epoxies form a wide category of thermosetting polymers for which cross-linking occurs at an epoxide end group. Such an epoxide group is characterized by a ring containing two carbon atoms and one oxygen atom as marked in Figure 2.3. The base molecule to which these end-groups are attached can differ widely, hence different grades of epoxies exist with varying performance, tailored for specific applications. It is also possible to add other additives, for example to increase toughness or reduce viscosity. The overall advantages and disadvantages of epoxies, when compared to other thermosetting polymers (polyesters, vinyl esters etc.) are given here [2, 13]:

- | | |
|---|-----------------------------|
| + Low shrinkage during cure | - Relatively high cost |
| + Excellent adhesion to variety of fibers/substrates | - Relatively long cure time |
| + Excellent chemical and corrosion resistance | |
| + High strength | |
| + Tailoring of properties, due to the wide variety of starting materials, hardeners and modifiers | |
| + No byproducts/ emission of volatiles | |

The most widely used class of epoxy resins are the ones containing Diglycidyl Ether of Bisphenol A (DGEBA), having two epoxide groups, one at each end of the molecule (see also Figure 2.3) [14]. The polymerization reaction is initiated by adding an amino-based curing agent (hardener), having amino functional groups (NH_2) to the resin. These amino groups react with the epoxide groups such that a three-dimensional cross-linked network is formed. During curing no by-products are formed, and in the end one big solid macromolecule results. The cross-link density and cure rate of the final product are dependent on both the functionality of the chosen curing agent (and catalyst) and external cure conditions such as temperature. The cross-link density defines the mechanical properties of the epoxy [14].

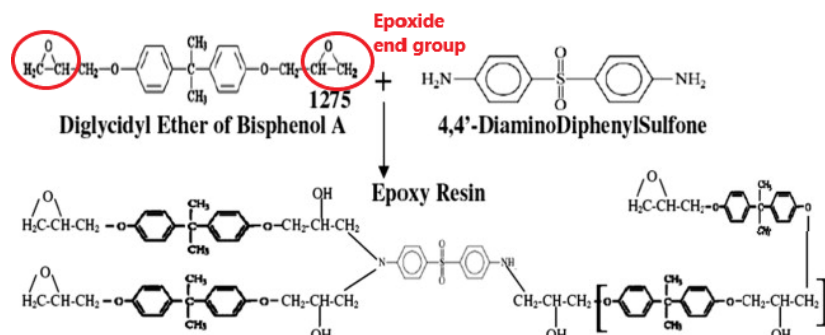


Figure 2.3: Chemical structure of DGEBA epoxy resin with DDS amine curing agent and resulting cross-linking reaction [15]

Epoxy systems are in general provided as two component systems, for which both components (resin & hardener) have to be mixed at a predefined mixing ratio. This mixing ratio will affect the cross-link density as well as the reaction rate, hence it is important to mix both components at the right proportions. Pre-mixed epoxy systems are also available, which can be found in pre-impregnated fabrics such as prepregs. The reaction of the epoxy is slowed down by the manufacturer in the B-stage, where the epoxy is in a highly viscous/tacky state and still has a low cross-link density. Note that the reaction is not completely stopped but only slowed down. To extend the shelf life, prepregs have to be stored in a freezer. Two types of prepregs exist: autoclave prepregs and out-of-autoclave prepregs, they will be further discussed at the end of Section 2.1.2.

Carbon fibers

Different types of carbon fibers exist with a variety of strengths and stiffnesses. Exceptional high specific stiffnesses can be achieved but this comes at the expense of lower specific strengths. Typical properties of high modulus (HM), intermediate modulus (IM) and high strength (HS) carbon fibers are presented in Table 2.1 in which also properties of other fibers such as glass, Kevlar and Twaron are given as comparison. Due to their relatively high cost, carbon fibers have not yet been widely applied in commercial applications. They are primarily used in weight critical applications in the aerospace, automotive and sporting goods industry where the high specific properties are considered more critical than cost. The cost of carbon fibers is dependent on the strength and stiffness of the fiber type, but also on the tow size (number of filaments per bundle). For example smaller 6K tows (6000 filaments per bundle) are more expensive than 24K tows. The main advantages and disadvantages w.r.t. other fiber types are [2, 16]:

- + Exceptionally high specific tensile strength and moduli
- + Even at high temperatures high tensile strength and modulus are retained
- + Very low coefficient of thermal expansion
- + High fatigue strengths
- + High thermal conductivity
- + Fiber properties are not affected by moisture and wide variety of solvents (at room temp.)
- High cost
- High electrical conductivity may cause 'shortening' in electrical equipment
- Low impact resistance
- Low strain to failure

Table 2.1: Typical properties of glass fibers, PAN based carbon fibers and aramid fibers [14]

Fiber type	Density [g/cm ³]	Filament diameter [μm]	Youngs modulus [GPa]	Tensile strength [MPa]	Failure strain [%]
E-glass	2.54-2.55	10	76-78	3100-3800	4.5-4.9
S-glass	2.48-2.49	10	88-91	4380-4590	5.4-5.8
HS Carbon	1.8	6-8	220-241	3450-4830	1.5-2.2
IM Carbon	1.8	5-6	290-297	3450-6200	1.3-2.2
HM Carbon	1.9	5-8	345-448	3450-5520	0.7-1.0
Kevlar 49	1.44	12	131	3600-4100	2.8
Kevlar 149	1.47	12	179	3400	2.0
Twaron	1.45	12	121	3100	3.5

Pre-impregnated fibers: Prepregs

The name prepreg refers to a thin sheet of continuous- fiber reinforcement that is already pre-impregnated with partially cured resin [17]. They are provided with a specific amount of resin and mix ratio such that consistency in the production process can be ensured. Different forms of fibers are possible; continuous tape, woven fabrics or mats. Epoxy is most commonly used as matrix material, nonetheless also other thermosetting or even thermoplastic matrices have been applied. Epoxy based prepregs are available in thicknesses ranging from 0.127mm to 0.54mm, which usually contain an epoxy content of 30 to 40wt.% [13].

During production of the prepregs the polymerization of the resin is already initiated and advanced into the B-stage. In the B-stage the epoxy still has a relatively low cross-link density. However it is viscous enough to not flow at room temperature and strongly adheres to the fibers. The prepreg sheets are backed with release

film and wound onto rolls for storage. At room temperature the shelf life of epoxy based prepregs would only be several days or weeks. However, this can be increased to 6-8 months when stored at -18°C [2].

Two main categories of prepregs exist; The first category are "Autoclave prepregs" which are fully impregnated with resin. They are suitable for autoclave processing because they require high consolidation pressures (typically 3 to 8 bar in an autoclave) to prevent void nucleation and growth [18]. Because the prepreg is fully impregnated the risk of dry spots is reduced.

The second category are the "Out-of-Autoclave (OoA) prepregs" which were initially developed for Vacuum-Bag-Only (VBO) processes and are therefore also known as VBO prepregs. They are only partially impregnated with resin and possess an in-plane permeability that allows entrapped air to be removed during a vacuum dwell at room temperature. The cure kinetics and rheology of these OoA prepregs have to be well designed. For example the viscosity of the resin should be high enough to prevent preliminary closing of the air channels. On the other hand during the initial cure stage, the viscosity should be sufficiently low to obtain fully saturated fibers before resin gelation [18].

2.1.3. Polymeric foam core materials

Polymeric foams are the most commonly used core materials in sandwich structures. They are available in a wide variety of materials, both thermoplastic and thermosetting. The basic principle of a polymeric foam is that it contains gaseous voids which are embedded into a polymer matrix. During the foaming process of the polymer, these gas pockets are formed using a chemical or physical blowing agent. The resulting voids can be interconnected, resulting in an open-cell foam or they can be isolated from each other with polymeric walls, referred to as a closed-cell foam. An example of the internal structure of both an open- and closed-cell polyurethane foam is given in Figure 2.4.

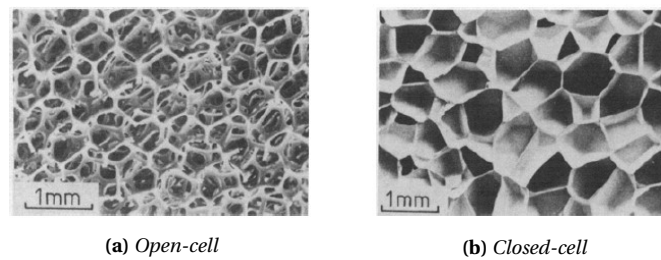


Figure 2.4: Internal structure of polyurethane foams [19]

For structural applications, closed-cell foams are generally used because they are more rigid than open-cell foams. Open-cell foams would also absorb too much resin during the production of sandwich panels. In addition to their role as structural member, foam cores could also function as thermal and acoustic insulation, fire retardant, impact resistance etc. The most common commercially available structural foams are PET, PMI, PU, PVC, SAN and syntactic foam, they are discussed in the next paragraphs. A comparison of their mechanical properties for varying foam densities is presented in Figure 2.5. From the graphs it can be observed that both the compressive and shear strength increase approximately linearly with foam density.

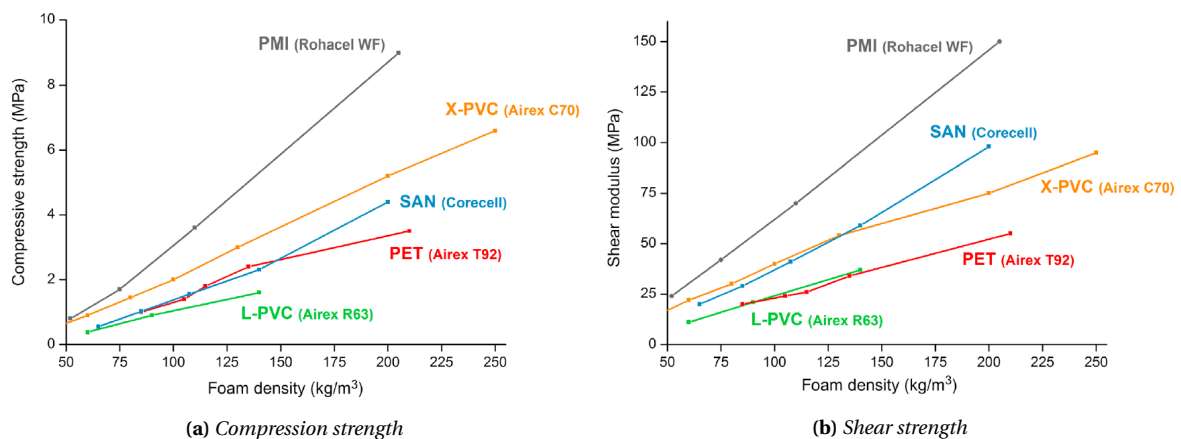


Figure 2.5: Comparison of mechanical properties for common commercial foam core materials at room temperature [20]

Polyethylene Terephthalate (PET) foams are available in a wide variety, both closed- and open-cell as well as thermosetting and thermoplastic in nature. PET foams exist with densities between 70-320kg/m³ and can typically be processed up to 150°C, with peaks even up to 180°C [21–23]. Additionally, they possess long thermal stabilities up to 100°C [21]. PET foams offer good compressive and tensile strength but when compared to other foams, stiffness and shear properties are relatively low (see also Figure 2.5b). Advantages of thermoplastic PET foams are that they are thermo-formable, recyclable and weldable. They can be joined to thermoplastic facesheet, to obtain thermoplastic sandwich panels with good impact resistance. Manufacturers of PVC cores include AIREX, Armacell, DIAB group and Gurit.

Polyvinylchloride (PVC) foams are usually closed-cell foams. They are available as both linear thermoplastic (L-PVC) and cross-linked thermosetting (X-PVC). L-PVC is more ductile, offering excellent impact resistance, but has lower mechanical properties and reduced temperature resistance than X-PVC. PVC foams have densities ranging from 35-250kg/m³ [24–26]. These foams can normally operate between -200°C to max. 70°C, however PVC foams have been developed that are processable up to 140°C [26]. A disadvantage of PVC foams is that CO₂ out gassing can happen over time and during prepreg curing, which could result in delaminations [20]. PVC foam cores are produced by manufacturers such as AIREX, DIAB group (Divinycel-H type foams) and Gurit.

Polymethacrylimide (PMI) foams are thermoplastic or thermosetting closed-cell foams. They offer the highest specific strength and stiffness properties of all foams and also the highest temperature resistance up to 220°C, but they are also the most expensive ones. Their tensile strength and modulus is typically 20% higher than X-PVC (see Figure 2.5). They also offer high impact strength, high thermal stability, low resin uptake and excellent solvent resistance [20]. PMI foam cores are commonly known under the tradename of ROHACELL™ produced by Evonik Industries. They come with densities ranging from 75 to 200kg/m³ [27]. A special type of PMI foam core was developed that can be "in-situ" foamed at the correct shape in a therefore designed mold [28]. It is named ROHACELL™ Triple F, and is one of the closest competitors to EX-CORE (see Section 3.5.3).

Polyurethane (PU) foams are open- or closed cell foams (see Figure 2.4) that can be both thermoplastic or thermosetting in nature. They are relatively inexpensive and can be used up to 135°C [29]. They are applied in automotive applications for which only moderate mechanical properties are required. They are also more brittle and less resistant to fatigue than PVC or SAN foams. PU foam cores are produced by Hexcel.

Styrene Acrylonitrile (SAN) foams are thermoplastic closed-cell foams which possess good mechanical properties and fatigue resistance in combination with high impact toughness. Hence it combines properties of both L-PVC and X-PVC. Gurit produces SAN foams under the tradename of Core-Cell which are processable up to 120°C and have densities in the range of 66 to 220kg/m³ [30].

Syntactic foams are by definition foams consisting of hollow spherical fillers that are incorporated in a binder matrix. EX-CORE can be classified as a syntactic foam, therefore this class of foams is discussed in more detail in Section 2.2.

2.1.4. Manufacturing aspects of foam cored sandwich structures

Most foam core materials are commercially available at low price in the form of sheet materials or thick blocks from which cores of the required dimensions can be cut or milled. Foam slices can also be bonded and stacked on top of each other to obtain the desired core thickness. In some cases cores can be thermally folded. Another more expensive option is to foam the core directly in the required shape and dimension in a specifically designed mold.

Sandwich structures are in general manufactured by joining the core material with the facings. This can be done in several ways. One option is to first cure the FRP facesheets and then adhesively bond them to the core. Another possibility is to use un-cured FRP facesheets and then co-cure them to the core, which means that they are simultaneously cured and bonded to the core in a single cure cycle. Several manufacturing methods can be used to do this, such as using a heated press, vacuum bagging with autoclave curing, match mold processing and liquid molding. A schematic of the first three processes is given in Figure 2.6.

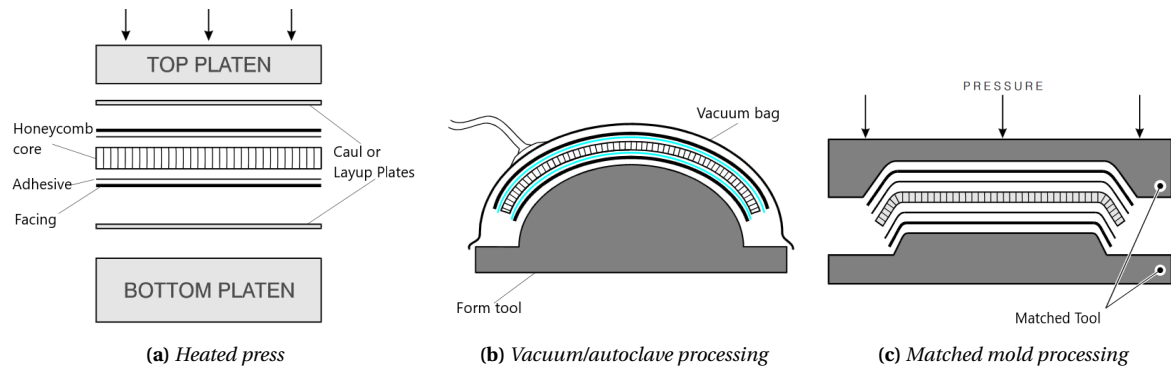


Figure 2.6: Different sandwich structures manufacturing processes [12]

2.2. Syntactic foams

Syntactic foams are a special class of closed-cell foams formed by incorporating spherical hollow particles in a binder matrix, as visualised in Figure 2.7. The mixture is then poured into a mold where it solidifies. As with conventional polymeric foams, a blowing agent could also be added that causes the foam to expand in the mold cavity. This is also the main idea behind EX-CORE as explained in Chapter 3.

Polymer matrices and more specifically thermosetting resins such as epoxies, polyesters, vinylesters and phenolics are most commonly used as binder because they offer the advantage of low processing temperatures and low viscosity, which makes it possible to mix the fillers without damaging them. The spherical fillers (in this case referred to as microspheres or microballoons) are often so small that the foam appears to be a homogeneous solid. In contrary to ordinary polymeric foams, pores are barely visible with the naked eye [31]. The microsphere walls can be made from glass, metal, polymers, ceramic or even carbon. The bulk density of the microspheres can vary from 70 to 500kg/m³ [31].

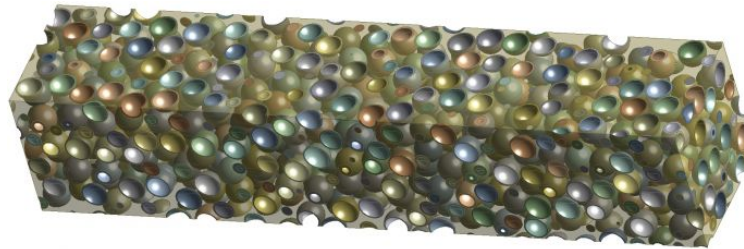


Figure 2.7: Schematic of a syntactic foam; hollow particles in a matrix [32]

Syntactic foams are highly tailorable due to the wide variety of fillers and properties that can be tuned such as; the material of the microsphere, microsphere diameter, shell thickness and used volume fractions. Other benefits of syntactic foams is that they possess high specific compressive strengths, good impact properties and low moisture absorption. Due to their closed-cell structure, they can withstand high hydrostatic pressures. They however generally have higher densities than ordinary polymeric foams, typically ranging between 180-800kg/m³ [33]. The compressive properties will be mainly dependent on the microspheres, while the tensile properties, are defined by the matrix material [34].

Compressive strength and stiffness for varying densities of epoxy/ hollow glass microspheres syntactic foams were collected by Pinisetty et al. [35] and plotting in the graphs given in Figure 2.8. From the graphs it can be seen that the compressive strength and modulus are both approximately linearly related with density. This behavior had also been observed for vinyl ester and polyetherimide syntactic foams [33, 35]. Syntactic foams are commercially available for in-situ foaming or as pre-molded foam sheets/blocks. Manufacturers include: DIAB group, Engineered syntactic systems, Synfoam and Trelleborg AEM.

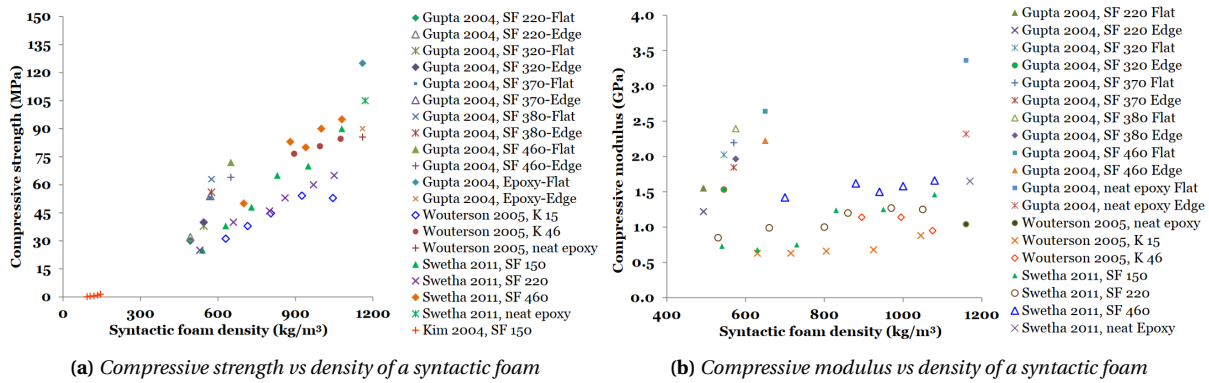


Figure 2.8: Compressive properties of epoxy hollow glass microsphere syntactic foams for various densities [35]

2.3. Cure process aspects and thermal modeling of thermoset composites

As will be discussed in more detail in Chapter 3, EX-CORE is in essence a syntactic foam consisting of hollow microspheres hold together by a thermosetting binder matrix. Some important principles on processing thermosetting composites are first of all presented, followed by relevant background on the theory of cure kinetics. In addition some examples of thermal models found in literature that simulate the heat transfer and reaction progress of thermosetting composites are discussed.

2.3.1. Cure process principles of thermosetting composites

When curing thermosetting composites three main processing parameters are predominantly of importance; temperature, pressure and time. The cure cycle defines the temperature versus time profile and controls the polymerization reaction of the thermosetting matrix. External pressure is required to makes sure that the laminate is sufficiently compacted and void formation and growth is suppressed. Figure 2.9 shows a typical autoclave pressure and temperature profile for a thermosetting resin. The corresponding viscosity and Tg profile of the resin is shown as well.

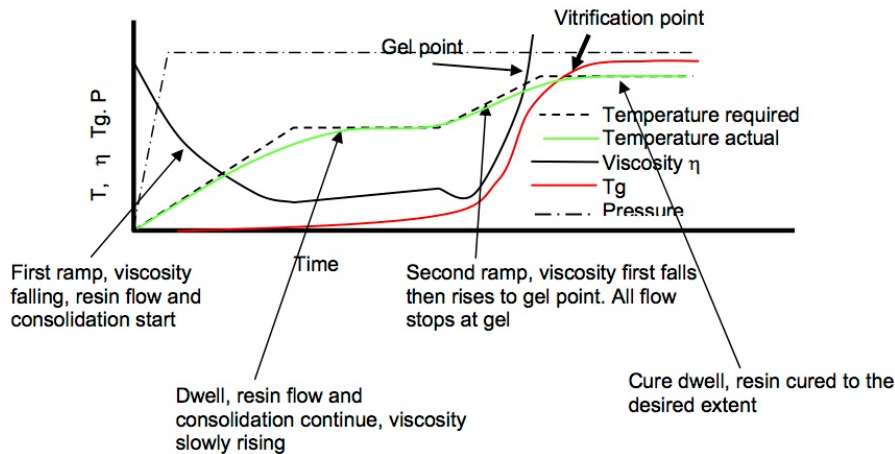


Figure 2.9: Classical two-stage cure cycle and corresponding viscosity profile (Figure from website: <http://aerospaceengineeringblog.com/autoclave-variability/>)

During the first stage of the cure cycle "softening" of the resin occurs; the relatively high viscosity of the resin drops when temperature increases [36]. The low viscous state of the resin allows it to flow and volatiles to escape. An intermediate isothermal dwell can also be opted for to extend the period of the resin being at low viscosity, during this dwell the viscosity will only slowly rise. A dwell is often also used to allow temperature homogenization throughout the composite. However, currently for most autoclave applications a straight ramp-up (without the first isothermal dwell) until the final cure temperature is being used. This because the industry shifted towards net-resin content systems that eliminate resin bleed time [37]. However, for out-of-autoclave/ vacuum bagging processes an intermediate dwell is required to ensure sufficient volatile extraction.

During the second ramp-up in Figure 2.9 it can be seen that the viscosity initially slightly drops as temperature is further increased. This is followed by a sudden high viscosity increase when the polymerization/cross-linking reaction of the resin takes place. The resin starts to gel and ultimately becomes solid. More precisely, "gelation" refers to the moment (at the "gel point") when an "infinitely large" cross-linked network molecule is obtained [38]. For epoxies gelation is often related to the point when a viscosity of 10kPa·s is reached (after passing the minimum viscosity point) [38]. The polymerization reaction progresses into the second isothermal dwell until the resin is fully cured. Another important term is "vitrification" which refers to the moment when the polymer chains are so closely packed that cooperative motion is blocked due to insufficient free volume. This is also the moment when the rate of cure is drastically reduced [38].

Next to a suitable temperature profile, pressure should be applied during curing of the composite. This is necessary for proper laminate compaction and to suppress void formation and growth. Pressure can be provided in several ways depending on the manufacturing process. In most cases it is provided by external means such as an autoclave, vacuum bag or press. Generally, it is beneficial to limit the pressure when the resin's viscosity is low, since too high pressure can result in air entrapment in the laminate. High pressure on the other hand is favorable right before gelation, this provides good laminate compaction and void growth suppression [37]. So to obtain a high quality laminate with low porosity and void content, the temperature and pressure profile should be properly tuned. This can also aid in obtaining shorter cure and process cycle times.

Another important aspect of thermosetting composites is that when they are cured, heat is generated due to the exothermic reaction nature of the thermosetting matrix. The liberated heat can only slowly dissipate through conduction to the outside edges of the composite. Especially for thick thermosetting composites, the internal heat cannot dissipate in time, which could rise the inner core temperature to such an extent that material degradation is at risk [39]. Another major point of concern are the large temperature gradients that cause non-uniform curing, increasing the potential of insufficient consolidation and residual stresses [40]. Consequentially, this effects the overall quality and performance of the product (warping, entrapped air, microcracks, delaminations, volatiles etc.) [39, 40]. To get a better understanding of the cure and thermal behavior of thick thermosetting composites, several numerical models were developed as discussed in the next section.

2.3.2. Finite difference thermal models for thick thermosetting composites

Several studies have been dedicated to simulating the heat transfer, temperature- and degree of cure distributions as a function of part geometry and cure cycle. One-, two- or three-dimensional numerical models were developed that make use of Finite Element Methods (FEM) or Finite Differencing Methods (FDM) [40–46]. In the next paragraphs two studies devoted to modeling the cure behavior of thick thermosetting composites using FDM are shortly discussed, as they are most representative for the current research. These thermochemical models make use of the conservation of energy principles with heat transfer equations that are coupled with cure kinetics (see Section 4.2.1). To solve the partial differential equations, transient FDM were used to discretize time and space. In addition material properties such as thermal conductivity and heat capacity had to be experimentally/analytically determined.

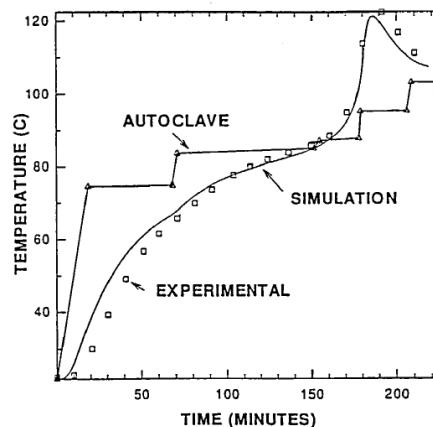


Figure 2.10: Comparison of experimental and simulated temperature over time for a 2.54 thick glass/polyester laminate. [40]

Bogetti & Gillespie: Two-dimensional cure simulation of thick thermosetting composites

Bogetti & Gillespie [40] created a two-dimensional cure simulation of thick thermosetting composites. They modeled several graphite/epoxy and glass/polyester composite parts at three different cross-sections; a flat plate, a ply drop geometry and a right angle bend. Verification of the model was done by comparing the temperature and degree of cure profiles with available exact solutions, which showed excellent agreement. Validation with experimental results from glass/polyester laminates also gave an excellent correlation, as shown in Figure 2.10. They concluded that the degree of cure gradients through-the-thickness were strongly dependent on part geometry, cure kinetics, cure cycle temperature and thermal anisotropy.

Shi: Heat transfer in thick thermoset composites

During his PhD dissertation Shi [45], created a three-dimensional heat-transfer model for simulating the temperature and degree of cure simulations in thick thermosetting composites. Material properties of a glass-fiber/epoxy composite and epoxy resin were experimentally and/or analytically determined such as density, heat capacity, thermal conductivity and cure kinetics. The thermal behavior of the glassfiber/epoxy composites was studied and both an analytical and numerical model was created. Again, it was concluded that the high exothermic heat release and low thermal conductive material resulted in large temperature- and cure gradients and high temperature overshoots in the core of the material. Both the experimental and simulated results showed that the maximum temperature in the core increases with part thickness and cure temperature. To obtain the simulation results the Heat Transfer Module of COMSOL Multiphysics 4.4 with MATLAB was used. The results were validated with experimental data, obtained from samples made with a vacuum infusion process. Comparisons of the those results for various laminate thickness and cure temperature are shown in Figures 2.11 and 2.12, respectively.

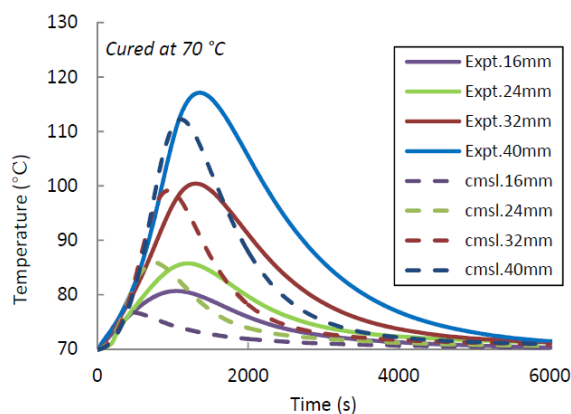


Figure 2.11: Experimental and simulated results for glass-fiber/epoxy laminates at various thicknesses cured at 70°C. [45]

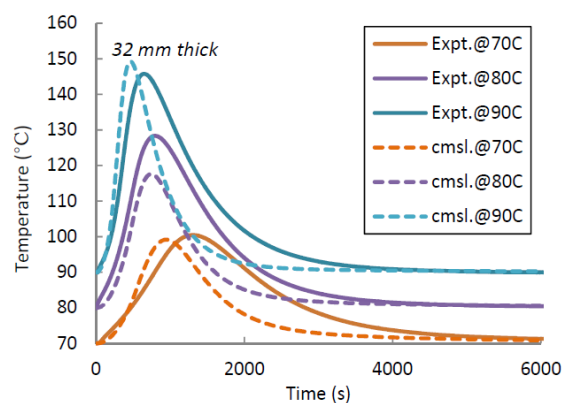


Figure 2.12: Experimental and simulated results for 32mm thick glass-fiber/epoxy laminates cured at various temperatures. [45]

2.3.3. Thermoset cure kinetic theory and models

Both of the previously discussed models use the theory of cure kinetics to simulate the heat generation and exothermic reaction progress of the thermosetting resin. This cure kinetics theory describes the reaction rate of the curing resin as a function of temperature and degree of cure. The theory makes use of the *Arrhenius Equation* (2.1) to determine the reaction rate constant k [1/s], which is dependent on temperature T [K] [47–49]:

$$k = Ae^{-\frac{E}{RT}} \quad (2.1)$$

in which A [1/s] is a pre-exponential constant or the Arrhenius frequency factor. It represents the frequency that molecules will collide with the correct orientation [50]. The activation energy E [kJ/mol] is the minimum energy that the molecules must acquire for the reaction to initiate. R represents the universal gas constant of 8.314 J/(molK), and the combined term RT represents the average kinetic energy of the molecules. The Arrhenius Equation can be seen as an exponential decay function, where the expression $e^{-E/RT}$ represents the fraction of molecules (at a certain temperature) with energies equal or larger than the activation energy [50]. A high temperature in combination with a low activation energy will therefore result in a large rate constant and fast reaction.

A cure kinetic model of certain reaction order (n & m) is used to relate the reaction rate $\frac{d\alpha}{dt}$ [1/s] with the reaction constant(s) k and the degree of cure α . Where α can vary from 0 (not cured) to 1 (fully cured). The degree of cure can be seen as the disappearance of epoxide functional groups with the formation of chemical bonds/cross-links [48]. The governing equation of three common cure kinetics models are given in Equations 2.2 to 2.4:

$$n^{th} \text{ order: } \frac{d\alpha}{dt} = k(1 - \alpha)^n \quad (2.2)$$

$$\text{Autocatalytic: } \frac{d\alpha}{dt} = k\alpha^m(1 - \alpha)^n \quad (2.3)$$

$$\text{Modified Autocatalytic: } \frac{d\alpha}{dt} = (k_1 + k_2\alpha^m)(1 - \alpha)^n \quad (2.4)$$

In these equations, the $(1 - \alpha)$ term can be seen as the concentration of epoxide functional groups. So for the n^{th} order model the reaction rate $\frac{d\alpha}{dt}$ is (next to k) only dependent on the epoxide group concentration, with the maximum rate at $t=0$. Many epoxy resins are however autocatalytic, meaning that the reaction product acts as an extra catalyst for the reaction. The additional term $k_2\alpha^m$ takes this effect into account [47, 48]. For epoxy-amine resins (as used in this research) this catalyzation product would be the generated hydroxyl groups. However, when using Equation 2.3, the initial rate of reaction is 0, which is not necessary the case when impurities such as catalyzing ions or water are present [48]. The governing equation of the autocatalytic model is therefore modified as shown in Equation 2.4.

The reaction order parameters n & m , as well as the reaction parameters E & A are specific for each epoxy system and are constant with temperature and degree of cure. For thermosetting resins these parameters can be determined with Differential Scanning Calorimetry (DSC) experiments, for which both dynamic or isothermal tests are possible [51]. In essence, the DSC apparatus is used to measured the heat flow ϕ [mW] of the curing resin, which can then be related to the rate of reaction by Equation 2.5:

$$\frac{d\alpha}{dt} = \frac{\phi}{H_T} \quad (2.5)$$

where H_T [mJ] is the total heat of reaction or reaction enthalpy. The experimental DSC results can be fitted to the cure kinetic model in various ways using numerical or graphical methods 4.2.1 [47, 52, 53]. For more information on cure kinetic testing using DSC see also Sections 4.2 and 4.3.

3

The EX-CORE concept and its development

EX-CORE is a novel type of expandable core material developed at Donkervoort Automobielen B.V. that makes it possible to create complexly shaped sandwich structures with mold defining features all around in an innovating one shot process. In recent years, EX-CORE evolved from a basic idea to a unique technology implemented at Donkervoort to create sandwich structures for their cars. So far EX-CORE has demonstrated its envisioned goal of saving cost and time at Donkervoort. Now, Donkervoort has the ambition to further invest in the development of EX-CORE with as goal to make it suitable for larger scale automotive manufacturing and for other industries as well.

The concept of EX-CORE will be explained in Section 3.1. Then in Section 3.2 an overview of previous EX-CORE research with their findings is given. The current EX-CORE constituents and their properties will be discussed in Section 3.3, followed by an explanation of a typical EX-CORE production process in Section 3.4. Finally in Section 3.5, important drivers for further EX-CORE development towards large scale automotive manufacturing are discussed.

3.1. The concept of EX-CORE

EX-CORE is in essence a closed-cell syntactic foam containing a physical blowing agent that will volumetrically expand once a certain temperature is reached. When molded in an enclosed rigid mold, EX-CORE acts as a pressure generating mechanism. This allows for consolidation and co-curing FRP prepreg facesheets to the EX-CORE foam. This process is unique since it does not require vacuum bagging or external pressure from an autoclave. In addition EX-CORE allows creating near-net shaped complex sandwich structures with mold defined features on all sides of the product in a one-shot process. The function of EX-CORE can be seen both from a material and production point of view; first of all its structural function of light weight core material and secondly, its internal pressure mechanisms allowing one-shot manufacturing of sandwich structures.

EX-CORE consists of a thermosetting matrix in which three types of microspheres are embedded. One of them is essential for the pressure generating mechanism of EX-CORE, namely thermoplastic expandable microspheres containing a gaseous blowing agent. They are sold by AkzoNobel under the name of Dry Unexpanded Expancel[®], or in short Expancel[®] DU. Its basic working mechanism is shown in Figure 3.1.

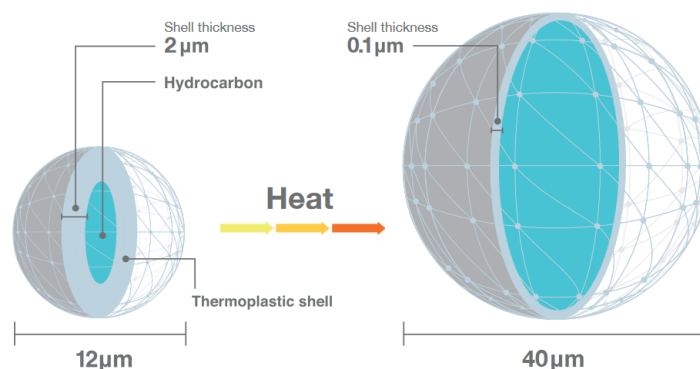


Figure 3.1: Schematic of expansion mechanism of Expancel[®] DU microspheres by AkzoNobel [54]

At elevated temperatures the hydrocarbon blowing agent wants to expand, this expansion (and so internal pressure increase) is restricted by the thermoplastic wall of the microspheres until the glass transition temperature of the thermoplastic material is reached. At this temperature the shell softens and sudden expansion of the microspheres will occur. The volume of the sphere increases around 40 times, which also results that the thermoplastic wall becomes thinner due to material stretching. At this point the sphere is plastically deformed and will not return to its original size upon cooling [55]. The expansion principle of the Expancel[®] DU microspheres is exploited in EX-CORE to fill up cavities in a complexly shaped enclosed heated mold and ultimately consolidate FRP prepreg facesheets.

Different grades of Expancel[®] DU are offered by AkzoNobel, their unexpanded diameters vary from 5 to 40 μm with expansion onset temperatures ranging from 80 to 173°C [56]. The volume of the spheres keeps on increasing (even up to 60 times) when the temperature is further increased beyond the onset expansion temperature [54]. However at the maximum allowable temperature, the thermoplastic shell becomes too thin and the microsphere starts to deflate.

Once cured, the thermosetting matrix ensures that a dimensionally stable foam is obtained, preventing re-expansion at elevated operational temperatures. Next to the expandable DU microspheres, un-expandable thermoplastic and glass microspheres are used in EX-CORE (see Section 3.3). They make it possible to further tailor the density and mechanical properties of EX-CORE. In total all the microspheres can fill up to 80-90% of the volume in EX-CORE.

In Section 2.3.1 the importance of a properly tuned temperature and pressure profile to obtain a high quality composite was explained. In addition it can help to achieve shorter cure and process cycles times. An important remark should be made for the EX-CORE process; the pressure generation in EX-CORE is directly related to the used volume fraction of Expancel[®] DU and so it cannot be varied during curing. In addition, the pressure is initiated once the onset expansion temperature of Expancel[®] DU is reached, beyond this point the pressure will keep on increasing at increasing temperature until the maximum temperature of Expancel[®] DU is reached. Consequentially, changing the temperature profile of the EX-CORE cure cycle has a direct effect on the generated pressure profile.

3.2. Previous research and developments

The idea behind EX-CORE arose in 2007, when Donkervoort desired a more cost-effective and less time consuming production method for the door beam of the Donkervoort D8-GT. As shown in the CAD drawings in Figure 3.2 the door beam has a complex shape. In the car it is visible from all sides and thus requires a high surface finish and visual carbon wave pattern all-around.

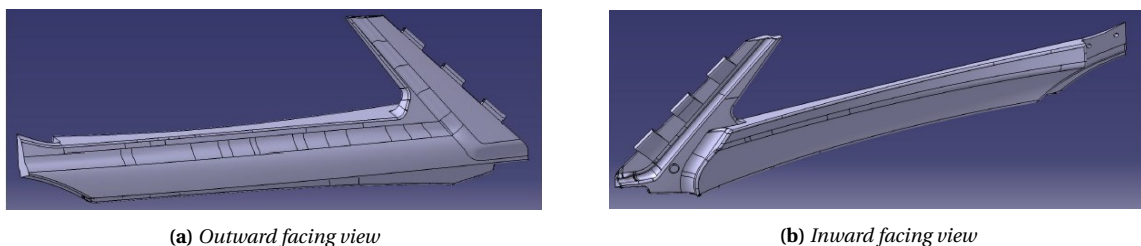


Figure 3.2: CAD drawings of the door beam (passenger side) of the Donkervoort D8 GTO [57]

The originally used core was CNC milled from Divinycell H45 (48kg/m³). In addition the door beam itself had to be produced in two main steps. First, two carbon fiber shells had to be produced with hand lay-up, vacuum bagged and then cured in an oven. In the second step, the milled core is wrapped in glue film and placed in between the pre-cured shells. The assembly is then put into the mold, vacuum bagged and cured in the oven. Only with this two-step process it was possible to obtain a high surface finishing all around the product. However, it remained difficult to control the tolerances between the pre-cured facings, milled foam core and mold dimensions. Not only was the 3D milled foam core a large contributor to the cost, the time-consuming two step process also resulted in high labor costs. It was reasoned that by developing an expandable core material, a cost-effective one shot process might be achieved for which the tolerance issues were also prevented. This eventually resulted in EX-CORE. Remark that in all the previous research EX-CORE was named X-core, but in 2018 its name changed to EX-CORE for licensing purposes.

3.2.1. Houwers 2013: Pure Expancel[®] DU/DE core and addition of thermoset binder

The first research towards expandable foam cores at Donkervoort was performed by Houwers [58] during his internship in 2013. He initially experimented with foam mixtures which he made from solely two types of gas filled thermoplastic microspheres: Expancel[®] 031 DU 40, which will expand at temperatures in excess of 80°C [56] and secondly, a pre-expanded variant; Expancel[®] 551 DE 40. The later one has an exceptional low density of 30kg/m³ and is therefore commonly used as a lightweight filler. More detailed characteristics of both constituents are provided in Section 3.3. A first sample was created with a weight ratio of 7:1 DU/DE. This was based on a similar research performed by Vaikhanski & Nutt [59] who obtained the highest quality crack-free foams with this ratio. They also discovered that foams made of purely DU are not desirable since they will possess large crack formations. The DE increases the structural integrity of the foam, reducing the number of cracks. Remark that due to the applied heat the thermoplastic shells of the microspheres starts to soften and this in combination with the pressure generated by DU, cause the microspheres to weld together.

The 7:1 DU/DE sample created by Houwers possessed similar characteristic than the one created by Vaikhanski & Nutt [59]; the foam is not very stiff nor strong and can be crushed by hand. Such a DU/DE mixture had also been placed in a mold that was covered with a 1.3mm aluminum lid. As shown in Figure 3.3 the lid deformed beyond yielding, indicating the significance of the pressure generated by large amounts of DU. An additional issue with the cured foam arose once re-heated; a cured sample with carbon fiber prepreg facesheets was de-molded and then re-heated to 105°C. This resulted in re-expansion of the cure which teared the facesheets apart from one another, as shown in Figure 3.4.



Figure 3.3: Deformation of 1.3mm aluminum mold lid after curing of Expancel[®] 7:1 DU/DE mix [58]



Figure 3.4: Re-expansion of Expancel[®] DU/DE sample with CF/epoxy facings after reheating at 105°C [58]

To prevent this re-expansion, it was proposed to add a thermosetting binder to the foam, which once cured should be strong enough to withstand the re-expansion of Expancel[®] DU at elevated temperatures. Samples with epoxy as binder were manufactured which resulted in a drastically increased density of the foam from $\pm 30\text{kg/m}^3$ to 450kg/m^3 . Nonetheless, it was argued that the epoxy also considerably increases the foam's mechanical properties. Additionally, the epoxy made the pre-cured mixture easier to handle, since it now became a viscous paste instead of loose powder. Complex-shaped products were successfully created in a one-shot process using this new composition. Examples are shown Figures 3.5 and 3.6. These results were very promising, convincing Donkervoort to continue the expandable foam research. Houwers recommended further testing with different epoxy resins, to further decrease the amount of surface porosity in the facesheets and lower the density of the foam.



Figure 3.5: Complex shaped demonstrator sandwich structure produced in one shot with DU/DE/epoxy core mixture and CF/epoxy facesheets [58]



Figure 3.6: Gear knob produced in one shot with DU/DE/epoxy core mixture and CF/epoxy facesheets [58]

3.2.2. Minde 2014: Manufacturing process & Approaches for density decrease and improvement of surface porosity

In 2014 the research was continued by Minde as part of his Master's Thesis [60]. He had as goal to develop and demonstrate the one-shot production process for the door beam of the D8 GTO (depicted in Figure 3.2). He experimented with different mix compositions of Expancel[®] DU/DE, other types of epoxy resins and fillers. In the first part of his research he aimed at reducing the foam's density. He came up with several approaches, with varying success, such as:

1. **Addition of inner F50 foam core:** A lightweight 50kg/m³ foam core with smaller dimensions than the mold was incorporated and the resulting 3mm gaps were filled with DU/DE/epoxy paste. The cured sample showed large air inclusions and the method was not practical.
2. **Addition of Divinycell H45 foam cubes:** The cubes had a density of 48kg/m³, so the density of the foam reduced. However, this method was again not practical and all the foams cubes had to be cut by hand at 3x3x3mm. A maximum packing factor of only 0.58 could be achieved, which is 6% lower than for spheres of equal size.
3. **Addition of polystyrene beads** Two sizes of polystyrene beads were added having diameters in the range of 0.1-1mm and 2-5mm. An optimal packing factor was obtained using 86% large and 14% small beads. Unfortunately, it was later diagnosed that they formed a weak link in the foam because of their poor mechanical properties and low melting point. At around 80°C the polystyrene beads started to shrink, which required a larger amount of DU fill to fill up the free volume. Minde recommended to use another lightweight filler in the same size range.

In the second part of his research the focus shifted towards reducing the surface porosity in the facesheets. The following mitigations strategies were investigated:

1. **Application of vacuum** The product/mold assembly was prepared as usual, but then entirely vacuum bagged and subsequently cured in the oven under vacuum. The surface porosity did not noticeably improve. It was reasoned that the out-gassing of the foam core probably only took place at elevated temperatures when the prepreg's viscosity was already too high for gases to escape.
2. **Addition of dry glass fabric** A dry ply of glass fabric was substituted in between the mold surface and prepreg. The reasoning behind this was that it might provide a path for gases to escape. When cured it became clear that there was not enough excess resin to impregnate the extra dry ply, resulting in an even worse surface finish.
3. **Addition of barrier layer** The hypothesis was that a barrier layer between the core and the prepreg facings would prevent out-gassing from the foam into the prepreg. Several types of barriers were tested such as PET foil, adhesive film, polypropylene etc. The most promising results were obtained with 0.023mm thick PET foil, which resulted in a significant improvement in surface quality of the door beam as can be seen in Figure 3.7. The quality of the core-to-facesheet bond was however questionable and peel test were recommended.
4. **Varying the grades of DU & DE** Samples were created with different grades of Expancel[®] DU and DE to investigate the effect on the foam quality and surface porosity. Minde used three grades of dry unexpanded Expancel[®] 031, 461 & 551 DU and two grades of dry expanded Expancel[®] 551 & 920 DE. He found that 031 DU in combination with 920 DU provided the best surface quality, with the fewest surface porosity and no discolorations. These two grades of Expancel[®] are currently still being used in EX-CORE production. Their properties will be discussed in Section 3.3.

Minde performed Thermo-Mechanical-Analysis (TMA) experiments on various grades of Expancel[®] DU at different temperature cycles. An example TMA plot for pure Expancel[®] 031 DU is shown in Figure 3.8. A sudden expansion at 84°C could be observed and it could also be confirmed that the amount of expansion is dependent on temperature. For example in Figure 3.8 it can be seen that the sample's volume kept on increasing during heat-up from 84 to 100°C. Minde also monitored the temperature during production of the first proof of concept door beam, which indicated that the exothermic reaction of the resin caused temperature overshoots exceeding 140°C, which could be related to shrinkage cracks in the core.

The final EX-CORE foam Minde created had a density of 168kg/m³. He performed mechanical tests and obtained a compressive strength of 1.27MPa and a shear strength of 0.64MPa. Using this foam Minde managed to produce the door beam in a one-shot process. The imposed strength criteria were met with an increased density of 25% (compared to Divinycell H45). The new process resulted in a decrease of manual labor

by 45% and a total cost reduction around 65%. The surface quality of the CFRP prepreg facings did improve but they still had a large amount of surface porosity. Further research was recommended to improve this.



Figure 3.7: Door beam with low amount of surface porosity produced with PET foil between core and CFRP prepreg facings [60]

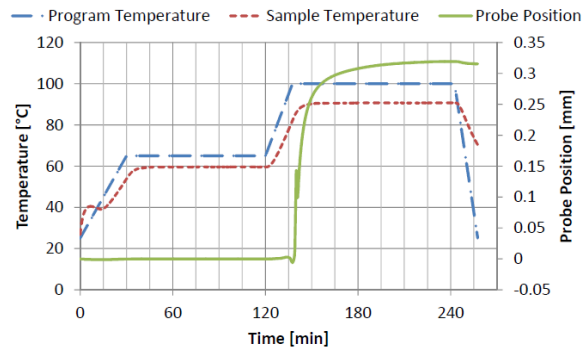


Figure 3.8: TMA graph of Expancel® 031 DU showing expansion vs oven- and sample temperature [60]

3.2.3. Santos & Boegem 2015: Material testing

In 2015, two interns helped to improve the fundamental knowledge of EX-CORE. Santos developed a test setup for determining the compressive properties of EX-CORE in-house at Donkervoort. The test bench was not conform ASTM standards, but made quick comparative testing of various EX-CORE samples possible. His most promising foam composition was also tested at the TU Delft according to ASTM standards. He found that the Donkervoort test bench underestimated the compressive strength and stiffness by 5% and 45%, respectively. The 266kg/m³ foam had a compressive strength of 4.65MPa.

Boegem [61] experimented with larger volumes of a wide variety of EX-CORE compositions. Mixtures with high DU content could result in explosive behavior of the foam during de-molding. Mixtures with high volume content of resin resulted in large voids in the foam. Boegem investigated the suitability of the EX-CORE technology for the manufacturing of the upper-door window frames of the Donkervoort D8 GTO-RS. He concluded that EX-CORE would cause a process time reduction around 65% and unit cost reduction around 60%.

3.2.4. Berckmoes 2016: Integrally heated tooling

In 2016, Berckmoes [62] did his internship at Donkervoort on the development of an integrally heated tooling (IHT) system. He investigated the idea of implementing a heating element inside a mold, which would allow to better control the mold temperatures and heat-up rates to cure EX-CORE parts and reduce the energy consumption when compared to oven curing. Berckmoes successfully developed an IHT mold system for the floor panels of the Donkervoort D8 GTO-RS. The main idea behind the IHT is to implement carbon fiber braids in the mold that function as a resistance heating element, i.e. the internal resistance of the braids will generate heat when current is provided through them. Thermocouples are also incorporated in the mold to monitor its temperature. This in combination with a proportional-integral (PI) controller makes it possible to control the mold temperature based on the difference between the desired temperature and measured temperature by the thermocouples. The PI controller and corresponding software was developed in corporation with Twenco CME B.V. The software is run on a windows computer connected to the PI controller. It allows to implement a pre-defined cure cycle and live monitoring of the process. A schematic representation of the entire setup is shown in Figure 3.9. IHT tooling is currently also being used to produce other sandwich products at Donkervoort such as the door window frames of the D8 GTO-RS.

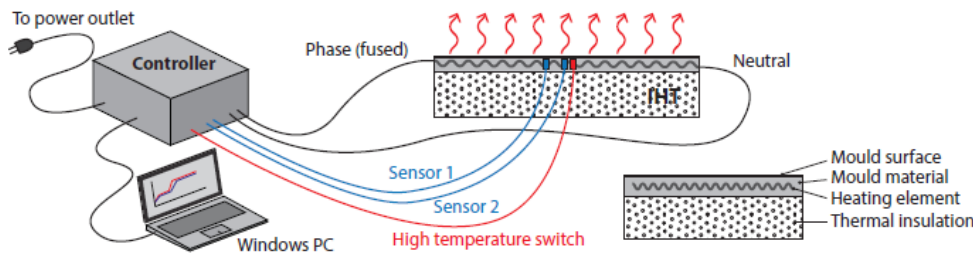


Figure 3.9: Schematic visualization of integrally heated tooling setup [57]

3.2.5. Vial 2016: Relating constituents to EX-CORE material properties

In 2016 Vial performed his Master's Thesis on EX-CORE. His research focused on investigating the influence of the various EX-CORE constituents on the material properties of EX-CORE. This to get a better understanding of how EX-CORE could be tailored for specific needs. In the first part of his Thesis, he changed some of the constituents of EX-CORE to improve mechanical properties and process-ability.

First of all, the polystyrene beads were replaced by hollow glass microspheres; Q-Cel[®] 5028, which offered better mechanical properties and high thermal stability. Although that they increased the density of the foam by ~50%, the compressive properties improved by ~150% and so their use could be justified.

Secondly, he searched for a different type of epoxy system than the SR8500/KTA317 with a lower viscosity at room temperature, reduced exothermic reaction and long pot life that did not require aging. The previous SR8500/KTA317 had to be aged for 24hours at room temperature. Also, once aged this resin did not flow anymore, hence to obtain the required shape the core had to be aged inside the mold. Air products and Chemicals Inc. proposed an epoxy system named Ancarez[®] RZ4010 in combination with 4 possible curing agents: A2781, UMX-50F, UMX-144C and UMX-157A. The temperature for 150g resin of each combination was monitored when cured at 60°C. The graph is provided in Figure 3.10a, from which it can be seen that the lowest exothermic peaks are achieved for the A2781 and UMX-144C hardeners.

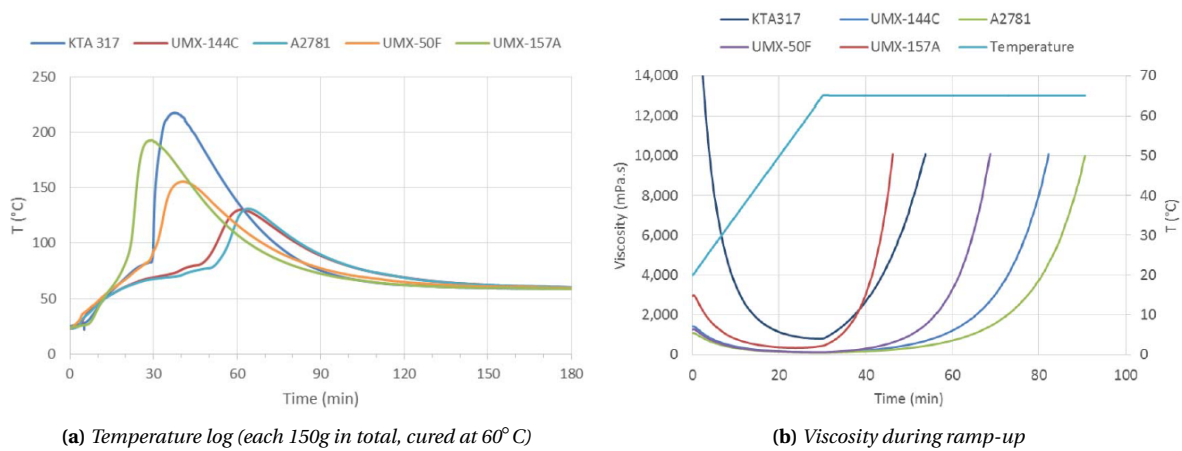


Figure 3.10: Temperature and viscosity measurements of various hardeners combined with Ancarez RZ4010[®] epoxy resin. Courtesy of Air Products and Chemicals Inc. [63]

Rheology measurements were also performed by Air products and Chemicals Inc. A comparison of the viscosity measured for the various resin systems during a temperature ramp up to 65° is given in Figure 3.10b. It can be seen that the A2781 and UMX-144C hardeners extended the low-viscous state of the resin by 2-3 times when compared to the KTA317 hardeners. In the end the UMX-144C hardener was selected because of its relatively low exothermic heat release, slower reaction progress, good compatibility with other EX-CORE constituents and outstanding compressive properties when compared to the other curing agents.

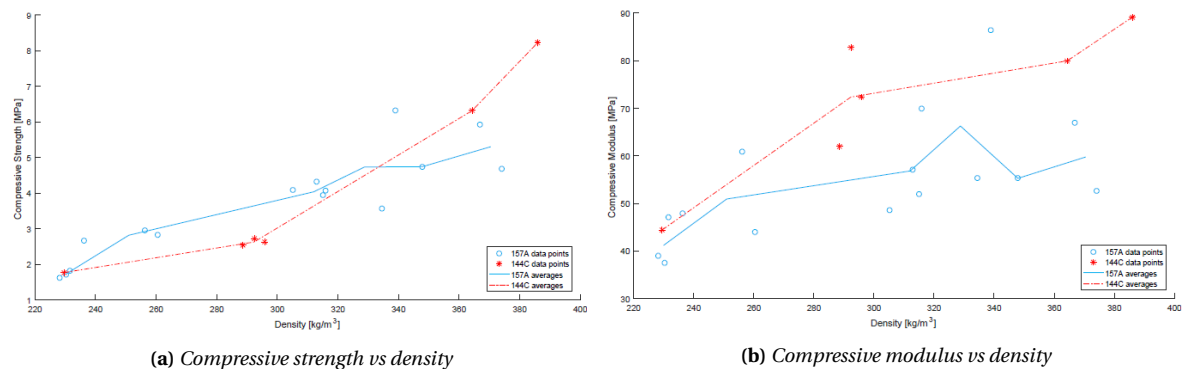


Figure 3.11: Compressive properties comparison for two different types of hardeners at a range of foam densities [63]

The compressive properties of the lower exothermic, slower reacting UMX-144C hardener and the higher exothermic, faster reacting UMX-157A hardener are compared in the graphs in Figure 3.11. Interestingly, it can be seen that the compressive strength for densities higher than 330kg/m^3 becomes higher for the UMX-144C, while the modulus of the UMX-144C is higher over the entire density range. Compressive tests also confirmed the positive effect on the compressive strengths of samples when the cure cycle increased from 2 to 3 hours at 100°C .

Vial also inspected the micro-structure of EX-CORE samples with a scanning electron microscope (SEM). In Figure 3.12, a SEM image of an EX-CORE sample containing the 144C hardener is shown. The large sphere on the left side is Q-Cel[®] which, in contrast to DU Expancel[®] and DE microspheres, maintains its spherical shape. It can also be observed that the resin successfully filled up the interstitial voids between the microspheres, ensuring that the foam is both dimensionally and thermally stable after curing.

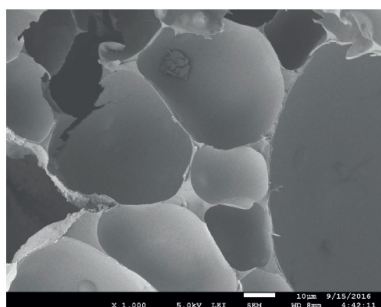


Figure 3.12: SEM image (x1000) of EX-CORE mix (14%DU, 33.2%DE, 19.6%resin, 33.2%Q-Cel) [63]

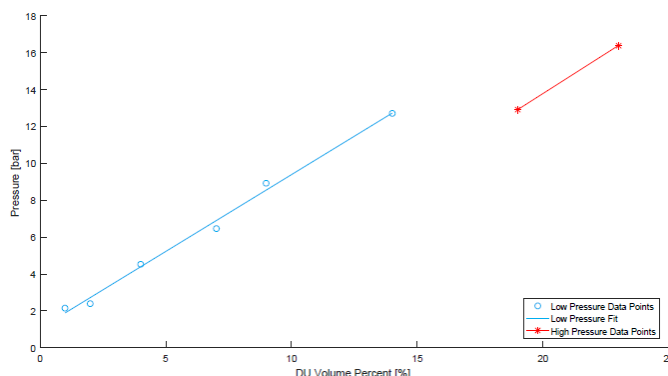


Figure 3.13: Relation between volume fraction of Expancel[®] 031 DU and pressure generated by EX-CORE at mold surface [63]

By making use of force sensitive sensors (Flexiforce[®] HT201) Vial could determine the amount of pressure generated at the mold surface by EX-CORE samples with various volume fractions of Expancel[®] 031 DU microspheres (with remaining $\sim 20\text{vol.}\%$ resin and $50/50\text{vol.}\%$ DU/Q-Cel). The resulting pressure vs vol.%DU plot is given in Figure 3.13, from which it can be seen that typical autoclave pressures of 6-8 bar can be achieved with not even 10% DU. The discrepancy in the graph was supposed to be related to the collapsing of microspheres and/or mold deformation. Vial obtained a linear relation, given in Equation 3.1, relating the volume fraction of Expancel[®] 031 DU (ϕ_{DU}) to the generated pressure. Remark that an improved relation was obtained in the research by Eversdijk in 2017, this will be discussed in Section 3.2.7.

$$P[\text{bar}] = 1.0653 + \phi_{DU} \cdot 83.24 \quad (3.1)$$

Finally, Vial set up a designed experiment for which he manufactured 13 samples with varying volume fractions of EX-CORE constituents. This made it possible to create a mathematical model that relates the volume fractions of the EX-CORE constituents to foam density and compressive properties. The resulting response surface of the simplex strength model is shown in Figure 3.14. This model predicts the mix composition possessing the highest specific compressive properties for a certain foam density. These optimal mixes are indicated by the black dots in Figure 3.14. They represent foam densities ranging from 150 to 400kg/m^3 with increments of 10kg/m^3 . A similar model had also been constructed for the compressive modulus

According to this theoretical model, the lightest possible foam composition which would satisfy the compressive strength requirement of 3.6MPa would have a density of 239kg/m^3 . Although that it is heavier than the 168kg/m^3 mix developed by Minde, the compressive strength doubled.

During the period of Vial's research, floor panels and door window frames for the Donkervoort D8 GTO-RS were for the first time manufactured in a one-shot process using EX-CORE. A 330kg/m^3 had been used that resulted in products with acceptable surface quality. The products still had some areas with surface porosities that required surface finishing. Nonetheless, the products could subsequently be integrated into the cars. Remark that this 330kg/m^3 foam is heavier and with a compressive strength of 7.08MPa stronger than required. This because it had been formulated before the mathematical model was completed. Vial recommended more research on improving the surface porosity of EX-CORE sandwich structures, as became the subject of the next research.

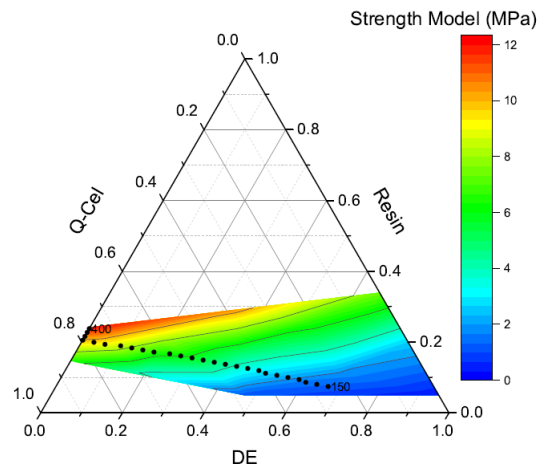


Figure 3.14: Response surface of simplex model showing the relation between volume fractions of EX-CORE constituents (at 4vol.% DU) and attained compressive strength. The black dots indicate the points of maximum specific strength for densities ranging from 150 to 400 kg/m^3 with intervals of 10kg/m^3 . [63]

3.2.6. Berckmoes 2017: Effect of EX-CORE foam processing on surface defects in carbon fiber-epoxy sandwich composites

One year later, in 2017, Berckmoes continued his research at Donkervoort performing his Master's Thesis. His goal was to develop processing guidelines that would aid in improving the surface defects in EX-CORE sandwich structures, allowing repeatable one-shot production. [57]. In his research he focused on investigating possible relationships between processing parameters and surface porosity in the CF/epoxy- prepreg facesheets of EX-CORE sandwich panels. For this purpose, Berckmoes designed and integrally heated mold, in which square test samples of variable height could be produced. Also, an optical inspection setup was constructed that allowed to identify and compare the amount of surface porosity of the square test samples under identical test conditions. The setups consisted out of a metal frame which aligns a uniform light source (400W LED panel), a digital camera and the sample at a specific angle and distance from one-another. The setup was locked in the configuration that resulted in the most optimal light contrast between the surface pores and the smooth glossy surface. The principle of light scattering is presented in Figure 3.15.

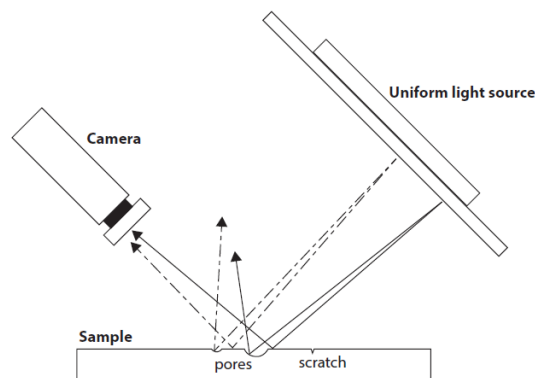


Figure 3.15: Schematic of light scattering principle used to quantify the amount of surface porosity [57]

During his research a wide variety of test samples were created to investigate the effect of prepreg type (autoclave vs VBO), prepreg wave pattern & density, lay-up, volume fraction of DU, mold filling, cure temperature & heat-up rate, sample thickness and barrier layers. At the start of Berckmoes his research it was assumed that a process window would exist in which EX-CORE sandwich structures could be produced repeatably with a consistent outcome and high surface quality. This however proved to be more challenging, also because Berckmoes found that there are more parameters involved than initially thought. Nonetheless, at the end of his research Berckmoes formulated processing guidelines that would aid in manufacturing EX-CORE sandwich structures with low amounts of surface defect. They are summarized on the next page.

1. Type of prepreg and laminate

In combination with EX-CORE, fully-impregnated prepregs suitable for autoclave processing should be used. So no semi-impregnated VBO prepregs. The difference between both prepreg types was explained in Section 2.1.2. As resin in the prepregs, the c-m-p CP0093 epoxy is advised. Other epoxy resins possessing a similar viscosity profile, gel- and cure time can be considered as well. Important cure related properties of the c-m-p CP0093 epoxy are noted here:

- Cure temperature between 80° and 170°
- Minimum viscosity of 350-450mPa·s around 105-110° this at a heat-up rate of 1-2°
- Gel time of 110min at 90°, 36min at 105° and 14min at 120°
- Time to reach 98% degree of cure is 300min at 90°, 120min at 105° and 60min at 120°

In general, the amount of surface porosity decreases when the laminate possesses a lower out-of-plane permeability. The weave density and composition of the laminate therefore have a large influence on surface quality. Three types of weaves were investigated, namely a 200g/m² 3k, 245g/m² 3k and a 420g/m² 12k, all 2x2 twill weaves. Using the 12k as surface ply is not recommended. Also the 245g/m² 3k (lowest permeability) is more beneficial in reducing the surface porosity than the 200g/m² 3k. Therefore the best results are obtained when two plies of 245g/m² 3k are used at the surface of the product. Additional plies can also be added, as this will further reduce the permeability. Mitigating nearly all the surface porosity is only possible when the out-of-plane gas escape from the core during EX-CORE expansion is prevented, for example with an impermeable barrier layer (such as vacuum foil) between the core and the facings. This however will affect the core-to-facesheet bond.

2. EX-CORE formulation

A 270kg/m³ foam mix is suggested which was also extensively used in parallel research by Eversdijk [64]. It was formulated using the mathematical model developed by Vial [63]. With this foam composition, the model predicts the highest specific compressive properties at this density. It will therefore be referred as the "270-optimal" mix. The pseudo-components of this mix are presented in Table 3.1. Note that the pseudo-components refer to the mix formulation in which the DU content is not yet incorporated since it can be varied in accordance with the desired pressure. To obtain the final true mix composition, the pseudo-component percentages should be multiplied with (100- vol.% DU)/100.

Table 3.1: Pseudo component volume percentages of the "270-optimal" mix

Density [kg/m ³]	Resin	DE	Q-Cel
270	14.9%	32.3%	52.8%

This mix in combination with the two layers of 245g/m² 3k can yield EX-CORE products for which almost all surface porosity is mitigated. The given guidelines are therefore based on results from samples created using this foam. When lower foam densities (with lower resin content) are required, it is strongly recommended to implement an impermeable barrier layer. This because foams with a lower resin content, contain more entrapped air between the microspheres, that should be prevented from penetrating into the facesheets. It is also recommended to use 10wt% of black pigmented epoxy resin, which would help masking EX-CORE penetration and/or manufacturing errors.

3. Degree of mold filling

It is important that the mold cavity is 100% filled with EX-CORE. Local under-filling should be prevented since this can cause a local decrease in pressure. Excessive under-filling is more problematic since this can cause insufficient laminate compaction (especially when the DU content is not revised) but more importantly, the extra amount of entrapped air will lead to an increase in surface porosity when no barrier layer is present between the core and the facesheets.

4. Expancel DU volume fraction

Essentially, higher volume fractions of Expancel[®] DU will result in higher pressures, which in turn will reduce the amount of surface porosity. If the mold is 100% filled, 031 DU volume fractions between 1.5 and 7.5vol.% would provide sufficient consolidation pressure to compact the laminate. To achieve a surface porosity content of only 0.025% (the benchmark and lowest value achieved in the research), 7.5vol.% of 031 DU would be required when using the 245g/m² 3k/3k lay-up without barrier layer. Remark that 7.5% 031 DU corresponds to ± 8.5bar pressure, which should be taken into account when designing the mold.

5. Cure cycle window

A simple two-step cure cycle window is recommended that is presented in Figure 3.16. A heat-up rate between 1- 1.5°C is suggested, followed by a cure dwell between 90 and 120°C. The dashed line indicates the time required to reach 98% cure of the prepreg resin. The cure cycle can also be extended beyond this line, but this is not essential.

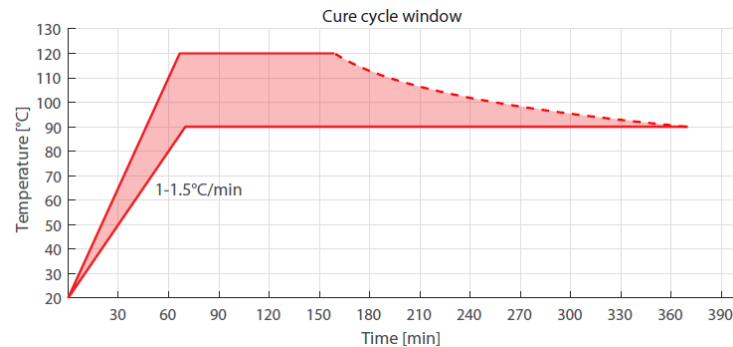


Figure 3.16: Cure cycle window suggested by Berckmoes [57]

Ultimately, two sets of floor panels for the D8 GTO-RS were manufactured according to these guidelines. Although that they still contained between 2.5% and 4.5% of surface porosity, surface defects such as large air inclusions, waviness of the surface ply, and contaminations of the surface with EX-CORE were no longer present. It is a standard practice to sand the parts and apply one layer of transparent filler. For the flat floor panels, it required not extra effort to fill up the pores with a slightly thicker layer of filler. For complex structures this is however more challenging, requiring a thicker layer of filler, which adds to the weight of the part.

3.2.7. Eversdijk 2017: Relating process parameters to EX-CORE properties through experimental testing and modeling

In 2017 also Eversdijk performed his Master's Thesis on the subject of EX-CORE [64]. His research objective was to gain better insights into the relation between process parameters and properties of the final EX-CORE product. Eversdijk selected the "270-optimal" mix as basis for the rest of his research, it was selected because of its optimal compressive properties and good processing characteristics. In the first part of his research, an integrally heated mold was produced (similar as the one created by Berckmoes[57]) that allowed manufacturing square test samples and temperature monitored during curing. In the first test series, Eversdijk focused on monitoring the temperature distribution at the surface of the mold by making use of thirteen DS18B20 digital temperature sensors placed in a grid pattern. During a 110°C cure cycle, temperature peaks up to 134°C were measured. Also temperature variations up to 28.5°C were observed over the 175x175m mold surface, which could be related to dry spots and surface porosities that covered >40% of the cured prepreg surface.

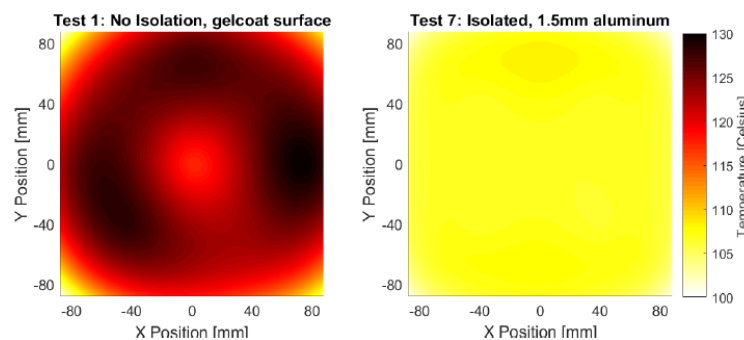


Figure 3.17: Surface temperature plots, with and without 1.5mm aluminum plate Eversdijk [64]

It was proposed to use a more conductive mold surface which could aid in reducing the temperature peaks. A 1.5mm aluminum plate was placed in between the mold lid and sample, which decreased the temperature difference to only 3.3°C and consequently reduced the amount of surface porosity to 2-6%. Surface temperature plots were constructed to visualize the measured temperatures. Two examples with and without the 1.5 aluminum plate are given in Figure 3.17.

The pressure generation in EX-CORE was also further investigated by Eversdijk because it was thought to be effected by more factors than solely the volume fraction of Expancel[®] DU. In addition some discrepancies were discovered w.r.t. the previous pressure measurements performed by Vial [63] such as the lack of repeated measurements, concentrated placement of the sensors, and not taking into account the temperature drift of 0.16% per degree Celsius [65]. Also in establishing the pressure-DU relation in Equation 3.1, the true density of Q-Cel[®] 5028 of 260kg/m³ had been used instead of the bulk density of 160kg/m³. A corrected pressure-DU relation 3.1 was determined, given in Equation 3.2:

$$P[\text{bar}] = 1.0653 + \phi_{DU} \cdot 99.34 \quad (3.2)$$

here ϕ_{DU} is again the volume fraction of Expancel[®] 031 DU. An oil-based pressure measuring tool was developed by Eversdijk. Unfortunately in the end it was found to be affected by thermal expansion differences, and no usable results could be obtained.

In another part of his research Eversdijk analyzed the core temperatures of thick 270-optimal mix samples. He manufactured a first set of samples (A-series) applying a two step cure cycle with a 1.5°C/min heat-up to the final cure at 110°C. In the core of 30, 55 and 80mm samples he measured peak temperatures of 130, 154 and 167°C, respectively. He also found that the expansion temperature of 85°C was first reached at the sample edges. This could be related to density variations in the foam, which were measured by X-ray tomography. As can be seen in Figure 3.18, the density is relatively constant throughout the thickness of the foam, however near the edges the density is approximately 7.5% lower.

A second series of samples (B-series) was cured at a different cure cycle that had an additional intermediate dwell at 50°C for 113min. This reduced the peak temperature in the core to only 119°C. But more interestingly, due to the exothermic reaction, the center region of the core now reached the 85°C onset expansion temperature before the edges did. As a consequence, more extreme density gradients in the foam could be observed, with a 37.5% decrease in density near the edges, as shown in Figure 3.18.

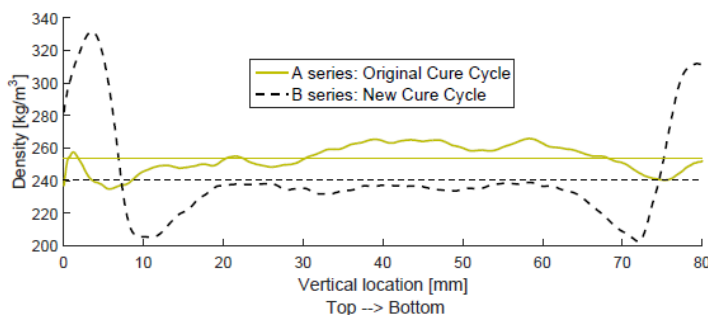


Figure 3.18: Density gradients in 80mm thick 270-optimal mix samples at the two tested cure cycles, measured using X-ray tomography [64]

The effect of density gradients on the compressive strength of the samples was investigated by making use of Digital Image Correlation (DIC). In all cases, failure initiated in the regions of lowest densities. And because the minimum density was higher in the A-series, this resulted that their compressive strength was on average 15% higher. Remarkably, these higher peaks in these A-series samples did not noticeably effect the compressive strength. In summary it was demonstrated that a functionally graded foam can be obtained which properties can be tuned. This would make it possible to create EX-CORE products with higher specific flexural properties.

Lastly, Eversdijk developed a thermal model/tool in MATLAB that was capable to predict the temperatures and degree of cure distribution as a function of time in rectangular geometries of EX-CORE cured under specified cure cycles. In essence the two-dimensional model is constructed using a transient finite difference method that allows to solve the energy balance equation for a system with internal heat generation. Where the later is caused by the exothermic reaction of the epoxy resin, which was modeled using the theory of cure kinetics. Theoretical models were also implemented that predict the thermal conductivity and specific heat capacity of the requested EX-CORE formulation. The working principles of the model will be extensively reviewed in Chapter 5, where the author will also explain the alterations made to the model as required for the current research.

The model is validated using experimental results of "270-optimal" mix foam samples (1vol.% DU) of variable heights between 30 and 80mm cured with dwell temperatures ranging between 50 and 110°C. Although that a time scale factor of 0.85 was required to achieve time to peak values within 10min of the experimental results, the model was capable to predict the maximum temperature in the center within 5°C and at the edges within 4°C. Comments on the validity of the model when using a different mix formulation or ramp-up (other than 1.5°C/min) cannot be made due to the lack of experimental data. Nonetheless with the current accuracy, the model will facilitate further research. The user can trail run several variations of a cure cycle to determine which maximum temperatures will be reached, where/when the onset expansion temperature is reached, when the sample is fully cured etc. Only 1 experimental validation test is then required to validate if the model prediction of the new process and/or EX-CORE formulation is as expected.

3.2.8. Mattheus 2017: Exploration with reinforcing fillers and diluents & Proof of concept for EX-CORE component dosing and mixing automation

The internship of Mattheus in 2017 at Donkervoort formed the starting point of the EX-CORE development towards larger scale applications [66]. In the first part of the internship many exploratory test were performed with reinforcing fillers in EX-CORE (up to 10%) such as carbon nanotubes (Tubal™ Matrix 201), glass microspheres (MicroPerl®) and 1mm chopped carbon fibers. Unfortunately, the specific compressive strength of the tested foam samples did not or only marginally improve.

A second series of experiments was performed to check if EX-CORE could be diluted with volatile diluents such as benzyl alcohol, thinner etc. The idea was that these diluents could aid in mixing extremely lightweight (and so low resin content) EX-CORE formulations. In the end it became clear that none of the tested diluents were suitable because they had a detrimental effect on the mechanical properties.

Nonetheless, promising results were obtained in the second part of the internship were a proof-of-concept automated mixing and dosing setup was developed for EX-CORE which demonstrated that the amount of manual labor in the EX-CORE process could be reduced. Firstly, it was demonstrated that various EX-CORE mix types could be homogeneously mixed automatically. This was done by making use of a modified kitchen robot with silicone dust covers and adapted dough hook. Next, a small 12V peristaltic pump was tested and found suitable for pumping the liquid hardener, however it was not strong enough for the more viscous epoxy resin (Ancarez® RZ4010). Therefore a larger peristaltic pump was designed that could be powered by a 230V stepper motor. For the dosing of the micro-spheric fillers, three similar screw powder feeders were designed, manufactured and successfully tested.

To automate the weighing of all the components, an Arduino Mega was used and coded. An electronics box with user interface was designed containing all the vulnerable electronics. The user can select the desired mix type, DU content and total mix volume and the system automatically calculates and weights the required components (one at a time). The Arduino processed the real-time measured component weight as read by a digital scale, and based on this controlled the speed of the powder feeders and pump in such a way that all the components could be automatically weighted within 0.1g accuracy.

3.2.9. Ten Hoeve 2018: EX-CORE production machine

The proof-of-concept developed by Mattheus formed a good starting point for the graduation project undertaken by Ten Hoeve at Donkervoort in 2018 [67]. His goal was to further upscale the test setup to a prototype suitable for the production of larger volumes (at least 15L) of EX-CORE without any intervention of the user. For example in the previous proof-of-concept, the user had to transfer the components from the scale to the mixing bowl. Several mayor alterations w.r.t. to the proof-of-concept have been proposed and/or tested, such as using butterfly valves instead of screw powder feeders. It was also opted to use a gear pump instead of a peristaltic pump to dose the resin, since the peristaltic hose ruptured to fast. Also a larger mixing bowl and mixing rod were constructed onto a pillar drill machine and proved successful in mixing 23L of EX-CORE at once in 15min. In the end a proposal for an "EX-CORE production machine" was done, for which CAD drawings are given in Figure 3.19. It includes i.e. a 40L mixing bowl, 3x 13L hoppers with attached butterfly valves, a gear pump including stepper motor, a scale etc.

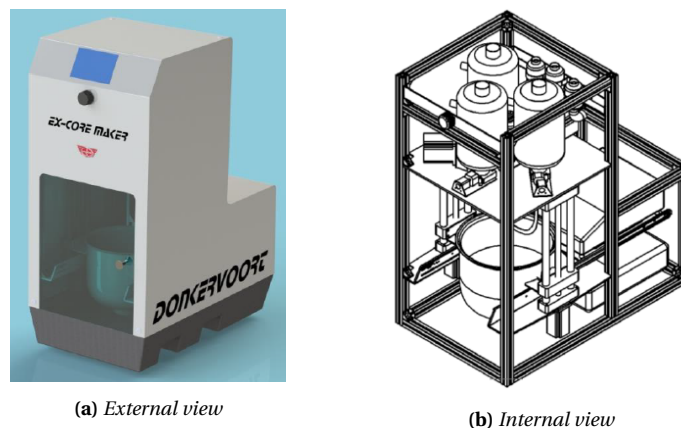


Figure 3.19: Visualization of the "EX-CORE production machine" concept as proposed by Ten Hoeve [67]

3.3. EX-CORE constituents (at the start of the current research)

EX-CORE is a syntactic foam that consists of three types of microspheres which are embedded in an epoxy matrix. EX-CORE can come in many different formulations, meaning that the volume fractions of the constituents can be altered depending on the required pressure, mechanical properties, and foam density. Nonetheless, the type and grade of microspheres and epoxy system as currently used in EX-CORE for sandwich productions at Donkervoort had been defined in previous research. The characteristics of these constituents are discussed in this section. Note that in the current research a new epoxy resin system (SR 1280 & Ancamine[®] 2442) and also a new grade of Expancel[®] DU (043 DU 80) will be chosen. The properties of these "new" constituents will later be discussed in Sections 4.1.2 and 7.1.

3.3.1. Thermoplastic expandable microspheres: Expancel[®] DU

The concept of EX-CORE relies on the used physical blowing agent in the form of thermoplastic expandable microspheres, traded by AkzoNobel under the name of Dry Unexpanded Expancel[®] or in short Expancel[®] DU. The working principle of these expandable microspheres was already discussed in Section 3.1. It are specifically these microspheres that cause EX-CORE to expand. When enclosed in a mold they will exert pressure to consolidate facesheets, allowing one shot production of complex-shaped structures. At the start of this research, the 031 DU 40 grade is used in EX-CORE. It is delivered as powder that can easily be mixed in the epoxy resin. Its properties as provided by AkzoNobel are presented in Table 3.2. The bulk density had been previously determined by Vial to be 370kg/m³ [63].

Table 3.2: Properties of Expancel[®] 031 DU 40 as provided by AkzoNobel [56]

	Particle size [μm]	Expansion temperature ¹		Density [kg/m^3]	Solvent resistance ²
		Tstart [$^{\circ}\text{C}$]	Tmax [$^{\circ}\text{C}$]		
031 DU 40	10-16	80-95	120-135	≤ 12	3

¹ Obtained from TMA measurements

² On a scale from 1 to 5, with 5 being excellent chemical resistance

The 031 DU 40 grade had been previously selected because it has the lowest range of expansion temperature of all DU grades, making it compatible with the cure cycle of the epoxy-based prepregs used at Donkervoort. The expansion profile of Expancel[®] 031 DU 40, is given in Figure 3.20. It can be seen that around 85-90 $^{\circ}\text{C}$ the expansion suddenly initiates followed by a non-linear increase until 120-135 $^{\circ}\text{C}$, then the expansion of Expancel[®] 031 DU 40 reduces. At this point the microspheres start to deflate as gas escapes from inside the microsphere. This is because at increasing temperatures the thermoplastic shell of the microsphere softens and becomes too thin due to the volume increase of the microsphere.

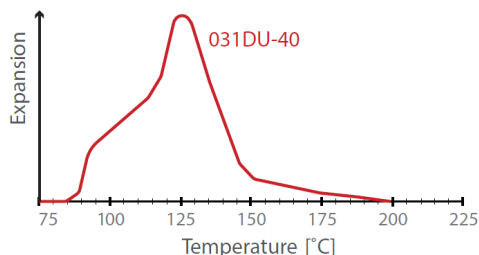


Figure 3.20: Expansion curve for Expancel[®] 031 DU 40 by AkzoNobel. The data on the y-axis was not provided. [54]

3.3.2. Thermoplastic expanded microspheres: Expancel[®] DE

As mentioned in Section 3.2.1 it is not favorable to develop foams relying solely on DU expansion since this would result in low quality foams with high amount of cracks. To overcome this problem and to lower the density of the foam, pre-expanded Expancel[®] microspheres, known as Dry Expanded Expancel[®] or Expancel[®] DE are added to the mixture. A broad range of these DE microspheres are produced by AkzoNobel. In EX-CORE the 920 DE 80 d30 grade is used. The properties as provided by AkzoNobel are presented in Table 3.3. The bulk density had been previously determined at Donkervoort to be $\pm 15\text{kg/m}^3$.

Table 3.3: Properties of Expancel[®] 920 DE 80 d30 as provided by AkzoNobel [68]

	Particle size [μm]	True density ¹ [kg/m^3]	Solvent resistance ²
920 DE 80 d30	55-85	30 ± 3	5

¹ Density of a single Expancel[®] DE microsphere

² On a scale from 1 to 5, with 5 being excellent chemical resistance

Note that in the remainder of this report Expancel[®] DU and Expancel[®] DE microspheres will be simply referred to as DU and DE.

3.3.3. Hollow glass microspheres: Q-Cel[®]

Hollow Glass Microspheres (HGM) are added to EX-CORE as reinforcing fillers. More specifically, Q-Cel[®] 5028 produced by Potters Industries are used in EX-CORE. Available characteristics are given in Table 3.4.

Table 3.4: Properties of Q-Cel[®] 5028 as provided by Potters Industries [69, 70]

	Particle size (mean) [μm]	True density ¹ [kg/m^3]	Bulk density [kg/m^3]	Compr. Strength/Max. working pressure [Mpa]
Q-Cel 5028	<75	290	160	6.9

¹ Density of a single Q-Cel[®] microsphere

3.3.4. Epoxy matrix; Ancarez[®] RZ4010/ Ancamide[™] 3399

To prevent re-expansion of the EX-CORE foam at elevated temperatures, a thermosetting resin matrix had to be used in EX-CORE. This ensures that a rigid structure is obtained after curing. The Ancarez[®] RZ4010 epoxy resin in combination with the Ancamide[™] 3399 curing agent (in previous research also referred to by the laboratory code of UMX-144C) are currently being used in EX-CORE. Ancarez[®] RZ4010 is an DGEBA (DiGlycidyl Ether of Bisphenol A) based epoxy, while Ancamide[™] 3399 is an amine based hardener. They are both obtained from Air Products and Chemicals Inc.

This system was selected in the research of Vial [63] (see Section 3.2.5) because of its relatively low exothermic reaction peak, workable pot life up to 3 hours and most of all, its good compatibility with other EX-CORE constituents and prepreps applied at Donkervoort; For instance it can be processed in the expansion range of Expancel[®] 031 DU 40 (80-120°C). The epoxy matrix not only provides thermal stability of the EX-CORE, but also greatly increases its strength and stiffness. However, with a density of 1150kg/m^3 , much higher than the other components, the density of the foam increases as well. Temperature and viscosity plots of the resin system were already discussed in Section 3.2.5.

3.4. Typical manufacturing process of EX-CORE products

At this moment in time, EX-CORE is successfully being applied in floor panels and door window frames integrated in the latest Donkervoort D8 GTO-RS. To gain a better insight into how these parts are produced with EX-CORE, the typical phases in the current production process are summarized here:

1. **Preparation phase** First, the mold sections are cleaned and covered in release agent. The pre-cut prepreg layers (conditioned at room temperature) are then manually placed into the mold. Next, the EX-CORE components are weighted and mixed one-by-one in this order: resin, hardener, DU, Q-Cel and finally DE. Depending on the mix formulation, the obtained mix can vary from a dry powdery mixture to a somewhat viscous paste. Next, the prepregged mold is manually filled with EX-CORE, targeting 100% mold filling. The mold is then closed and fastened with bolts. Then, the sensor and braid plugs are connected to the PI controller and finally the mold assembly is covered with insulation blankets.

Remark that the weighing and mixing had for a long time be done manually, but now the EX-CORE mixing and dosing setup developed by Mattheus [66] or more recently Ten Hoeve [67] can be used.

2. **Curing process** The integrally heated mold and PI-controller (explained in Section 3.2.4) allow for heating the mold according to a pre-defined cure cycle. For the 8mm thick floor panels, this cure cycle already takes at least 3 hours (with 1.5°C/min ramp-up to 110°; see proposed cure cycle window in Section 3.2.6).
3. **Post-processing** After the part has cooled down (not included in cure time), the part can be taken out of the mold. The part is then visually inspected for surface defects. It is a standard practice to sand the part, followed by the application of a transparent filler. If major surface porosities are present, a thicker layer of transparent filler is used to fill up the pores.

3.5. Drivers for EX-CORE development towards large series automotive manufacturing

In this section the most important findings w.r.t. the future development of EX-CORE towards large series automotive manufacturing are presented. The information given here is discussed in more detail in the literature study report written prior to the current research [10].

3.5.1. Evolution of CFRP composites in the automotive industry

The use of CFRPs for structural applications has already been well established in high value markets such as aerospace, military and the high-end (race, sports & luxury) automotive industry. Here it is driven by the desire to increase performance through lowering weight [1]. Due to their high specific properties, anisotropy, tailor-ability etc. CFRPs offer the highest potential for weigh savings compared to the current aluminum and steel alloys, but this comes at a high cost, as illustrated in Figure 3.21 [1, 2].

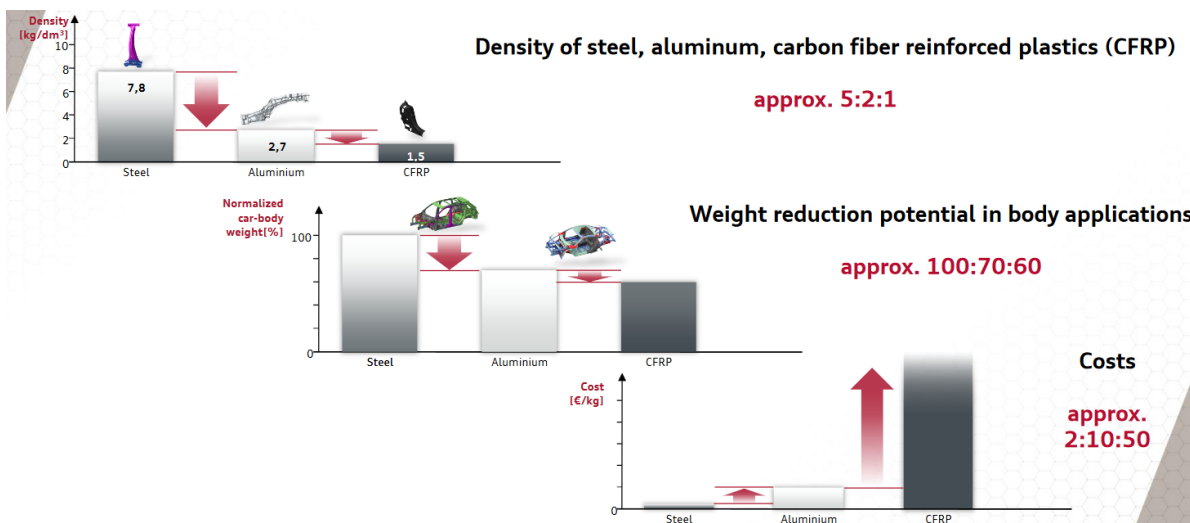


Figure 3.21: Comparison of density, cost and potential weight reduction for a typical body in white steel/aluminum/CFRP component [71]

For a long time autoclave processing (prepreg lay-up) was the standard manufacturing method for the production of high quality structural composite parts in both the aerospace and automotive industry. Despite that in the last decade more cost-effective out-of-autoclave manufacturing processes have been developed, it became clear during the literature study that until now the use of CFRPs in the automotive industry still remained mainly confined to small series (1-1000 units/year) automotive applications. There are many reasons for this but the main issue remains their relative high cost price compared to metals, which prevented a breakthrough in the medium (1000-10.000/year)- to large (>10.000/year) series automotive market [3–5]. The only "affordable" vehicle that is build for a large part out of CFRPs and which is produced at a large scale (approx. 100/day) is the BMW i3 electric vehicle, for which sub-10 minute part cycle times were reported [72].

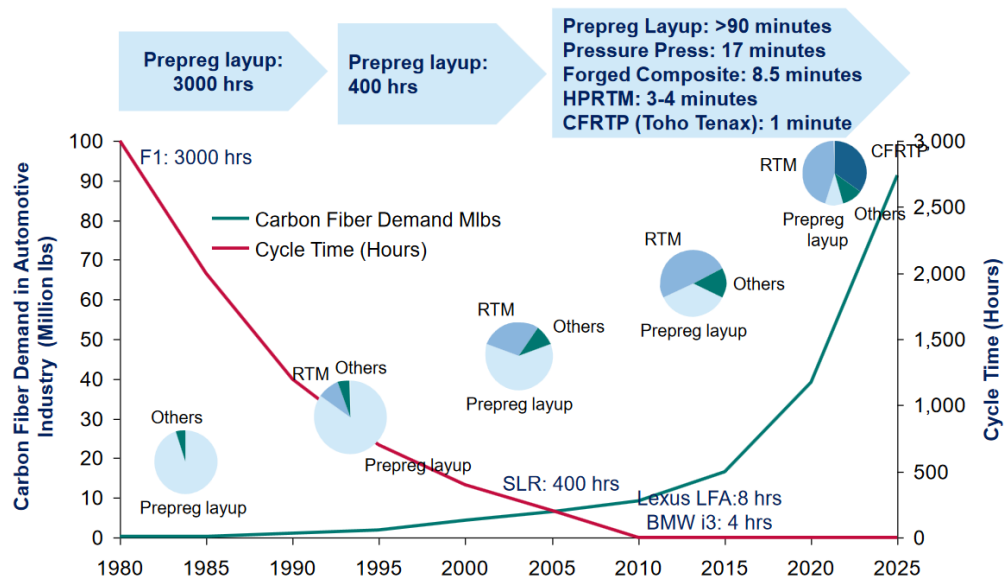


Figure 3.22: Carbon fiber demand and CFRP part cycle time vs time in the automotive industry [3]

Nevertheless, several studies expect a large increase in the demand of CFRP composites for large series automotive applications in the next two decades [3, 6, 7]. This is also illustrated in Figure 3.22 which gives a good overview of the evolution & prospects of carbon fiber demand and CFRP part cycle times in the the automotive industry. The key drivers for change are the stringent CO₂ reduction regulations which are being implemented around the world [8]. Hence Automotive OEM's are forced to search for new types of powertrains and ways to cut down the structural weight of the cars [5]. Because of the weight savings that CFRP can offer, there is a strong intention by OEMs to apply CFRP for structural parts. Consequently, they are challenged to develop more cost-effective CFRP production technologies that can produce CFRP parts within short cycle times [1, 9].

Promising fast production processes include High-Pressure Resin Transfer Molding (HP-RTM) [13, 73–75] and Wet Compression Molding (WCM) [13, 76, 77], which can achieve part cycle times of several minutes. The reader is referred to the literature report [10] for more details on the working principles and recent developments w.r.t. these and other CFRP manufacturing processes used (or under development) in the automotive industry.

3.5.2. Advantages of EX-CORE w.r.t. other CFRP composite technologies

The EX-CORE technology can offer several unique advantages compared to other CFRP composite manufacturing processes. Complexly shaped sandwich structures with small tolerances and a high surface finish on all sides of the products can be manufactured in one-shot process. This reduces the amount of process steps and hence production- and labor costs. On top of this, because a high surface finish can be obtained, little to no post-production is required for EX-CORE products. With other manufacturing technologies a multi-step approach would be necessary, especially if small tolerances and class-A surface finish are required all around the product. Remark also that composite vehicle structures are commonly produced by bonding several sub-components [78, 79].

Next to its function as a lightweight core material, increasing the flexural stiffness of the sandwich structure (performance), the EX-CORE material also allows for integral component functionality of noise- & thermal insulation (comfort) and impact damage (safety). Furthermore, the EX-CORE process does not require any externally applied pressure from an autoclave or vacuum bagging and hence reduces the amount of consumables and tooling. Additionally because an integrally heated mold can be used, the amount of energy required for curing the part can also be reduced. So to conclude with, large cost reductions can be achieved in terms of labor, required machinery, energy and consumables.

3.5.3. EX-CORE's closest competitors

At this moment, there are no foam core materials and/or production technologies comparable to EX-CORE on the market. This was confirmed by the patent attorney firm Arnold & Siedsma in 2017 [80]. The closest comparable products to EX-CORE on the market are Rohacell[®] Triple F and Syncore[®], but they have some distinct disadvantages as discussed in the following paragraphs. A comparison of the available mechanical properties is also given in Table 3.5.

Rohacell[®] Triple F by Evonik is a syntactic foam developed for in-mold/in-situ foaming [28]. The first disadvantage w.r.t. EX-CORE is that a separate mold is required to produce the foam core. In another production process the core will be combined with the facesheets to obtain a sandwich panel. This makes it a more time consuming and costly process that is also more prone to tolerance issues. Secondly, external pressure tooling is required, hence this limits the complexity of the parts that can be made.

Syncore[®] by Henkel is presumably the product which is closest comparable to EX-CORE [81]. It is a syntactic foam that also makes use of expandable microspheres, but it is provided in thin films with a maximum thickness of only 6.35mm. Additionally, these films can only be used in combination with vacuum bagging, hence they are not suitable for one-shot processing with closed molds. The application areas of Syncore[®] are thin sheet materials in combination with prepregs which cannot conflict with the EX-CORE business case [80].

Table 3.5: Mechanical properties for different grades of ROHACELL[®] Triple F, SynCore[®] and EX-CORE [10]

Property	Unit	ROHACELL [®] "75"- "200" Triple F				SynCore [®] 9823.1 9872.1 HC9875			EX-CORE		
		Nominal density	kg/m ³	75	110	150	200	673	673	916	80
Tensile strength	MPa	1.3	1.9	2.3	2.7	27.6	33.1	34.5	Unknown		
Tensile modulus	MPa	90	143	199	262	2600	2760	4000	Unknown		
Compr. strength	MPa	1.0	1.7	2.8	4.7	62.0	55.2	150	1.00	1.30	4.76
Compr. modulus	MPa	64	117	172	229	1380	2590	n/a	50	96	300
Shear strength	MPa					61.4	46.9	48.2	0.41	0.60	1.43
Shear modulus	MPa	Unknown				1000	1034	n/a	4.39	20.54	11.40

3.5.4. Main drivers for the future development of EX-CORE

From the previous two sections it became clear that EX-CORE has the potential to offer several advantages compared to other technologies, not only from a material point of view, but also from a production point of view. Unsurprisingly, EX-CORE has caught the attention of OEMs such as Porsche, Volkswagen, Lamborghini, Daimler and Jaguar/Landover. Understandably, Donkervoort has the ambition to further develop EX-CORE for larger series applications.

Most recently, with the EX-CORE technology, Donkervoort has been awarded the "European Innovation Grant in High-Tech Materials and Advanced Manufacturing Technologies" within the scope of the Horizon 2020 EU program. This program has as goal to support and accelerate the market introduction of unique innovations, and such realize faster economic growth. EX-CORE was selected out of 2300 nominees from across Europe. Donkervoort, together with 2 other dutch companies, has been awarded a total grant of 5.1 million euro [82]. This grant will aid in launching EX-CORE on the international automotive market. To make this commercialization possible, more research is not only required on the upscaling and automation of the EX-CORE process, but also the EX-CORE material itself should be redesigned.

At the start of the literature study it was still relatively unknown what the wishes and requirements of OEM's are w.r.t. CFRP part and production process characteristics for high volume applications. Especially because they are entirely different than the ones for small series production at Donkervoort. An effort was made in the literature study to grasp the most important drivers for EX-CORE's future development [10]. Important conclusions are given here:

- **Part cycle times**

In order to become competitive with cycle times of other promising CFRP manufacturing processes suitable for high volume automotive applications, such as HP-RTM and WCM, the part cycle times of EX-CORE should be drastically reduced from several hours down to several minutes (preferably below 10min).

- **CFRP part price/kg**

It was researched that in the next 5 to 10 years, it is likely that typical automotive chassis components should be able to be manufactured at a cost price around 15-25euro/kg. Or in other words, this is the price that OEM's are targeting. This is i.a. based on a price drop of carbon fiber to 10euro/kg, which has been predicted by several research institutes.

- **Mechanical properties**

The mechanical properties of Rohacell® Triple F form a good indication to which EX-CORE has to compete with. They were presented in Table 3.5.

- **Applications**

OEM's see for instance potential for EX-CORE in applications such as rear spoilers, floor panels, wheel arches, trunk panels etc. Such parts have typical thicknesses of $\pm 1-2$ cm

With respect to the part cycle times, it became clear that a major limiting factor for obtaining sub-10 min cycle times is the long time required for curing the EX-CORE foam. Remark that currently solely the cure process of EX-CORE already requires 3 hours or more (see Section 3.2.4 and 3.4). Therefore and due to the limited time frame of the Master's Thesis it was decided to focus on researching the possibilities of re-designing the EX-CORE foam in such a way that major cure cycle time reductions can be achieved. The obtained knowledge will provide more insight into the capabilities and limitations of fast-curing EX-CORE, and so the current research which will contribute to the development of EX-CORE towards large scale automotive manufacturing.

4

Defining cure kinetics of new candidate epoxy resins by DSC

An important step in reducing the cure time of EX-CORE components is to replace the current epoxy matrix system Ancarez[®] RZ4010/Ancamide[™] 3399 with a fast curing, so called snap cure epoxy system. In this chapter the selection of suitable snap cure epoxies is first discussed in Section 4.1. Then in Section 4.2, the essential theory on resin cure kinetics and Differential Scanning Calorimetry (DSC) is covered. DSC will be used to determine the cure kinetics of candidate epoxy matrices. The principles and post-processing of the experimental DSC measurements are presented in Section 4.3. The required cure kinetic parameters are then determined by fitting a suitable cure kinetic model with the experimental DSC data. This cure kinetic model, on its turn, will be integrated into the numerical thermal EX-CORE model covered in Chapter 5. Finally, in Section 4.4, the experimental and cure kinetic model results for the different epoxies will be discussed.

4.1. Selection of new candidate snap-cure epoxy resins

Eversdijk [64] investigated the cure kinetics of the current epoxy resin system Ancarez[®] RZ4010/Ancamide[™] 3399 used as matrix in EX-CORE. His experimental and cure kinetic model results can be reviewed in Appendix B of this report. These results show that it takes 46min to reach a 98% cure at an isothermal cure temperature of 110°C, this increases to 56min at 105°C etc. It should be noted that these results are for the curing of the pure epoxy resin, not for the EX-CORE foam or sandwich panels. As will become clear in Chapter 5, EX-CORE is a poor conductor, increasing the cure times even more, especially for thick structures.

Berckmoes [57] defined in his processing guidelines an optimal two-step cure cycle profile (see also Section 3.2.6, Figure 3.16). When using the fastest heat-up rate of 1.5°C/min in combination with the highest cure temperature of 120°C, the total cure process should take at least 2 hours 40min. When lowering the cure temperature to 110°C this increases to 3 hours etc. Note that after this cure cycle the power to the mold is shut down and the mold is left to cool back to room temperature before it is opened and the product is taken out. So approximately one additional hour for cooling down has to be taking into account.

The current cure cycle times are a long way from the preferred <10min reference cure cycles times for large series automotive production. The first step in reducing the cure cycles times of EX-CORE products is to replace the current epoxy-amine matrix Ancarez[®] RZ4010/Ancamide[™] 3399 with a fast curing, so called snap-cure epoxy system. In the following sections the resin selection criteria are discussed, leading to a new epoxy resin and 3 new candidate hardeners/curing agents.

4.1.1. Resin selection criteria

Many different epoxy resins and hardeners are commercially available, tailored for a variety of applications. They vary in; viscosity profile, cure time, reactivity, onset reaction temperature, exothermic heat release, glass transition temperature, mechanical properties, shelf life etc. The current EX-CORE epoxy resin Ancarez[®] RZ4010 and hardener Ancamide[™] 3399 was selected in the research of Vial [63], as discussed in Section 3.2.5. The hardener was i.a. selected based on its relatively low exothermic reaction, low viscosity profile, slow reaction behavior, good compatibility with other EX-CORE components and improved compressive properties with respect to other proposed hardeners.

The requirements for the new epoxy matrix were defined at the start of this research. They are listed and explained here in order of importance.

1. *The (snap-cure) epoxy should be able to reach a 98% cure in less than 10 minutes.*

The 10min upper bound is based on the preferred <10min cycle time, discussed in Section 3.5.4. The 98% degree of cure indication is commonly used in practice.

2. *The cure temperature should be above 80° C but preferably below 120° C.*

The lower bound was set to 80°C because this corresponds to the onset temperature of Expancel® 031 DU 40. Hence curing at a temperature below this expansion temperature would not be desirable since no pressure would be generated. Other DU grades are also available with different expansion- (and maximum-) temperatures, but all of them have expansion temperatures in excess of 80°C [56].

The maximum cure temperature of 120°C was initially chosen based on the 120-135°C maximum temperature of the currently used 031 DU 40 Expancel® grade as discussed in Section 3.3.1 [56]. Although that cure time reduces when cure temperature increases, higher cure temperatures and resulting temperature overshoots due to the exothermic reaction could negatively effect the microspheres used in EX-CORE. Note also again that other grades of Expancel® DU exist with higher maximum temperatures, even up to 235°C [56]. So another grade of DU could be used, that makes it possible to cure at a higher temperatures. Therefore the upper boundary of 120°C is no strict requirement.

The maximum temperatures of the other microspheres used in EX-core and possible influence on the maximum cure temperature was also investigated:

Q-Cel® is a hollow glass microsphere for which again the maximum temperature was not available. However, the safety data sheet mentions the glass material to be an amorphous sodium borosilicate [83]. Glass in general has a high thermal resistance and with the T_g of borosilicate glass around 525°C [84], it can be safely assumed that Q-Cel® will not be affected by the temperatures occurring during EX-CORE processing.

The maximum temperatures of the pre-expanded Expancel® DE microspheres are not available, nor were the expansion curves or exact material composition provided by Akzonobel when asked for. It can however be expected that the "co-polymer" shell is also effected at elevated temperatures. This would probably occur at similar temperatures as the unexpanded microspheres since their walls are made from similar co-polymers.

3. *The cured epoxy matrix should have a Tg of at least 115° C.*

EX-CORE components may not degrade or deform when exposed to the sun. Figure 4.1 shows the surface temperature for different mat paint colors when exposed to the sun at different surrounding temperatures. The lower boundary of Tg is based on the worst case scenario for a mat black surface at 45°C. Note that glancy coated surface absorbs around 5% less.

4. *The onset of reaction or thermal block temperature of the epoxy should be above 45° C.*

To prevent curring and exothermic heat release during mixing it is desirable that the resin does not react with the hardener at room temperature. This allows large batches of EX-CORE mixtures to be mixed beforehand, without the necessity of immediate use or storage in a freezer.

5. *The epoxy matrix should be low viscous/liquid at room temperature; a viscosity below 5000mPa·s at 25° C is preferred.*

The resin should be liquid/low viscous at room temperature because this will make homogeneous mixing easier. The current Ancarez® RZ4010 resin has a viscosity of 8000-15000mPa·s at 25°C [85], which is a relatively high viscous resin at room temperature, making manual mixing with the microspheres labor intensive. As a reference for the new resin the maximum viscosity was therefore set to 5000mPa·s at room temperature.

6. The point of maximum viscosity drop should occur around the onset expansion temperature of Expancel[®] DU; for the current 031 DU 40 grade this is at 80-95°C.

Finally, it is also preferable that the viscosity drop occurring during heating is as low as possible and that this drop occurs around the onset expansion temperature of Expancel[®] DU; for the current Expancel[®] 031 DU 40 grade this occurs at 80-95°C. This allows for volatiles/air to escape through the viscous resin when pressure is generated inside the product. Most suppliers provide viscosity profiles for their resin, it is however difficult to compare such profiles since they are dependent on the heat up rate. For example when the heat up rate is increased, the minimum viscosity is lowered and both the gel time and the time required to reach the minimum viscosity is reduced [86]. This is visualized in Figure 4.2.

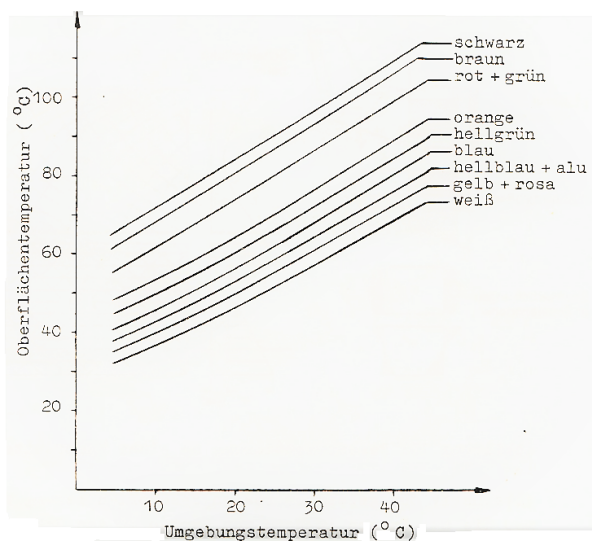


Figure 4.1: Surface temperature of different mat paint colors in function of surrounding temperature. (Internal source Donkervoort.)

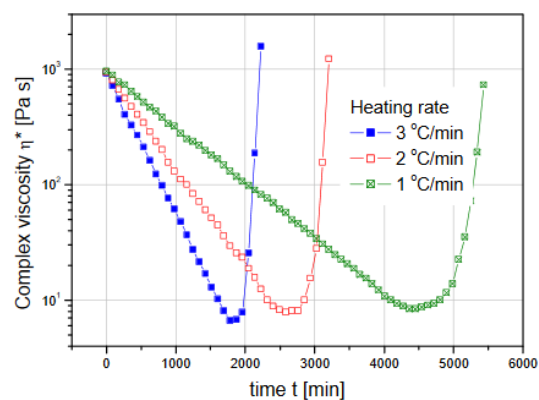


Figure 4.2: The effect of heat-up rate on the viscosity profiles of a curing thermoset resin [87].

4.1.2. Acquiring new candidate "fast curing" epoxy resins

During the literature study performed prior to this thesis work, initial research was performed on snap-cure epoxy systems and prepregs [10]. It became clear that many epoxy resin systems and prepregs exist with sub 5 minute cure times. However, most of them are not suitable for complex structural automotive parts and/or are only commercially available when incorporated in prepregs. Some fast curing epoxy resin systems recently developed for high-volume structural automotive components include the following:

- VORAFORCE/VORAFUSE[™] 5300 epoxy resin by Dow Automotive Systems [9, 71, 88, 89]
 - 90 to 180s mold cycle times at 120°C
 - Tg of 120°C
 - Ultra-low viscosity of 15mPa-s
 - Room storage stability up to 30 days
- EPIKOTE[™] 06170/ EPIKURE[™] 06170 epoxy resin by Hexion [90, 91]
 - 45sec cure at 115-145°C
 - Tg of 115-125°C
- Araldite[®] 3031/ARADUR[®] 3032 epoxy resin by Huntsman [92, 93]
 - 45sec cure at 130°C and 30sec at 140°C
 - Tg of 120°C

The previously mentioned resins could offer great potential in reducing the cure cycle times of EX-CORE. Unfortunately, after contacting the manufacturers and distributors, it became clear that those epoxies were either not commercially available, in-stock and/or were not purchasable in small order quantities. Additionally, about twenty different epoxy manufacturers, distributors and suppliers from Donkervoort were contacted, with the question whether or not they had resins available that could fulfill (most of) the formulated requirements. Finally, a new resin system by Sicomin was ordered and two new curing agents/hardeners samples were obtained from Evonik. Their specifications are summarized in the next paragraphs.

Epoxy resin SR 1280 & hardener SZ 8525 by Sicomin

The epoxy resin SR 1280 and hardener SZ 8525 by Sicomin are offered as one epoxy system, but the resin and hardener can also be ordered separately. The epoxy system offers high reactivity and short cycle times. It is originally designed for wet lay-up, pressure molding and hot processing (90-120°C) applications. The SR 1280 resin has a viscosity of 1780±360 mPa·s at 25°C and a density of 1.159g/cm³ at 20°C. It is a Diglycidyl Ether of Bisphenol A (DGEBA) type of resin, similar to the Ancarez[®] RZ4010 resin. The main difference is that with SR 1280 a reactive diluent (butanediol diglycidyl ether) similar to Epodil 750 by Evonik [94] had been added by the manufacturer with a concentration of 10-25% according to the safety data sheet [95]. The hardener SZ 8525 has a density of 0.94g/cm³ and viscosity of 33±5 mPa·s. According to the material data sheet [96], the SR 1280/SZ 8525 system should be mixed at a mix ratio of 100:24 (by weight). This will result in a viscosity of 1300±260 mPa·s at 20°C. When cured for 10min at 120°C (time to reach cure temp not included) a T_g of 104°C is reached, so slightly below the 115°C T_g of requirement 3. Note that this resin system also does not satisfy requirement 4 since it does (although slowly) react at room temperature. [96]

Hardener Ancamine[®] 2337s by Evonik

Ancamine[®] 2337s is a modified aliphatic amine hardener that is designed for use as a latent curing agent in epoxy resins. It comes in the form of powder, but offers easy dispersion in liquid resins. It has a density of 0.25g/cm³ and is commonly used in coatings, adhesives, potting and hot-melt prepregs. Depending on the mixing ratio (100:30 to 100:60) in a standard bisphenol A based epoxy resin a T_g of 115 to 185°C can be reached, at a 30min cure at 120°C. It has an onset reaction temperature of 71°C, after which it offers very rapid reactivity. Requirement 4 is therefore complied with. However, to reach a sub 10min cure as defined in requirement 1, a cure temperature above 120°C would probably be required. [97, 98]

Hardener Ancamine[®] 2442 by Evonik

Ancamine[®] 2442 is also a modified aliphatic polyamine hardener in powder form that is used as a latent curing agent in one-component epoxy formulations. It has a density of 0.95g/cm³. Typical applications include powder coatings, prepregs and one-component adhesives. The main difference with Ancamine[®] 2337s is that the Ancamine[®] 2442 has a slightly higher onset activation temperature of 93°C (measured by DSC at 10°C/min scan). [99, 100]

4.2. Theory on resin cure kinetics and Differential Scanning Calorimetry

Cure kinetics describe the reaction rate of a curing resin as a function of temperature and degree of cure. The reaction rate can be related to the heat release of a thermosetting resin. A frequently used thermal analysis method to measure this heat flow is Differential Scanning Calorimetry (DSC). The experimental DSC data can then be used to fit a cure kinetic model. During the current research a cure kinetic model of certain reaction order is created for each of the tested resins. The cure kinetic model is then implemented in the transient numerical EX-CORE model, as will be explained in Chapter 5. This makes it possible to determine the heat release and degree of cure at every time step of the simulation for a certain volume and mix composition of EX-CORE. The essential theoretical background on resin cure kinetics is presented in Section 4.2.1. Here the used governing equations and selected cure kinetic model will be discussed. Then in Section 4.2.2 the principles of heat flow measurements by DSC are explained.

4.2.1. Resin cure kinetics

The main principle behind utilizing DSC to obtain cure kinetics of a thermosetting resin is that the reaction rate $\frac{d\alpha}{dt}$ [1/s] is proportional to the measured heat flow ϕ [mW] as given by Equation 4.1:

$$\frac{d\alpha}{dt} = \frac{\phi}{H_T} \quad (4.1)$$

where H_T [MJ] is the total heat of reaction or reaction enthalpy. The fraction of reaction completed; the degree of cure α [-] of the resin can be calculated with Equation 4.2. It can vary from 0 (not cured) to 1 (fully cured).

$$\alpha = \frac{H_c(t)}{H_T} \quad (4.2)$$

in which H_c [MJ] is the cumulative liberated heat up to time t . The reaction progress of the resin can be simulated by a cure kinetic model of certain reaction order. Three different types of cure kinetic models were

already explained in Section 2.3.3, namely the n^{th} order, the autocatalytic and the modified autocatalytic model. In all models one or more reaction rate constants k are implemented. These rate constants are calculated by the *Arrhenius Equation* and relate the reaction rate with the temperature T [K]:

$$k = Ae^{-\frac{E}{RT}} \quad (4.3)$$

where A [1/s] is a pre-exponential constant or the Arrhenius frequency factor, E [kJ/mol] is the activation energy and R represents the universal gas constant of 8.314 J/(molK). For more detailed background formation on the Arrhenius equation and meaning of the parameters, see Section 2.3.3.

In the current research, epoxies will be cured with amine types of hardeners. These type of reactions are autocatalytic, meaning that the reaction product also acts as a catalyst for the reaction. This has as a result that the peak reaction occurs after $t=0$ and so the simplest n^{th} order model cannot be used [47, 48]. For all the resin systems tested in this research, the modified autocatalytic model represented by Equation 4.4 is used. This allows a non-zero initial reaction rate, which can take into account the effect of impurities such as catalyzing ions or water [48]. Note that this model was also used in the research by Eversdijk [64] to model the kinetic behavior of the former EX-CORE epoxy-amine resin Ancarex[®] RZ4010/Ancamide[™] 3399.

$$\frac{d\alpha}{dt} = (k_1 + k_2\alpha^m)(1-\alpha)^n \quad (4.4)$$

k_1 is the initial reaction rate at $t=0$, while the term $k_2\alpha^m$ takes into account the influence of the reaction products on the reaction rate [47]. α again represents the degree of cure, or more specifically the fraction of epoxide reacted at time t [47]. So the term $(1-\alpha)$ can be seen as the concentration of epoxide functional groups still available for reaction. The reaction order parameters m & n and the reaction parameters E & A are constant with temperature and degree of cure. They are specific for each type of epoxy system and can be obtained by fitting the kinetic model given by Equation 4.4 to the experimental DSC data.

Fitting of the model can be done in several ways. For example a numerical method was proposed by Ryan & Dutta [52, 53] that uses the initial and maximum reaction rate to determine the cure kinetic parameters of epoxy. A downside of this method is that it uses the assumption of the total reaction order ($m+n$) to be equal to 2. A graphical analytical method was developed by Kenny [47] that does not impose any assumption on the reaction order, however it requires a bit more work. This method was used in several other research papers to model the cure kinetic behavior of epoxy-amine systems [48, 49]. This method was had also been successfully applied in the research by Eversdijk [64] and is therefore also the preferred method for the current research. The model fitting procedure and determination of the cure kinetic parameters for the new epoxies is explained in Section 4.3.3.

4.2.2. Differential Scanning Calorimetry (DSC)

A widely used thermal analysis method to measure the heat release during the exothermic reaction of a thermosetting polymer is Differential Scanning Calorimetry (DSC). The basic principle of a DSC apparatus is that the heat flow to or from a crucible containing the sample is measured and compared with the heat flow of an inert reference empty crucible, when they are both heated, cooled or kept at constant temperature. Two classes of DSC instruments exist, namely powder-compensation DSC and heat-flux DSC, for which a schematic representation is given in Figure 4.3. In powder-compensation DSC, the heating (or cooling) of the sample and reference crucible is done independently at a controlled rate in separate chambers [101]. The temperature is monitored and the heat flow changed accordingly to keep both samples at the same temperature. So if the sample crucible contains an epoxy, the required heat flow to this sample is lower due to the generated heat from the exothermic reaction. In contrary, with heat-flux DSC both the sample and reference crucible are in the same chamber heated at the same rate [101]. The temperature difference between both crucibles is measured and related to the heat flow. The measured heat release can then be used to fit the cure kinetic model.

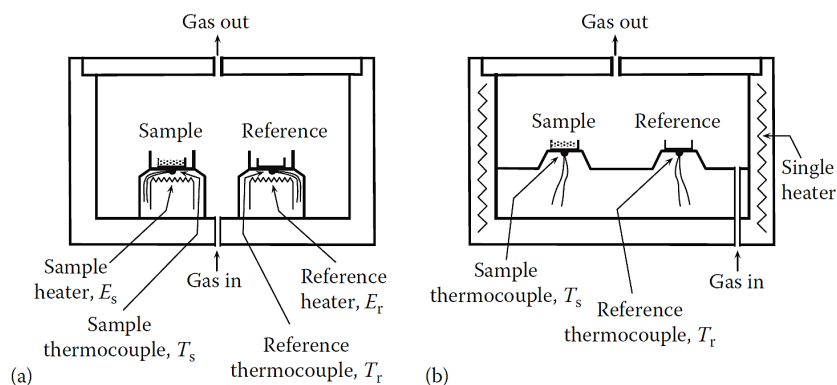


Figure 4.3: Schematic of a) powder compensation DSC and b) heat flux DSC. The sample is placed in an inert crucible. An empty crucible is used as reference. [101]

4.3. Resin cure kinetics determination with DSC

Both isothermal and dynamic DSC tests can be used to characterize the cure kinetics of thermosetting resins [51]. In this research isothermal DSC tests are performed similarly as done by Eversdijk [64] for the former EX-CORE resin. Although that isothermal tests are more time consuming, they are generally more reliable than dynamic tests since they introduce fewer experimental variables [51]. The data is therefore also easier to interpret. The experimental setup and DSC test procedures are covered in Section 4.3.1. The next step is to process the raw DSC data and finally compute the cure kinetic parameters using the graphical analytical method by Kenny [47], as explained in detail in Sections 4.3.2 and 4.3.3, respectively.

4.3.1. Experimental setup and isothermal DSC test methodology

To perform the DSC experiments, ASTM test standard E2070-13 "Kinetic parameters by Differential Scanning Calorimetry using isothermal methods" [102] was consulted. This method dictates that a minimum of four isothermal experiments are required over a temperature range of 10K. The isothermal temperatures have to be selected such that the time to complete the exothermic reaction is between 15 and 100min. To obtain suitable results, several papers mention slight alterations to the E2070-13 isothermal method [47, 51, 103, 104]. For example instead of placing the sample at room temperature in the test chamber and then rapidly ramping up ($\pm 20\text{K}/\text{min}$ to $40\text{K}/\text{min}$) to the isothermal temperature, in some cases the test chamber was preheated to the isothermal temperature after which the sample was quickly inserted [103]. Also the sample crucible is not always hermetically sealed, depending on whether or not out-gassing of the resin is expected.

A pre-calibrated *Seiko Instruments Exstar 6000* heat flux DSC apparatus available at the Delft Aerospace Structures and Materials Laboratory (DASML) was used to perform the heat flux measurements. For each tested resin system at least 4 isothermal DSC tests were performed at temperatures starting from 90°C with intervals of 5°C up to maximum of 110°C (and even up to 160°C for the SR 1280/Ancamine 2442 epoxy system). The exact step-by-step approach performed for the isothermal DSC tests can be found in Appendix A. This approach is followed for all epoxies tested in this research. Important aspects and differences with the E2070-13 isothermal method and/or approach by Eversdijk [64] are addressed here:

- *The DSC test chamber was pre-heated to the isothermal test temperature.*
DSC measurements with a heat-up starting from room temperature to the isothermal test temperature caused part of the reaction already taking place during the ramp-up phase [64]. This would result in poor results. Note that the *Seiko Instruments Exstar 6000* has a max. ramp-up rate of $20\text{K}/\text{min}$.
- *Before every DSC test a new amount of resin was mixed with hardener.*
This ensured minimal pre-cure of the epoxy before testing.
- *The lid of the aluminum crucibles were perforated with a needle, this allows to pressure inside the crucible to equilibrate.*
The *Seiko Instruments Exstar 6000* is not equipped with a pressurized test chamber. To ensure equal pressure inside the crucible as in the test chamber a small pinhole ($\pm 50\mu\text{m}$) was created with a needle. The weight of all the samples was measured before and after DSC testing. No weight losses larger than 2% were observed, validating the use of non-hermetically sealed crucibles.

- *Data collection was initiated immediately after sample insertion.*

Eversdijk [64] started data collection when the isothermal temperature was reached within $\pm 1\text{K}$, this occurred approximately 15-20s after sample insertion. However, for the new fast-curing epoxy systems, the reaction already started before the isothermal temperature was reached within $\pm 1\text{K}$. More specifically, heat flows were already observed when the isothermal temperature was reached with a maximum difference of -3K (this after less than 15s). Therefore it was decided to start data collection immediately after sample insertion.

An overview of the newly tested DSC resin systems is presented in Table 4.1, where they are given a reference number from 1 to 5. The former Ancarez[®] RZ4010/Ancamide[™] 3399 EX-CORE matrix system had been previously tested by Eversdijk [64] and was given the reference number 0a. By means of comparison and to get acquainted with the DSC apparatus DSC experiments were again performed on this former resin system in the current research. These tests are given the reference number 0b. The first newly tested resin system is the SR 1280/SZ 8525 both from Sicomin. The Ancamine[®] hardeners were initially tested with the former Ancarez[™] RZ4010 resin. However, it proved to be difficult to homogeneously mix these powder hardeners with the high viscous RZ4010 resin (viscosity of 8000-15000mPa·s at 25°C [85]) (see Ref. nr. 2 & 3). Therefore it was decided to mix them with the available low viscous resin SR 1280 from Sicomin having a viscosity of $1780 \pm 360 \text{ MPa}\cdot\text{s}$ at 20°C (Ref. nr. 4 & 5) [96]. The Ancamine[®] hardeners proved to be much easier and more homogeneously mixable in this SR 1280 resin.

Table 4.1: Overview of former and newly DSC tested resin systems, used mix ratio (by weight) and given test reference number.

DSC test ref. nr.	Type of resin	Type of hardener	Mix ratio r	Notes
0a	Ancarez [®] RZ4010	Ancamide [™] 3399	100:60	Former test by Eversdijk in 2017 [64]
0b	Ancarez [®] RZ4010	Ancamide [™] 3399	100:60	Redo test 0a for current research
1	SR 1280	SZ 8525	100:24	
2	Ancarez [™] RZ4010	Ancamine [®] 2337s	100:60	
3	Ancarez [™] RZ4010	Ancamine [®] 2442	100:60	
4	SR 1280	Ancamine [®] 2337s	100:60	
5	SR 1280	Ancamine [®] 2442	100:60	
5.2	SR 1280	Ancamine [®] 2442	100:20	See Section 8.4

The used epoxy mix ratios r can be seen in Table 4.1. The epoxy mix ratio of the former EX-CORE matrix (Ref. Nr. 0) was 100:60. For the new epoxies, only for the Sicomin resin SR 1280 & hardener SZ 8525 (Ref. Nr. 1) an "optimal" resin mix ratio (100:24) was given on the datasheet specifically for this combination of resin/hardener [96]. For the Ancamine[®] hardeners, the datasheets mentioned typical formulations with DGEBA epoxies ranging from 100:60 to 100:30. It was decided to initially test with a mix ratio of 100:60 as this would result in the fastest reaction rates.

Note that at a later stage during the research, DSC tests with the SR 1280/Ancamine[®] 2442 epoxy system at 100:20 resin mix ratio were also performed. This at temperatures ranging from 90°C to 160°C. These DSC tests and results will be discussed in detail in Section 8.4 and are referred by the reference nr 5.2.

4.3.2. Data processing part 1) Experimental results from isothermal DSC scans

The raw data obtained from the DSC experiments is imported into MATLAB for post-processing. The data processing method is explained by making use of the heat flow DSC results obtained for the SR 1280 & Ancamine[®] 2442 (Ref. Nr. 5). This epoxy system will later be chosen as best candidate epoxy matrix for further research. The data processing is however similar for all epoxy DSC tests discussed in this report. All the representative plots and results for both the newly tested resins as well as the former results by Eversdijk [64] are presented in Appendix B.

For all tested resins at least 5 isothermal DSC tests were performed. In only a few cases in-consistent results were obtained w.r.t. the other tests performed for that epoxy. In that case the in-consistent isothermal test was disregarded. In all cases at least 4 "good" isothermal test results were obtained, which is the minimum amount required to fit the cure kinetic model.

A visual representation of the post-processing method covered in this section is given in Figure 4.4. The graph shows the heat-flow ϕ [mJ/s] plotted as function of time. The first post-processing step on the raw heat flow data is to obtain the baseline heat flow. When the resin is fully cured, the exothermic reactivity is zero. However, at this point, the measured heat flow is still non-zero. This is caused by the own signal of the DSC apparatus. To correct for this a horizontal baseline is established extending from the end of the exothermic reaction to the point where this baseline intersects the heat-flow curve during the initial stage of curing [102]. The heat flow data is now corrected by subtracting the baseline value from it. Next the area under the resulting heat flow curve is integrated to obtain the total heat of reaction or reaction enthalpy H_T [mJ]. The reaction rate $d\alpha/dt$ can now be determined by dividing the instantaneous heat flow $\phi(t)$ by H_T as given by Equation 4.1. The degree of cure at time t ($\alpha(t)$) is then calculated by integrating the heat flow up to time t (resulting in $H_c(t)$) and dividing it by H_T as represented by Equation 4.2.

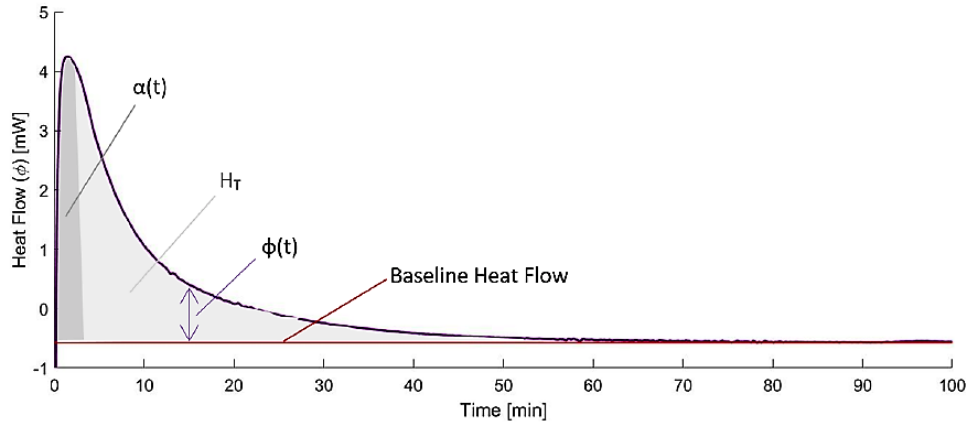


Figure 4.4: Representation of raw heat flow data curve obtained from an isothermal DSC experiment. Post-processing steps that are indicated: baseline heat flow construction, heat flow (ϕ) at time t , total heat of reaction calculation H_T by integration, completed reaction fraction (degree of cure) α at time t . [64]

When dividing the heat flow data by the resin mass in the crucible the specific heat flow ϕ_{spec} [mW/g] and total specific heat of reaction $H_{T_{spec}}$ [mJ/g] of the resin are obtained. The specific heat flow is plotted as a function of time for the example of the SR 1280 & Ancamine[®] 2442 resin system (Ref. Nr. 5) in Figure 4.5. In Table 4.2 the total specific heat of reaction values obtained for all 5 isothermal tests are given. The average of these values is taken and will later be used in the thermal model. Note that the specific total heat of reaction should be similar for each isothermal test. This because in the end the same total amount of heat/energy is released when the resin is fully cured, only the rate at which this occurs differs. More specifically, the reaction rate increases when the isothermal temperature is increased. The reaction is also completed sooner at higher cure temperature. This behavior can be observed in the reaction rate plot in Figure 4.6. The results obtained for H_T , $\alpha(t)$ and $d\alpha/dt$ can now be used to fit the cure kinetic model and obtain the required cure kinetic parameters. This procedure is explained in the next section. Note that similar heat-flow and reaction rate graphs for the other tested resins are given in Appendix B.

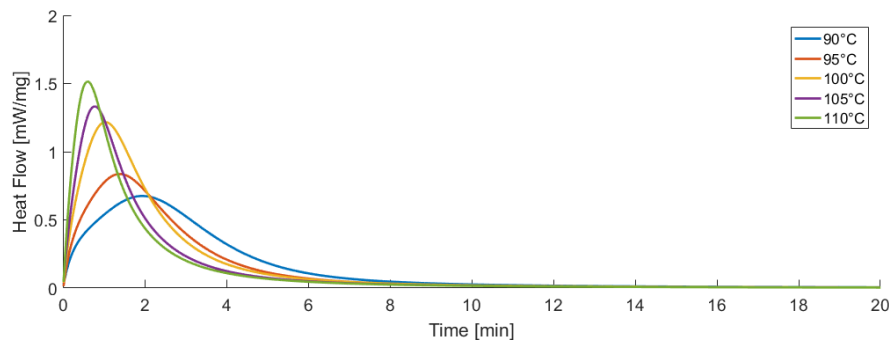


Figure 4.5: Specific heat flow ϕ_{spec} vs time at different isothermal DSC tests. Tested resin SR 1280 & hardener Ancamine[®] 2442 at mix ratio 100:60.

Table 4.2: Specific total heat of reaction. Tested resin SR1280 & hardener Ancamine[®] 2442 at mix ratio 100:60.

T_{iso} [°C]	$H_{T_{spec}}$ [J/g]
90	170.04
95	161.94
100	186.46
105	164.86
110	163.99
Avg.	169.46

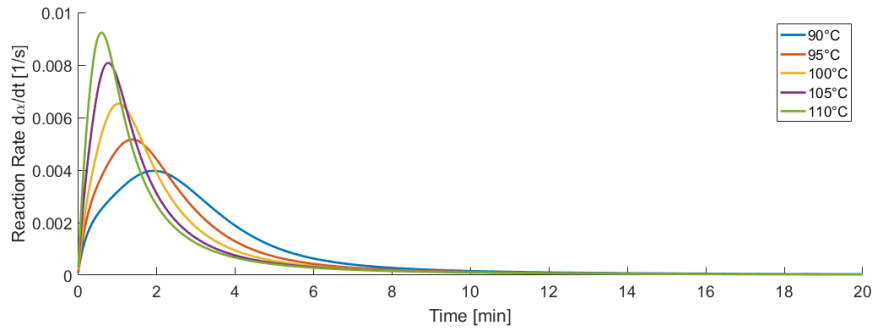


Figure 4.6: Reaction rate $\frac{d\alpha}{dt}$ vs time for resin SR 1280 & hardener Ancamine® 2442 at mix ratio 100:60.

4.3.3. Data processing part 2) Computing cure kinetic parameters from experimental DSC results

It became clear in Section 4.2.1 that the *modified autocatalytic model* is the most suitable cure kinetic model for the epoxy-amine resins used in this research. The governing equation of the *modified autocatalytic model* is given by:

$$\frac{d\alpha}{dt} = (k_1 + k_2\alpha^m)(1 - \alpha)^n \quad (4.5)$$

with

$$k_1 = A_1 e^{-\frac{E_1}{RT}} \quad (4.6)$$

$$k_2 = A_2 e^{-\frac{E_2}{RT}} \quad (4.7)$$

The following cure kinetic parameters thus have to be determined:

- m = reaction order
- n = reaction order
- k_1 = Initial reaction rate constant 1, comprised of:
 - A_1 = Arrhenius frequency factor 1
 - E_1 = activation energy 1
- k_2 = reaction rate constant 2, comprised of:
 - A_2 = Arrhenius frequency factor 2
 - E_2 = activation energy 2

To attain these cure kinetic parameters, the graphical-analytical method by Kenny [47] was selected in Section 4.2.1. This method requires the cure kinetic equation to be re-arranged in several logarithmic formats. The entire procedure is explained in the following paragraphs. Again the data obtained for the SR 1280 & Ancamine® 2442 resin system (Ref. Nr. 5) is used as an example. Similar plots and results for the other tested resins can be found in Appendix B.

First of all, the initial reaction rate constant k_1 is obtained by taking the reaction rate at the start of the cure reaction when $t = 0$ and $\alpha = 0$. Equation 4.5 thus simplifies to:

$$\left[\frac{d\alpha}{dt} \right]_{t=0} = k_1 \quad (4.8)$$

A first estimate of the reaction order n is then determined by taking the natural logarithm of both sides of Equation 4.5, resulting in:

$$\ln \left(\frac{d\alpha}{dt} \right) = \ln(k_1 + k_2\alpha^m) + n \ln(1 - \alpha) \quad (4.9)$$

Now $\ln \frac{d\alpha}{dt}$ is plotted as a function of $\ln(1-\alpha)$ for each isothermal experiment. An example of such a plot can be seen in Figure 4.7 for a 110°C isothermal DSC test. When inspecting Equation 4.9, it can be reasoned that the slope of the linear behavior is the reaction order parameter n . A linear regression fit is generated, the slope of the fit is taken as the first initial estimate for n .

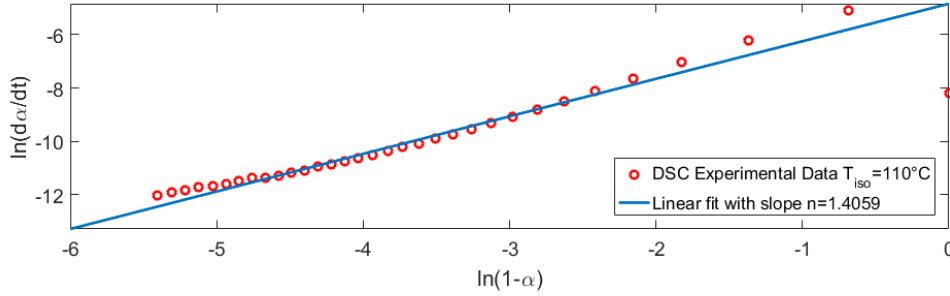


Figure 4.7: $\ln(d\alpha/dt)$ plotted as function of $\ln(1-\alpha)$ for the 110°C isothermal experiment for DSC/resin ref. Nr. 5

The values for k_1 and n are determined for each isothermal DSC scan, these values can now be used to determine the reaction rate constant k_2 and reaction order m . Therefore Equation 4.5 is re-arranged in a different form:

$$\ln\left(\left[\frac{\frac{d\alpha}{dt}}{(1-\alpha)^n}\right] - k_1\right) = \ln(k_2) + m\ln(\alpha) \quad (4.10)$$

When substituting the values for k_1 and n , a plot of $\ln\left(\left[\frac{d\alpha/dt}{(1-\alpha)^n}\right] - k_1\right)$ as a function of $\ln\alpha$ can be made. An example of such a plot is given in Figure 4.8 for the same 110°C isothermal experiment as before. Again a linear behavior can be observed over almost the complete range. This allows taking the slope and zero intercept as initial values for m and k_2 . To do this, a linear fit is generated from the straight portion of the experimental data between $\ln\alpha = -5$ and $\ln\alpha = -1$ (see Figure 4.8). The data below $\ln\alpha = -5$ represents the initial period of cure up to $\alpha = 0.007$. Here the deviation from the linear behavior is caused due to the time required for temperature equilibration after the sample is inserted. This data should therefore not be considered in the fit [53]. The portion after $\ln\alpha = -1$ should also not be considered in the fit since here vitrification of the epoxy-amine resin takes place which causes differences in thermal properties of the epoxy such as the specific heat [105], influencing the heat flow measurements.

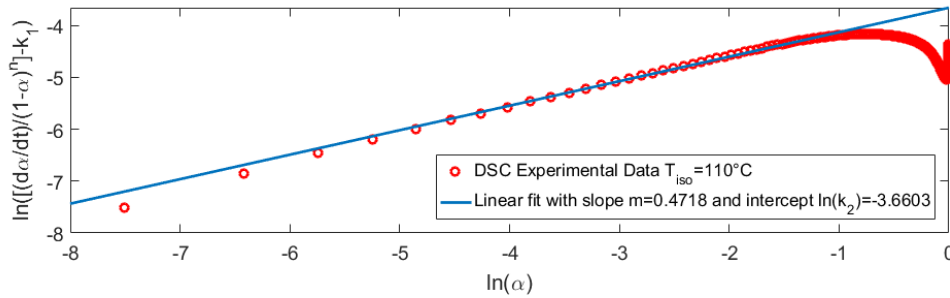


Figure 4.8: $\ln\left(\left[\frac{d\alpha/dt}{(1-\alpha)^n}\right] - k_1\right)$ plotted as function of $\ln\alpha$ for the 110°C isothermal experiment for DSC/resin ref. Nr. 5

At this stage initial values for the parameters n , m , k_1 and k_2 have been obtained. However, more precise results can be obtained when applying an iterative procedure that uses the previously determined values of parameters m , k_1 and k_2 to update n . The value of n can then again be used to update the values for m , k_1 and k_2 etc. To perform this iteration, Equation 4.5 is re-arranged as follows:

$$\ln\left(\frac{\frac{d\alpha}{dt}}{k_1 + k_2\alpha^m}\right) = n\ln(1-\alpha) \quad (4.11)$$

Equation 4.11 allows to plot $\ln\left(\frac{d\alpha/dt}{k_1+k_2\alpha^m}\right)$ as function of $\ln(1-\alpha)$. Similarly as before the slope gives the updated value for n . This value is then implemented in Equation 4.10 and new values for k_2 and m can be obtained. This iterative procedure is continued until all 4 parameters converge with less than 1% difference between subsequent calculations. Normally 2 or 3 iterations were required.

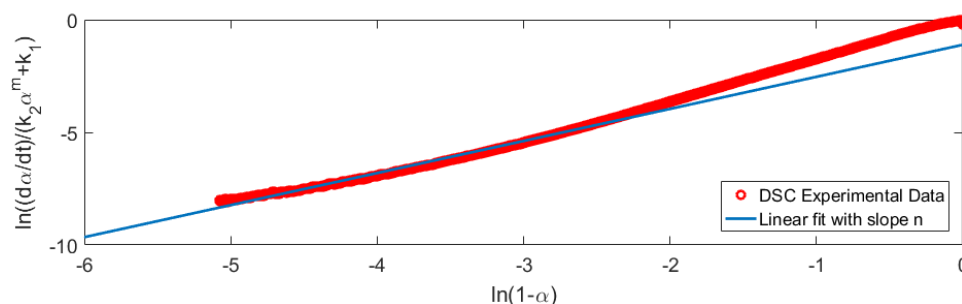


Figure 4.9: $\ln\left(\frac{d\alpha/dt}{k_1+k_2\alpha^m}\right)$ plotted as function of $\ln(1-\alpha)$ for the 110° C isothermal experiment for DSC/resin ref. Nr. 5

The parameters values obtained after each iteration for the example of the SR 1280 & Ancamine® 2442 resin system (Ref. Nr. 5) are given in Figure 4.9. Similar plots are given for the other tested resin systems. They can be found in Appendix B.

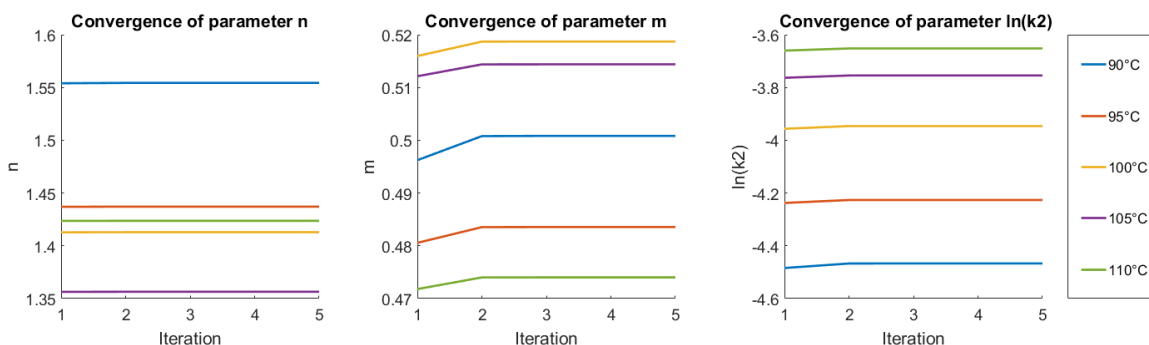


Figure 4.10: Convergence plots of cure kinetics fit parameters n , m and $\ln(k_2)$ for 5 iterations at different isothermal DSC temperatures. Tested resin SR 1280 & hardener Ancamine® 2442 at mix ratio 100:60.

The next step is to determine the Arrhenius frequency factors A and activation energies E . They can be determined by taking the logarithm of the Arrhenius Equation (Eq. 4.3) resulting in:

$$\ln(k) = \ln(A) - \frac{E}{RT} \quad (4.12)$$

Equation 4.12 can now be used to plot $\ln k_1$ and $\ln k_2$ versus $1/T$ for all the isothermal DSC tests performed for the specific resin type. This results in the so called Arrhenius plots. Here the slopes is used to determine E , while the intercept is used to determine the value for A . If the assumption of the Arrhenius reaction behavior is correct, a straight line should be obtained. This indicates that the reaction mechanism is not changing with temperature, or more specifically that the reaction orders m and n are constant. This implies that the average value of n and m obtained for the different isothermal experiments can be taken. The Arrhenius plots for k_1 and k_2 obtained for the SR 1280 & Ancamine® 2442 resin system (Ref. Nr. 5) is given in Figure 4.11.

Again similar plots for the other tested resins can be found in Appendix B. For all the plots a good linear regression fit can be observed for $\ln k_2$. This validates the Arrhenius type of reaction. Slightly larger variations can be observed for $\ln k_1$. Note again that k_1 represents the initial rate of reaction obtained during the initial stage of the DSC experiment. At this stage the sample temperature was not yet fully stabilized which could cause the fluctuation observed for $\ln k_1$.

All cure kinetic parameters n , m , E_1 , E_2 , A_1 and A_2 have now been determined. The parameter values for all the tested resins are presented in the next section together with a comparison and discussion of the autocatalytic model vs. experimental results.

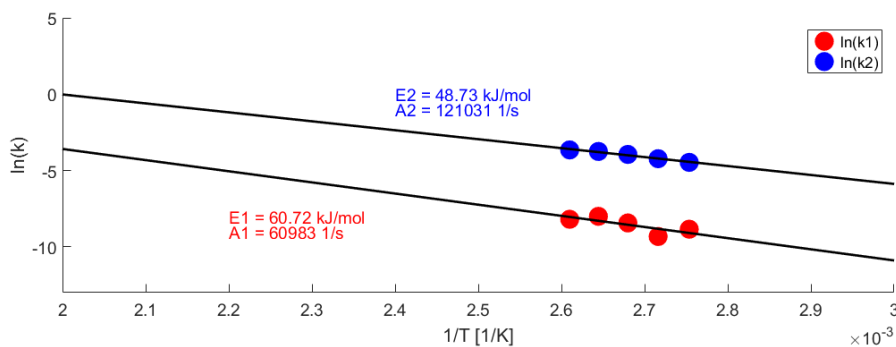


Figure 4.11: Arrhenius plots relating temperature with rate constants k_1 and k_2 . Indicated values for the activation energies (E) and pre-exponential factors (A) obtained from a linear regression slope fit and y-axis intercept respectively. Tested resin SR 1280 & hardener Ancamine[®] 2442 at mix ratio 100:60.

4.4. Autocatalytic cure kinetic model results

In this section an overview of the calculated cure kinetic parameters for the different isothermally tested epoxy resin systems (see Table 4.1) is first of all given in Section 4.4.1. These parameters are implemented in the modified autocatalytic model (Equation 4.5) to simulate the experimental isothermal DSC data. The resulting autocatalytic model fits are discussed in Section 4.4.2, where they are also compared to the experimental data.

4.4.1. Cure kinetic parameter results

For each of the tested epoxy systems, the obtained cure kinetic parameters are presented in Table 4.3. The specific total heat of reaction H_{Tspec} is also given. Note again that the test reference numbers refer to the different epoxy systems as presented in Table 4.1.

Table 4.3: Overview of the autocatalytic-model cure kinetic fit parameters and specific total heat of reaction for the different DSC tested resin systems.

DSC test ref. nr.	Cure kinetic fit parameters						H_{Tspec} [J/g]
	n [-]	m [-]	E1 [kJ/mol]	E2 [kJ/mol]	A1 [1/s]	A2 [1/s]	
0a	1.343	0.167	7.84	50.78	4.925E-04	2.582E+04	312
0b	1.140	0.178	83.07	58.83	1.236E+07	4.649E+05	189
1	1.335	0.287	64.60	59.08	8.420E+04	1.187E+06	278
2	1.610	0.407	119.61	58.12	2.278E+13	3.094E+06	99
3	1.667	0.545	42.71	55.11	1.987E+02	1.277E+06	132
4	1.620	0.381	37.19	54.27	5.328E+01	8.597E+05	91
5	1.437	0.498	60.73	48.73	6.098E+04	1.210E+05	169

Some remarkable results can be observed when comparing the results for DSC test 0a and 0b both for the current epoxy system Ancarez[®] RZ4010/Ancamide[™] 3399; It can be observed that the total heat of reaction reduced from 312J/g as obtained by Eversdijk [64] to only 189J/g obtained in the current research. The DSC test were performed in a similar fashion on the same DSC apparatus and both the resin and hardener were obtained from the same (opened) barrel. The DSC tests by Eversdijk were performed around 1 year earlier than the current research. It is therefore probable that the hardener Ancamide[®] 3399 had aged/degraded in the mean time. At Donkervoort it was already known that this hardener was susceptible to moisture uptake, that is i.a. why it always was stored in air-tight barrels. However, this did not prevented that air was entrapped in the re-closed barrel. Part of the hardener could therefore have reacted with moisture from the air in the barrel, resulting in less functional groups still available for reaction with the resin during DSC testing. Unfortunately no "fresh" or recently manufactured Ancamide[®] 3399 was available to test this theory. A recommendation is given in Chapter 12 that discusses how moisture uptake can be limited by saturating opened barrels with nitrogen gas.

When comparing the total specific heat flows from the newly tested resins, it can be observed that the Sicomin hardener (used in ref. nr. 1) results in around twice- to three- times as much total specific heat, when compared to the Ancamine[®] hardeners 2337s (ref. nr 2 & 4) and 2442 (ref. nr 3 & 5), respectively. It can also be seen that comparable specific heat flows are obtained when the same hardeners are used but the resin is changed from the Ancarez[®] RZ4010 resin (ref. nr 2 & 3) to the Sicomin SR 1280 resin (ref. nr 4 & 5). Namely, 99J/g vs 91J/g for the Ancamine[®] hardeners 2337s and 132J/g vs 169J/g for the Ancamine[®] hardeners 2442. This is logical since both are DGEBA epoxy resins with similar epoxide group formulations with as main difference the viscosity of both resins, where the Sicomin SR 1280 is pre-diluted by the manufacturer.

4.4.2. Autocatalytic model results and comparison with isothermal DCS measurements

The cure kinetic parameters presented in Table 4.3 are now implemented in the modified autocatalytic model (Equation 4.5) to simulate the experimental isothermal DSC data. The reaction rate and degree of cure vs time are plotted for all the resin systems tested in this research. They can be found in Appendix B. In these plots both the simulated model results and the experimental DSC data are compared, this to evaluate the correctness of fit of the modified autocatalytic model.

The reaction rate vs time plot for the 5 isothermal DSC test performed on the SR 1280 & Ancamine[®] 2442 (Ref. Nr. 5), is shown in Figure 4.12. The model results are plotted in solid lines while the experimental DSC results are given by the dashed lines. An almost perfect model fit with the experimental data can be observed for the 95°C, 100°C and 110°C temperatures. For 90°C and 105°C a slight deviation from the experimental data is present, but still considered of good quality and similar to the fits observed in literature [49]. The corresponding degree of cure plot for the SR 1280 & Ancamine[®] 2442 (Ref. Nr. 5) is shown in Figure 4.13. It can be seen that especially at higher temperatures, the model slightly overestimates the degree of cure α . However, overall the fit is again of similar quality as observed in literature [47].

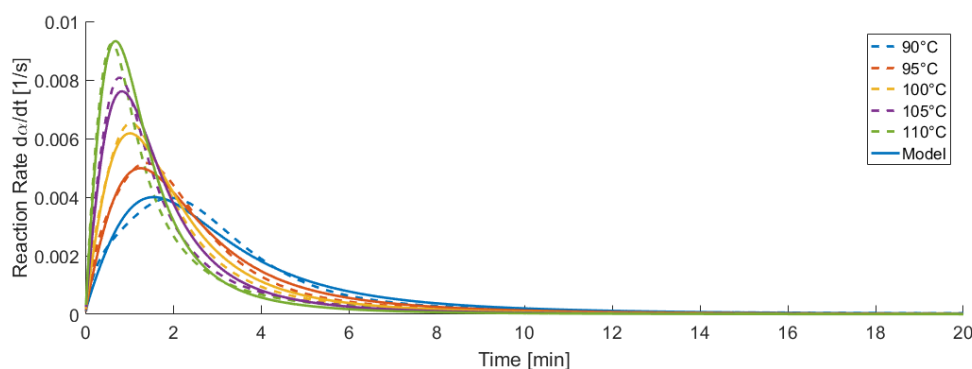


Figure 4.12: Reaction rate $\frac{d\alpha}{dt}$ vs time for both the experimental DSC isothermal tests (solid line) and autocatalytic model (dashed lines) when implementing the cure kinetic fit parameters from Table 4.3. Tested resin SR1280 & hardener Ancamine[®] 2442 at mix ratio 100:60.

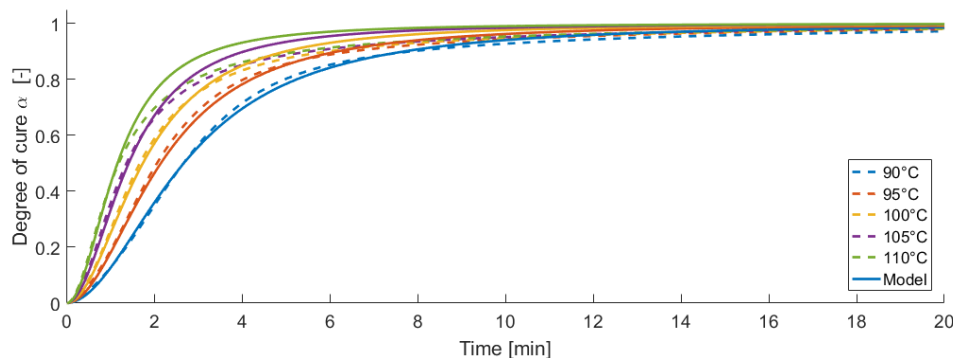


Figure 4.13: Degree of cure vs time for both the experimental DSC isothermal tests (dashed line) and autocatalytic model (solid lines) when implementing the cure kinetic fit parameters from Table 4.3. Tested resin SR1280 & hardener Ancamine[®] 2442 at mix ratio 100:60.

Similarly, reasonably good model fits are obtained for the other tested resins in this research. This indicates that the modified autocatalytic model using the graphical-analytical model of Kenny [47] is successful in predicting the behavior of the epoxy-amine epoxy resins used in this research. And so the models can be implemented in the numerical model with the cure kinetic parameters as presented in Table 4.3.

The degree of cure progress has been modeled for all tested resin systems (see degree of cure vs time graphs in Appendix B). From this the time to obtain 98% cure for the different tested epoxy systems could be determined at selected isothermal cure temperatures, as given in Table 4.4. When looking at these results it can be concluded that the newly tested resins indeed reaches 98% cure much faster than the current Ancarez[®] RZ4010/Ancamide[™] 3399 epoxy matrix used in EX-CORE (ref. nr. 0a). Note that the comparison should be done w.r.t. the original results (ref. nr. 0a) obtained by Eversdijk [64] since the most recent test (ref. nr. 0b) indicated that the resin had been aged/degraded as explained in Section 4.4.1.

When comparing the results at the different cure temperatures it can be clearly observed that the required cure time reduces if cure temperature increases. From the newly tested resins, the Sicomin epoxy system SR 1280/SZ 8525 (ref. nr 1) is the slowest, requiring 13.9min to obtain 98% at 110°C, while the SR 1280/Ancamine[®] 2442 (ref. nr. 5) proved to be the fastest, requiring only 7.2min at 110°C. In other words this means a reduction in cure time between 70-84% when compared to the 46min cure at 110°C for the current EX-CORE matrix.

Table 4.4: Time to obtain 98% cure at 5 isothermal temperatures for the different tested resin systems. Determined with the modified autocatalytic model.

DSC test Ref. nr.	Time required for 98% cure [min]				
	90°C	95°C	100°C	105°C	110°C
0a	137.0	109.0	87.2	56.7	46.0
0b	57.3	44.0	33.9	26.4	20.6
1	38.5	29.5	22.8	17.7	13.9
2	21.5	16.5	12.7	9.9	7.7
3	23.2	18.1	14.2	11.3	9.0
4	21.9	17.2	13.6	10.8	8.6
5	16.8	13.5	10.9	8.8	7.2

It is important to note that the given times represent the simulated cure times required for the pure epoxy resins when cured at constant isothermal temperature. As will become clear in the next chapter, the EX-CORE foam and more specifically the microspheres used in it, are poor conductors which will significantly increase the required cure time. This is especially the case for thick EX-CORE components, for which it takes several minutes to reach the (isothermal) cure temperature in the core. The numerical thermal model presented in Chapter 5 will make it possible to estimate the temperature and degree of cure distribution at each time step during the cure cycle for a certain EX-CORE composition and rectangular sample dimension. This allows to estimate the required cure time for EX-CORE products.

Remark again that the use of the former (non-diluted) resin Ancarez[®] RZ4010 in combination with Ancamine[®] types of hardeners (Ref. nr 2 & 3) is not recommended. This because of its too high viscosity which makes homogeneous mixing of the powder hardeners difficult. Therefore only epoxy systems nr 1, 4 & 5 were further explored. To explore the suitability of these epoxy systems with the microspheric fillers used in EX-CORE, a first set of EX-CORE sample were produced with these three new systems. This first experimental test phase is covered in Chapter 6.

5

Numerical EX-CORE thermal model

In the previous chapter a cure kinetic model was created that allows simulating the reaction rate and degree of cure of the pure epoxy systems when cured at different temperatures. EX-CORE however consists out of several types of microspheres embedded in an epoxy matrix. In addition, the volume fractions of the constituents can also be varied. Analytic models do exist for filled composites that can predict the temperature distribution in filled composites for steady-state simple geometries and/or boundary conditions [45]. However, no analytic solutions are available for transient problems with internal heat-generation. Therefore a numerical heat conduction-based model was developed by Eversdijk [64] that predicts the thermal behavior of EX-CORE mixtures during a specified cure cycle. A two-dimensional transient finite-difference method had been set up in MATLAB that uses the energy balance equation for a system with internal heat generation. This generated heat is determined by implementing the cure kinetic model as discussed in Chapter 4. The thermal model makes it possible to estimate the temperature and degree of cure distribution as a function of time and location in the core. The framework of this model is also extensively used in the current research during which some alterations to the model had to be made.

To get an understanding of the models working principle and solution methodology, the finite differencing method, used assumptions and derived governing equations similar as used by Eversdijk [64] are discussed in Section 5.1 of this chapter. Next, in Section 5.2 the utilized mesh is explained. Then in Sections 5.3 to 5.6 the determination and implementation of thermal properties such as thermal conductivity, specific heat and cure kinetics are covered. After that, in Section 5.7, an overview of the alterations made by the author to the numerical model is given. The updated model again had to be verified with an analytical solution, as presented in Section 5.8. Afterwards also a new sensitivity study is performed in Section 5.9. Note that validation of the model with experimental data will be covered in Chapter 9. In Section 5.10 an overview of the numerical model is given in the form of a flow chart. Finally, a conclusion is given in Section 5.11.

5.1. Finite difference method

In contrast to analytical solutions that solve the governing differential equations to provide the temperature (or degree of cure) at any point in the domain, numerical methods replace the continuous differential equations with discrete algebraic approximations and only evaluate the temperature at a finite/discrete number of points. The *finite difference method* is such a numerical technique that discretizes the physical domain into smaller regions or elements. Each region is given a reference point or node, to which the average temperature of the representative region is assigned. All the nodes combined form a so called meshed grid or nodal network. Since the temperature in EX-CORE changes with position as well as time, a so called *transient* analysis has to be done, meaning that a discretization of time (in Δt) in addition to space is required [106].

The conservation of energy principle is used to determine the temperature for each node, such that the temperature distribution for the complete mesh is obtained. Normally, smaller elements do not only increase the resolution/detail, but also improve the accuracy of the numerical solution w.r.t. the exact analytical solution (if available) but this will also increase computation time. The same is true when smaller time steps are used.

Heat transfer in solids and fluids at rest is dictated by conduction, which means that energy exchange takes place from the regions of high temperature to the regions of low temperature [107]. Heat flows cannot be measured directly but can be derived from the temperature gradients inside the body by making use of Fourier's law [106, 107]. So when the temperature inside a body is known as a function of time and location, the heat flows can be determined. In this section the required assumptions, governing equations and chosen explicit solution strategy as implemented in the numerical thermal model are discussed.

5.1.1. Assumptions

Eversdijk [64] treated EX-CORE as a homogeneous, isotropic solid with internal heat generation caused by the exothermic reaction of the epoxy. The same and other assumptions formulated by Eversdijk apply for the updated numerical model presented in this report. However, two additional assumptions should be taken into account; one w.r.t. to the mold edges (see nr. 9) and one w.r.t. the onset reaction temperature of the Ancamine[®] hardeners (see nr. 10). An explanation of all the required assumptions is given here:

Identical assumptions:

1. *Homogeneity* is assumed in EX-CORE. On a microscale EX-CORE consists of a mixture of microspheres mixed in an epoxy matrix. The present analysis is however done on a scale of tens of mm. Vial [63] inspected the microstructure of EX-CORE under a Scanning Electron Microscope (SEM) from which an image is given in Figure 5.1. These results confirm the assumption that all the components in EX-CORE are thoroughly mixed and evenly distributed. Identical compositions can therefore be assumed in each volume segment of the body. Thermal properties such as thermal conductivity and specific heat capacity can therefore also be assumed constant throughout the volume.

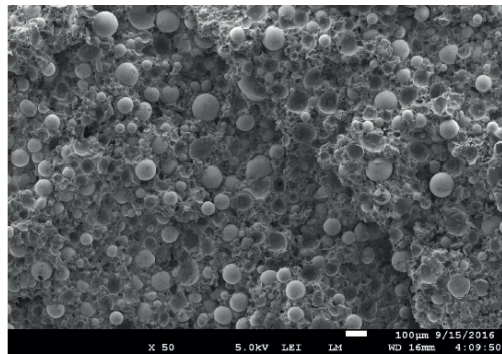


Figure 5.1: Scanning electron microscopic image of EX-CORE, showing that the three types of microsphere are evenly dispersed into the epoxy matrix. [63]

2. *Isotropy* in the material can be assumed, for similar reasons as stated in 1. This has as a consequence that conductivity is equal in all directions
3. *Thermal material properties are assumed to be constant; being independent of time and temperature.* A large variety of components is used in EX-CORE that could behave differently when temperature changes. Exploring such effects for all the constituents, is outside the scope of the research and would also over-complicate the model analysis.
4. *Convective heat transfer* by fluid or gas transfer is *assumed not to be present* in the body, this to not over-complicate the analysis. This assumption is valid because the pre-cured EX-CORE is a paste-like mixture which is dimensionally stable when placed in the mold. In addition it is also tightly compacted in the mold cavity. Gases are present in the microspheres but they are encapsulated by the thermoplastic walls of the microspheres and so convective currents are not present outside the wall of the microspheres. Interstitial voids could be entrapped in the mixtures with low resin content, but their heat convection is considered to be of negligible influence to the heat transfer, especially when compared to the conduction phenomena. Resin flow could be present when the viscosity of the resins drops at increased temperature during the initial stage of curing. Modeling this resin flow is essential for determining the heat flow in processes such as resin transfer molding (RTM) or vacuum infusions that evidently involve resin flows. However, for the EX-CORE process the mixture is placed in an enclosed mold that prevents resin flow out of the mold. Hence the no-resin flow assumption is reasonable.

5. *Radiative heat emittance* on the side surfaces of EX-CORE is *not taken into account* in the analysis. This because EX-CORE can be considered as a solid in physical contact with the mold surface which is maintained at a prescribed temperature (see assumpt. nr. 9). Heat transfer through radiation is of negligible influence at the used curing temperatures ($<160^{\circ}$) when compared to the heat transfer through conduction [45].
6. *Constant pressure* is considered throughout the analysis. As discussed in chapter 3, the pressure generated by Expancel[®] DU as used in EX-CORE is dependent on temperature. Variations in temperature in EX-CORE could therefore result in resin flows through the thickness [64]. To model these effects, precise knowledge on local pressures inside EX-CORE and resin viscosities would be required. Such data is however not available at this stage of the research. Another aspect is that the generated pressure could also affect the thermal interface resistance between EX-CORE and the aluminum mold edges. Similarly not enough knowledge is available to take this phenomena into account. Hence both phenomena are considered outside the scope of the model analysis.
7. A *two-dimensional Cartesian coordinate system* is used such that rectangular cross-sections of infinite depth can be analyzed. Since the model is two-dimensional, this implies that no temperature gradients exist in depth direction. This makes it possible to approximate the thermal behavior of EX-CORE products with various dimensions for which the depth is several times larger than the width or height, and for which edge phenomena in depth direction are minimal. Examples are the floor panels or door sections as currently produced at Donkervoort with EX-CORE.

New additional assumptions:

9. *All mold edges maintain the prescribed (isothermal) cure temperature.* In the current research the top and bottom lids of the tile mold are preheated at the required isothermal cure temperature. The sample is prepared in an aluminum casing, which allows to quickly transfer it in between the preheated mold lids. The mold is then insulated from the outside environment with insulation blankets. Note that this procedure is explained in full detail in Appendix E. In addition, the inner mold temperature is tracked with thermocouples and controlled with PI-controller software that regulates the current to the heat-tracings (see also Section 3.2.4). Therefore it is reasonable to assume that the mold temperature does not deviate from the pre-scribed heating/cure profile. Since the heated mold is considered thermally insulated from the environment, this also implies that heat convection and radiation from the mold surface to the external environment is not considered.

An important note should be made on this; in the model analysis all the mold edges/nodes are assumed to be at the prescribed cure temperature from the beginning of the analysis. However, in reality the aluminum sample casing is transferred in the pre-heated (top & bottom) mold lids and so heats-up from room temperature. The casing consists of milled aluminum side edges and the bottom is made with two layers of aluminum tape. Although that aluminum is highly conductive, it could take some time to heat-up the aluminum side edges which could impair the model accuracy. To investigate this, the heat-up of the aluminum side edges had been implemented in the model and compared with the original model. This procedure and comparison of the results can be found in Appendix C. From these results it can be concluded that the assumption of constant mold temperature for the aluminum side edges does not impair the model accuracy. For example it does not measurably effect the estimated maximum core temperature and/or time required to obtain 98% degree of cure. In addition, modeling the heat-up of the aluminum edges would significantly reduce the required minimum time step for stability (see stability criteria Equation 5.10); from $\Delta t_{crit} \approx 1.5\text{sec}$ for typical EX-CORE mixtures to 0.0045sec for modeling the heat transfer in Aluminum. In practice this implies that the total time to run a single simulation increases from $\pm 30\text{s}-3\text{min}$ to $>1\text{hour}$. This would impair the functionality of the model as a quick analysis tool.

10. A *constant onset reaction temperature; independent of heat-up rate* is implemented in the numerical model. On the datasheets of the Ancamine[®] hardeners 2337s & 2442, onset reaction temperatures of 71°C and 93°C (at $10^{\circ}\text{C}/\text{min}$ DSC heat-up rate) respectively were mentioned. This implies that the reaction is mostly prevented or blocked below this temperature. According to the manufacturer Evonik, this is caused by a physical (not chemical) thermal block of the hardener. The cure kinetics determined in Chapter 4 however do not take this phenomenon into account. In the cure kinetic model, at reduced temperatures (below the specified onset reaction temperature), the reaction rate simply further

reduces as predicted by the implemented Arrhenius equation (see Section 4.2.1). To account for this phenomenon in the numerical model it was decided to implement a condition that no heat generation is allowed to take place in the element until the onset reaction temperature of the resin is reached for that element. This is simply done by setting $\dot{q} = 0$ in that case (see Section 5.6).

Initially the onset reaction temperature as stated on the datasheets of Ancamine[®] hardeners 2337s & 2442 were implemented, namely 71°C and 93°C. The datasheet mentions that they are determined for a DSC heat-up rate of 10°C/min. However, when the heat-up rate changes, the onset reaction temperature will change as well. This was validated with additional DSC experiments (see Section 9.3). During curing of EX-CORE heat-up rates are not constant in time nor space. However, to not over-complicate the model analysis, a constant onset-reaction temperature had to be assumed. As will be discussed in Section 9.3 reaction onset temperatures were determined at different heat-up rates. This allowed to implement better corresponding (constant!) values for the reaction onset temperature (corresponding to the average heat-up rate as observed in EX-CORE samples) to validate the model.

5.1.2. Governing equations

The *energy balance method (or control volume method)* as discussed in [106] allows for setting up the governing equation in term of conservation of energy of a control volume instead of deriving this from less intuitive finite differencing formulations derived from differential equations. Besides that the differential equations do not have to be known before the analysis, this method is also suitable to implement internal heat generation and can handle boundary conditions more easily. Furthermore, the same set of algebraic equations are obtained as when an standard finite differencing method would be used [106].

The energy balance for a transient heat conduction problem with a discretized control volume $V = \Delta x \Delta y$ can be written as follows:

$$\left(\begin{array}{c} \text{Heat transferred into} \\ \text{volume element } V \\ \text{through all surfaces} \\ \text{during } \Delta t \end{array} \right) + \left(\begin{array}{c} \text{Internal heat} \\ \text{generation within} \\ \text{volume element } V \\ \text{during } \Delta t \end{array} \right) = \left(\begin{array}{c} \text{Internal energy} \\ \text{change within} \\ \text{volume element } V \\ \text{during } \Delta t \end{array} \right)$$

in equation format this results in:

$$\Delta t \cdot \sum_{AllSides} \dot{Q} + \Delta t \cdot \dot{q}_{int} \cdot \Delta x \Delta y = \Delta E_{element} \quad (5.1)$$

where \dot{Q} [W/m] is the rate of heat transfer. For internal nodes this is dominated by conduction, whereas for the boundary nodes convection or radiation could also take place. However as mentioned in the assumptions both effects are neglected in the analysis. \dot{q}_{int} [W/m³] is the internal heat generation rate, which in this case is caused by the exothermic reaction of the epoxy matrix in EX-CORE. To obtain the heat generation rate for a volume element V this term should be multiplied with the volume, represented by $\Delta x \Delta y$. \dot{q}_{int} itself is calculated from the cure kinetics of the resin as will be further explained in Section 5.6. Finally, the internal energy change $\Delta E_{element}$ [J/m] is equal to: $\Delta E_{element} = m C_p \Delta T = \rho V C_p \Delta T$, with C_p [J/kgK] the specific heat capacity and ρ [kg/m³] the density of the element. ΔT [K] is the change of temperature inside the element. Equation 5.1 is now divided by Δt and rewritten as follows:

$$\sum_{AllSides} \dot{Q} + \dot{q}_{int} \Delta x \Delta y = \rho \Delta x \Delta y C_p \frac{\Delta T}{\Delta t} \quad (5.2)$$

This equation will be applied for all the nodes in the mesh grid. How this is done is explained in the following paragraphs for an example element with central node at location m,n.

The heat flow rates \dot{Q} through all 4 surfaces of element (m,n) are visualized in Figure 5.2. These heat flow rates can be related to the temperature difference between the central node in the element and its adjacent nodes by making use of the conductance K between the elements. The heat flow rates per unit length (in dept direction) are represented by \dot{Q}_N , \dot{Q}_E , \dot{Q}_S & \dot{Q}_W [W/m] and calculated with Equations 5.3 to 5.6, respectively. Note that a positive heat flow into element (m,n) is obtained when the temperature of the neighboring element is higher than its own temperature. This sign conventions is used throughout the entire analysis.

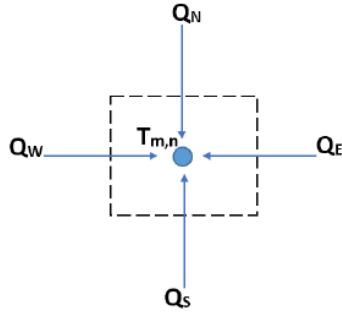


Figure 5.2: Heat flows Q per unit length (in dept direction) from neighboring elements, into element represented by central node (m,n) [64]

$$\dot{Q}_N = K_{m,n+1/2}(T_{m,n+1} - T_{m,n}) \quad (5.3)$$

$$\dot{Q}_E = K_{m+1/2,n}(T_{m+1,n} - T_{m,n}) \quad (5.4)$$

$$\dot{Q}_S = K_{m,n-1/2}(T_{m,n-1} - T_{m,n}) \quad (5.5)$$

$$\dot{Q}_W = K_{m-1/2,n}(T_{m-1,n} - T_{m,n}) \quad (5.6)$$

The thermal coupling between the adjacent elements in the numerical mesh is described by thermal conductances K [w/mK]. For a two-dimensional model, they have to be determined per unit length perpendicular to the x-,y-plane (in dept direction) as visualized in Figure 5.3 [108].

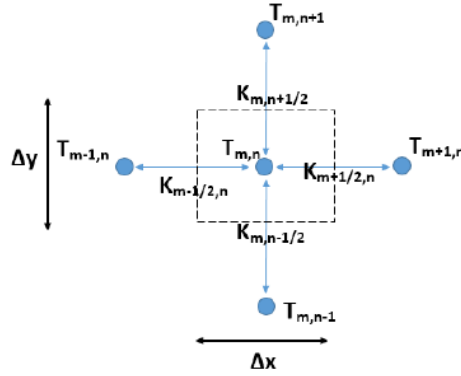


Figure 5.3: Representation of thermal coupling through conductances K between element (m,n) and its neighboring elements [64]

How the conductances K are calculated/derived is explained in full detail in [108]. For example the conductance between element (m,n) and element $(m+1,n)$ is determined as follows:

$$K_{m+1/2,n} = \frac{\Delta y}{\frac{\Delta x}{2k_{x_{m,n}}} + \frac{\Delta x}{2k_{x_{m+1,n}}} + R_{m+1/2,n}} \quad (5.7)$$

Here the conductance term $K_{m+1/2,n}$ represents the total heat flow through the right boundary of element (m,n) per unit length perpendicular to the x-,y-plane. $k_{x_{m,n}}$ & $k_{x_{m+1,n}}$ [W/mK] are the thermal conductivities in x-direction for element (m,n) and element $(m+1,n)$, respectively. The first term in the denominator $\Delta x/(2k_{x_{m,n}})$ denotes the thermal resistance in x-direction for half of element (m,n) . Similarly, the second term $\Delta x/(2k_{x_{m+1,n}})$, represents the thermal resistance in x-direction for half of element $(m+1,n)$. The third term $R_{m+1/2,n}$ is an optional additional thermal resistance that is used when a thermal contact resistance is present at the boundary between elements (m,n) & $(m+1,n)$. This thermal contact resistance is influenced by the surface roughness between adjacent surfaces. A higher surface roughness reduces the effective contact between both surfaces which in turn reduces the thermal conductance and thus heat flow over the interface surface [109].

The heat flow terms are now implemented in Equation 5.2. Additionally, ρ and C_p can be combined into the volumetric heat capacity C [J/m³K] which denotes the energy required to increase the temperature of a unit volume element by 1K. The following equation is then obtained:

$$\dot{Q}_N + \dot{Q}_E + \dot{Q}_S + \dot{Q}_W + \Delta x \Delta y = C \Delta x \Delta y \frac{\Delta T}{\Delta t} \quad (5.8)$$

To obtain the temperature change in an element over a time step Δt , ΔT in Equation 5.8 is replaced by $T^{i+1} - T^i$. Where T^i represent the temperature at the current time step and T^{i+1} the temperature at the next time step. This results in Equation 5.9:

$$T^{i+1} = T^i + \frac{\Delta t}{C\Delta x\Delta y} (\dot{Q}_N + \dot{Q}_E + \dot{Q}_S + \dot{Q}_W + \dot{q}_{int}\Delta x\Delta y) \quad (5.9)$$

This Equation is solved for all nodes in the nodal network and this for consecutive time-steps with increments Δt . To do this and explicit solution methodology is selected as explained in Section 5.1.3.

5.1.3. Solution methodology and stability criteria

When implementing Equation 5.37 in the transient numerical model one has to choose how the heat flow rates \dot{Q} and internal energy generation rate terms \dot{q}_{int} are determined, more specifically in an explicit or implicit manner (or a mix of both) [106]. The *explicit (or forward difference) method* uses the temperatures at the previous time step (i) to calculate \dot{Q} & \dot{q}_{int} during the next time step ($i + 1$). The temperatures at time (i) are already available and can therefore be directly implemented. On the contrary, the *implicit (or backward difference) method* uses the temperatures at the new time step ($i + 1$) to calculate \dot{Q} & \dot{q}_{int} at that time step. This requires solving all the nodal temperatures simultaneously for each time step. Each method has its benefits w.r.t. stability, accuracy, speed and implementation [106].

The *explicit method* is most commonly used and is the easiest to implement, but has as a major limitation that it is unconditionally stable. To avoid instabilities for the nodal temperatures, a limit on the allowable time step Δt should be imposed as defined by the stability criteria. As stated in [106]: "*the stability criteria is satisfied if the coefficient of all $T_{m,n}^i$ and $T_{m,n}^{i+1}$ expressions (called the primary coefficient) are greater than or equal to zero for all nodes (m,n)*". When grouping all the terms involving $T_{m,n}^i$ and $T_{m,n}^{i+1}$, the term with the smallest coefficient should be used. For a two-dimensional transient heat conduction model, such as the one used in this analysis, the following stability criteria given in Equation 5.10 is then obtained:

$$\frac{\alpha\Delta t_{cr}}{l^2} \leq \frac{1}{4} \quad (5.10)$$

in which α [m^2/s] is the thermal diffusivity of the material, that is calculated with $\alpha = \frac{k}{\rho C_p}$. For a specified mesh size $l = \Delta x = \Delta y$ the largest allowable/critical time step Δt_{crit} to ensure stability can thus be calculated using Equation 5.10.

The *implicit method* is unconditionally stable at every time step and so does not require a stability criteria on the allowable time step Δt [106]. This allows to use a larger time step to obtain a solution. However, because the implicit method requires to solve for all the nodal temperatures simultaneously at every time step, it requires additional computational time to solve and is more complicated to implement. In general, implicit methods are therefore better suitable for long (time wise) computations that can use larger Δt and so will faster obtain a solution when compared to the explicit method. To limit the complexity of the MATLAB code, Eversdijk [64] opted for the explicit solution strategy. The same approach is followed in the current research where is build upon the original MATLAB code as created by Eversdijk.

5.2. Mesh

A two-dimensional rectangular mesh is implemented in the numerical model that makes it possible to simulate the thermal behavior of an infinitesimally long EX-CORE sample with height a and width b . The height a is subdivided into N elements with length Δy , while the width b is subdivided into M elements with length Δx . In this model analysis only square elements are used, such that $\Delta x = \Delta y$. A representation of a mesh with arbitrary rectangular dimensions and nodal spacing is given in Figure 5.4. The relative positions of the nodes with respect to their neighboring nodes are indicated with the indices m & n . Phantom nodes are implemented along the EX-CORE boundary to model the heat transfer along the interface between the aluminum mold and EX-CORE. These phantom nodes act as an infinite heat source at prescribed temperature T_∞ which correspond to temperature of the heated aluminum mold T_{mold} . In the mesh used to model EX-CORE three types of nodes are used, namely central nodes, edge nodes and corner nodes. Each type of node requires a different form of Equation 5.9 since the heat flow terms \dot{Q} will be affected by the presence of an adjacent mold boundary or not. The equations for each type of node are discussed in the next sections.

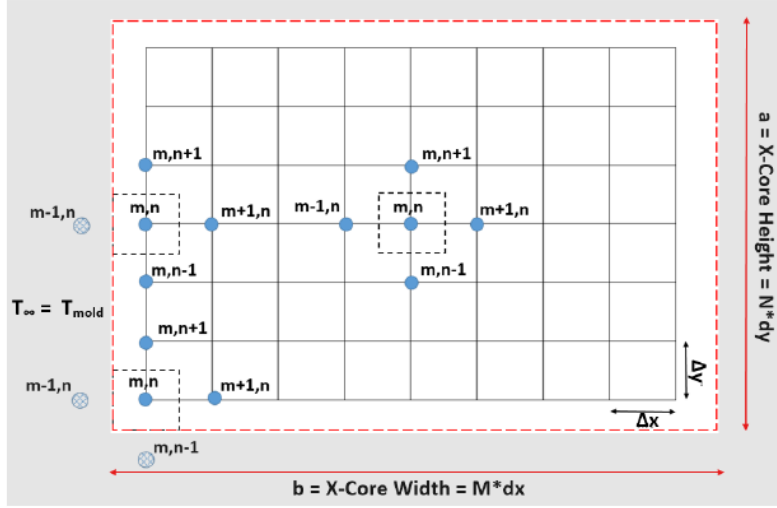


Figure 5.4: Schematic of mesh used to model EX-CORE sample surrounded by aluminum mold (in gray). Central nodes and boundary nodes are illustrated. [64]

5.2.1. Central nodes

As the name indicates, the central nodes cover the central region of the EX-CORE model, more specifically covering elements (2:M,2:N). So central nodes do not have adjacent boundary/phantom nodes. Because the adjacent EX-CORE nodes are in direct contact with each other and are of identical composition, the interface resistance R can be set to zero. Additionally as mentioned in Section 5.1.1 it was assumed that EX-CORE is a homogeneous isotropic solid. This implies that the thermal conductivity is the same in all direction, such that $k_{x_{m-1,n}} = k_{x_{m,n+1}} = k_{x_{m+1,n}} = k_{x_{m,n-1}} = k_{eff}$. When also taking into account that $\Delta x = \Delta y$, Equation 5.7 is reduced to the effective thermal conductivity of the EX-CORE materials denoted by k_{eff} as shown in Equation 5.11. k_{eff} for EX-CORE will be derived in Section 5.4.

$$K_{m+1/2,n} = \frac{\Delta y}{\frac{\Delta x}{2k_{x_{m,n}}} + \frac{\Delta x}{2k_{x_{m+1,n}}} + R_{m+1/2,n}} = \frac{\Delta x}{\frac{\Delta x}{k_{eff}} + 0} = k_{eff} \quad (5.11)$$

A schematic of a central node and its neighboring node numbering is visualized in Figure 5.5, the resulting heat flow rates are shown in Equations 5.12 to 5.15.

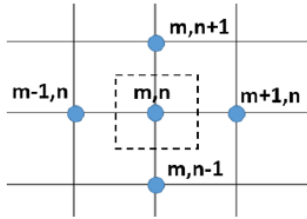


Figure 5.5: Central node [64]

$$\dot{Q}_N = k_{eff}(T_{m,n+1} - T_{m,n}) \quad (5.12)$$

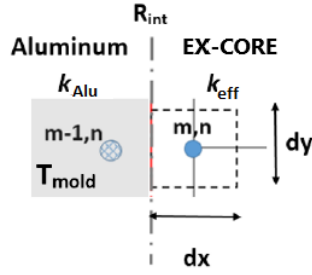
$$\dot{Q}_E = k_{eff}(T_{m+1,n} - T_{m,n}) \quad (5.13)$$

$$\dot{Q}_S = k_{eff}(T_{m,n-1} - T_{m,n}) \quad (5.14)$$

$$\dot{Q}_W = k_{eff}(T_{m-1,n} - T_{m,n}) \quad (5.15)$$

5.2.2. Boundary nodes

To model the heat-flow between EX-CORE and the aluminum mold, the conductances K of the boundary nodes in the nodal network should include the thermal interface resistance term R_{int} as explained with Equation 5.7. Two type of boundary nodes exist, edge nodes and corner nodes. A schematic of an edge boundary node in contact with the aluminum node is shown in Figure 5.6.



$$K_{m-1/2,n} = \frac{\Delta y}{\frac{\Delta x}{2k_{eff}} + \frac{\Delta x}{2k_{alu}} + R_{int}} = K_{int} \quad (5.16)$$

Figure 5.6: Interface between EX-CORE and aluminum mold at an edge boundary node [64]

The thermal conductance K between nodes $(m-1,n)$ and (m,n) as shown in Figure 5.6 is calculated with Equation 5.16 and will be further referred to as the interface conductance K_{int} . How the thermal conductivity of EX-CORE k_{eff} is calculated will be explained in Section 5.4. The value for k_{alu} was set to 210 W/mK, which is the thermal conductivity of 6060-T6 grade Aluminum [110].

The thermal interface resistance R_{int} is not exactly known for the EX-CORE/aluminum interface. It is dependent on the surface roughness between the adjacent surfaces that could cause imperfect contact (on a microscale). This results in reduced heat flow through conduction over the interface [106]. To obtain exact values for R_{int} experimental testing would be required.

In the research by Eversdijk [64], R_{int} was initially set to $1.6 \cdot 10^{-5} \text{ m}^2\text{K/W}$. This value was based on known values from literature, more specifically the experimentally determined values from Chapelle et. al [111] who obtained thermal interface resistance ranging from $0.3 \cdot 10^{-5}$ and $1.6 \cdot 10^{-5} \text{ m}^2\text{K/W}$ between epoxy and metallic wires. However, after validation of the model with experimental results Eversdijk concluded that R_{int} had to be re-evaluated. It was reasoned that because of the large volume of microspheres embedded in the epoxy matrix, a worse surface contact than with neat epoxy resin is obtained and therefore the thermal resistance should be higher than the initial assumption of $1.6 \cdot 10^{-5} \text{ m}^2\text{K/W}$. This value was taken as lower bound for the updated interface resistance.

The upper bound value was obtained from research on thermal contact resistance between steel pipes and insulating materials, in which interface resistances between 0.37 and $0.18 \text{ m}^2\text{K/W}$ were obtained for steel pipes in contact with fiber glass or calcium silicate [112]. The value of $0.37 \text{ m}^2\text{K/W}$ was used as upper bound because both insulating materials are solids, in contrary to the more viscous state of the EX-CORE resin matrix that could fill up gaps.

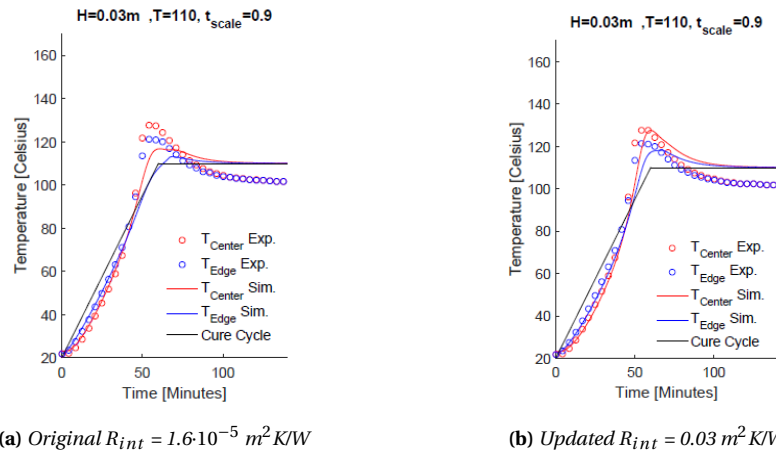


Figure 5.7: Comparison of model fit results by Eversdijk for 30mm thick "270opt" mix EX-CORE sample with the original (a) and updated (b) interface resistance R_{int} [64]

Eversdijk varied the interface resistance between both boundaries and compared the corresponding model data to experimental results for a 30m thick sample with his optimal 270mix composition. Finally, a value of $0.03 \text{ m}^2\text{K/W}$ was selected as this gave an improved model fit. A comparison of his model fit for the original

and new R_{int} value can be seen in Figure 5.7. This updated value was also applied in other validation model data by Eversdijk, resulting in all cases in reduced errors; the maximum error at the edges reduced from 12 to 4°C, while the maximum errors at the core were reduced from 13 to 5°C [64]. In the current research R_{int} was therefore also be set to 0.03m²K/W.

Edge nodes

Edge nodes exist along the left, right, top and bottom boundary edges of the EX-CORE model region. More specifically, they occur at the following nodal locations: (1,2:N), (M,2:N), (N,2:M) and (1,2:N), respectively. The difference with central nodes is that the thermal conductivity between the mold and EX-CORE boundary is defined by the interface conductance K_{int} instead of k_{eff} , the thermal conductivity in EX-CORE. In Figure 5.8 a representation of a left boundary edge node is given, with the corresponding heat flow rate formulations given by Equations 5.17 to 5.20. Note that heat flow rates for the other edge nodes are derived in a similar way, where K_{int} is implemented in either \dot{Q}_E , \dot{Q}_S or \dot{Q}_W for the top, right and bottom edges respectively.

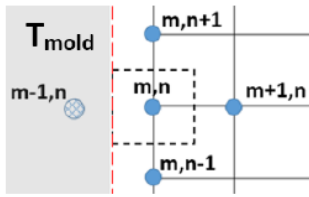


Figure 5.8: Edge node [64]

$$\dot{Q}_N = k_{eff}(T_{m,n+1} - T_{m,n}) \quad (5.17)$$

$$\dot{Q}_E = k_{eff}(T_{m+1,n} - T_{m,n}) \quad (5.18)$$

$$\dot{Q}_S = k_{eff}(T_{m,n-1} - T_{m,n}) \quad (5.19)$$

$$\dot{Q}_W = K_{int}(T_{m-1,n} - T_{mold}) \quad (5.20)$$

Corner nodes

Four corner nodes are present in the model at nodal locations (1,1), (1,N), (N,M) and (M,1). At each corner, two heat flow rates are dependent on the interface conductance term K_{int} . As an example the left bottom node schematic is shown in Figure 5.9, with the corresponding heat flow rates given in Equations 5.21 through 5.24. Again in a similar way, the equations for the other three corner nodes can be derived.

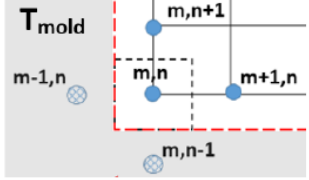


Figure 5.9: Corner node [64]

$$\dot{Q}_N = k_{eff}(T_{m,n+1} - T_{m,n}) \quad (5.21)$$

$$\dot{Q}_E = k_{eff}(T_{m+1,n} - T_{m,n}) \quad (5.22)$$

$$\dot{Q}_S = K_{int}(T_{m,n-1} - T_{mold}) \quad (5.23)$$

$$\dot{Q}_W = K_{int}(T_{m-1,n} - T_{mold}) \quad (5.24)$$

5.2.3. Boundary conditions

To model EX-CORE curing inside a heated mold certain boundary conditions are required. It was explained in the assumptions that "All mold edges maintain the prescribed (isothermal) cure temperature." This implies that the phantom nodes, which represent the aluminum mold surface in the model analysis are assigned a specific mold temperature T_{mold} at every time step as prescribed by the cure cycle profile defined by the user. In the current research a constant T_{mold} is used since the used aluminum mold is pre-heated to a certain isothermal cure temperature before the sample is inserted. As explained in Section 5.2.2, the heat transfer between the mold surface (phantom nodes) and EX-CORE boundary nodes is dependent on both thermal conductance and interface resistance.

5.2.4. Initial conditions

As a starting point for the model analysis at $t=0s$, initial conditions should be defined by the user. First of all, the initial nodal temperatures should be supplied. An initial EX-CORE temperature should be entered, that is used for all EX-CORE center-, edge- and boundary-nodes. However, the initial temperature of the mold can be chosen to be different from EX-CORE's temperature. This is especially the case in the current research where a preheated mold is used. Finally, also the degree of cure of the resin can be entered as a value between 0 and 1. How this degree of cure is implemented in the model analysis is covered in Section 5.6.

5.3. Thermal properties of EX-CORE components

In the following Sections an explanation is given on how the thermal conductivity and specific heat of different EX-CORE mixtures are computed. Since EX-CORE is assumed to be an homogeneous isotropic solid, these thermal properties are referred to as the effective thermal conductivity k_{eff} and effective specific heat $C_{p_{eff}}$ of the bulk EX-CORE material. Before these effective thermal properties of EX-CORE can be determined, the (thermal-) properties of the separate EX-CORE components should be known. As explained in the current section, these properties are derived from literature. They are summarized in Tables 5.1, 5.2 & 5.3 where the sources are given as well. Later in Sections 5.4 and 5.5, the theoretical model used to calculate k_{eff} and $C_{p_{eff}}$ are discussed. Note that these theoretical models are similar as the ones used in the research by Eversdijk, however some EX-CORE components differ in the current research, while also some material properties have been updated/corrected.

Epoxy resins

Next to the previous EX-CORE resin Ancarez[®] RZ4010 & hardener Ancamide[™] 3399 from Airproducts/Evonik (discussed in Section 3.3.4) one new type of resin (SR 1280 by Sicomin) and three new types of hardeners (SZ 8525 by Sicomin and Ancamine[®] 2337s & Ancamine[®] 2442 both from Evonik) are used in this research. They were introduced in Section 4.1.2. The densities of all the resins and hardeners can be found in Table 5.2. When using the volume fractions of the used resin mix ratio, the density of the resin matrix phase in EX-CORE ρ_{matrix} is obtained. The densities for specific combinations of epoxy systems and mix ratios used in this research are presented in Table 5.3. The thermal conductivities k and specific heat capacities C_p of the used resins and/or hardeners were not known nor provided on the datasheets. However, the used resin systems are all epoxy-amine based, therefore k and C_p were derived from literature for similar epoxy-amines. Note that the same values for k and C_p were used for all epoxy systems, these values were also implemented by Eversdijk [64].

Hollow glass microspheres: Q-Cel[®]

The first type of microsphere used in EX-CORE is Q-Cel[®] 5028 which is a hollow glass microsphere (HGM) with an amorphous sodium Borosilicate shell [70] and air entrapped inside.

Thermoplastic expanded microspheres Expancel[®] DE

Thermoplastic expanded microspheres Expancel[®] DE are the second type of microspheres used in EX-CORE. Only one grade of Expancel[®] DE will be used, namely 920 DE 80 d30. The exact material compositions of Expancel[®] DE (& DU) are not mentioned on the datasheets nor were they provided when consulting the manufacturer *Akzonobell*. However, a careful inspection of the provided material Safety Data Sheets (SDS) [113] revealed a 15-20% concentration of isopentane. So it can be derived from this that the gas inside 920 DE 80 d30 is isopentane. Unfortunately, this latest revision of the SDS did not mention the exact material composition of the thermoplastic shell. Only the general term "copolymer" was mentioned. Nonetheless, older revision of SDS for Expancel[®] DE & DU found by Eversdijk [114] revealed more specific information. As main weight fraction of the used substances the co-polymers acrylonitrile and methacrylonitrile were mentioned. From this it could be derived that the shell is probably made from polyacrylonitrile (PAN) [64].

Thermoplastic expandable microspheres Expancel[®] DU

The third type of microspheres are thermoplastic expandable microspheres known as Expancel[®] DU. During this research two grades of Expancel[®] DU will be used: the originally used grade 031 DU 40 and a new more resistant grade 043 DU 80. This grade also has a higher onset expansion temperature (95-115°C instead of 80-95°C) [56]. Again exact material compositions of Expancel[®] DU could not be obtained. However, inspection of the SDS revealed a 25-30% concentration of isobutane gas for 031 DU 40 [115]. So this reveals that isobutane is the blowing agent inside 031 DU 40. For the 043 DU 80 grade, both a 10-15% isobutane and 10-15% isopentane composition was mentioned on the SDS [116]. So the material properties for the 043 DU 80 blowing agent were derived by taking the average of the isopentane and isobutane properties as provided in Table 5.1. Again PAN was assumed as material for the shell of both Expancel[®] DU grades.

Table 5.1: Density (ρ), thermal conductivity k and specific heat C_p of EX-CORE component materials at room temperature. Similar values as used by Eversdijk [64], again confirmed with literature.

Component	Material	ρ [kg/m ³]	Source ρ	k [W/mK]	Source k	C_p [J/kgK]	Source C_p
Binder	Epoxy-amine resin	*	*	0.363	[117–119]	2217	[105, 120, 121]
Q-Cel wall	Borosilicate glass	2230	[84, 122]	1.140	[84]	750	[122]
Q-Cel gas	Air	1.161	[123]	0.024	[123, 124]	1140	[123]
DE wall	PAN	1240	[125, 126]	0.200	[119]	1300	[125]
DE gas	Isopentane	3.212	[127, 128]	0.015	[129]	1680	[129]
DU wall	PAN	1240	[125, 126]	0.200	[119]	1300	[125]
031DU40 gas	Isobutane	2.440	[128, 130]	0.015	[129, 130]	1580	[129, 130]
043DU80 gas	50% Isobutane & 50% Isopentane	2.826	[127, 128, 130]	0.015	[127, 129, 130]	1630	[129, 130]

* see epoxy matrix densities in Table 5.3

Table 5.2: Densities of resins and hardeners used in this research.

	ρ [kg/m ³]	Source
Resins		
Ancarez [®] RZ4010	1170	[85]
SR 1280	1159	[96]
Hardeners		
Ancamide [™] 3399	940	[131]
SZ 8525	940	[96]
Ancamine [®] 2337s	250	[98]
Ancamine [®] 2442	950	[100]

Table 5.3: Effective resin matrix phase densities ρ_{matrix} for the different epoxy systems at the given resin mix ratios (Derived from densities in Table 5.2).

DSC test Ref. nr.	Resin mix ratio (resin:hardener)	ρ_{matrix} [kg/m ³]
0 (a & b)	100:60	1.084
1	100:24	1.117
2	100:60	0.825
3	100:60	1.088
4	100:60	0.818
5	100:60	1.081
5.2	100:20	1.124

5.4. Thermal conductivity of EX-CORE

Thermal conductivity is a material property that is a measure for how easy a material conducts heat. It is denoted by k and has the units [W/mK] [106]. Values for K are well known for common homogeneous materials. For filled composites such as EX-CORE, the effective thermal conductivity of the bulk material k_{eff} should be determined from theoretical models as discussed in Section 5.4.1. It will become clear that k_{eff} is affected by both the conductivity of the separate components as well as the geometrical structure of the composite. Suitable methods will first of all be used to calculate the effective thermal conductivity of the various microspheres used in EX-CORE, they are explained in Section 5.4.2. Then, in Section 5.4.3, the effective thermal conductivity of EX-CORE as bulk material will be estimated. Finally, remarks on the validation of k_{eff} for EX-CORE are given in 5.4.4.

5.4.1. Theoretical models for effective thermal conductivity of particle filled composites

For syntactic foams with high volume content (>50%) of microspheres, as is the case in EX-CORE, the walls of the microspheres can be in physical contact with each other. At a certain volume fraction, referred to as the "percolation threshold", conductivity paths are formed throughout the composite [132]. This effect is especially important for syntactic foams with highly conducting microspheres w.r.t. the binder matrix, (for example aluminum microspheres in an epoxy matrix). Then a large increase in conductivity occurs at the percolation threshold because a highly conductive path/network is formed. The parallel and series model are the two most simple theoretical models that can be used to determine the boundaries of k_{eff} for particle filled composites such as syntactic foams [133, 134]. They are shortly introduced in the next paragraph.

Parallel and series model

The parallel and series model determine the upper and lower boundary for the thermal conductivity k_{eff} of a two-phase material (resin & microspheres) [135]. This is done by modeling the material in layers representing the two components. As the name indicates, the parallel model positions these layers parallel to the heat flow, while in the series model the heat flow is assumed to be perpendicular to the layers, this is visualized in Figure 5.10. The equations for both models are the following [135]:

$$\text{Parallel: } k_{eff} = (1 - v_f)k_b + v_fk_f \quad (5.25)$$

$$\text{Series: } k_{eff} = \frac{1}{\frac{1-v_f}{k_b} + \frac{v_f}{k_f}} \quad (5.26)$$

In which v_f is the volume fraction of the filler/microspheres, while k_b and k_f represent the thermal conductivity of the binder and filler/microspheres, respectively. These equations usually provide the upper (parallel) and lower bounds (series) of k_{eff} . However, more advanced analytical models for filled composites have been developed in recent years that give predictions of k_{eff} within both bounds [134]. They make use of the self-consistent field theory to predict the effective thermal conductivity of a heterogeneous material provided that the thermal conductivities and volume fractions of the constituents are known. They then consider the heterogeneous material as macroscopically homogenic [133, 136]. The Maxwell-Garnett model is such a well-known model that was also implemented in the numerical EX-CORE model. Its working principles and the reasons why it was selected are discussed in the following paragraphs.

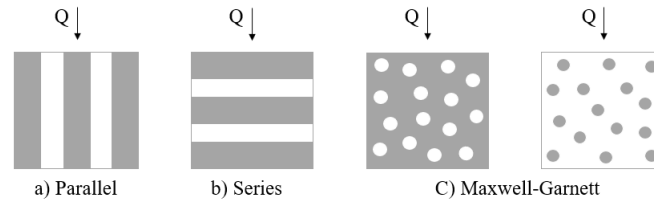


Figure 5.10: Two phase material representations of parallel, series and Maxwell-Garnett model for thermal conductivity.

Maxwell-Garnett model

The Maxwell-Garnett model is a commonly used method to determine k_{eff} for spherical filled composites. This model assumes that the fillers are homogeneously mixed, which is valid since it was also one of the assumptions as stated for the EX-CORE model in Section 5.1.1. The Maxwell-Garnett equation is as follows:

$$\text{Maxwell-Garnett: } k_{eff} = k_b \frac{k_f + 2k_b + 2v_f(k_f - k_b)}{k_f + 2k_b - v_f(k_f - k_b)} \quad (5.27)$$

This model was also selected by Eversdijk [64] and implemented in the numerical EX-CORE model. The main reasons for choosing this model were the following:

Firstly, in a research by Zhu et. all [134] the Maxwell-Garnett relation was i.a. implemented to determine the thermal conductivity of a hollow glass microsphere (HGM) filled syntactic foams with an epoxy-matrix. Two types of tested microspheres (K1 & K20 by 3M) have a true density close to that of Q-Cel[®] 5028, namely 125 & 200kg/m³ compared to 290kg/m³ of Q-Cel[®] 5028. They experimentally determined k_{eff} for HGM volume fractions up to 60% and found good correlation with the Maxwell-Garnett model. Because of its resemblance with EX-CORE components this could also be true for the EX-CORE syntactic foam. In addition the heaviest EX-CORE mixes defined by Vial [63] have a maximum Q-Cel[®] volume fraction of 65.8% [63], which only slightly exceeds the upper limit of 60% volume fraction, validated by Zhu et. all [134].

Secondly, it is said that most of the theoretical models that make use of the self-consistent field theory do not give accurate results when the percolations threshold volume fractions is reached [136]. However, as said Zhu et. all [134] found that the Maxwell-Garnett relation can be used to predict k_{eff} for HGM epoxy filled composites with HGM volume fractions up to 60%. In addition, this effect would also not be prominent in EX-CORE since the thermal conductivity of the fillers is relatively close to that of the epoxy matrix. When inspecting Table 5.1 it can be seen that the largest deviation occurs between the glass shell of Q-Cel[®] (1.14W/mK) and the epoxy matrix (0.363W/mK). It could therefore be expected that no sudden changes in thermal conductivity occur at high volume fractions of Q-Cel[®] in EX-CORE. Hence the Maxwell-Garnett model can be implemented in the numerical thermal model of EX-CORE.

5.4.2. Effective thermal conductivity of microspheres

The Maxwell-Garnett relation presented in Equation 5.27 is expressed for only one type of filler, but in EX-CORE three different types of microspheric particles occur. To deal with this a method was proposed by Mishra [117] that allows to obtain the effective thermal conductivity of the various fillers combined. This approach was also implemented in the numerical thermal EX-CORE model. To begin with, the total volume fraction of all the microspheres present in a known EX-CORE mixture is calculated as follows:

$$v_f = (v_{DU} + v_{DE} + v_{q-cel}) \quad (5.28)$$

Next, the relative volume fraction of each type of microsphere w.r.t. to v_f is obtained. Here DU is used as example:

$$v_{rDU} = \frac{v_{DU}}{v_f} \quad (5.29)$$

The effective thermal conductivity of the combination of filler will then be calculated with:

$$k_f = k_{DU} \cdot v_{rDU} + k_{DE} \cdot v_{rDE} + k_{Q-cel} \cdot v_{r_{qcel}} \quad (5.30)$$

k_{DU} , k_{DE} & k_{Q-cel} , the thermal conductivities of DU, DE and Q-Cel are not directly known, but can be determined using *Hashin's equation* presented in Equation 5.31 [133, 137]. Although incorrectly formulated in the report of Eversdijk [64], Equation 5.31 was in the end also implemented in his final version of the numerical model to calculate the effective thermal conductivity of a single DU, DE and Q-Cel microsphere:

$$k_{1microsphere} = k_w \left(1 + \frac{v_g}{\frac{1-v_g}{3} + \frac{k_w}{k_g - k_w}} \right) \quad (5.31)$$

Here k_w and k_g represent the thermal conductivities of the wall material and inner gas of the microsphere, respectively. v_g is the volume fraction of the gas w.r.t. to the total volume of the microsphere.

v_g (& ρ_{true}) determination

Values for v_g had to be estimated based on 1) *the material densities of the wall and gas inside the microspheres*. These densities were already given in Table 5.1. and 2) *the true density of the microspheres ρ_{true}* . Only the true densities for Q-Cel and DE were provided on the data sheets [68, 70]. The true densities for DU had to be estimated. First of all, this was done by taking the bulk densities that could be experimentally determined. Vial [63] for example measured for 031 DU 40 a bulk density of 370kg/m³. Similarly, the density for 043 DU 80 (a new grade that will be used in this research as well) had been determined to be 500kg/m³. The bulk densities can not be higher than the corresponding true densities, because in the bulk microspheric mixture, interstitial air will be entrapped between the microspheres, resulting in a lower (bulk) density. When the packing factor of the bulk material would be known, the true density could be obtained. In theory this packing factor specifies how close the spheres are packed inside a unit cell (the smallest repeating unit in the bulk volume) or it is simply the ratio of the volume of the spheres in the unit cell over the total volume of the unit cell.

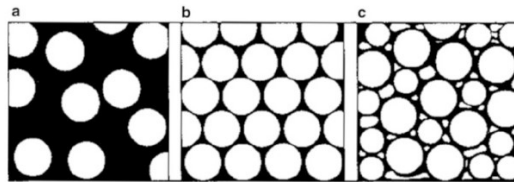


Figure 5.11: Graphical representation of the internal structure of syntactic foams: **a)** random dispersion of spheres (2-phase) **b)** hexagonal closed-packed structure with uniform sized spheres (2-phase) **c)** microspheres, dispersed voids and resin matrix (3-phase) [33]

Because the datasheet of DU [56] mentions a particle size variation between 10-16 μ m (at unspecified distribution) for 031 DU 40 and 16-240 μ m for 043 DU 80 microspheres, the exact packing factor of the spheres in the bulk DU mixture could not be determined. So an estimation had to be made based on packing factor values obtained from literature. For a two-phase system where all spheres are of equal dimension, the highest

packing factor that can be achieved is 0.74, this can only occur when the spheres are positioned in a hexagonal closed-packed structure (see Figure 5.11b). For mixtures with different sizes of spheres (Figure 5.11c), packing factors up to 0.8 can be achieved [37]. Based on this information and considering that the bulk DU mixture is not optimally structured, an estimate for the packing factor of DU of 0.65 seemed reasonable.

The true density of (unexpanded) DU is then determined by dividing the known bulk density of DU by the packing factor of 0.65. The resulting true densities ρ_{true} can be found in Table 5.4. Note also that *Eversdijk* [64] previously implemented an incorrect true density for 031 DU 40 (unexpanded) of 120kg/m^3 in the numerical model. This would be physically impossible because this would mean that the measured bulk density of 370kg/m^3 [63] (with interstitial air having a density $\approx 1\text{kg/m}^3$ at room temperature) would be higher than the "true density of 120kg/m^3 ". The newly obtained ρ_{true} values for DU should therefore be more accurate.

With all the required parameter values known, the volume fraction of the gas inside the microsphere v_g can finally be determined by making use of Equation 5.32, in which now v_g is the only unknown.

$$\rho_{true} = (1 - v_g)\rho_w + v_g\rho_g \quad (5.32)$$

were ρ_w and ρ_g are the densities of the microsphere's wall and inner gas, respectively.

$k_{1microsphere}$ determination

Next, values for the effective thermal conductivity of a single DU, DE and Q-Cel microspheres ($k_{1microsphere}$) could be obtained using Equation 5.31. The respective results are presented in Table 5.4. These values can now be used in Equation 5.30 to determine the effective thermal conductivity of the combination of fillers k_f for a specific EX-CORE mixture with known volume fractions.

Table 5.4: True densities for EX-CORE microspheres used to estimate v_g and from this determine the respective thermal conductivities of a single microsphere $k_{1microsphere}$

Type of microsphere	ρ_{true} [kg/m ³]	v_g [-]	$k_{1microsphere}$ [W/mK]
Q-Cel 5028	290	0.870	0.1257
920 DE 80d30	30	0.978	0.0179
031 DU 40 (unexpanded)	569	0.542	0.0832
031 DU 40 (expanded)	15	0.990	0.0166
043 DU 80 (unexpanded)	769	0.381	0.1130
043 DU 80 (expanded)	21	0.985	0.0171

A remark should be made on the properties of Expancel[®] DU. Under elevated temperatures, this component will expand, which can result in an increase in volume of the sphere up to 37 times [63]. This free-expansion of DU is under normal processing conditions (100% mold filling) prohibited due to the surrounding viscous EX-CORE paste entrapped in an enclosed mold. This way pressure is generated, which is required to consolidate the prepreg facesheets. Nonetheless, in the numerical model the state of DU can also be chosen as "expanded", where in the calculations the "expanded true volume" is simply the "unexpanded true volume" divided by 37. Also ρ_g had to be divided by 37 since the DU expansion is caused by the expansion of the gas and such the gas density decreases. Note that this was incorrectly not taken into account by *Eversdijk* [64], but had been updated in the current version of the numerical model. The obtained values for v_g and $k_{1microsphere}$ for both states are given in Table 5.4. The effect of these two boundary cases on modeling the effective thermal conductivity in EX-CORE is evaluated in Section 5.4.3.

The thermal conductivity values obtained for Expancel[®] DU & DE could not be validated due to the lack of comparative experimental data or literature. However, in the research by *Eversdijk* [64] the obtained values for Q-Cel 5028 were already compared to the thermal conductivity of similar HGM produced by 3M[™] as used in the research of *Zhou et al* [134]. The resulting comparative data is presented in Table 5.5, from which it can be observed that the thermal conductivity of Q-Cel 5028 lies in between that of HGM having a lower and higher true density. This is as expected and so the result obtained for Q-Cel 5028 is realistic.

Table 5.5: Comparison of thermal conductivities of similar HGM to Q-Cel 5028, derived from Zhou et al [134] [64]

Type of HGM	True density [kg/m ³]	Thermal conductivity [W/mk]
K1	125	0.064
K20	200	0.086
Q-Cel 5028	290	0.126
S38HS	380	0.137
S60HS	600	0.200

5.4.3. Effective thermal conductivity of EX-CORE

All the properties required to determine the effective thermal conductivity of EX-CORE, k_{eff} , have now been determined. All what is left is taking an EX-CORE mixture from which the volume fractions are known. A code has been generated in MATLAB that asks the user to enter an EX-CORE mix composition, DU percentage and asks to select the unexpanded or expanded state of DU. The code makes use of the material & thermal properties of the components as presented in the previous paragraphs to calculate the effective thermal conductivity k_{eff} of the chosen EX-CORE mixture based on the Maxwell-Garnett model. As will become clear in Chapter 6, a specific mix composition, referred to as the "270kg/m³ optimal mix" or simplified "270opt" [63] was selected as a suitable mixture to use as a baseline in the current research. The corresponding pseudo-volume fractions (i.e. excluding DU) can be found in Table 5.6. Note that the final volume fractions of the EX-CORE mix are determined by multiplying the pseudo-volume fractions by (100-%DU)/100.

Table 5.6: Pseudo component volume fractions of the "270-optimal" mix [63]

EX-CORE mix	Resin	Q-Cel	DE
270opt	0.149	0.528	0.323

Comparison of K_{eff} models and effect of changing DU percentage, grade and expansion state

The pseudo "270opt" mix is used as an example to investigate the effect of changing the volume content, expansion state and grade of DU on k_{eff} . More specifically, a DU content of 1, 5 and 10% for both states and both grades has been selected. The resulting k_{eff} values as determined by both the parallel, series and Maxwell-Garnett model are shown in Table 5.7.

Table 5.7: Comparison of effective thermal conductivity results k_{eff} of the EX-CORE 270 opt mix obtained with the series, parallel & Maxwell-Garnett model. The DU grade, expansion state and DU percentages were varied.

DU vol. %	DU state	k_{eff} [W/mK]		
		Series	Parallel	Maxwell-Garnett
<i>270opt mix with 031DU40</i>				
1%	unexpanded	0.0441	0.126	0.117
1%	expanded	0.0439	0.125	0.116
5%	unexpanded	0.0450	0.124	0.115
5%	expanded	0.0411	0.121	0.112
10%	unexpanded	0.0461	0.122	0.114
10%	expanded	0.0382	0.115	0.107
<i>270opt mix with 043DU80</i>				
1%	unexpanded	0.0442	0.126	0.117
1%	expanded	0.0439	0.125	0.116
5%	unexpanded	0.0453	0.125	0.117
5%	expanded	0.0413	0.121	0.112
10%	unexpanded	0.0468	0.125	0.117
10%	expanded	0.0384	0.1155	0.107

As expected, from Table 5.7 it can be observed that the Maxwell-Garnett model results lie in between the lower and upper bounds as predicted by the series and parallel model. The difference between similar mixes with different grades of DU is at most 2.8%, this for the 10% unexpanded 270 opt mixes. The difference between the unexpanded and expanded results is at most 8.6%. This occurs for the 270opt mix with 10% 043DU80. Remark that the k_{eff} results are the same for all epoxy-amine resin systems used as binder in EX-CORE. This because the volume fraction of the binder (v_f) is constant for a specific mix and also because the same conductivity value of 0.363W/mK is used for all epoxies.

Comparison of k_{eff} for different EX-CORE mix compositions

The effective thermal conductivity, k_{eff} , for commonly used EX-CORE mixtures is presented in Table 5.8. The given mix compositions result in a mix density between $\pm 230\text{kg/m}^3$ and $\pm 330\text{kg/m}^3$. They all have a 4vol.% DU content set at the unexpanded state. The k_{eff} results for both the 031DU40 & 043DU80 grade are given. It can be observed that when the mix density increases, k_{eff} increases as well. This is because the volume fractions of relatively high conductive epoxy matrix and Q-Cel increase with mix density. When the mix density increases by 100kg/m^3 from 330 to 230kg/m^3 , k_{eff} increases around 31%.

Table 5.8: Effective thermal conductivities k_{eff} of common EX-CORE mixes

EX-CORE mix	Resin	Mix volume fractions			k_{eff} [W/mK]
		DU (grade)	DE	Q-Cel	
230opt	0.120	0.04 (031DU40)	0.427	0.413	0.098
		0.04 (043DU80)			0.099
270opt	0.143	0.04 (031DU40)	0.310	0.506	0.116
		0.04 (043DU80)			0.117
330opt	0.176	0.04 (031DU40)	0.126	0.658	0.143
		0.04 (043DU80)			0.145

5.4.4. Note on validation of the effective thermal conductivity of EX-CORE

The method to obtain the effective thermal conductivity of EX-CORE as presented in Section 5.4 provides similar conductivities as the ones obtained for the HGM-epoxy syntactic foams researched by Zhu et. all [134]. However, what makes EX-CORE unique is that three types of microspheres are used, both HGM and thermoplastic in nature. Additionally, in total a very high volume fraction of these microspheric fillers is present. It is therefore recommended to experimentally validate the obtained theoretical model results (see also the recommendations given in Chapter 12). A suitable method prescribed in ASTM standard E1225 and also used by Zhu et. all [134], would be the Guarded Heat Flow meter technique [138]. Another possibility is to use the Laser-Flash method as stipulated in ASTM standard E1461 [139]. Unfortunately, the required setups were not available to the author, nor were they in the previous research by Eversdijk [64]. Nonetheless a new sensitivity study, similar to the one previously performed by Eversdijk, is executed to evaluate the effect on the temperature distribution of the updated numerical model w.r.t. changes in the thermal conductivity (& specific heat capacity) of EX-CORE. This is explained in Section 5.9.

5.5. Specific heat capacity of EX-CORE

The specific heat capacity of a material is defined as "the energy required to raise the temperature of a unit of mass of a substance by one degree (or Kelvin)" [106]. It is referred to by C_p and gains the units [J/kgK]. Similar as with the thermal conductivity, the effective specific heat of EX-CORE as bulk material ($C_{p_{eff}}$) is a function of the C_p of the individual components. Again EX-CORE is then considered as an homogeneous isotropic material. In this section it is explained how the effective specific heat of a variety of EX-CORE mixtures can be predicted.

The specific heat of a filled composite can be calculated with the general rule of mixtures that uses the mass fractions m_f of the separate components [140]. The rule of mixtures for EX-CORE can be written as follows:

$$C_{p_{eff}} = C_{p_{binder}} m_{f_{binder}} + C_{p_{DU}} m_{f_{DU}} + C_{p_{DE}} m_{f_{DE}} + C_{p_{Q-cel}} m_{f_{Q-cel}} \quad (5.33)$$

However, it is known that this simple rule of mixtures tends to slightly under-estimate the predicted specific heat values. This issue can be corrected for by rewriting the rule of mixtures, resulting in Equation 5.34. This relation had been successfully used for mixtures with high volume fractions of fillers, for which coefficient of fit (R^2) values between 0.92-0.99 had been obtained [140].

$$C_{p_{eff}} = \left(C_{p_{binder}} m_{f_{binder}} + C_{p_{DU}} m_{f_{DU}} + C_{p_{DE}} m_{f_{DE}} + C_{p_{Q-cel}} m_{f_{Q-cel}} \right) \cdot \left(1 + A \cdot m_{f_{binder}} m_{f_{filler}} \right) \quad (5.34)$$

In Equation 5.34, A is a correction factor, which for spherical fillers should be set to 0.2. The total mass fraction of the fillers, $m_{f_{filler}}$ can be calculated with $m_{f_{filler}} = m_{f_{DU}} + m_{f_{DE}} + m_{f_{Q-cel}} = 1 - m_{f_{binder}}$. As said the specific heat values of the individual components thus have to be known. The material decomposition of the various components was already explained in Section 5.3 for which the specific heat capacity values of the separate materials were listed in Table 5.1.

5.5.1. Specific heat capacity of epoxy-amine resins

In Table 5.1 the specific heat capacity of the epoxy-amine resins had been listed as 2217 J/kgK. This value had already been selected by Eversdijk [64], who took the average of three values (2.0, 2.30 & 2.35 J/kgK) he found in literature for epoxy-amine resins (before the vitrification phase) [105, 120, 121]. A remark should be made on this; one of the assumptions made in Section 5.1.1 was that; "*Thermal material properties are assumed to be constant, being independent of time and temperature.*" In reality the specific heat capacity of an epoxy resin undergoes a phase transition during cure, where the C_p can drop by around 10% at the vitrification point (vitrification was explained in Section 2.3.1). However, before this point C_p is not strongly affected by the degree of cure or temperature [105]. Because this is also the region of interest in the numerical model analysis the assumption of using a constant C_p is acceptable, this will also be confirmed by the C_p sensitivity study performed in Section 5.9.

5.5.2. Effective specific heat capacity of microspheres

The effective specific heat of a single DU, DE and Q-Cel microsphere, defined by $C_{p_{DU}}$, $C_{p_{DE}}$ & $C_{p_{Q-cel}}$ can be calculated with the simple rule of mixtures that uses the mass fractions of the inner gas (m_{f_g}) and surrounding wall (m_{f_w}) as follows:

$$C_{p_{microsphere}} = C_{p_{gas}} m_{f_{gas}} + C_{p_{wall}} m_{f_{wall}} \quad (5.35)$$

The mass fractions can be determined with the known material densities of the gas (ρ_g) and wall (ρ_w) and the volume fraction of the gas v_g that was calculated with Equation 5.32. As an example m_{f_g} is calculated with Equation 5.36. Using the same analogy, m_{f_w} can be obtained.

$$m_{f_g} = \frac{\rho_g v_g}{\rho_g v_g + \rho_w (1 - v_g)} \quad (5.36)$$

The effective specific heat values for the different microspheres are presented in Table 5.9. The obtained values lie close to the ones of the microsphere wall material (shown in Table 5.1), this is logical since the relatively dense material of the wall gains a high mass fraction.

Table 5.9: Effective specific heat $C_{p_{1microsphere}}$ for the different type of microspheres present in EX-CORE.

Type of microsphere	$C_{p_{1microsphere}}$ [J/kgK]
Q-Cel 5028	751.4
920 DE 80d30	1339.8
031 DU 40 (unexpanded)	1300.7
043 DU 80 (unexpanded)	1300.5

5.5.3. Effective specific heat of EX-CORE

Now that the specific heat capacities of the individual EX-CORE components have been obtained, the effective specific heat capacity of different EX-CORE mixtures ($C_{p_{eff}}$) can be determined. First, the mass fractions of the specific EX-CORE mix are calculated based on the known volume fractions and bulk densities of the microspheres and epoxy matrix. Finally, $C_{p_{eff}}$ of EX-CORE is calculated with Equation 5.34.

Evaluation of DU content variations

$C_{p_{eff}}$ will change when the DU percentage and/or grade is altered. In addition the chosen type of epoxy matrix will also influence the final $C_{p_{eff}}$ of the EX-CORE mixture since the mass fractions are altered. The effect of these variations is presented in Table 5.6 were $C_{p_{eff}}$ values for several compositions of the 270-optimal mix are given.

Table 5.10: Effective specific heat capacity $C_{p_{eff}}$ for examples of 270opt mixes, with varying DUvol.%, two type of DU grades and two type of resin systems (Resin nr.1 and resin nr.5).

DU vol. %	$C_{p_{eff}}$ [J/kgK]			
	031DU40		043DU80	
	Resin Nr0	Resin Nr5	Resin Nr0	Resin Nr5
1	1798	1778	1796	1776
5	1777	1757	1768	1748
10	1749	1730	1733	1713

It can first of all be observed that when the volume fraction of DU increases, the effective specific heat capacity of EX-CORE decreases. This is because then the mass fraction of the epoxy matrix (with highest $C_{p_{eff}}$ of all components) decreases. For a DU increase from 1 to 10% the $C_{p_{eff}}$ decrease is however minor, with only 2.7-3.6%. Secondly, it can be noted that the $C_{p_{eff}}$ values are somewhat lower for resin system nr.5 when compared to resin system 0. This is because resin system nr.5 has a slightly lower ρ_{matrix} (see Table 5.1) which results again in a lower mass fraction of the epoxy matrix. A similar reasoning can be done to explain the higher $C_{p_{eff}}$ values of 270opt mixes with 031DU70 compared to similar ones with 043DU80. This is because of the lower true density of 031DU40, which results in a higher mass fraction of the epoxy matrix.

Remark that the expansion state of DU did not have to be taken into account since it does not have an influence on the $C_{p_{eff}}$ values. This is because when DU expands, only the volume fractions of the DU microsphere will change, but the relative mass fractions stay unaffected. Therefore the effective specific heat of "expanded" DU is the same as for the "unexpanded DU".

Comparison of $C_{p_{eff}}$ for different EX-CORE mix compositions

The effective specific heat capacities for the same EX-CORE mix compositions as presented earlier in Table 5.8 are evaluated in this paragraph. Note that the comparison is done for EX-CORE mixes all containing the SR 1280/Ancamine® 2442 binder (resin nr. 5) and the new 043DU80 grade. Because now variations in mass fractions (in stead of volume fractions) will influence $C_{p_{eff}}$, the obtained mass fractions of those mixes are presented in Table 5.11 and the resulting $C_{p_{eff}}$ values are listed. The $C_{p_{eff}}$ values for the three EX-CORE mixes all vary around 1750J/kgK. It can be seen in Table 5.9 that Q-Cel has the lowest specific heat of all microspheres (751J/kgK) while the epoxy binder has the highest specific heat (2217J/kgK) of all components. The mass fraction of resin increases at increasing mix density, but at the same time DE is traded for Q-Cel, which counteracts the effect of $C_{p_{eff}}$ increase when resin content increases.

Table 5.11: Effective specific heat $C_{p_{eff}}$ for the EX-CORE mixes of Table 5.8 but now the corresponding mass fractions are given.

EX-CORE mix	Mix mass fractions				$C_{p_{eff}}$ [J/kgK]
	Resin (Nr.5)	DU (043DU40)	DE	Q-Cel	
230opt	0.582	0.090	0.033	0.296	1753.5
270opt	0.593	0.077	0.020	0.310	1754.9
330opt	0.599	0.063	0.007	0.332	1747.3

5.5.4. Note on validation of the effective specific heat capacity of EX-CORE

Eversdijk [64] performed in his research DSC experiments to "validate" the specific heat capacities of EX-CORE mixtures predicted by the theoretical model. He tested 5 cured EX-CORE samples with varying mix compositions and performed the tests in accordance with ASTM standard E2169 [141]. Because only cured samples were allowed to be tested in the *Perkin Elmer Sapphire DSC standard 115V* DSC apparatus, in the model analysis the specific heat capacity of the resin had to be set to the post vitrified value of 1850J/kgK to be able to compare with the theoretical results[121].

When comparing the experimental and theoretical $C_{p_{eff}}$ results, difference between +31.2% and -15.8% were obtained, and such the model could not be validated based on these results. Eversdijk reasoned that these large deviations are most probably caused by weight variations and geometry of the sample; First of all, differences in surface contact of the powdery EX-CORE sample and the bottom of the DSC crucible will change the heat flow to EX-CORE. This is also in contrast to the perfect flat surface of the sapphire standard used for calibration. In addition, when the lid is pressed with more or less force, the surface contact changes as well. Secondly, the weight of the EX-CORE sample could also contribute to the variations. For example McHugh et al. [105] concluded that the optimal sample weight is accomplished if the product of the sample mass and its specific heat is equal to the similar product of the sapphire standard. This was only achieved for one sample, for which the smallest deviation (-6.8%) from the theoretical results was achieved. Additionally the sample with the largest weight deviation also gained the largest $C_{p_{eff}}$ deviation. Although that the experimental $C_{p_{eff}}$ values were in the range of the model prediction, the large deviations did not allow validating the theoretical results for $C_{p_{eff}}$.

Nonetheless, a sensitivity study had been performed by Eversdijk [64]. From his results he concluded that variations of $C_{p_{eff}}$ for the expected bound of EX-CORE mixes (1862-1774J/kgK) only lead to a temperature variation about 4°C. From this he concluded that highly accurate experimental validation performed by an experienced lab technician is not of the highest priority. Since the numerical model has been updated in the current research, a new sensitivity study had to be performed on $C_{p_{eff}}$ to confirm the effect of $C_{p_{eff}}$ variations. This process is explained in Section 5.9. The obtained results also support the conclusion made by Eversdijk.

5.6. Implementation of cure kinetics into the numerical thermal model

In Section 5.1.2 it was addressed that the exothermic heat release during curing of the epoxy resin is implemented in the energy balance equation as follows;

$$T^{i+1} = T^i + \frac{\Delta t}{C\Delta x\Delta y} (\dot{Q}_N + \dot{Q}_E + \dot{Q}_S + \dot{Q}_W + \dot{q}_{int}^i \Delta x \Delta y) \quad (5.37)$$

here \dot{q}_{int} is the internal heat generation rate of the element during time step Δt . To calculate this term, first the cure kinetic parameters as determined in Section 4.4.1 are implemented in the governing equation of the modified autocatalytic model:

$$\frac{d\alpha}{dt} = (k_1 + k_2\alpha^m)(1 - \alpha)^n \quad (5.38)$$

with

$$k_1 = A_1 e^{-\frac{E_1}{RT}} \quad (5.39)$$

$$k_2 = A_2 e^{-\frac{E_2}{RT}} \quad (5.40)$$

Equation 5.41 is used to determine \dot{q}_{int}^i [39, 45]:

$$\dot{q}_{int}^i = \rho_{epoxy} V_{epoxy} H_{Tspec} \left(\frac{d\alpha}{dt} \right)^i \quad [W/m^3] \quad (5.41)$$

in which ρ_{epoxy} [kg/m³] is the density of the selected epoxy matrix. These densities can be found in Table 5.3 for the specific resin mix ratios. V_{epoxy} is the epoxy volume fraction in an element, which is equal to the volume fraction used in EX-CORE. H_{Tspec} [J/kg] is the specific total heat of reaction. Values for H_{Tspec} in J/g can be found given in Table 4.3. $(\frac{d\alpha}{dt})^i$ is the reaction rate [1/s] at time step i . When multiplying the former terms $\rho_{epoxy} \cdot V_{epoxy} \cdot H_{Tspec}$ with $\frac{d\alpha}{dt}$ the amount of heat released per second for the element's volume is obtained in [W/m³].

Next to the temperature, the degree of cure α is also tracked for each element. This is done as follows:

$$\alpha^{i+1} = \alpha^i + \left(\frac{d\alpha}{dt} \right)^i \Delta t \quad (5.42)$$

here α^i is the degree of cure at the current time step i and α^{i+1} the degree of cure at the next time step $i+1$.

As already explained in the 9th assumption in Section 5.1.1: *A constant onset reaction temperature: independent of heat-up rate* is implemented in the numerical model for the Ancamine[®] 2337s & 2442. At temperatures below this onset reaction temperature, also referred as the (physical) thermal block temperature, exothermic reaction of the resin is prevented. To take this effect into account in the numerical model, a condition is implemented that prevents heat-generation to take place at a node if the current nodal temperature is below the specified onset reaction temperature of the resin. More specifically, this is then done by setting $\dot{q}_{int} = 0$ in the model analysis.

5.7. Updates and alterations w.r.t. previous numerical thermal model by Eversdijk

The numerical thermal EX-CORE model created by Eversdijk [64] formed the basis for the latest version of the numerical model used in the current research. The model has been updated and some erroneous inputs and calculations have been corrected. In Section 5.7.1 an overview of all the alterations w.r.t. to the previous model by Eversdijk is given. Then in Section 5.7.2 the effect of the alterations is evaluated by comparing the output data of the previous model with the updated model for the original EX-CORE formulation.

5.7.1. Overview model updates

1. Firstly, material properties and cure kinetics of new epoxy systems have been implemented. Also a new grade of Expancel[®] DU, namely 043DU80 is included. The user can select the required epoxy system and DU grade at the start of the analysis.
2. Secondly, for the powder hardeners Ancamine[®] 2337s & 2442 a constant onset reaction temperature had to be implemented in the model analysis. For more information on this see the corresponding assumption in Section 5.1.1 and the implementation explained in Section 5.6.
3. In the previous model version an incorrect true density of 120kg/m³ for 031DU40 had been implemented. This value would be impossible since this is lower than the 370kg/m³ measured bulk density of 031DU40. An updated true density of 569kg/m³ is now used. How this value is obtained is explained in Section 5.4.2.
4. A mistake had been spotted in the calculation of the gas volume fraction v_g of DU in the expanded state. Namely, when using Equation 5.32 to obtain v_g , not only should the true density ρ_{true} be divided by 37 (DU can expand upto 37 its volume [63]) but also should the gas density ρ_g be divided by 37 since DU expansion is caused due to the expansion of the inner gas, and so the gas density decreases.
5. In the last version of Eversdijk his model, he implemented a time scaling factor of 0.85 ($t_{new} = t_{unscaled} / 0.85$) to obtain time to peak values within 10min of experimental results. As will become clear from the new validation results discussed in Chapter 9, a time scaling factor is no longer required in the current model analysis.

6. A mistake has been discovered w.r.t. to the way in which the nodal temperatures and degree of cure α had been updated. In the previous version of the model, the nodal temperature and degree of cure had been calculated as presented in Algorithm 1. Remark that the temperature and degree of cure values for every element in the nodal network are stored in an (N x M) matrix, here referred to as T_n and α_n , respectively.

Algorithm 1: Nodal temperature (T_n) and degree of cure (α_n) matrix incorrectly updated

```

Import data, model initialization,  $k_{eff}$  &  $C_{peff}$  calculation etc. ;
while  $t < \text{Max. simulation time}$  do
  for  $x=1:M$  do
    for  $y=1:N$  do
      Calculating  $\frac{d\alpha}{dt}$ ,  $\dot{q}_{int}^i$ ,  $\dot{Q}_N$  etc. ;
       $T_n^i(y, x) = T_n^i(y, x) + \frac{\Delta t}{C\Delta x\Delta y} (\dot{Q}_N + \dot{Q}_E + \dot{Q}_S + \dot{Q}_W + \dot{q}_{int} \Delta x \Delta y)$ ;
       $\alpha_n^i(y, x) = \alpha_n^i(y, x) + \left(\frac{d\alpha}{dt}\right)^i \Delta t$ ;
    end
  end
   $t = t + \Delta t$ 
end

```

It can be seen in Algorithm 1 that the temperature matrix T_n^i (& similarly α_n^i) at the current time step (i) is incorrectly updated anytime a nodal location (y, x) is analyzed. So for example when the temperature at the next nodal location in the loop i.a. (y+1, x) is analyzed (still at the current time step i), the temperature of its neighboring node (y, x) had already incorrectly been updated with its temperature at the next time step (i+1). This has i.a. as a consequence that the temperature progresses faster in time and also that the temperature distribution is inaccurate. In analogy this also applies for the degree of cure. However, as becomes clear in Section 5.7.2 the effect is only minor.

Algorithm 2: Nodal temperature (T_n) and degree of cure (α_n) matrix correctly updated

```

Import data, model initialization,  $k_{eff}$  &  $C_{peff}$  calculation etc. ;
while  $t < \text{Max. simulation time}$  do
  for  $x=1:M$  do
    for  $y=1:N$  do
      Calculating  $\frac{d\alpha}{dt}$ ,  $\dot{q}_{int}^i$ ,  $\dot{Q}_N$  etc. ;
       $T_n^{i+1}(y, x) = T_n^i(y, x) + \frac{\Delta t}{C\Delta x\Delta y} (\dot{Q}_N + \dot{Q}_E + \dot{Q}_S + \dot{Q}_W + \dot{q}_{int} \Delta x \Delta y)$ ;
       $\alpha_n^{i+1}(y, x) = \alpha_n^i(y, x) + \left(\frac{d\alpha}{dt}\right)^i \Delta t$ ;
    end
  end
   $T_n^i = T_n^{i+1}$ ;
   $\alpha_n^i = \alpha_n^{i+1}$ ;
   $t = t + \Delta t$ ;
end

```

The correct way of updating the nodal temperature and degree of cure is presented in Algorithm 2. This is also how it is implemented in the latest version of the numerical model. It can be seen that while looping all the nodal locations (x, y) at the current time step (i), the temperatures and degrees of cure for the next time step (i+1) are stored in a separate matrix T_n^{i+1} and α_n^{i+1} respectively. Only when all the nodal locations have been analyzed, the T_n^i and α_n^i matrix are overwritten with the updated values stored in the T_n^{i+1} and α_n^{i+1} matrices. This procedure is repeated for the next time step.

5.7.2. Comparison output data original vs updated numerical thermal model

To investigate the effect of the updates made to the numerical model, output results of the former and updated numerical model are compared. The comparison is done for 230opt, 270opt and 330opt mix formulations containing the original epoxy matrix system Ancarez[®] RZ4010/ Ancamide[™] and the Expancel[®] 031 DU 40 grade, all isothermally cured at 110°C. The comparison is also done for 3 different sample thicknesses of the 270-opt mix. An overview of the comparison test variations is given in Table 5.12. To enable proper comparison, all "former" model predictions are obtained with no time scale factor included.

Table 5.12: Overview of EX-CORE thermal model comparison test variations

	Mix type	h [mm]
test 1	270opt	30
test 4	270opt	55
test 5	270opt	80
test 2	230opt	30
test 3	330opt	30

Table 5.13: Comparison of effective- thermal conductivity k_{eff} and specific heat Cp_{eff} calculated with former and updated model

Mix type	k_{eff} [W/mk]			Cp_{eff} [J/kgK]		
	Former	Upd.	Diff.	Former	Upd.	Diff.
230opt	0.093	0.097	-0.004	1759.9	1750.1	9.8
270opt	0.110	0.114	-0.004	1763.5	1753.2	10.3
330opt	0.136	0.141	-0.005	1758.6	1748.6	10.0

As illustrated in Table 5.13, updates nr. 3 listed in Section 5.7.1 slightly affects the predicted effective thermal conductivity (k_{eff}) and specific heat (Cp_{eff}) of EX-CORE with a maximum difference of 0.005W/mK and 10.3J/kgK, respectively. As will become clear from the model sensitivity study performed in Section 5.9, these differences have insignificant effect on the resulting temperature distribution accuracy. More specifically, to obtain an model accuracy of 5°C k_{eff} should be known within 0.092W/mK and similarly Cp_{eff} should be known within 152J/KgK. This is hence both more than a factor 10 higher than the observed differences in Table 5.13.

The effect of update nr. 6 was evaluated by comparing four different output parameters in the former and updated model. Namely, the maximum temperature in the center of the sample (T_{center}) and at 90% sample height (T_{edge}) and also the time to reach the peak temperature (t_{peak}) and 98% degree of cure everywhere throughout the sample. The results for all the performed model simulations are summarized in Table 5.14. It can be seen that the updated model predicts T_{center} 2.7°C to 5.1°C lower than the former model did. With the highest deviation obtained for the 80mm thick 270-opt mix test. Also T_{edge} predictions are slightly lower then before, with a maximum difference of 2.4°C obtained for the 230-opt mix sample. Interestingly, update nr. 6 has only minor effect on the predicted time to peak and 98% cure time. Maximum differences of only 0.7min and 0.6min, respectively are obtained for the 80mm thick sample. As said the updated numerical model predictions will be validated with experimental data as will be discussed in Chapter 9.

Table 5.14: Comparison of maximum center temperature T_{center} , maximum edge temperature T_{edge} (at 90% sample height), time to peak t_{peak} and 98% cure time calculated with former and updated numerical model

	Max. T_{center} [°C]			Max. T_{edge} [°C]			t_{peak} [min]			98% cure time [min]		
	Former	Upd.	Diff.	Former	Upd.	Diff.	Former	Upd.	Diff.	Former	Upd.	Diff.
test 1	167.5	163.5	4.0	141.5	139.5	2.0	16.9	17.1	-0.2	44.1	44.3	-0.2
test 4	172.1	167.9	4.2	136.5	135.1	1.4	28.8	29.3	-0.5	44.6	44.8	-0.2
test 5	178.5	173.5	5.1	132.7	131.6	1.1	38.6	39.3	-0.7	48.7	49.3	-0.6
test 2	166.2	161.3	4.9	139.5	137.1	2.4	16.5	16.8	-0.3	44.5	44.7	-0.2
test 3	167.9	165.3	2.7	143.7	142.4	1.3	17.4	17.4	0.0	43.5	43.7	-0.2

5.8. Verification of numerical thermal model

As discussed in the previous section, the numerical model has been modified since the last verified model version created by Eversdijk [64]. Because the sequence has been altered in which the nodal temperatures (& degree of cure) are updated, it is necessary to once more verify the numerical solution with an analytical solution that is known to be correct under certain simplified geometries and boundary conditions. The verification procedure presented in this section is similar to the one previously performed by Eversdijk [64]. A similar method has also been used by Bogetti & Gillespie [40] to verify their two-dimensional cure model for thick thermosetting composites. More details on the analytical solution principles can be found in [123]. Unfortunately there are no analytical solutions available for two-dimensional transient heat-transfer problems that involve an internal heat generation. For model verification it is therefore required to put the internal heat generation term $\dot{q} = 0$. In addition when insulated boundary conditions are applied at the edges of the two-dimensional numerical model it can be compared with analytical one-dimensional transient heat transfer solutions [40]. Such solutions are available in a graphical format, known as Heisler charts. A graphical-analytical solution exist for an infinitely long plane wall with thickness $2L$. A first set of charts represent the temperature at the mid plane of the wall at a certain time, while a second set of charts is available to determine the temperature at any location away from the mid plane [123]. Both charts can be found in Appendix D, while the method and results are covered here. The analytical results are then used to evaluate the convergence of the numerical model at different mesh sizes and time steps.

5.8.1. Graphic-analytical one-dimensional solution using Heisler charts

Before the Heisler charts can be used, the Biot- and Fourier numbers should be obtained. Both are dimensionless parameters which are based on material properties. The Biot number Bi [-] can be calculated with equation 5.43:

$$Bi = \frac{hL}{k} \quad (5.43)$$

with L [m] the half wall thickness, h the convection coefficient [W/m^2K] and k the thermal conductivity [W/mK]. The Heisler charts are only valid when the Fourier number $F_0 > 2$ [123]. F_0 [-] is given by equation 5.44:

$$F_0 = \frac{\alpha t}{L^2} \quad (5.44)$$

where t [s] is time and α represents the thermal diffusivity given by equation 5.45:

$$\alpha = \frac{k}{\rho C_p} \quad (5.45)$$

with C_p the specific heat [J/kgK] and ρ [kg/m^3] the density. When the previous parameters are known, the value of θ_0 can be read from the first set of Heisler charts for each time step. θ_0 can then be used to relate the boundary temperature at the wall edges to the temperature at the mid plane of the wall through equation 5.46:

$$\theta_0 = \frac{T_0 - T_\infty}{T_i - T_\infty} \quad (5.46)$$

in which T_0 is the new mid plane temperature, T_∞ the temperature of the surrounding medium and T_i the initial temperature of the material, all in $^\circ C$. Next, a second set of Heisler charts can be used to determine θ_y . This parameter can then be used to relate the temperature at the mid plane of the wall to the temperature at any location away from the wall, as presented in equation 5.47:

$$\theta_y = \frac{T_y - T_\infty}{T_0 - T_\infty} \quad (5.47)$$

in which T_y [$^\circ C$] is the temperature away from the mid plane of the wall. In this analysis locations at $\frac{y}{L} = 0.4, 0.6, 0.8$ are selected. For EX-CORE, the convection coefficient h is unknown. However, when a sudden change in surface temperature is applied, the convection coefficient becomes infinite, making the Biot number infinite as well. T_∞ has to be replaced by the imposed surface temperature T_s . This does not require the convection coefficient to be known. So when using the first set of Heisler charts the line corresponding to

$Bi^{-1}=0$ should be used. The Fourier number on the other hand can be determined at the selected interval times. The following parameter values were selected to generate the verification data from both the numerical model and the graphical-analytical Heisler chart solutions:

- $k = 0.12 W/mK$
- $C_p = 1700 J/kgK$
- $\rho = 260 kg/m^3$

These values match closely the "270opt" mix with a 4vol.% DU content, as frequently used in this research. As total wall/sample thickness $2L=30mm$ was used. The initial temperature T_i was set to $0^\circ C$ with an implied top an bottom surface temperature of $30^\circ C$. To obtain the Fourier numbers for the first set of Heisler charts, time steps from 200s were used up to a maximum of 2000s. This combination of time step and half thickness L makes that the Fourier number is just exceeding 0.2 at the first 200s time step, ensuring the validity of the Heisler charts.

5.8.2. Convergence of numerical model solution

The mesh geometry and boundary conditions used to generated the numerical model verification data is adjusted to represent the one-dimensional plane wall. A schematic of the mesh geometry and boundary conditions can be seen in Figure 5.12.

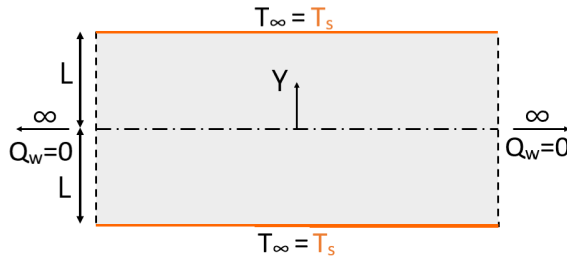


Figure 5.12: Schematic of mesh geometry, boundary conditions and orientation y/L away from mid plane.

Mesh size [mm]	$\Delta t / \Delta t_{crit}$
10	1
	1/2
5	1/4
	1/8
2.5	1/16
	1/32
1.25	1/64

Figure 5.13: Schematic of convergence study procedure; selection of mesh size and critical time step factor reduction.

The immediate surface temperature at the top and bottom edge nodes is fixed to $T_s = 30^\circ C$, while the initial temperature of all other nodes is set to $T_i = 0^\circ C$. At the left and right sides insulation boundary conditions have to be applied, so $Q_w = 0$ at the right node edge and $Q_E = 0$ at the left node edge. As explained in Section 5.1.3, the maximum allowable time step Δt_{crit} for the explicit method to be stable can be determined by equation 5.48:

$$\frac{\alpha \Delta t_{crit}}{l^2} \leq \frac{1}{4} \quad (5.48)$$

However, model convergence is not guaranteed. Therefore a convergence study on both mesh size and time step is performed to find out which combination of mesh size and time step results in convergence to the exact numerical solution. Note that according to equation 5.48, when the mesh size $l = \Delta x = \Delta y$ is altered, the minimum critical time step for stability Δt_{crit} is influenced. This implies that both the mesh size and time step has to be studied simultaneously. First an initial mesh size l of 10mm has been selected. Next, the critical time step required for stability t_{crit} is calculated using equation 5.48. After obtaining the numerical solution for this combination of mesh size and time step, the time step is halved and a new solution is calculated. For the same mesh size this process is repeated until the time step becomes $\frac{1}{64} \Delta t_{crit}$. Then the mesh size is halved, and the new Δt_{crit} for this mesh size is determined. The time step is then again stepwise reduced until $\frac{1}{64} \Delta t_{crit}$. This procedure is continued for a mesh size up to 1.25mm. A schematic of this procure is shown in Figure 5.13.

For all the 28 combinations of mesh size and time step factor, the error with the analytical solution is recorded at each of the four locations $\frac{y}{L} = 0.4, 0.6, 0.8$ and at each time step (1 to 2000s in steps of 200s). The maximum absolute errors for each mesh size and time step factor are recorded and presented in Table 5.15, starting from a mesh size of 5mm. An error of less than 2% in the numerical solution is deemed sufficiently accurate since the analytical solution had been obtained in a graphical manner. In addition, the solution is found to be sufficiently converged when the error change for the next mesh size/time step iteration is less than 1%.

Table 5.15: Maximum absolute errors of numerical model w.r.t. analytic-graphical solution at different mesh sizes and time steps.

Mesh size [mm]	$\Delta t / \Delta t_{crit}$					
	1	1/2	1/4	1/8	1/16	1/32
5	23.35%	20.88%	13.14%	9.30%	9.56%	9.69%
2.5	9.36%	8.70%	7.04%	4.60%	4.39%	4.39%
1.25	4.29%	4.13%	3.35%	2.52%	1.84%	1.84%

From Table 5.15 it can be seen that the numerical solution is sufficiently converged at a mesh size of at least 1.25mm in combination with a time step of $\frac{1}{16} t_{crit}$. This gives a maximum error of 1.84%. A further reduction in time step is not required, as this will reduce the error by less than 0.01%. So for all numerical simulations performed during this research, the verified mesh size of 1.25mm will be used in combination with a time step of $\frac{1}{16} t_{crit}$. The comparison of the numerical and analytical solution at this combination of mesh size and time step is shown in Figure 5.14.

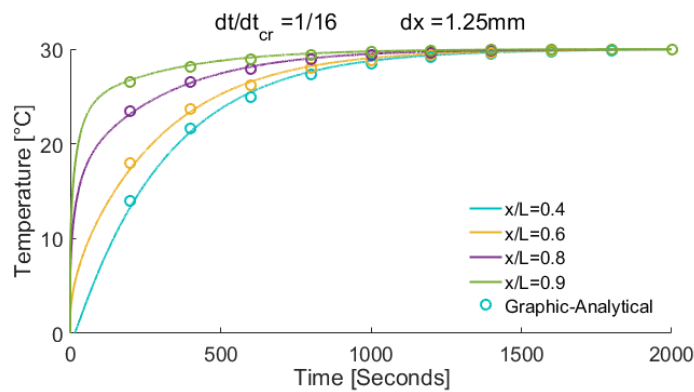


Figure 5.14: Converged numerical model solution at mesh size 1.25mm and time step $\frac{1}{16} \Delta t_{cr}$

The cure kinetic model which is implemented in the numerical model could not be verified since comparative exact analytical data is not available. Nonetheless, the numerical solutions could be compared with experimental data. This validation is covered in Chapter 9 and should give a good indication on the accuracy of the overall numerical model, including the heat generation term.

5.9. Numerical model sensitivity on thermal conductivity and specific heat capacity

A sensitivity study had been performed by Eversdijk [64] to evaluate how accurately the effective thermal conductivity (k_{eff}) and specific heat capacity (C_{peff}) of EX-CORE have to be calculated. From his study Eversdijk concluded that in order to obtain a numerical temperature distribution accuracy of 5°C, the effective thermal conductivity and specific heat capacity value of EX-CORE have to be determined with 0.03W/mK and 143J/kgK accuracy, respectively. However, these results do not necessary apply any more for the current model with the updates and differences discussed in Section 5.7. Therefore a new sensitivity study is performed for the latest version of the model created by the author.

To assess how sensitive the updated numerical model is to variations in k_{eff} and C_{peff} , only these parameters were separately varied over the expected boundaries obtained for the mixes presented in Tables 5.8 and 5.11. This results in a range for k_{eff} from 0.098 to 0.145W/mK and for C_{peff} from 1747.3 to 1754.9J/KgK. The temperature progress is plotted in Figure 5.15 for a 30mm thick EX-CORE sample cured at an isothermal temperature of 110°C and with as matrix resin system nr. 5 (T_{onset} set at 83°C) and 7.5% of the new 043 DU 80 grade. The maximum center & top edge temperatures for the range of k_{eff} and C_{peff} are given in Table 5.16.

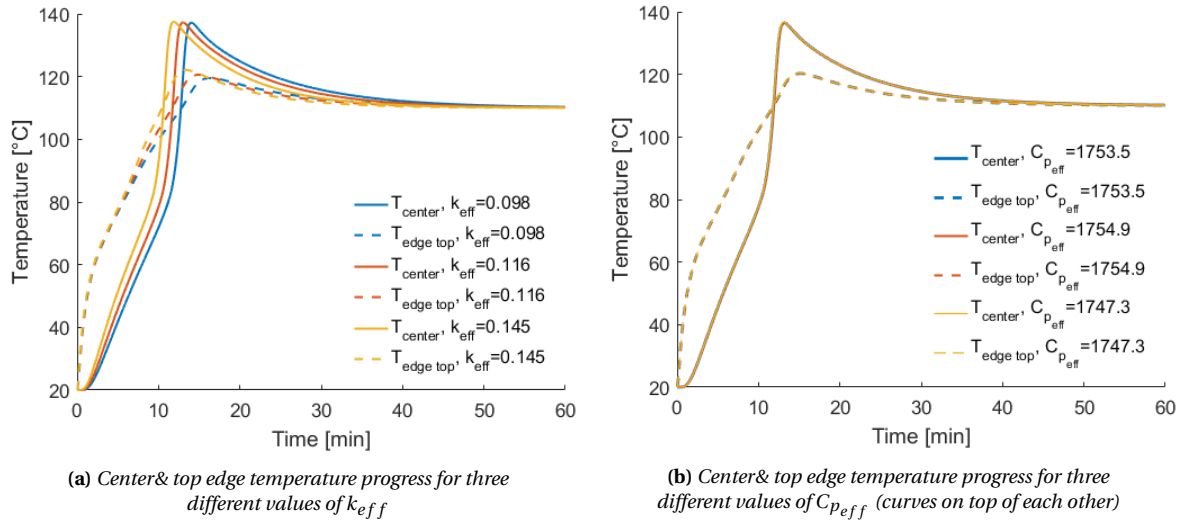


Figure 5.15: Model sensitivity w.r.t. changes in a) k_{eff} and b) C_{peff}

Table 5.16: Sensitivity of maximum center & top edge temperature for the range of k_{eff} and C_{peff} .

EX-CORE mix	k_{eff} [W/mK]	T_{center} [°C]	$T_{edgetop}$ [°C]	C_{peff} [J/KgK]	T_{center} [°C]	$T_{edgetop}$ [°C]
230	0.098	137.2	119.5	1753.5	136.5	120.3
270	0.116	137.3	120.6	1754.9	136.5	120.3
330	0.145	137.5	122.1	1747.3	136.7	120.4

It can be seen from the graphs that the k_{eff} range causes a larger variation in temperature then C_{peff} does, for which the curves are approximately on top of each other. This is also because the expected C_{peff} values are quite close together. Nevertheless, for the expected k_{eff} range, the maximum temperature difference is only 2.6°C for the top edge. It can be concluded that to obtain an accuracy of 5°C w.r.t. the effective thermal conductivity, the value of k_{eff} should be determined within 0.092W/mK. For effective specific heat the value needs to be determined with 152J/kgK to obtain a 5°C accuracy. These values are in the range of the ones obtain by Eversdijk [64].

5.10. Flow chart of the numerical model and output example

In this section an overview of the required inputs and resulting outputs of the transient FDM thermal EX-CORE model is given in the form of a flow chart as shown in Figure 5.16. Here the inputs that the user can choose at the start of the analysis are shown in (light-) blue such as mix composition, geometrical properties, initial conditions and cure cycle. During the analysis, a simulation of the two-dimensional transient temperature distribution of the sample is shown. An example of such a temperature distribution is shown in Figure 5.18. When the modal analysis is finished, an overview of the nodal temperatures and degrees of cure versus time is plotted. An example of such a plot is given in Figure 5.17. The temperature values should be read from the left y-axis, while the degree of cures values should be read from the right y-axis. Note that the 98% degree of cure time indication is always the time when at least 98% degree of cure is reached in every location/node in the sample.

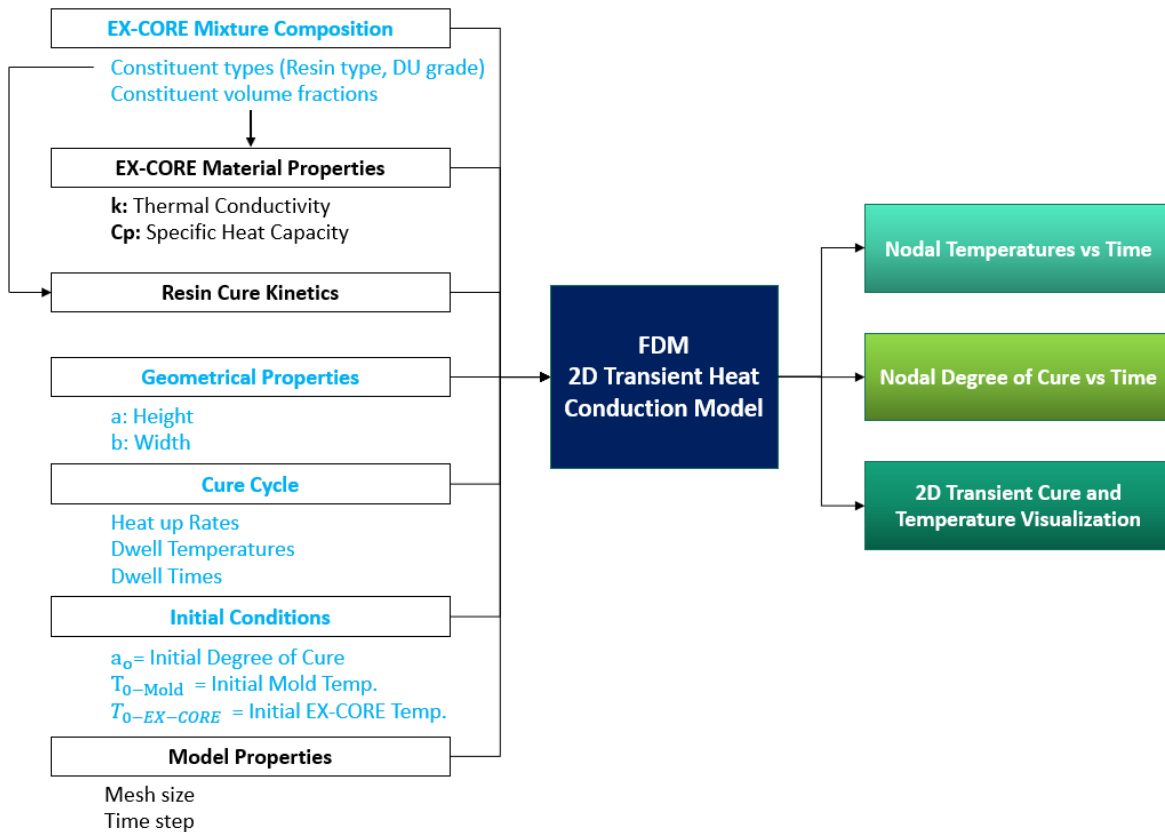


Figure 5.16: Flow chart of the numerical EX-CORE model. The required user inputs are indicated in (light-) blue.

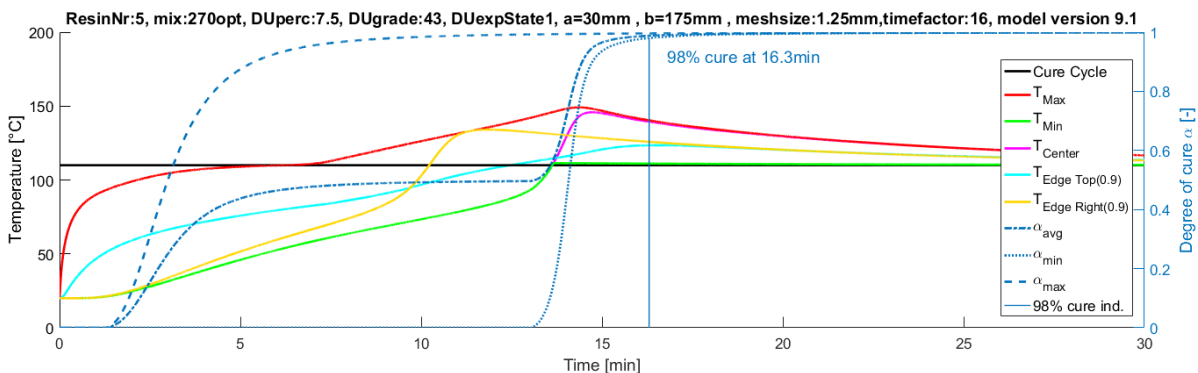


Figure 5.17: Example output plot from the numerical model, showing temperature and degree of cure plotted versus time for various locations in the sample.

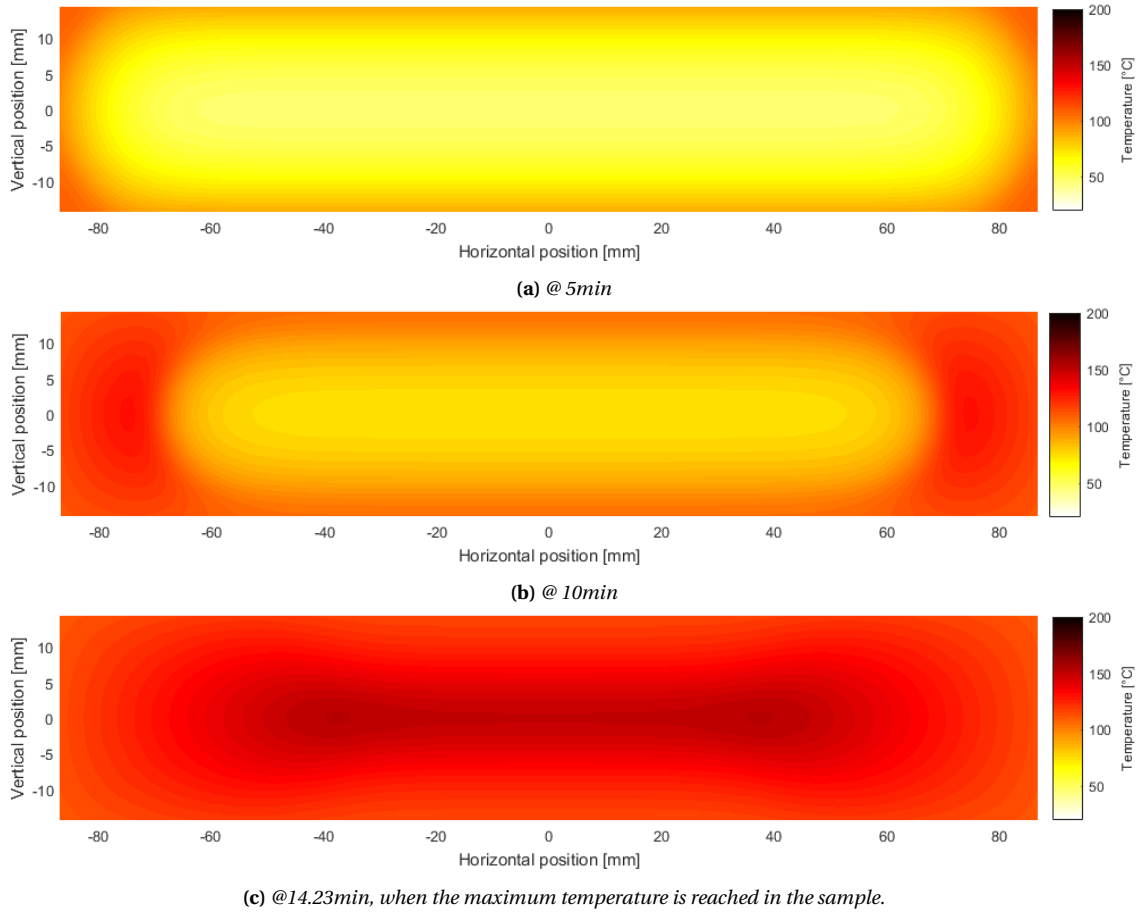


Figure 5.18: Example of 2D transient temperature distribution visualization at various moments in time for the example shown in the graph of Figure 5.17

5.11. Conclusions

A two-dimensional transient finite difference model was developed that allows simulating the temperature and degree of cure distribution over time for a specific EX-CORE mix and sample geometry under a specified cure cycle. The energy balance method was used to establish the governing equation with internal heat generation caused by the exothermic reaction of the epoxy resin. The reaction behavior was experimentally measured with DSC and implemented in the model using the theory of cure kinetics. Theoretical models were also implemented to determine the effective thermal conductivity and specific heat capacity of the EX-CORE mixture. Remark that the original numerical model created by Eversdijk [64] was updated and some faulty input parameters and calculation methods were corrected. The working of the (simplified) numerical model therefore again needed to be verified with an analytical solution. When using a mesh size of at least 1.25mm in combination with a time step of $1/16 t_{crit}$, a converged numerical solution was obtained with an error of less than 2% with the analytical solution. A sensitivity study was performed to evaluate how accurately the effective thermal conductivity and specific heat capacity have to be obtained. It was concluded that to obtain an accuracy of 5°C, they should be determined with 0.092W/mk and 152J/kgK respectively. The numerical model will be validated with experimental results, however this will be covered in Chapter 9. In that chapter more conclusions on the overall accuracy of the numerical model w.r.t. experimental results are given. Remark that the updated model code is written in MATLAB as Eversdijk wrote the original code in MATLAB. However, the model does not make use of MATLAB specific functions and so it can be rewritten in any open source software such as PythonTM or Scilab.

6

Test phase 1: Exploratory isothermal EX-CORE curing with new epoxies

From Chapter 4 it became clear that three types of hardeners; the SZ 8528, the Ancamine[®] 2337s and the Ancamine[®] 2442 in combination with the SR 1280 resin might be suitable candidate matrices that could reduce the cure time of EX-CORE. As explained in this chapter some initial EX-CORE samples with these epoxies as matrix were produced to explore their compatibility with the microspheric fillers and the EX-CORE process. First, the methodology and experimental set-up will be discussed in Section 6.1. Similar procedures and tooling were also used for various other produced samples discussed in subsequent chapters. Secondly, in Section 6.2 an overview of the produced samples during the first test phase and discussion of the results will be given.

6.1. Methodology and experimental set-up

In this first test phase, several samples were produced in the same sample mold, all isothermally cured at 110°C. The only variable was the chosen resin system and the required cure time. During curing, the generated pressure (& core temperature) of EX-CORE was monitored with sensors. The used mold and sensor tooling are discussed in detail in Section 6.1.2. All the samples have the same base mix formulation, meaning that the used volume fractions of epoxy and fillers are the same for all samples. The "270-optimal" mix formulation was selected as explained in Section 6.1.1. How the EX-CORE mix, mold and samples are prepared and manufactured is briefly covered in Section 6.1.3. A more detailed step-by-step sample manufacturing procedure can be found in Appendix E. If not mentioned otherwise, the same experimental setup and sample manufacturing procedures as discussed in this chapter are also applied for subsequent sample production covered in following chapters.

6.1.1. EX-CORE base mix selection: "270-optimal" mix

The $\pm 270 \text{ kg/m}^3$, "270-optimal" mix formulation was selected in previous research by Berckmoes [57] and Eversdijk [64] based on its good processing characteristics and predicted optimal specific compressive properties at that density. More specifically, the mathematical model developed by Vial [63] predicted that this mix composition would result in the highest compressive properties at this foam density. Therefore it is referred to as the "270-optimal" mix. It was decided to use the 270-optimal mix as basis in the current research as well. Although that the resulting mix density might become different and mechanical properties might not be "optimal" anymore when using a different epoxy resin, this mix formulation should give the best chances of success. In addition, due to its extensive use in previous research, comparisons with previous EX-CORE experiments and/or products can be made. The pseudo-components of this "270-optimal" mix are given in Table 3.1. Note again that the pseudo-components refer to the mix formulation in which the DU content is not yet incorporated since it can be varied in accordance with the required pressure. To obtain the final true mix composition, the pseudo-component percentages should be multiplied with $(100 - \text{vol.}\% \text{ DU})/100$.

Table 6.1: Pseudo component volume percentages of the "270-optimal" mix

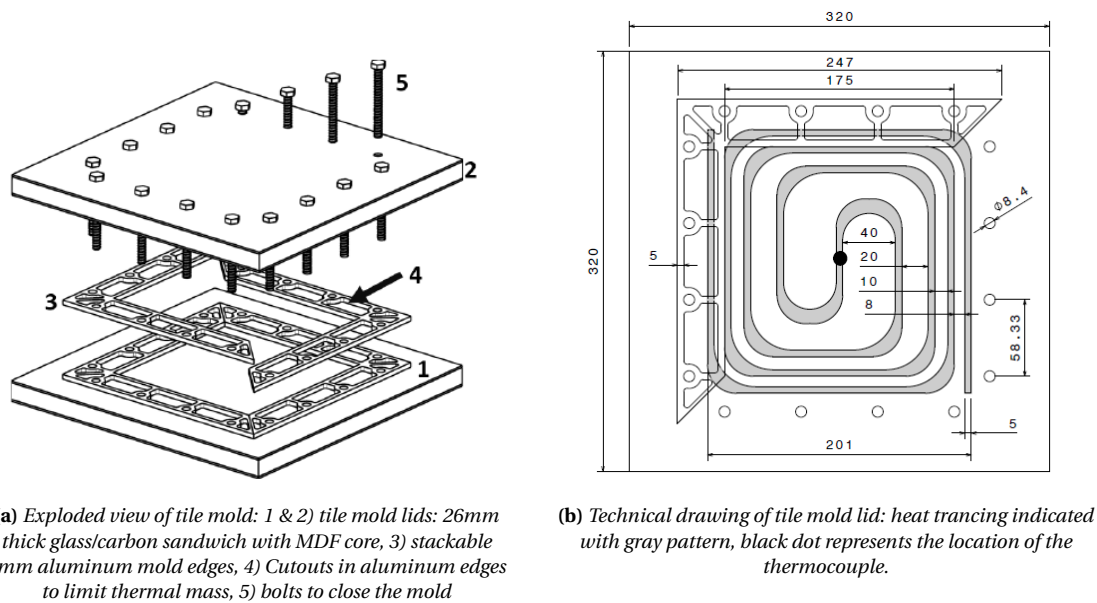
Mix	Resin	DE	Q-Cel
270-optimal	14.9%	32.3%	52.8%

6.1.2. Tooling for sample production

Two similar integrally heated sample molds, referred as "tile molds" were manufactured, re-designed and extensively used in previous parallel research by Berckmoes [57] and Eversdijk [64]. The tile mold allows for producing 175x175mm square samples ("tiles") of variable thickness ranging from 5 to 80mm with increments of 5mm. One of the tile molds was again extensively used in the current research. The original design and adaptations made to the tile mold in this and previous research are explained in the following paragraphs. The additional pressure and temperature sensors and the required Arduino® setup are also discussed.

Tile mold

The construction of the tile mold is explained by making use of Figure 6.1, where the numbers in brackets refer to the labels indicated in the exploded view in Figure 6.1a. First of all, the tile mold consist out of two stiff bottom & top lids that contain the heating elements (1 & 2). These lids are actually sandwich panels with a core of Medium Density Fiber Board (MDF) and facesheets made from a combination of carbon fiber/epoxy and glass fiber/epoxy. With 320x320mm they have some overlap with the side walls, which allows for placing insulation in between (1). The MDF core was selected because it has a relatively high compressive strength of 10MPa and is also cheaper compared to polymer foams. With a total laminate thickness of 26mm, Berckmoes [57] calculated the maximum deflection in the center to be 0.13mm at 10bar of EX-CORE pressure.

**Figure 6.1:** Drawings of tile mold used for sample production [64]

In both the upper and lower lid of the tile mold, carbon fiber heating braids and a type J thermocouple are integrated. In combination with the PI temperature controller (explained in Section 3.2.4), the mold can be heated according to a predefined temperature profile with any desired heating rate up to 3°C/min and maximum of 120°C. Higher heat-up rate should be possible since only around 40% of power is required to achieve a 3°C/min between 110°C and 120°C [57]. The carbon fiber heat tracing pattern (in gray) and central location of the thermocouple (black dot) are visualized in Figure 6.1b. To obtain a more even temperature distribution, it was chosen to implement a more dense spacing of the carbon fiber braid when approaching the edges of the mold, this to counteract the expected higher heat loss near the edges.

In between the two lids, 5mm thick stackable aluminum mold edges are placed, which allow for reaching a maximum stacking height of 80mm (3). The high thermal conductivity of the aluminum sides assists in transferring the heat from the mold lids to the sides of the sample. To minimize the thermal mass that has to be heated, large cut-outs were designed in the aluminum side edges (4). The resulting air pockets will also aid in limiting the transverse heat flows from inside the mold to the outside environment. Finally, to fasten the mold, originally 16 M8 bolts were used (5).

As already discussed in more detail in Section 3.2.7, Eversdijk [64] monitored the temperature distribution at the surface of the tile mold, and found that temperature variations as large as 28.5°C with peaks up to 134°C occurred when cured at 110°C (see also Figure 3.17). In the end, he proposed to use a 1.5mm aluminum cover plate in between the mold lid and the sample (shown in Figure 6.2b), which reduced the maximum temperature difference to only 3.3°C. This also significantly reduced the amount of surface porosity in the prepreg facing of samples from >40% to 2-6%. Another benefit of the aluminum plates is that they can be easily polished and/or replaced if necessary.

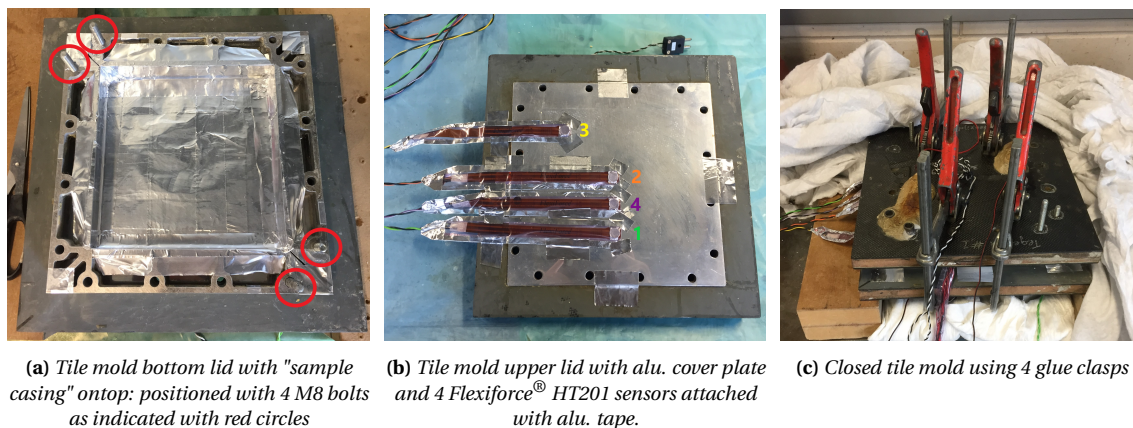


Figure 6.2: Pictures of tile mold used for sample production

To make the tile mold setup suitable for the current research, some alterations had to be done:

First of all, in previous research the EX-CORE mix could directly be placed into the cavity of the tile mold framed by the lower lid (including aluminum plate) and stacked aluminum side edges. Next, the mold was closed and consequently heated from room temperature. However, in the current research, the mold lids are preheated at a certain cure temperature. This allows for curing the samples at an isothermal cure temperature, without being limited by the maximum heat-up rate of the mold. Because it takes ± 5 -10 minutes to manually fill up the entire mold cavity with EX-CORE it is not possible to manually apply EX-CORE while the mold is being heated. Then part of the "snap-cure" EX-CORE paste would already start to cure and/or expand. The idea came up to create a conductive "sample casing" in which the un-cured EX-CORE mix could be prepared. The casing could then be quickly transferred in between the heated mold lids for curing. This sample casing was created from stacked aluminum edges which were connected to each other with aluminum tape to form a rigid casing. The bottom of the casing was created from two layers of aluminum tape. Due to the high thermal conductivity of the aluminum and minimal thermal mass, the heat from the hot tile mold lid could be quickly transferred to the EX-CORE sample. The sample casing is shown in Figure 6.2a, where it is displayed on top of the bottom mold lid, kept in position by 4 bolts (indicated with red circles).

Secondly, in all previous research the tile mold was closed and fastened with 16 M8 bolts. This proved to be very time-consuming, taking at least 10 minutes to complete. In combination with the preheated mold and fast curing EX-CORE, closing the mold this way would take too long, especially because the EX-CORE can already expand during that time period. Additionally, fastening the bolts when the mold is heated is also not practical nor safe. It was proposed to use 4 glue clasps that allowed for quickly closing and locking the mold. The closed mold is shown in Figure 6.2c. In addition 4 bolts were prepositioned into the bottom mold lid. Their only function was to keep the sample mold horizontally in place. They were not fastened. Both alterations allowed for quickly transferring the sample casing in between the preheated mold lids and consequently closing the mold, all in less than one minute.

Force Sensitive Sensors (FSR): Flexiforce® HT201;

In previous research by both Vial [63] and Eversdijk [64], FSRs of the type Flexiforce® HT201 by Tekscan were used to estimate the amount of pressure generated at the mold surface of EX-CORE samples with various DU contents. Eversdijk concluded that the Flexiforce® HT201 sensors are not reliable to obtain accurate pressure measurements. Nonetheless they are suitable to determine the moment of EX-CORE expansion and can be used for relative pressure measurements/comparisons between different samples. Because of their flat and flexible shape they can be easily integrated into the mold. In addition, they are the only commercially available pressure sensors in their kind which can be used up to 204°C [65]. Therefore they are again used in the current research, for example to investigate the timing of EX-CORE expansion. A Flexiforce® HT201 pressure sensor is shown in Figure 6.3:

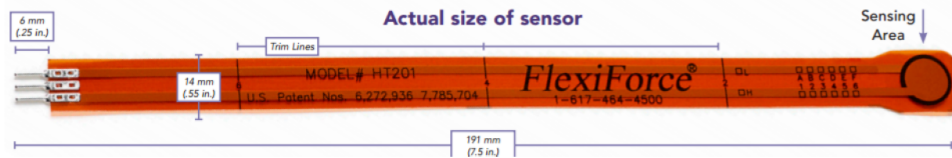


Figure 6.3: Force-sensitive resistor; Flexiforce® HT201 by Tekscan [64]

Four new Flexiforce® HT201 sensors were ordered and each separately calibrated. How this calibration was done is explained in Appendix F. Remark that the calibration data given there is only valid when the Flexiforce sensors are used in combination with the $10\text{k}\Omega \pm 1\%$ resistors and a 5V Arduino® processor (see Figure 6.5). It is also important to note that the sensors have an output change of 0.16% per degree Celsius according to the datasheet [65]. This value has been experimentally verified by placing the four sensors under constant loading in an oven, and then measuring the signal drift when the temperature was increased from room temperature up to 120°C. An output change of $\pm 0.14\%/^{\circ}\text{C}$ was obtained, in line with the 0.16% value provided by the datasheet. Therefore a $0.16\%/^{\circ}\text{C}$ temperature drift is taken into account when processing the analogue sensor data as monitored by the Arduino®.

Before attaching the sensors to the tile mold (as shown in Figure 6.2b), they are covered in vacuum foil "Scabro Vacfilm 450V" to protect them from contamination. Then they are attached to the aluminum plate with aluminum tape and covered with at least 3 layers of release agent Loctite® 700-NC™ Frekote™. As can be seen in Figure 6.2b, three sensors are placed on the centerline of the mold, while one sensors is placed in the corner. This is done to investigate possible pressure distributions on the mold surface. The sensor numbering given in Figure 6.2b refers to the numbers as given to the sensors during calibration (Appendix F). The same numbering is also used in the graphs in Appendix H where the pressure vs time is plotted for various samples created during this research.

Temperature sensors: NCT thermistor EPCOS B57560G104F

The NCT thermistor sensors B57560G104F by EPCOS were selected because of their small size (see Figure 6.4) and high operating range up to 300°C [142]. NTC stands for negative temperature coefficients, meaning that the their resistance decreases with increasing temperatures. When combined with a $4.7\text{k}\Omega \pm 1\%$ resistor it was calculated that they should give have an accuracy of $\pm 1.7^{\circ}\text{C}$ at 110°C [143]. The sensors were calibrated by making use of a pre-calibrated PT100 sensor. How this is done is explained in more detail in Appendix G. To protect the sensors from short-circuiting, they were covered with PTFE heat shrink tubing with an operating temperature up to 250°C [144]. In addition, they were covered with vacuum foil to prevent contamination during sample production.

Data processing using Arduino® Nano setup

The pressure and temperature sensor data is processed using an Arduino® Nano with SD card logger module. The sensor output is logged every second and stored on the SD card. The setup as shown in Figure 6.5 was already available from previous research but the Arduino® had to be re-programmed. The entire setup can be powered with a 5V USB adapter or by connecting the Arduino® itself to a computer. The four $10\text{k}\Omega \pm 1\%$ resistors on the right are incorporated to maximize the read-out sensitivity of the Flexiforce® HT201 sensors. For similar reasons, $4.7\text{k}\Omega \pm 1\%$ resistors are used in combination with the NTC sensors (upper left). Each NTC and Flexiforce® sensor requires its own analog connection to the Arduino®.

Multiple digital temperature sensors (the DS18B20 as previously used by Eversdijk [64]) can also be connected, requiring only 1 signal wire to the Arduino[®] due to their unique MAC address. A disadvantage of these sensors is that they have an output range of maximum 127.75°C [145]. Because higher temperature are expected during this research, the digital sensors were not used anymore. Unfortunately, other digital sensors with a higher maximum output were not commercially available

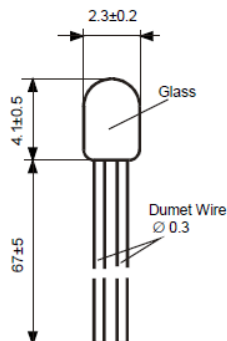


Figure 6.4: Technical drawing of NCT thermistor EPCOS B57560G104F [142]

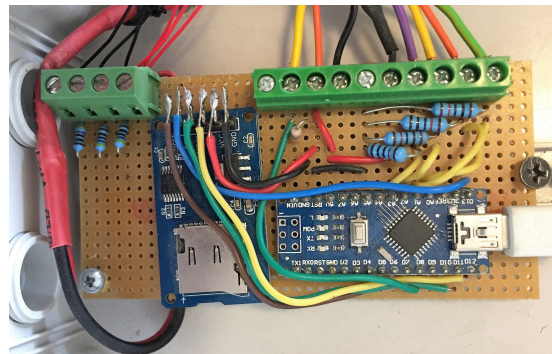


Figure 6.5: Arduino[®] Nano setup, including SD card reader

6.1.3. Manufacturing of samples in the tile mold

Before EX-CORE samples can be produced, the mold, the sample casing and the sensors have to be prepared. For example the aluminum plates have to be cleaned and attached to the mold lids, sensors have to be attached and the sample casing needs to be constructed with aluminum tape. Also, at least 3 layers of release agent should be applied. Finally, the mold lids are preheated at the desired cure temperature. The entire tile mold preparation procedure is explained in Appendix E, Section E.1 Part A where step-by-step instructions are given.

All EX-CORE mixtures are manually produced without using any mixing apparatus and/or automated weighing/dosing setup. The weighing is done manually using a Kern PFB 6000-1 digital balance with 0.1g accuracy. The manual procedure was preferred because the different types of resins and hardeners could contaminate the current "automated" weighing & mixing setup available at Donkervoort. In addition, manual processing gives better insight into the viscosity and ease of mixing of the EX-CORE blend. The step-by-step EX-CORE constituent weighing and mixing procedure is explained in Appendix E, Section E.1 Part B.

Subsequently the step-by-step EX-CORE molding & curing in the pre-heated tile mold is explained in full detail in Appendix E, Section E.1. Part C. In short; a predefined amount of EX-CORE mixture is manually placed inside the cavity of the sample casing such that 100% mold filling is ensured. Then the mold casing is transferred in between the pre-heated mold lids. Next, the mold is closed using four glue claps and covered with at least 6 layers of bleeder fabric (insulation). Then the Arduino[®] is reset, such that pressure and temperature recording is initiated.

For all samples the required cure time was predicted using the numerical thermal model. To ensure proper curing, the sample cure time was taken as the simulated time when at least 98% cure is reached everywhere in the sample. During sample curing, the time was tracked and the sample was immediately taken out of the mold once this predicted cure time was reached.

6.2. First two series of EX-CORE samples produced with new epoxy matrices (R1 & R2)

In this section an overview of the produced samples during the first exploratory test phase is given. Each manufactured sample is given a unique label. The used naming convention is explained in Appendix E, Section E.2. This first test phase consist out of two series of samples that were produced, referred to as R1 and R2. A discussion of the sample results is given w.r.t. the measured pressure and temperature, but also whether or not the samples are sufficiently cured and expanded etc. The obtained pressure (& if measured the core temperature) are plotted as a function of time for every sample produced in this research. These plots can be found in Appendix H.

6.2.1. Test series R1: Initial exploration

The goal of the first test series was to explore the suitability of the new candidate epoxy matrices in EX-CORE and compare their compatibility with the microspheres and the EX-CORE process. The three types of new hardeners SZ 8528, Ancamine[®] 2337s and Ancamine[®] 2442 in combination with the new SR 1280 resin were used to create EX-CORE samples. All samples were 30mm thick, which is a representative sample thickness also commonly used in previous research. The samples were cured at an isothermal cure temperature of 110°C. Higher cure temperatures (and such shorter cure cycles) could also be possible but the (higher) resulting exothermic reaction peaks could negatively affect the EX-CORE properties. Therefore it was decided to initially stick to a 110°C cure temperature.

As explained in Section 6.1.3, the cure time of the different samples is not the same. The total sample cure time is taken as the time to obtain a 98% cure, which is estimated using the numerical model for the specific EX-CORE formulation, sample thickness and 110°C isothermal cure temperature. The obtained cure time was rounded above to the nearest integer. It is important to note that when this R1 (& R2) test series was manufactured, the onset-reaction temperatures (T_{onset}) of 71°C and 93°C, for the Ancamine[®] 2337s & 2442 hardeners respectively were not yet incorporated in the numerical model. So the condition of setting $\dot{q}_{int} = 0$ if T_{onset} was not yet reached at the node (explained in Section 5.6) was not yet implemented. The obtained cure time (given in Table 6.2) is therefore shorter than it should be. For the samples with the Ancamine[®] 2337s hardener (R1-TM1-3 & R1-TM1-4), this difference is only 18sec while for the sample with the Ancamine[®] 2442 hardener (R1-TM1-5), having the highest onset reaction temperature, this difference is more pronounced, namely 3min 24sec. Nonetheless, as will become clear in the following paragraphs, even with a larger cure time deviation, the samples with the Ancamine[®] 2442 hardener are in reality better cured than the ones with the Ancamine[®] 2337s hardener.

Table 6.2: Overview of R1 series manufactured samples

Sample label	Sample height	Mix	Resin type	Hardener type	Epoxy ratio r	031 DU 40 vol.%	Cure temp.	Cure time
R1-TM1-1	30mm	270-opt	SR 1280	SZ 8525	100:24	1%	110°C	15min
R1-TM1-2	30mm	270-opt	SR 1280	SZ 8525	100:24	4%	110°C	15min
R1-TM1-3	30mm	270-opt	SR 1280	Ancamine [®] 2337s	100:60	4%	110°C	>20min
R1-TM1-4	30mm	270-opt	SR 1280	Ancamine [®] 2337s	100:60	4%	110°C	20min
R1-TM1-5	30mm	270-opt	SR 1280	Ancamine [®] 2442	100:60	4%	110°C	15min
R1-TM1-6	30mm	270-opt	SR 1280	None used!	\	4%	110°C	>15min
R1-TM1-7	30mm	270-opt	SR 1280	SZ 8525	100:24	4%	110°C	15min

In Table 6.2, an overview of all the produced R1 series samples, their formulation, sample thickness, cure temperature and cure time is given. Table 6.3 gives a good overview of important results and/or measurements obtained during and after production/curing of the samples. For ease of comparison, the same table formats will be used for all manufactured samples discussed in this report. Before discussing the created samples and results, a clarification is given w.r.t. to some of the parameters presented in the columns of Table 6.3.

- **The maximum surface pressure** is the maximum pressure measured by any of the four Flexiforce[™] sensors placed at the mold surface (see Figure 6.2b). As said, pressure plots including the individual pressure sensor measurements and average pressure over time can be found in Appendix H for each sample.
- **Time to reach 0.5bar** refers to the required time when (on average) 0.5bar pressure was recorded by the four Flexiforce[™] sensors. It became clear that the 0.5bar point gave a good indication for the onset of EX-CORE expansion. This point (if reached) is also indicated in the plots in Appendix H.
- **Temperature at 0.5bar**; Similarly, this refers to the average temperature in the core (if measured) when the 0.5bar average was reached. This should give a good indication of the temperature at which EX-CORE/ Expancel[®] DU starts to expand.
- **Maximum core temperature** is the maximum temperature measured in the core by any of the used NTC sensors (if implemented).

- **Sample curing** gives an indication on how well the sample is cured. A score from 0 (not cured) to 5 (fully cured) is given based on visual/manual inspection of the sample. For example, the dimensional stability and compressibility of the sample is inspected. A more rubbery/compressible sample indicates that the sample is not yet sufficiently cured, while a stronger rigid sample implies that the sample is sufficiently cured. Another good indication of whether or not the sample is fully cured, is the odor of the sample when it is taken out of the mold. A strong epoxy smell reveals that the sample is not yet fully cured.
- **Sample expansion** specifies the degree of sample expansion caused by the pressure generation of the EX-CORE mixture. Again a relative score from 0 (not expanded) to 5 (excellent expansion) was given based on visual inspection and pressure measurements at the surface of the samples using the Flexiforce™ sensors. A rough surface with visual pores indicates that EX-CORE did not sufficiently expand and/or the timing of EX-CORE expansion is not optimal. For example because EX-CORE is already cured too far before expansion in the core takes place. To be able to better compare the expansion mechanism in EX-CORE, an imprint of an M8 bolt head was pressed into the EX-CORE mixture before curing. In case of excellent expansion, this imprint will not be visible anymore in the sample after curing. When no expansion occurred, the imprint will still have the original dept. When poor/insufficient expansion occurred, the contours of the bolt will still be visible, for example as marked in Figure 6.8.

Table 6.3: Overview of R1 sample results, pressure and temperature measurements & rating of sample curing and expansion

Sample label	Room temp.	Sample mass	Max. surf. pressure	Time to reach 0.5bar (avg.)	Temp. at 0.5bar	Max. core temp.	Sample curing ¹	Sample expansion ²
R1-TM1-1	25°C	258.7g	0.16bar	/	/	/	5	0
R1-TM1-2	20°C	252.0g	3.25bar	5.7min	/	/	5	3
R1-TM1-3	20°C	205.5g	0.34bar	/	/	/	1	0
R1-TM1-4	20°C	196.0g	0.86bar	/	/	/	3	1
R1-TM1-5	18°C	219.5g	2.34bar	10min	/	/	4	3
R1-TM1-6	22°C	/	0.50bar	/	/	115°C	0	1
R1-TM1-7	22°C	263.0g	2.23bar	6min	95°C	175°C	5	3

¹ On a scale from 1 to 5, with 5 being fully cured.

² On a scale from 1 to 5, with 5 being excellent expansion.

The first sample **R1-TM1-1**, was produced using the SR 1280 resin in combination with the SZ 8525 hardener (epoxy system ref. nr. 1) and was cured for 15min. This sample was produced with only 1vol.% of 031 DU 40 (a commonly used percentage in previous research by Eversdijk [64]). This amount of DU proved to be way to little since no pressure increase has been measured at all. The rough surface of the cured sample can be seen in Figure 6.6. The location/imprints of the pressure sensors is also indicated. Nonetheless, when taken out of the mold after only 15min, the sample was already completely rigid/cured. So this was a very promising result w.r.t. cure time reduction of EX-CORE.

A similar sample **R1-TM1-2** with an increased DU content of 4vol.% DU was manufactured. This time pressures up to 2.64bar were measured. However, small pores in the surface could still be spotted. Also, as can be seen in Figure 6.7, in de cross-section of the sample a crack can be observed. At that time it was thought that this crack was caused due to the high exothermic peak in the core of the sample (degradation), especially because the thermal model predicted a maximum temperature up to 178°C in the core. Additionally, in the cross-section of the sample a yellow discoloration can be spotted (not noticeable in the figure) near the location of the crack. Later when more samples were produced, it became clear that the crack most probably emerged when the hot sample was taken out of the mold. This because due to the high temperature a significant amount of pressure is built up in the core, which the cured EX-CORE sample cannot withstand when taken out of the mold. The R1-TM1-2 sample was prepared half an hour (lunchtime) before it was placed in between the preheated mold lids. It was noticed that in these 30min the sample had already warmed up to ± 35°C due to the exothermic reaction of the resin.

The same sample formulation was again used for sample **R1-TM1-7**, but this time the sample was directly placed in between the preheated mold lids once prepared. In addition, the temperature was monitored using 3 NTC sensors that were placed inside the core on the diagonal line (similar as shown in Figure 6.9). A

maximum core temperature of 175°C was measured, close to the model prediction of 178°C. Remarkable this time, no crack was visual in the cross-section of the cured sample. Next to the difference of 30min warm-up time, there is another difference w.r.t how both samples were allowed to cool down: Sample R1-TM1-2 cooled down to room temperature inside the aluminum sample casing, while the hot sample R1-TM1-7 was directly taken out of its hot casing, and such could cool down without any restrictions. This difference could also affect the occurrence of the crack. From this sample onwards, hot samples are directly taken out of their aluminum sample casing after curing.

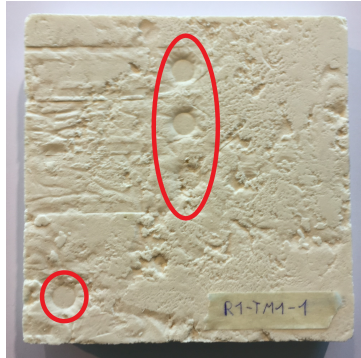


Figure 6.6: Sample R1-TM1-1. Imprint of flexiforce sensors indicated.



Figure 6.7: Cross-section of sample R1-TM1-2. Crack indicated.

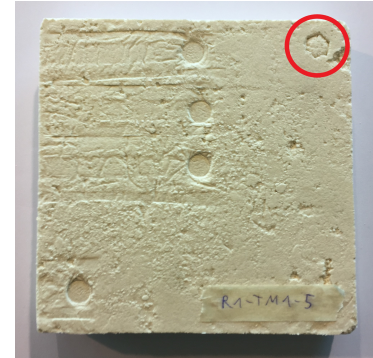


Figure 6.8: Sample R1-TM1-5. Imprint of M8 bolt indicated.

Sample **R1-TM1-3** was produced with the Ancamine[®] 2337s hardener (resin system ref. nr. 4). Unfortunately during curing, a current plug connection to the tile mold became loose (unnoticed), causing the mold temperature to drop back to 80°C. Therefore, a similar sample **R1-TM1-4** was produced, which was taken out of the mold after 20min. The "cured" sample could still be compressed by hand, also after several weeks. Additionally, a strong epoxy odor could be noticed. Also, the sample did only marginally expand; the surface was still rough and porous and a maximum pressure of only 0.86bar was measured.

Sample **R1-TM1-5** was manufactured with the Ancamine[®] 2442 hardener (resin system ref. nr. 5) which was taken out of the mold after 15min. The surface of the sample was relatively rough/grainy and the contours of the M8 bolt in the corner were still visual, as shown in Figure 6.8. The sample was dimensionally stable but could still be slightly squeezed by hand. It had an epoxy odor that indicated that the sample was not yet completely cured. However, the next day the sample was completely rigid and did not smell anymore.

Finally, sample **R1-TM1-6** was manufactured with the SR 1280 resin but without any hardener! This test had as goal to investigate the moment of EX-CORE expansion without the influence of the exothermic reaction heat. Three NTC sensors were placed inside the sample, as shown in Figure 6.9. It is known that pure Expancel[®] 031 DU 40 starts to expand around 80-95°C (see Section 3.3.1). However, it was expected that in combination with surrounding fillers and epoxy matrix a higher temperature would be required to initiate DU expansion in EX-CORE. For example for sample R1-TM1-7 is was obtained that 0.5bar was reached at 95°C, this around 6min (and 5.7min for similar sample R1-TM1-2 for which the core temperature was not measured).

Initially sample R1-TM1-6 was cured for 20min at 110°C. Surprisingly, (see plot of sample R1-TM1-6a in Appendix H) no pressure increase was registered even though that the temperature in the core reached 110°C. Therefore it was decided to increase the mold temperature to 130°C (plot R1-TM1-6a in Appendix H) and reheat the sample. Now only a ± 0.25 bar increase in pressure was registered, such that 0.5bar pressure was measured when the core reached 106.5°C. Only 2 minutes later, the pressure suddenly dropped. This occurred when the measured temperature in the core was 117-133°C. As explained in Section 3.3.1, the maximum temperature of Expancel[®] 031 DU 40 is 120-135°C which falls within the measured temperature range. Without any surrounding solid cured shell/network of epoxy, the microspheres starts to deflate. When opening the mold, it could also be observed that the final uncured EX-CORE sample was shrunken on each side and slightly discolored yellowish, as shown in Figure 6.10.

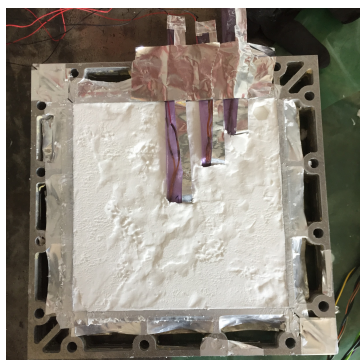


Figure 6.9: Location of NTC sensors in EX-CORE mix of R1-TM1-6



Figure 6.10: Shrunken sample R1-TM1-6 after heating in 130°C mold

6.2.2. Test series R2: Reduced sample thickness of 10mm

As mentioned already in Section 6.2.1, the condition of setting $\dot{q}_{int} = 0$ to simulate the onset reaction temperature of 71°C or 93°C for the Ancamine[®] hardeners 2337s and 2442, was not yet implemented in the numerical model when sample series R1 and R2 were produced. At that time the idea came up to create thinner 10mm samples, which would minimize the time discrepancy/effect of the thermal block. This because the thermal block temperature is much quicker reached in the core of thinner samples, and the delay of reaction initiation is therefore limited. In addition, the time when this onset reaction temperature should be reached everywhere in the sample (when cured at 110°C) was estimated using the numerical model. This time difference was then added to the estimated 98% cure time obtained with the model.

Two R2 series samples, both 10mm thick and with 4vol.% 031 DU 40 were produced, as summarized in Table 6.4. In both samples 1 NTC sensors was incorporated, and positioned in the center of the sample. The first sample, **R2-TM1-1** contained the Ancamine[®] 2337s hardener, while the second one, the **R2-TM1-2** was manufactured with the Ancamine[®] 2442 hardener. Both were again cured at 110°C. For sample R2-TM1-1 the 12min cure time was the summation of the simulated 98% cure time (10.3min) and the simulated time to reach 71°C everywhere in the sample (1.7min). Similarly, for sample R2-TM1-2, an 11min cure time was predicted (7.4 + 3.4min).

Table 6.4: Overview of R2 series manufactured samples

Sample label	Sample height	Mix	Resin type	Hardener type	Epoxy ratio r	031 DU 40 vol.%	Cure temp.	Cure time
R2-TM1-1	10mm	270-opt	SR 1280	Ancamine [®] 2337s	100:60	4%	110°C	12min
R2-TM1-2	10mm	270-opt	SR 1280	Ancamine [®] 2442	100:60	4%	110°C	11min

An overview of the R2 sample results is presented in Table 6.5. After 12min curing, the mold lid of sample **R2-TM1-1** was opened. The sample was very brittle and "burst" upward, as can be seen in Figure 6.11. The sample was also easily crushable. Successful results were however obtained for sample **R2-TM1-2** containing the Ancamine[®] 2442 hardener. This cured sample is shown in Figure 6.12. After 11 min curing, the sample was taken out of the mold. It had a relatively smooth surface and the contours of the M8 bolt imprint were not visual anymore. The maximum peak temperature measured in the core was only 128°C, while a maximum pressure of 1.25bar was reached. Expansion already initiated (0.5bar point) after 2.4min, this around 91°C. The sample was so "hard" that it caused significant effort to cut out the NTC sensor.

Table 6.5: Overview of R2 sample results, pressure and temperature measurements & rating of sample curing and expansion

Sample label	Room temp.	Sample mass	Max. surf. pressure	Time to reach 0.5bar (avg.)	Temp. at 0.5bar	Max. core. temp.	Sample curing ¹	Sample expansion ²
R2-TM1-1	22°C	/	0.77bar	/	/	125°C	2	2
R2-TM1-2	22°C	78g	1.25bar	2.4	91°C	128°C	5	4

¹ On a scale from 1 to 5, with 5 being fully cured.

² On a scale from 1 to 5, with 5 being excellent expansion.



Figure 6.11: *Brittle sample R2-TM1-1, bursting out of mold when opened.*



Figure 6.12: *Cured sample R2-TM1-2. Cut outs made to free NTC sensor*

6.2.3. Conclusions test series R1 & R2

Based on the results of the first produced sample series R1 and R2 discussed in this chapter, several conclusions could already be made:

First of all, with the SZ 8525 hardener fully cured and good expanded EX-CORE samples were obtained in less than 15min. Care should however be taken when pre-mixing the hardener with the resin. In contrary to the other Ancamine[®] hardeners, SZ 8525 already quickly reacts at room temperature. For example from sample R1-TM1-2 it became clear that in less than 30min, the temperature of the EX-CORE mixture already increased with $\pm 15^{\circ}\text{C}$ due to the exothermic reaction of the epoxy. This could form a limitation for large series production where large volumes of EX-CORE have to be produced.

Secondly, high exothermic peaks up to 178°C were measured and predicted for 30mm EX-CORE samples with the SZ 8525 hardener cured at 110°C . As already became clear from the DSC test results in Chapter 4 (see Table 4.3), the total specific heat of reaction with the SZ 8525 hardener (278J/g) is more than twice as high than obtained with the Ancamine[®] hardeners (91J/g & 169J/g). These high exothermic reaction peaks could negatively affect EX-CORE properties, especially because the current 031 DU 40 grade has a maximum temperature of only $120\text{-}135^{\circ}\text{C}$. It would therefore be beneficial to investigate the use of another type of DU grade in EX-CORE with a higher maximum temperature. This will become the subject of the next chapter. There more samples manufactured with the newly chosen DU grade and the SZ 8525 hardener will also be discussed.

Thirdly, none of the EX-CORE samples manufactured with the Ancamine[®] 2337s hardener (R1-TM1-3/4 & R2-TM1-1) were sufficiently cured nor dimensionally stable. Since no promising results were obtained with this hardener, further testing with Ancamine[®] 2337s is not recommended.

Finally, promising 30mm and 10mm thick samples (R1-TM1-5 & R2-TM2-2) were manufactured with the Ancamine[®] 2442 hardener in only 15min and 11min, respectively. All samples were cured to such an extend that they were dimensionally stable when they were taken out of the hot mold. In addition, the good sample expansions can be attributed to the measured pressures of 2.34bar & 1.25bar. Experimental testing with this hardener was therefore continued, as discussed in the next chapter.

7

Test phase 2: A new Expancel[®] DU grade

From the previous chapter it became clear that both the SZ 8525 and the Ancamine[®] curing agent in combination with the SR 1280 resin gave promising results when used as matrix in EX-CORE. Further research with both epoxy matrices was therefore continued in the second test phase as discussed in this chapter. But first of all, a more resistant grade of Expancel[®] DU, namely 043 DU 80 was selected to replace the current 031 DU 80 grade. Why this new grade was selected is explained in Section 7.1. Then, in Section 7.2 the methodology and improved experimental set-up used to monitor the temperature distribution in EX-CORE samples is discussed. Next, the manufactured samples in the second test phase and their results are covered in Section 7.3. Finally, in Section 7.4 one of the two curing agents will be selected as best candidate curing agent to reduce the cure cycle times of EX-CORE.

7.1. Selecting the new Expancel[®] 043 DU 80 grade

In this section it is explained why a new Expancel[®] 043 DU 80 grade was selected in the current research to replace the original Expancel[®] 031 DU 40 grade used in EX-CORE. As can be seen in Figure 7.1, the original Expancel[®] 031 DU 40 grade has the lowest onset reaction temperature of all available DU grades, namely 80-95°C. Unfortunately, it also has the lowest maximum temperature of 120-135°C. At this maximum temperature range, the thermoplastic shell of the DU microspheres softens and starts to deflate as the blowing agent in the microspheres escapes. This is especially detrimental when the surrounding epoxy matrix is still in a low viscous state. In contrary if the maximum DU temperature is reached when the epoxy is already suffi-

Expancel	Particle Size µm ⁽¹⁾ D(0.5)	Thermomechanical Analysis ⁽²⁾			Solvent Resistance ⁽³⁾
		Tstart, °C	Tmax, °C	Density kg/m ³	
551 DU 40	10–16	94–99	141–149	≤ 17	3
461 DU 20	6–9	100–106	143–151	≤ 30	4
461 DU 40	9–15	100–107	144–152	≤ 20	4
051 DU 40	9–15	108–113	142–151	≤ 25	4
031 DU 40	10–16	80–95	120–135	≤ 12	3
053 DU 40	10–16	96–103	138–146	≤ 20	3
093 DU 120	28–38	120–130	189–204	≤ 6.5	5
909 DU 80	18–24	120–130	175–190	≤ 10	5
920 DU 20	5–9	120–145	155–175	≤ 25	5
920 DU 40	10–16	123–133	168–178	≤ 17	5
920 DU 80	18–24	123–133	180–195	≤ 14	5
920 DU 120	28–38	122–132	194–206	≤ 14	5
930 DU 120	28–38	122–132	192–207	≤ 6,5	5
950 DU 80	18–24	138–148	188–200	≤ 12	5
951 DU 120	28–38	133–143	190–205	≤ 9	5
980 DU 120	25–40	158–173	215–235	≤ 14	5
New product					
043 DU 80	16–24	95–115	147–167	≤ 10	5

Figure 7.1: Properties of Expancel[®] DU grades by AkzoNobel [56]

ciently cured, the gas escape is restricted due to the impermeable epoxy shell/network that is formed around the microsphere. The 120-135°C maximum temperature of 031 DU 40 thus limits the maximum cure temperature at which EX-CORE can be cured, which in turn limits the minimum cure time that can be obtained. For example it was demonstrated in Table 4.4 that the 98% cure time of the tested epoxy systems significantly reduced when cured at higher temperatures. For example it be seen that the cure time approximately doubled when cured at 95°C instead of 110°C.

Another reason to opt for a new DU grade is the suspicion at Donkervoort that the thermoplastic shell (of unknown copolymer material composition) of the 031 DU 40 grade is possibly negatively affected by the epoxy matrix. As can be seen in Table 4.4, the solvent resistance score of 031 DU 40 is only 3 out of 5. Several tests with mixtures containing 4% to 20% of 031 DU 40 in pure epoxy resins, epoxy/hardener systems and even in water where performed to investigate the expansion behavior of DU. The mixtures were prepared in transparent mixing cups that were placed in a small Tefal oven preheated at 110°C. This oven allowed to observe the expansion behavior from behind the glass oven-door. The temperature of the oven and in the mixtures was also monitored with NTC sensors.

In summary, it was observed that the 031DU/resin/hardener and pure DU mixtures (sample 5a in Figure 7.4) as expected expanded out of the mixing cup. These expanded mixtures were also still intact when cooled back to room temperature. However, when 031 DU 40 was mixed in pure epoxy resins (both Ancarez[®] RZ4010 and SR 1280), it was observed that gas bubbles originated in the liquid mixture that grew larger when they slowly floated upwards. These bubbles can be spotted in Figure 7.2. This caused the mixture to increase approx. twice in volume. Once the bubbles reached the surface of the mixture they collapsed. Ultimately, all gases had escaped out of the mixture and it shrunk back to its original volume. The final cooled down mixtures are shown in Figure 7.3. It is still unsure how these bubbles originated. The temperature of the mixtures was in all cases not more than 95-110°C, so below the maximum temperature of 031 DU 40. It could therefore be possible that epoxy degraded the thermoplastic shells of the DU microspheres which caused them to collapse and the blowing agent to escape, hence causing the large bubble formations. In addition, similar tests were performed with mixtures containing 4 to 20% of 031 DU 40 mixed in water. The mixtures started to foam, but they did not collapse anymore during heating, nor after cooling down. Resulting 031DU/water foamed mixtures can be seen in Figure 7.4. The working of 031 DU was clearly not affected in water.

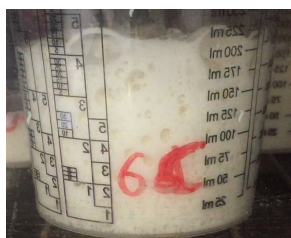


Figure 7.2: Picture taken of mixture containing 50g SR 1280 and 12.5g 031DU when heated in oven at 110°C

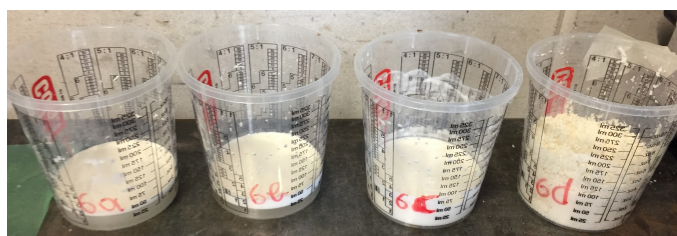


Figure 7.3: 031DU/SR1280 mixtures when cooled back to room temp. Composition: 6a) 50g SR 1280 & 2.08g 031DU, 6b) 50g SR 1280 & 5.55g 031DU and 6c) 50g SR 1280 & 12.5g 031DU



Figure 7.4: 031DU/water mixtures when cooled back to room temp. Composition: 5a) 50ml DU, 5b) 50g water & 2g 031DU and 5c) 50g water & 50g 031DU

Based on these and other tests performed at Donkervoort, it could not be confirmed with certainty that the shell of 031 DU 40 degraded due to contact with epoxy resin. The collapsing of the foamed mixture could for example also be caused due to differences in surface tension around the microspheres. Akzonobel, the

manufacturer of Expancel[®] DU was also contacted, but they considered it very doubtful that 031 DU 40 would be negatively affected by epoxy. Nonetheless, it was decided to opt for a new DU grade with an maximum solvent resistance score of 5/5.

Finally, the new 043 DU 80 grade was selected because of its relatively low onset expansion temperature range of 95-115°C, increased maximum temperature range of 147-167°C and maximum solvent resistance score. A small sample batch was received from AkzoNobel such that some first initial tests with this new DU grade could be performed. First of all, the bulk density of 043 DU 80 was experimentally determined to be 500kg/m³ which was implemented in the numerical model. Secondly, 043 DU 80 was mixed in pure SR 1280 epoxy resins, similar as tested with the 031 DU 40 grade (shown in Figures 7.2 and 7.3). This time, foamed mixtures were obtained which did not collapse. Also only minor bubble collapsing was observed at the surface. The resulting cooled down foamed mixtures can be seen in Figure 7.5. Depending on the used 043 DU 80 content, the foam structure varied from a wet-like shaving foam (11a and 11b) to a more rubbery like foam (11c and 11d).

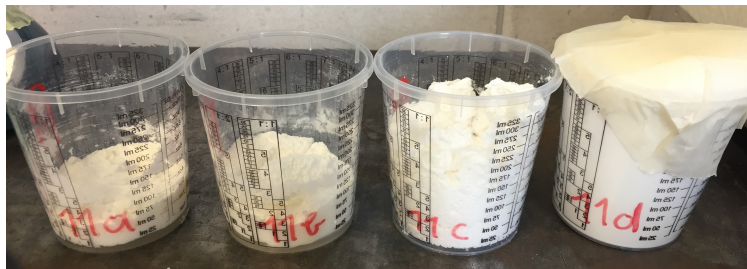


Figure 7.5: 043DU/SR1280 mixtures when cooled back to room temp. Composition: 11a)50g SR1280 & 2.08g 043DU, 11b) 50g SR1280 & 5.55g 043DU, 11c) 50g SR1280 & 12.5g 043DU and 11d) 10g 043DU

7.2. Methodology and experimental set-up

In the second experimental test phase several EX-CORE samples were produced with the new Expancel[®] 043 DU 80 grade, the SR 1280 resin, and the Ancamine[®] 2442 or SZ 8525 hardener. These samples were manufactured along the same methodology as discussed in Section 6.1. The EX-CORE samples were again cured in the preheated tile mold and the pressure and temperature of the samples was monitored with NTC and Flexiforce[®] sensors. However, an improved setup has been constructed that allowed to measure the temperature distribution along the mid plane of the samples using 15 NTC sensors. These temperature measurements will i.a. be used to validate the numerical model predictions as discussed in Chapter 9. The setup will be explained in Section 7.2.1. To process the 15 NTC sensor signals, also a new Arduino[®] Mega setup had to be constructed as discussed in Section 7.2.2.

7.2.1. Temperature monitoring with NTC sensor grid

To be able to measure the temperature distribution in EX-CORE samples and compare them with the numerical model prediction, an "NTC sensor grid" was constructed. The same NTC thermistors as used in the first test phase were again used (discussed in Section 6.1.2). To keep the sensors at the predefined position in the sample, a metal grid with a maze size of 4x4mm (similar as the one used in the research of Eversdijk [64]) was used. The grid was cut at the size of the tile mold cross-section, in this case 175mm x 30mm, where 30mm is the height of the samples produced in the second test phase. The sensors could easily be connected to the mazes of the grid using tacky tape. In total 15 NTC sensors were placed on the metal grid in such a way that the temperature sensitive sensor heads were located inside the mazes so that they were in contact with EX-CORE at both sides. A schematic representation of how the sensors were arranged is shown in Figure 7.6. The positioning of the 15 NTC sensors on the 30mm metal grid can be seen in Figure 7.7.

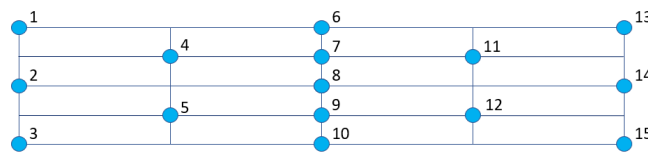


Figure 7.6: Schematic positioning of the 15 NTC sensors on grid

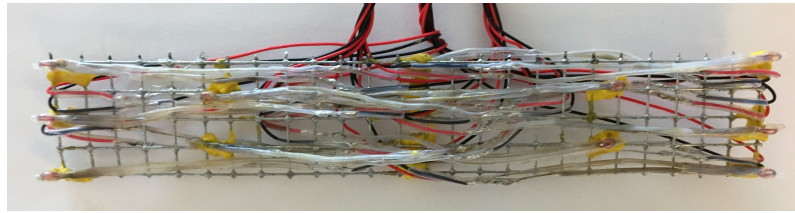


Figure 7.7: 15 NTC sensors including wiring, attached to 30mm high metal grid

As can be seen in Figure 7.6 the pattern concentrates sensors on the vertical center line. This is done because there the most severe temperature peaks and gradients were expected due to the exothermic reaction of the resin and insulating properties of EX-CORE. In both height and width direction sensors are distributed over 5 different positions. This allows to integrate the sensor data with the MATLAB "griddata" function based on the biharmonic spline fitting method "v4". This way a graphical representation of the temperature distribution of the sample over time can be made. The fitted temperature data was solely used for ease of visualization of the temperature profiles in the samples.

Each sensor required one connection to a unique analog port of the Arduino[®] and one connection to ground. To facilitate this, thin wires having PTFE (Teflon) sheaths were soldered to both sensors arms. To prevent short circuiting with the metal grid, all sensors and soldered connections were also covered with PTFE heat shrink tubing that is temperature stable up to 250°C [144]. All sensor wires were bundled per 5 sensors, which in turn were braided into one larger bundle that could run out the mold. At the end of the woven bundle, three 6-pin plastic connectors (already available at Donkervoort) were attached. From each connector, 5 pins were used for signal wires and 1 pin for ground connection. The connectors allowed to quickly (dis-)connect the sensor grid with the Arduino setup. The entire sensor grid, including the wire bundle was covered in vacuum foil "Scabro Vacfilm 450V", temperature stable up to $\pm 170^{\circ}\text{C}$. The vacuum foil was fixed with double sided Tesa 4965 tape that is temperature resistant up to 200°C. This made it possible to re-use the sensor grid multiple times.

The entire sensor grid setup was covered in at least 3 layers of release agent Loctite[®] 700-NC[™] Frekote[™]. Note that the inner side of the vacuum foil cover was also covered in release agent beforehand (except for the locations where tape had to be applied). This was done to prevent the vacuum foil from sticking to the sensor grid when temperatures in excess of 170°C occurred. Otherwise it proved to be very hard to demount the sensors when they had to be re-used on larger grids (for validation purposes as explained in Chapter 9). Vacuum foils with higher temperature resistance were unfortunately not available at Donkervoort.

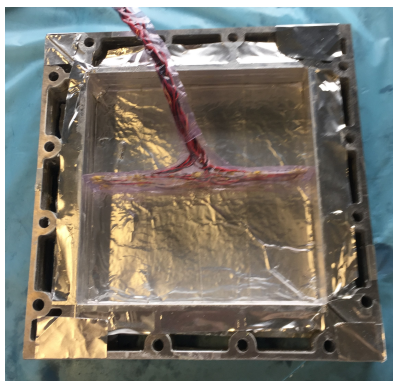


Figure 7.8: Positioning of 30mm NTC sensor grid inside the mid plane of 30mm high sample casing



Figure 7.9: Sample casing filled with EX-CORE and sensor grid positioned at mid plane

In all tests the NTC sensor grid is placed on the mid plane in the sample casing, as shown in Figure 7.8. The casing is then filled up with EX-CORE, depicted in Figure 7.9. This position was chosen because the mid plane acts as a plane of symmetry, such that the temperature distribution can be simulated and compared with the two-dimensional numerical model prediction. The grid could also have been placed on the diagonal symmetry plane, however there it was expected that the presence of the nearby aluminum corners would affect the boundary conditions too much. Another reason to opt for the mid plane is that there the highest

temperature peaks were expected due to the exothermic reaction of the resin and insulating characteristic of the EX-CORE foam. The NTC temperature grid measurements were later used to validate the numerical model, as discussed in Chapter 9.

7.2.2. Data processing using new Arduino® Mega setup

The Arduino® Nano as previously used for data processing (see Section 6.1.2) has only 5 analog input ports. It could therefore not be used to simultaneously monitor the signals of the 15 NTC sensors. Therefore an Arduino® Mega has been ordered that contains 16 analog input ports. A new similar setup has been soldered including an SD-card reader module and 15x 4.7kΩ±% resistors, one for each NTC sensors. In addition, 4x 10kΩ±% were implemented to accommodate the read out of the Flexiforce® sensors. The setup can again be powered with a 5V USB/phone charger adapter or by connecting the Arduino® Mega itself to a computer. The setup is shown in Figure 7.10. It can be covered with a lid to prevent contamination. The sensor data is logged every second on the SD-card.

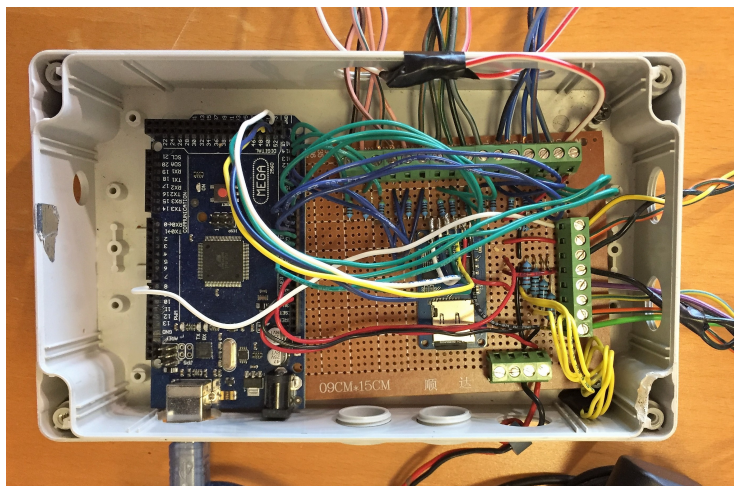


Figure 7.10: Arduino® Mega setup, including SD card reader

Note that the 4 Flexiforce® sensors each also require an analogue connection to the Arduino®. Unfortunately, no Arduino® micro-controllers exist with more than 16 analogue input ports. So this implies that the 15 NTC sensors cannot be simultaneously read-out together with the 4 Flexiforce® sensors using solely the Arduino® Mega. In some test, therefore only 12 NTC sensors were connected in combination with 4 Flexiforce® sensors. 3 NTC sensors at the left side of the grid (nr. 1 to 3 shown in Figure 7.6) were disconnected. Due to symmetry they should give similar temperature results than the ones measured by the right hand side sensors numbers 13 to 15. In later tests (from sample R4-TM1-4 onwards), both the Arduino® Nano and Mega setups were simultaneously used such that all 15 NTC and 4 Flexiforce® sensors could be processed. They were reset synchronously such that data processing initiated at the same moment.

7.3. Test series R3: EX-CORE samples with new 043 DU 80 grade

In the third test series R3, several samples were produced that contained the new Expancel® 043 DU 80 grade. As epoxy matrix either the SZ 8525 hardener or the Ancamine® 2442 in combination with the SR 1280 resin was used. These matrix systems gave the most promising results in previous test series R1 and R2. In total 7 additional samples were produced in the tile mold. An overview of their mix formulation, cure temperature and cure time is given in Table 7.1. Note again that the given cure times were obtained using the numerical model, still in a similar way as explained in Section 6.2.2. So the thermal block condition of setting $\dot{q}_{int} = 0$ was not yet implemented but an extra time difference (to reach the thermal block temperature) was added to the 98% simulated cure time. An overview of the most important sample results is given in Table 7.2. All manufactured R3 series samples are discussed in the following paragraphs. Again for all samples the obtained temperatures and pressure plots can be found in Appendix H.

Table 7.1: Overview of R3 series manufactured samples.

Sample label	Sample height	Mix	Resin type	Hardener type	Epoxy ratio r	043 DU 80 vol.%	Cure temp	Cure time
R3-TM1-1	30mm	270-opt	SR 1280	SZ 8525	100:24	4%	110°C	15min
R3-TM1-2	30mm	270-opt	SR 1280	None used!	/	4%	110°C	>1hour
R3-TM1-3	30mm	270-opt	SR 1280	Ancamine [®] 2442	100:60	4%	110°C	24min
R3-TM1-4	30mm	270-opt	SR 1280	SZ 8525	100:24	4%	110°C	15min
R3-TM1-5	30mm	270-opt	SR 1280	SZ 8525	100:24	1%	110°C	15min
R3-TM1-6	30mm	270-opt	SR 1280	Ancamine [®] 2442	100:60	4%	140°C	19min
R3-TM1-7	30mm	270-opt	SR 1280	Ancamine [®] 2442	100:60	4%	160°C	16min

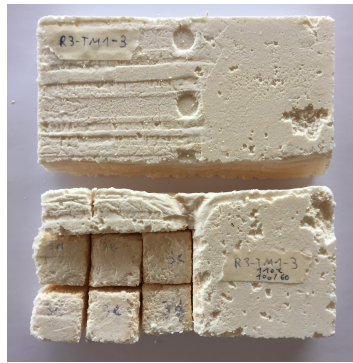
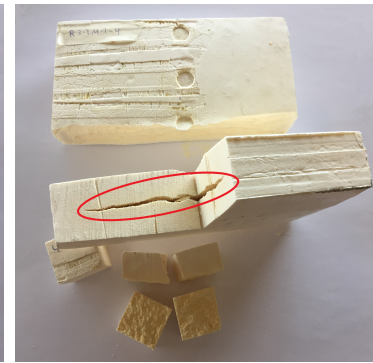
Table 7.2: Overview of R3 sample results, pressure and temperature measurements & rating of sample curing and expansion

Sample label	Room temp.	Sample mass	Max. surf. pressure	Time to reach 0.5bar (avg.)	Temp. at 0.5bar	Max. core. temp.	Sample curing ¹	Sample expansion ²
R3-TM1-1	24°C	243.8g	5.00bar	6.1min	85°C	172°C	5	5
R3-TM1-2	27°C	/	0.88bar	/	/	110°C	0	0
R3-TM1-3	27°C	224.7g	1.49bar	8.1min	107°C	141°C	4	2
R3-TM1-4	27°C	260.0g	3.48bar	8.3min	102°C	>145°C	5	5
R3-TM1-5	24°C	257.8g	4.01bar	6.4min	98°C	183°C	5	5
R3-TM1-6	24°C	259.1g	2.38bar	6.2min	109°C	165°C	5	3
R3-TM1-7	21°C	263.3g	3.09bar	5.2min	102°C	181°C	5	3

¹ On a scale from 1 to 5, with 5 being fully cured.

² On a scale from 1 to 5, with 5 being excellent expansion.

R3-TM1-1, the first R3 sample that was produced, was similar to sample R1-TM1-7 (see Section 6.2) but contained 4% of the new 043 DU 80 grade. Unfortunately, during sample curing the glue claps were poorly positioned, and such the high generated pressure caused the glue claps to move out of position causing the mold to open slightly at one side. This in turn caused EX-CORE to squeeze out of the mold slits as shown in Figure 7.11. The obtained data is therefore not representative.

**Figure 7.11:** Tile mold bursting open during curing of sample R3-TM1-1**Figure 7.12:** Sample R3-TM1-3; small blocks cut/used for compression testing**Figure 7.13:** Sample R3-TM1-4 with large crack visual in cut out

A similar sample **R3-TM1-4** was produced, for which it was ensured that the glue clasps could not move out of position during curing. After 15 minutes curing at 110°C, the hot sample was taken out of the mold lids and its sample casing. The hot sample felt fully cured and was sufficiently expanded, the surface finish was smooth and the M8 imprint was not visual anymore. However, during mold opening the top surface of the sample became convex. One half of the sample was cut and a large crack was clearly visual in the central region, as shown in Figure 7.12. This crack most probably originated during mold opening when the sample expanded due to the high internal pressure generated by DU at elevated temperatures. It was observed

that right before mold opening the temperature in the core was still increasing, exceeding 145°C (see plot R3-TM1-4 in Appendix H). It is therefore reasonable that, although the sample was sufficiently cured, the epoxy matrix network could not withstand the high internal pressure generation of the blowing agent inside DU. Note also that a relatively high maximum pressure of 3.48bar has been registered and that the sample expansion initiated (when 0.5bar was reached) around 102°C, so right in between the expansion range of 95-115°C of Expancel® 043 DU 80 [56].

An additional sample with the SZ 8525 hardener has been manufactured but with only 1vol.% of 043 DU 80, namely sample **R3-TM1-5**. This with the intention to lower the maximum pressure and thus possibly eliminate the expansion/bursting of the sample at mold opening. The temperature and pressure plot is given in Figure 7.14. It gives a good representation of typical measurement plots. As said, plots for all other produced samples can be found in Appendix H.

As can be seen in Figure 7.14, pressures up to 4 bar were recorded which is surprisingly slightly more than the 3.48bar measured in sample R3-TM1-4, containing 4vol.%DU. This higher pressure could be related to the higher temperature peaks that were measured in the core; as high as 183°C! Note that in Figure 7.14 the lower orange pressure curve from FSR 2 located in the center of the surface is disregarded in the average pressure calculation because this sensor was affected by the presence of the sensor grid located right under need it. In the figure it can also be seen that EX-CORE expansion (at the average 0.5bar point) is initiated after 6.4min when the average temperature in the core reached 98°C. This is only slightly above the lower boundary of the 95-115°C onset expansion temperature range of 043 DU 80. As expected, in the graph it can also be seen that the NTC temperature sensors located near the boundaries initially recorded higher temperatures than the NTC sensors located in the middle of the core (which is clearly visual for NTC sensors 6 and 13). Around minute 7 this alters since the temperature in core becomes higher due to the exothermic reaction of the epoxy. Ultimately, also sample R3-TM1-5 became convex when removing the upper mold lid after a 15 minute cure. This resulted in a large crack in one half of the sample as can be seen in Figure 7.15.

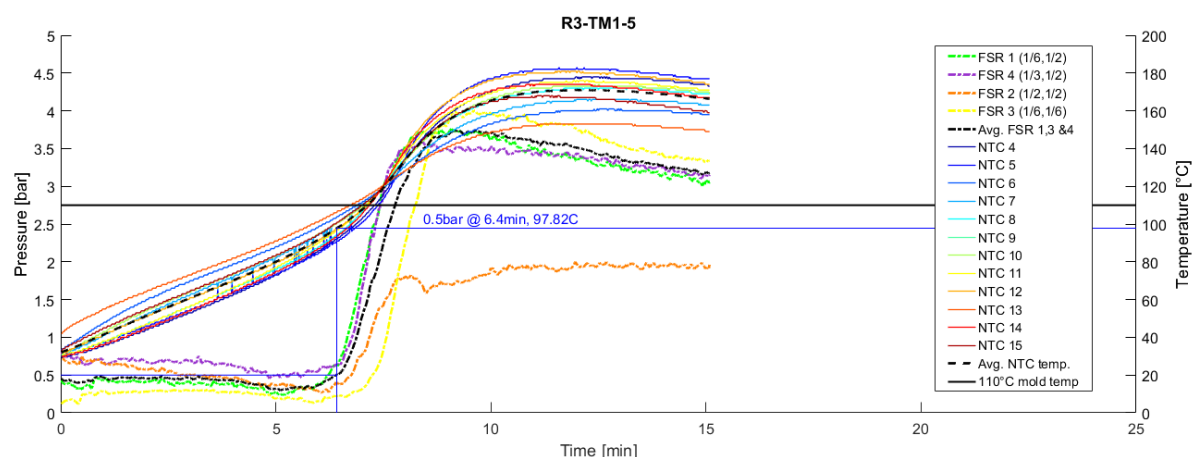


Figure 7.14: Measured pressure and temperature of sample R3-TM1-5 during 15min cure in pre-heated 110°C mold. (NTC9 temperature neglected due to erroneous/short-circuited signal.)

Sample **R3-TM1-2** was produced without any hardener. It was similar to sample R1-TM1-6 but now 4vol.% of the new 043 DU 80 grade has been used. It was first heated at 110°C for almost 1 hour. Unfortunately, again no increase in pressure was measured (plot R3-TM1-2a in Appendix H). Consequently, the mold temperature was increased to 120°C and after 45 more minutes it was even increased to 140°C for 30 minutes. In all cases no increase in pressure was recorded (see plots R3-TM1-2b and R3-TM1-2c in Appendix H). So although the more resistant 043 DU 80 grade has been used and the onset expansion temperature range of 95-115°C had been reached, the pressure generation mechanism did not seem to work in "EX-CORE" samples that did not contain any hardener, at least when only 4vol.% DU is used. It could therefore be that the used DU volume fraction is simply too low to obtain a measurable pressure difference in low viscous/non-curing EX-CORE mixtures. Similar samples with higher amounts of DU were not manufactured during this research, so this hypothesis could not be confirmed.

Sample **R3-TM1-3** was manufactured with the Ancamine[®] 2442 hardener and 4vol.% of 043 DU 80. It was cured at 110°C for 24 minutes. Note that this sample is similar to sample R1-TM1-5 but now the new DU grade was used and the sample was cured for 9 additional minutes (the simulated time required to reach the onset expansion temperature of 93°C everywhere in the sample). A maximum surface pressure of only 1.49bar was recorded. This could be related to the relatively low maximum temperature of 141°C that was recorded. Expansion initiated around 107°C. When the hot sample was taken out of the mold after 24min, some of the EX-CORE adhered to the aluminum top plate. This because the sample was also relatively brittle. Additionally, the hot sample could be slightly compressed by hand. The sample is shown in Figure 7.12. The rough surface is caused by the adherence of pieced to the top aluminum plate, when it was removed.

It was decided to create a similar sample, **R3-TM1-6**, but now cured at higher temperature, namely 140°C. This seemed worth the try because in the previous sample only a low temperature peak of 141°C was measured. In addition this higher cure temperature would reduce the required cure time by 5min (24min at 110°C to 19min at 140°C). Also a higher cure temperature could result in better expansion of the sample. Part of the resulting (original 140°C cured) R3-TM1-6 sample is shown in the lower part of Figure 7.16. The sample was not brittle any more and was completely rigid. It was also dimensionally stable when taken out of the mold; it did not became convex and no cracks were formed. It was measured that the maximum surface pressure increased to 2.38bar and the maximum core temperature to 165°C. The resulting sample had a relatively smooth surface finish, the M8 bolt imprint was not visual anymore. However, the sample had a slightly darker yellowish color. It should also be noted that a strong chemical smell could be observed. This could later be related to the behavior of the Ancamine[®] 2442 hardener at higher cure temperatures, as observed in additional performed DSC tests explained in Section 8.4.

Finally, another sample **R3-TM1-7** was produced with the Ancamine[®] 2442 hardener and 4vol.% of 043 DU 80 but now cured at an even higher cure temperature of 160°C, this for 16min. The resulting sample is shown in Figure 7.17. In this figure it can be seen that the surface seems to be more rough. The pinholes were caused because part of the EX-CORE stick to the aluminum plate when the mold was opened. The sample was again completely rigid and dimensionally stable when removed out of its mold casing. It was also slightly more darker yellow discolored. This time the temperature in the core of the sample increased up to 181°C. Also a slight increase in measured surface pressure was recorded, with a maximum pressure of 3.09bar.

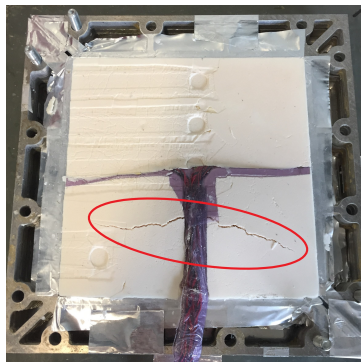


Figure 7.15: Sample R3-TM1-5 in aluminum sample casing; crack caused due to bursting upwards of sample

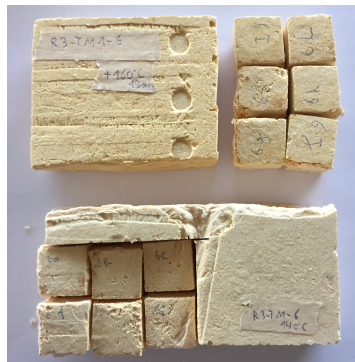


Figure 7.16: Sample R3-TM1-6; small blocks cut/used for compression testing. Lower part: originally cured at 140°C, upper part: extra post-cured at 160°C

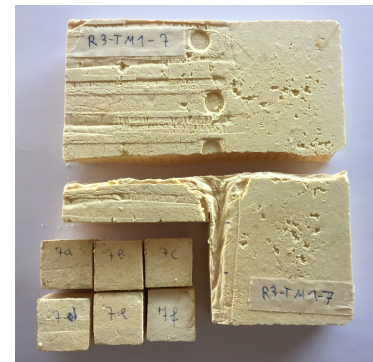


Figure 7.17: Sample R3-TM1-7; small blocks cut/used for compression testing

7.4. Conclusion: final selection of most promising epoxy system

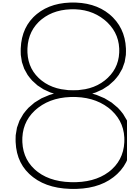
Based on the results of the produced sample series R3 with the new 043 DU 80 grade discussed in this chapter, it was concluded that the from the two remaining epoxy matrix systems, the Ancamine[®] 2442 hardener in combination with the SR 1280 resin, is most suitable for the fast curing EX-CORE processing. This epoxy system was therefore chosen to be further investigated in the current research. More specifically, the Ancamine[®] 2442 hardener was selected for the following reasons:

- As already became clear from test series R1 and R2, the use of the SZ 8525 has one major disadvantage. Namely, the SZ 8525 does not have a thermal block, which means that once mixed with resin, it will start

to react at room temperature. This is a major limitation for large scale production since it is not possible to prepare EX-CORE mixtures in large batches and/or store them for a certain amount of time before used in sandwich structure production/curing. This would also makes it difficult to obtain consistent results, as variations in pre-mixed storage times would effect the degree of cure, temperature peaks etc. The Ancamine[®] 2442 hardener does not have this problem since according to the datasheet it has an onset reaction temperature of 93°C (measured by DSC scan at 10°C/min) [99]. Note that in the current research additional DSC scans were performed to determine the effect of heat-up rate on the onset reaction temperature. This will be discussed in Section 9.3.

- Another disadvantage of the SZ 8525 hardener is that it has a much higher total specific heat of reaction H_{Tspec} than the Ancamine[®] 2442 hardener. More specifically, values of 287J/g (SZ 8525) and 169J/g (Ancamine[®] 2442) were obtained from the DSC tests discussed in Chapter 4 (see Table 4.3). Due to the high exothermic heat release of the SZ 8525 hardener, high temperature peaks up to 183°C were measured and predicted for 110°C cured 30mm thick EX-CORE samples with the SZ 8525 hardener. These high exothermic reaction peaks could negatively effect EX-CORE properties, especially when they exceed the maximum temperature of Expancel[®] DU when the epoxy matrix is not yet sufficiently cured. Then the DU microspheres starts to deflate due to the escape of the blowing agent.
- Although that sufficiently cured samples were obtained in less then 15min with the SZ 8525 hardener, all samples produced with the new 043 DU 80 grade were not dimensionally stable when they were taken out of the mold. Due to the high core temperatures, the samples could not withstand the internal pressure generated by the (restricted) expansion of the blowing agent inside the 043 DU 80 microspheres. When the mold lid was removed, the samples became convex and large cracks were formed throughout the core (see Figures 7.13). Even when only 1vol.% 043 DU 80 was used (sample R3-TM1-5 shown in Figure 7.15), a large crack resulted and up to 4bar of pressure was measured. The small crack spotted in a previous sample R1-TM1-2 made with the former 031 DU 40 (see Figure 6.7), most probably occurred in a similar way and was not caused by degradation as thought earlier.
- Promising 30mm thick EX-CORE samples with the Ancamine[®] 2442 curing agent were manufactured, namely the ones cured at 140°C (R3-TM1-6) and 160°C (R3-TM1-7). Although they were slightly discolored yellowish, they were rigid and seemed sufficiently cured. The hot samples taken out of the mold were also dimensionally stable and did not contain any cracks.

In the third test phase discussed in Chapter 8, various EX-CORE samples produced with the Ancamine[®] 2442 hardener will be compression tested. New samples were produced (with different resin mix ratio's than 100:60) but also some of the EX-CORE samples created in this R3 test series were tested under compression, namely samples R3-TM1-3, R3-TM1-6 and R3-TM1-7. From these samples six smaller approx. 30x30x30mm blocks were cut, which could already be seen in Figures 7.12, 7.16 and 7.17.



Test phase 3: Compression strength tests & epoxy mix ratio update

During the third test phase covered in this chapter compressive strengths of various EX-CORE samples containing the SR 1280/Ancamine[®] 2442 epoxy matrix were determined. Some R3 series samples already manufactured during the previous test phase were tested but also some additional samples (R4) were manufactured and tested to investigate the effect of cure temperature, cure time and epoxy mix ratio on the compressive strength of EX-CORE. The newly created R4 series samples are discussed in Section 8.1. Then, in Section 8.2 the determination of the lower boundary of epoxy mix ratio is explained. Next, in Section 8.3 the compressive strength determination procedure, test setup and compressive strength results of the various R3 and R4 tested samples will be discussed. As will become clear, a more optimal 100:20 epoxy mix was selected. Additional DSC tests were therefore performed with the SR 1280/Ancamine[®] 2442 epoxy system at mix ratio 100:20 as discussed in Section 8.4. Another series of samples (R5) was also produced to investigate the effect of a different mix formulation and increased DU content, this is covered in Section 8.5. Based on these test results the cause of crack initiation became clear, as explained in Section 8.6. Finally, a chapter summary with important conclusions is given in Section 8.7.

8.1. Test series R4: EX-CORE samples with various resin mix ratios cured at different temperatures

The R4 series samples were again produced in the preheated tile mold. During curing the generated pressure was recorded with the 4 Flexiforce[®] sensors. The temperature profile in the mid plane of the samples was measured with the 30mm NTC sensor grid and Arduino[®] Mega setup discussed earlier in Section 7.2. An overview of the manufactured R4 series samples is given in Table 8.1. Next, in Table 8.2 the overview of the pressure and temperature measurements is given. From sample R4-TM1-4 onwards it was tried to simultaneously monitor all 15 NTC sensors and the 4 Flexiforce[®] sensors using both the Arduino[®] Nano and Mega setups. Unfortunately, due to a bad contact in the 5V adapter cable (at that time unknown) the Arduino[®] Nano reseted itself, deleting the data on the SD card. Hence no pressure data of the R4-TM1-4 and -5 samples was available. From sample R5-TM1-2 onwards (see Section 8.5) this problem was recognized and a new 5V adapter was soldered to the Arduino[®] Nano setup. All R4 samples will be shortly discussed in the following paragraphs. Note that their compression test results will be presented and discussed in Section 8.3.2.

Table 8.1: Overview of R4 series manufactured samples.

Sample label	Sample height	Mix	Resin type	Hardener type	Epoxy ratio r	043 DU 80 vol.%	Cure temp	Cure time
R4-TM1-1	30mm	270-opt	SR 1280	Ancamine [®] 2442	100:30	4%	160°C	16+5min
R4-TM1-2	30mm	270-opt	SR 1280	Ancamine [®] 2442	100:60	4%	160°C	21min
R4-TM1-3	30mm	270-opt	SR 1280	Ancamine [®] 2442	100:20	4%	160°C	21min
R4-TM1-4	30mm	270-opt	SR 1280	Ancamine [®] 2442	100:20	4%	110°C	26min
R4-TM1-5	55mm	270-opt	SR 1280	Ancamine [®] 2442	100:20	4%	110°C	40min
R4-TM1-6	55mm	270-opt	SR 1280	Ancamine [®] 2442	100:60	4%	110°C	31min

Table 8.2: Overview of R4 sample results, pressure and temperature measurements & rating of sample curing and expansion

Sample label	Room temp.	Sample mass	Max. surf. pressure	Time to reach 0.5bar (avg.)	Temp. at 0.5bar	Max. core. temp.	Sample curing ¹	Sample expansion ²
R4-TM1-1	18°C	257g	/	/	/	190°C	5	5
R4-TM1-2	20°C	238g	3.6bar	4.9min	110°C	180°C	5	5
R4-TM1-3	18°C	264g	4.0bar	8.3min	102°C	190°C	5	5
R4-TM1-4	19°C	265g	/	/	/	151°C	5	3
R4-TM1-5	20°C	441g	/	/	/	152°C	5	2
R4-TM1-6	20°C	439g	1.9bar	16min	124°C	138°C	5	2

¹ On a scale from 1 to 5, with 5 being fully cured.

² On a scale from 1 to 5, with 5 being excellent expansion.

All previously manufactured R3 series samples contained the SR 1280/Ancamine[®] 2442 epoxy matrix at a mix ratio 100:60. This upper bound mix ratio (resin:hardener) was initially chosen because this would result in the fastest cure times as mentioned in Section 4.3.1. It was however unsure whether or not EX-CORE samples with higher compressive strengths could be obtained when using a different epoxy mix ratio. Therefore it was decided to create a sample similar to sample R3-TM1-7, also cured at 160°C but now created with an epoxy mix ratio of 100:30. This sample was labeled **R4-TM1-1**. Because DSC test had not been performed with this epoxy ratio, the cure kinetics were not available and so the 98% cure time could not be estimated with the numerical model. Therefore it was decided to take the sample out of the mold after 16min, similarly as done with sample R3-TM1-7. However, when the mold was carefully opened after 16min, it was clear that the sample was not yet fully cured and still wanted to expand. Therefore the mold was quickly re-closed and the sample was cured for 5 additional minutes. When opening the mold after a total cure of 21min, the sample was dimensionally stable. Although pressure data was lost, the sample seemed sufficiently expanded; the M8 imprint was not visible anymore at all. Sample R4-TM1-1 can be seen in Figure 8.1. As can be seen in the picture the cured sample was slightly discolored yellow.



Figure 8.1: Sample R4-TM1-1



Figure 8.2: Sample R4-TM1-2;
crack indicated

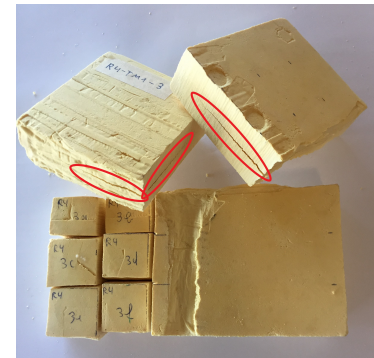


Figure 8.3: Sample R4-TM1-3;
cracks indicated

It will become clear in Section 8.3.2 that the compressive strength of sample R4-TM1-1 (100:30 epoxy ratio), was higher than sample R3-TM1-7 (100:60 epoxy ratio). However, from these sample results it could not be confirmed that the higher strength was caused due to the different mix ratio or due to the additional 5min cure time. Therefore sample **R4-TM1-2** was produced with the original 100:60 epoxy mix ratio, but now also cured at 21min. This time a small crack could be spotted in the center of the cured sample which is indicated in Figure 8.2. Again a slight yellow sample discoloration can be observed. A maximum pressure of 3.6bar was recorded during curing. From the compressive test results (see Section 8.3.2) it became clear the 5min extra cure time did not cause a meaningful increase in strength (sample R3-TM1-7 vs R4-TM1-2). It can therefore be concluded that the increase in strength (sample R3-TM1-7 vs R4-TM1-1) was caused due to the change in mix ratio from 100:60 to 100:30. Nonetheless, it was for example not sure if an even lower epoxy mix ratio would increase the compressive strength of EX-CORE even more.

To investigate the lower boundary of suitable epoxy mix ratio for the SR 1280/Ancamine[®] 2442 system, mixtures with a range of epoxy mix ratios were cured in plastic cubs in a small oven. The test is explained in more detail in Section 8.2. From this test it became clear that the lower epoxy mix ratio boundary was 100:20. It was therefore decided to manufacture sample **R4-TM1-3** with this 100:20 epoxy mixing ratio. To allow comparison with the previous samples, sample R4-TM1-3 was again cured at 160°C for 21min. The resulting cured sample is shown in Figure 8.3. Although that the hot sample was rigid when taken out of the mold, one half of the sample contained a large crack as indicated in Figure 8.3. A maximum pressure of 4 bar was recorded and the core temperature reached a maximum of 180°C right before the sample was taken out of the mold. As will be discussed in more detail in Section 8.3.2, the compressive strength was even higher than that of sample R4-TM1-1 (100:30 epoxy ratio) so it could be concluded that the optimal mix ratio (w.r.t. compressive properties) would be around 100:20. The determination of the most optimal exact epoxy mix ratio (i.a. 100:18 or so) was considered behind the scope of the current research. Therefore all subsequent samples were manufactured with a 100:20 epoxy mix ratio.

The next sample **R4-TM1-4** was again produced with the 100:20 epoxy mix ratio and was in formulation entirely similar to R4-TM1-3. However, this sample was cured at a lower cure temperature of 110°C to explore the compressive strength properties of this EX-CORE formulation when cured at a lower cure temperature. The 26min cure time of the sample was determined with the final version of the numerical model that included the condition of $\dot{q}_{int} = 0$ for nodes that do not yet have reached the thermal block temperature of 93°C (discussed in Section 5.6). At that time additional DSC tests were performed with the SR 1280/Ancamine[®] 2442 system at 100:20 mix ratio. These DSC test will be discussed in Section 8.4. The resulting cure kinetics were thus implemented in the numerical model. The cured R4-TM1-4 sample is shown in Figure 8.4. When taking the hot sample out of the mold, it was dimensionally stable and rigid. No cracks could be spotted in the cross-section of the sample. Unfortunately, the recorded pressure data was lost. Nonetheless from the surface of the sample it could be seen that EX-CORE did not sufficiently expand, the contours of the M8 bolt nut imprint were still visual and some pores could be seen in the surface of the sample. It should also be noted that the cured sample was not discolored as bright yellow as the 160°C cured samples. The lower cure temperature however reduced the compressive strength of EX-CORE (see Section 8.3.2).

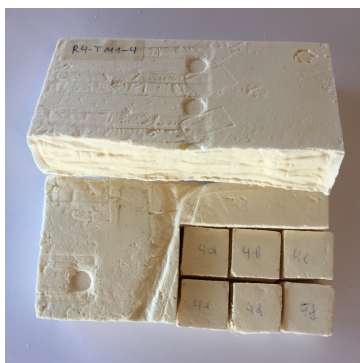


Figure 8.4: Sample R4-TM1-4

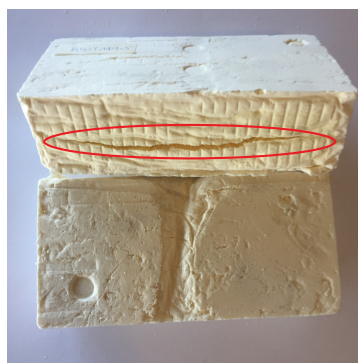


Figure 8.5: Sample R4-TM1-5;
crack indicated



Figure 8.6: Sample R4-TM1-6

Sample **R4-TM1-5** was in formulation entirely similar to the previous sample but now instead of 30mm it was 55mm thick. This thicker sample was i.a. created to validate the numerical model (see Chapter 9). For this purpose the 15 NTC sensors were repositioned on a larger 55mm metal grid, which is shown in Figure 8.7. The sample was cured for 40min at 110°C. It can be seen in Figure 8.5. Although the hot sample was sufficiently rigid/cured when taken out of the mold, it was not dimensionally stable; a large crack emerged throughout the cross-section of the sample which is indicated in Figure 8.7. Unfortunately again all pressure data was lost. From the surface of the sample it could however be clearly observed that the sample did only marginally expand; the surface was very rough and the imprint of the M8 bolt nut was still clearly visual.

Another 55mm thick sample was created for validation purposes. This sample was labeled **R4-TM1-6** and is shown in Figure 8.6. It was again cured at 110°C but in contrary to the previous sample an 100:60 epoxy mix ratio was used. This time a pressure of at most 1.9bar was recorded. The sample also did not looked

sufficiently expanded; its surface was rough and some pores could be observed. Nevertheless the sample was completely rigid and dimensionally stable when it was taken out of the mold after a 31min. Also no internal cracks could be discovered.

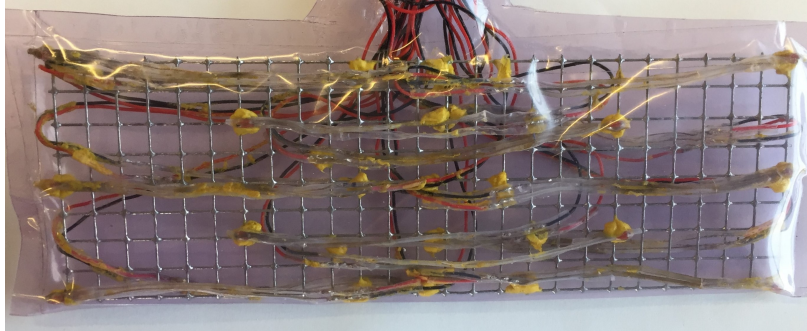


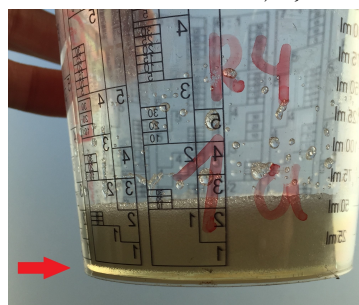
Figure 8.7: 15 NTC sensors including wiring attached to 55mm height metal grid. Entire setup wrapped in vacuum foil

8.2. Determination of the lower boundary of SR 1280/Ancamine[®] 2442 epoxy mix ratio

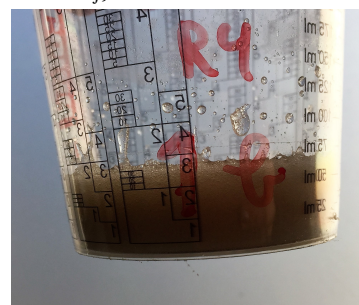
To determine the lower boundary of suitable epoxy mix ratios, six SR 1280/Ancamine[®] 2442 epoxy mixtures with varying epoxy mix ratios ranging from 100:10 to 100:60 were prepared in plastic mixing cups. In each cup 50g SR 1280 was mixed with the required amount of Ancamine[®] 2442 curing agent. The mixtures were cured for 30min in a small 110°C preheated Tefal oven available at Donkervoort. The resulting cured mixtures can be seen in Figure 8.8. When inspecting the cured mixtures it became clear that only for the 100:10 mixture (in mix cup 1a) a transparent layer of epoxy was visible on the bottom of the mixing cup, as indicated in Figure 8.8b. This implies that there was not enough hardener available to react with the resin. In contrary to all the other samples which were fully rigid, the "cured" 100:10 mixture was a highly viscous liquid (even after several weeks). It can thus be concluded that for the SR 1280/Ancamine[®] 2442 epoxy system, the lowest successfully tested mixing ratio is 100:20. It could be possible that a more specific mixing ratio (i.a. 100:18 or so) would also still be suitable, but investigating this was considered behind the scope of the current research.



(a) All cured mixtures on a row: used epoxy mix ratios from left to right; 1a) 100:10, 1b) 100:20, 1c) 100:30, 1d) 100:40, 1e) 100:50 and 1f) 100:60



(b) Close-up of cured 100:10 mixture (1a); unreacted layer of transparent resin visible at the bottom.



(c) Close-up of cured 100:20 mixture (1b); no unreacted layer of transparent resin visible at the bottom.

Figure 8.8: Cured mixtures of SR 1280/Ancamine[®] 2442 at 6 different mix ratios ranging from 100:10 (mix cup 1a) to 100:60 (mix cup 1f)

8.3. Compressive strength determination using Donkervoort's pressure jack

To determine the compressive strength of the EX-CORE samples, a compression test setup available at Donkervoort was used, which can be seen in Figure 8.9. This setup was developed by Santos in 2015 and consisted out of a pressure jack combined with a load cell based weighing balance, a dial gauge micrometer and a load readout display. The top part of the pressure jack can be moved manually with a torque wrench such that pressure can be applied on the sample.



Figure 8.9: Donkervoort's pressure jack with load cell, dial gauge micrometer and readout display.

Although the setup is not conform ASTM standards it allows for quickly testing various EX-CORE samples to get an idea of their compressive strength range. It is however important to take the drive compliance of the pressure jack into account because at high loads part of the deflection measured by the micrometer is actually the deflection of the jack itself instead of the deflection of the sample. This drive compliance was determined by Eversdijk [64] by placing a high stiffness solid block of steel in the pressure jack and then compressing this block. He obtained a drive compliance of $0.001438 \times \text{load [lbs]}$, which gives the amount of vertical displacement in mm that is caused by the deflection of the jack's structure for a certain load in lbs. When correcting for this drive compliance, the original obtained stress-strain curve shifts to the left and now for the same stress value a lower strain is obtained. An example of a stress-strain curve with and without drive compliance correction is given in Figure 8.10.

Eversdijk [64] manufactured several 270-optimal mix samples and compared their compression strength data obtained with Donkervoort's compression jack with tests conducted in accordance to ASTM standard D1621 [146] on the Zwick 250kN available at the Delft University of Technology. For proper comparison, sub-samples of the same sample were tested on either of both setups and compared. When applying the drive compliance correction Eversdijk [64] found a maximal difference of 0.48MPa (+8%) compared to Zwick 250kN test results.

Due to its simplicity and ability to quickly obtain test results, Eversdijk [64] recommended the use of Donkervoort's pressure jack for relative comparison of different sample formulations and/or initial estimates of strength values. He concluded that the setup is adequate in determining strength values if an uncertainty around 10% is acceptable. Therefore in the current research the Donkervoort's pressure jack was used. The test procedure is explained in Section 8.3.1. When later more exact determinations are required, a setup that is in accordance with ASTM standard D1621 [146] should be used such as the Zwick 250kN .

8.3.1. Compression test procedure and data processing

From the cured 175x751x30mm sample tile blocks, 6 equal sub-samples (labeled a to f) of approximately 30x30x30mm were cut and scoured with sandpaper. Before the sub-samples were compression tested, the density of each sub-sample was determined. Three measurements with a caliper were done on each side of the sub-sample, from which the volume was calculated. In addition, the samples were weighted to the nearest 0.1g. The resulting densities of each tested sub-sample are given in Appendix I.

The compression test procedure continued as follows: First, the sub-sample was placed on top of the load cell after which a pre-load in the range of 0-10lbs was applied. At this point the micrometer is set to zero and the test is initiated. Displacement steps of 25mm were performed and at each step the corresponding load was recorded. The sub-samples were compressed until a strain of at least 0.15% was reached. Note that during the entire test the displayed loads were filmed with a phone camera. At the end of the test the load data was retrieved from the film. This ensured a smooth continuation of the test without data recording interruptions which would have happened otherwise with live step-wise data recording.

To obtain the compressive strength of each tested specimen, the following data processing steps were performed: The stress-strain curves were determined from the measured loads and deflections using the initial height and surface area of the samples. As mentioned before, the stress-strain curves were also corrected to take the drive compliance of the pressure jack into account (see example in Figure 8.10).

ASTM standard D1621 [146] specifies a procedure to determine the compressive strength for specimens that show no clearly defined yield point before the 10% strain point, which is also the case for EX-CORE samples: It dictates that the compressive strength should be determined at 10% strain, but after determination of the new "zero-strain" point. This point is determined by extrapolating the steepest part of the curve and its intersection with the horizontal axis. The point is indicated as point O in Figure 8.11. In this figure, X_1 represents the new 10% strain margin, and thus point P represents the resulting compressive strength.

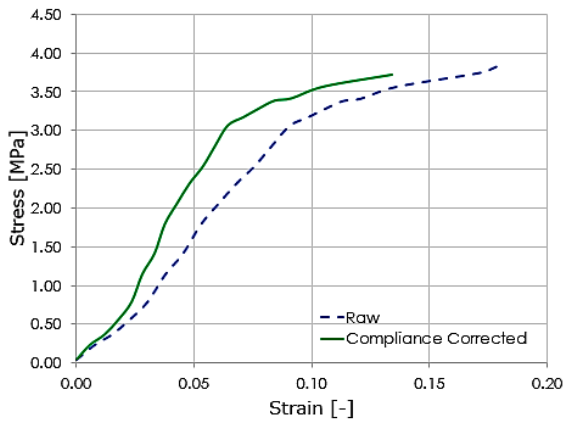


Figure 8.10: Example of stress-strain plot of sample R4-TM1-4c with and without drive compliance correction.

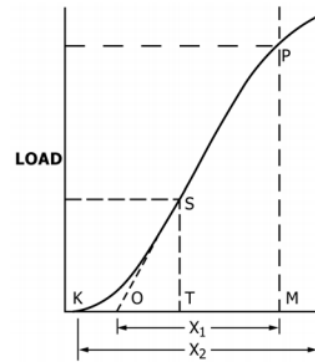


Figure 8.11: Schematic of new "zero strain" point O and 10% strain point P determination procedure)[146]

8.3.2. Compressive strength results R3 & R4 samples

In this section the compressive strength results of various tested R3 and R4 samples will be given and discussed. For ease of comparison an overview of the mix formulation, cure temperatures, cure times etc. of the compression tested R3 & R4 samples is given in Table 8.3. Note that part of the 140°C cured sample R3-TM1-6 was post-cured at 160°C for an additional 19min. It will simply be referred to as "R3-TM1-6 postcured" in this chapter. Its sub-samples were labeled 6g to 6l in Appendix I.

Table 8.3: Overview of R3 and R4 series samples that were compression tested.

Sample label	Sample height	Mix	Resin type	Hardener type	Epoxy ratio r	043 DU 80 vol.%	Cure temp	Cure time
R3-TM1-3	30mm	270-opt	SR 1280	Ancamine [®] 2442	100:60	4%	110°C	24min
R3-TM1-6	30mm	270-opt	SR 1280	Ancamine [®] 2442	100:60	4%	140°C	19min
R3-TM1-7	30mm	270-opt	SR 1280	Ancamine [®] 2442	100:60	4%	160°C	16min
R4-TM1-1	30mm	270-opt	SR 1280	Ancamine [®] 2442	100:30	4%	160°C	16+5min
R4-TM1-2	30mm	270-opt	SR 1280	Ancamine [®] 2442	100:60	4%	160°C	21min
R4-TM1-3	30mm	270-opt	SR 1280	Ancamine [®] 2442	100:20	4%	160°C	21min
R4-TM1-4	30mm	270-opt	SR 1280	Ancamine [®] 2442	100:20	4%	110°C	26min

As already mentioned before, from each tile sample 6 sub-samples were tested under compression. The corrected stress-strain curves of all sub-samples can be seen in Figure 8.12. These stress-strain curves were already corrected for both the drive compliance of the pressure jack and the new "zero-strain" point. The resulting compressive strengths vs specimen densities are plotted in Figure 8.13. An overview of the exact compression strength results, specimen densities and specific compressive strength results of all sub-samples can be found in Appendix I.

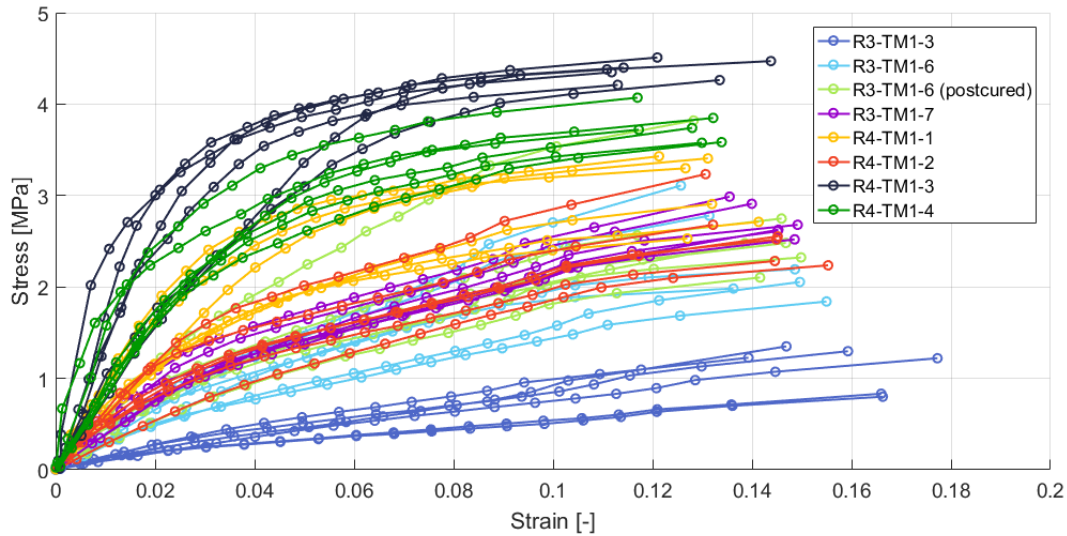


Figure 8.12: Stress strain curves of compression tests on samples R3-TM1-3,-6,-7 and R4-TM1-1,-2, -3 & -4 tested on the Donkervoort pressure jack.

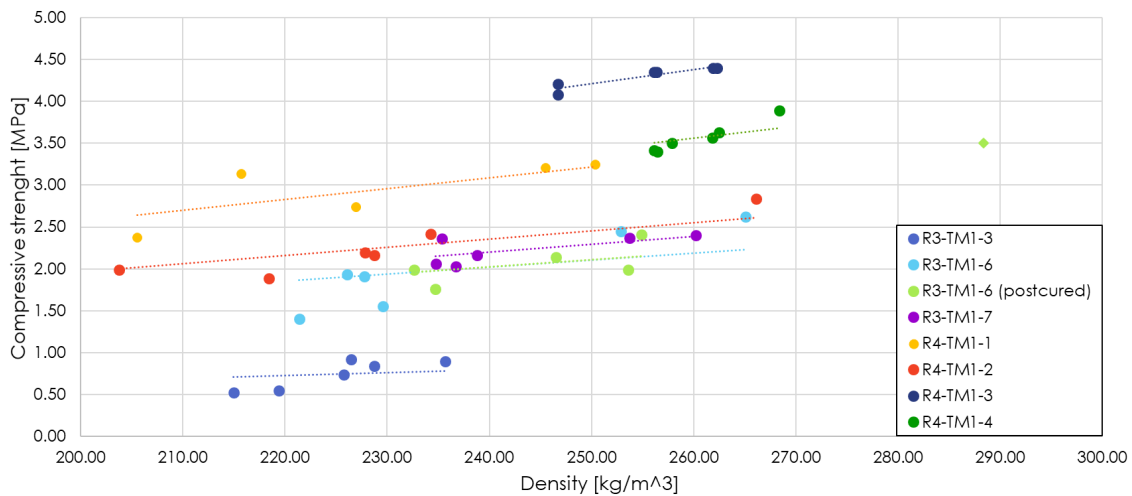


Figure 8.13: Compressive strength vs. density for samples R3-TM1-3,-6,-7 and R4-TM1-1, -3 & -4 tested on the Donkervoort pressure jack.

As indicated in the graph in Figure 8.13, one outlier can be observed (upper right). Compared to the other sub-samples of R3-TM1-6, sub-sample R3-TM1-6i has a much higher density and compressive strength value. On the surface of this compressed specimen one large lighter colored spot could be observed, indicated in Figure 8.13. This is most probably a Q-Cel rich area, which would explain the higher density and compressive strength of this specimen. Therefore the data of sub-sample R3-TM1-6i is neglected in further averaging calculations.

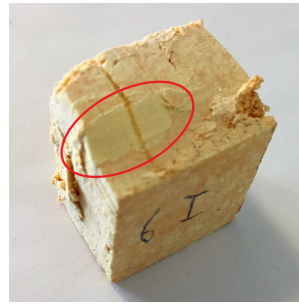


Figure 8.14: Sub-sample R3-TM1-6i (postcured); large brighter colored spot of compacted Q-Cel indicated

An overview of the average specific compressive strength values and standard deviation of each tested tile mold sample is given in the bar chart plot in Figure 8.15. For ease of comparison, the three variables: cure temperature, cure time and resin mix ratios are given as well. Note that all the other parameters (270-opt mix, 30mm sample thickness, 4 vol.% 043 DU 80, SR 1280/Ancamine[®] 2442 epoxy system etc.) are equal for each of the tested samples. As reference, the compressive strength of the original EX-CORE composition with the 270-optimal mix formulation (with 4vol.% of 031 DU 40 and the former epoxy matrix) is 4.76MPa [63, 64]. With a foam density of 270kg/m³ this results in a specific compressive strength value of 17.63kNm/kg. Note that the mechanical properties for various foam densities of EX-CORE, ROHACELL[®] Triple F and SynCore[®] were given in Table 3.5.

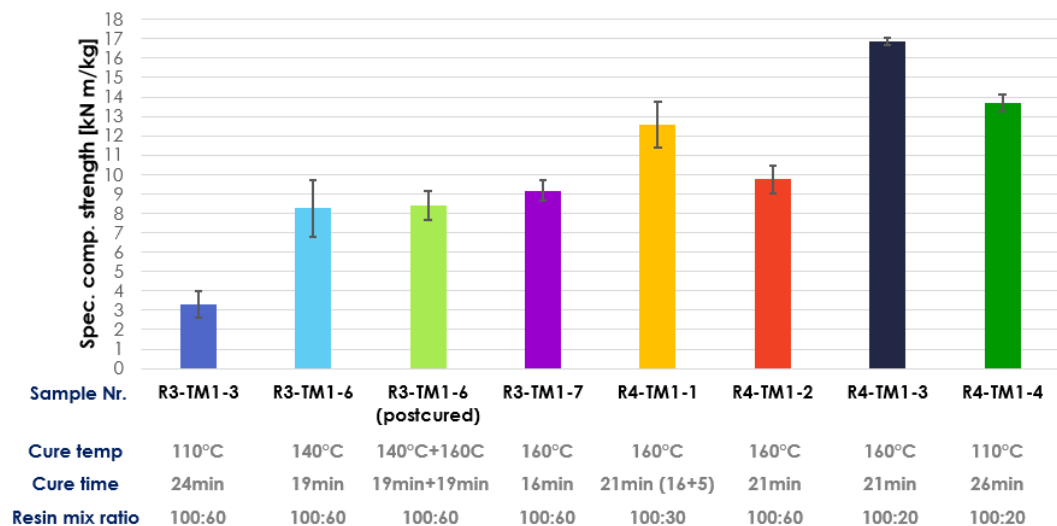


Figure 8.15: Comparison of average spec. compressive strength results including 68% confidence interval of one standard deviation for samples R3-TM1-3,-6,-7 and R4-TM1-1,-2, -3 & -4 tested on the Donkervoort pressure jack.

The first sample that was tested, **R3-TM1-3**, was cured at 110°C and contained the 100:60 epoxy ratio. An average specific compressive strength value of only 3.28kNm/kg was obtained, which is more than 5 times lower than the value of the original 270kg/m³ EX-CORE foam (17.63kNm/kg). As mentioned in Section 7.3, sample R3-TM1-3 was also relatively brittle in nature and so it easily crushed.

As can be seen in Figure 8.15, the specific compressive strength of sample **R3-TM1-6** with similar formulation but cured at 140°C, more than doubled to 8.27kNm/kg. The effect between a cure of 140°C and 160°C was however less pronounced; The specific compressive strength of sample **R3-TM1-7** which was cured at 160°C, was 9.17kNm/kg, still within the 68% confidence interval of sample R3-TM1-6 cured at 140°C.

Part of the cured sample R3-TM1-6 was also postcured for an additional 19min at 160°C, it was labeled **R3-TM1-6 (postcured)**. This had only negligible effect on the specific compressive strength, for which now an average value of 8.40kNm/kg was obtained, only 1.6% higher when cured solely at 140°C. Due to its marginal effect, postcuring was not investigated any further.

Because the highest specific compressive strength values obtained with the 100:60 epoxy mix ratio samples (9.17kNm/kg for sample R3-TM1-7) were still almost twice as low as the original EX-CORE foam (17.63 kNm/kg), it was decided to test samples with a lower epoxy mix ratio which could possibly increase the compressive strength properties of EX-CORE to an acceptable comparable value. Such a lower epoxy mix ratio would however increase the required time to reach 98% cure. Note again that the 100:60 upper bound mix ratio was originally chosen because this would result in the fastest cure times.

Sample **R4-TM1-1** was produced with an epoxy mix ratio of 100:30 of the SR 1280/Ancamine[®] 2442. Similar to sample R3-TM1-7 it was intended to be cured at 160° for 16min, such that the sole variable would be the epoxy mix ratio. However, as explained already in Section 8.1 when opening the mold after 16min, it became clear the sample was not yet sufficiently cured so the mold was quickly re-closed and the sample was left to cure for an additional 5min. After a total cure of 21min the sample was rigid and dimensionally stable enough to take it out of the mold. Remark again that the 98% cure time could not be determined with the numerical model since at that moment in time no DSC scans were performed other than with the 100:60 ratio. As can be seen in Figure 8.15 the specific compressive strength of sample R4-TM1-1 (mix ratio 100:30 cured for 16min at 160°C) was much higher than sample R3-TM1-7 (mix ratio 100:60 cured for 21min at 160°). Namely, the spec. compr. strength increased to 12.59kNm/kg. It could however not be confirmed whether this was caused due to changed resin mix ratio and/or the 5min extra cure time.

Sample **R4-TM1-2** was in formulation similar to sample R3-TM1-7 but was cured for 5 additional minutes to investigate the possible effect of extended cure time on compressive properties. From the compressive test results it became clear that the 5 min extra cure time only marginally increased the spec. compr. strength from 9.17kNm/kg to 9.74kNm/kg, which is an increase of only 6% and approx. 1 standard deviation away from the average result of sample R3-TM1-7. It can thus be concluded that the increase in spec. compr. strength in sample R4-TM1-1 (w.r.t. to R3-TM1-7) was caused due to the change in epoxy mix ratio from 100:60 to 100:30.

As already discussed in Section 8.1, it was not known if a mixing ratio lower than 100:30 (or in between 100:60-100:30) would result in an even higher compressive strength. Therefore a simple test with epoxy mixtures with various mix ratios cured in a small oven was performed. From this test it became clear that the lowest suitable mix ratio boundary was 100:20 (see Section 8.2).

To investigate whether a sample with the 100:20 epoxy mix ratio would obtain an even higher compressive strength, sample **R4-TM1-3** was manufactured with this 100:20 epoxy mix ratio. It was again cured at 160°C for 21min, the same as done with samples R4-TM1-2 (100:60) and R4-TM1-1 (100:30). A significant increase in spec. compr. strength was obtained, namely a value of 16.85kNm/kg (on average 4.3MPa for a density of 255kg/m³) which is close to the 17.63kNm/kg value for the original 270-opt EX-CORE foam. At that moment in time it was therefore decided to continue the research with the 100:20 epoxy mix value. New DSC tests were performed with the SR128/ Ancamine[®] 2442 epoxy system at 100:20 resin mix ratio. These DSC test will be discussed in Section 8.4.

Finally, sample **R4-TM1-4** was also produced with the 100:20 epoxy mix ratio and was in formulation similar to sample R4-TM1-3. It was however cured at 110°C to explore the effect on the compressive properties. It was cured for 26min, which was the 98% cure time estimated with the numerical model that included the cure kinetic parameters for the 100:20 mix ratio. In addition from then onwards in the numerical model the condition of $\dot{q}_{int} = 0$ for nodes that do not yet have reached the thermal block temperature of 93°C was implemented (discussed in Section 5.6). The reduction in cure temperature from 160°C (R4-TM1-3) to 110°C (R4-TM1-4) caused a reduction in specific compressive strength by 18.7%, namely from 16.85kNm/kg to 13.70kNm/kg. It could however not be distinguished whether this is caused due to a better/higher cross-linked epoxy network formation at higher cure temperatures or for example due to the resulting higher pressure and thus better compaction/melting of the thermoplastic microspheres at increased cure temperatures.

8.4. DSC tests of SR 1280/Ancamine[®] 2442 epoxy at 100:20 mix ratio

At the start of this research multiple DSC tests were performed to determine the cure kinetics of new candidate epoxy systems (see Chapter 4). Isothermal DSC scans ranging from 90°C to 110°C were for example executed on the chosen SR128/ Ancamine[®] 2442 epoxy system. However, they were only performed with a mix ratio of 100:60 for this epoxy system. Since much higher compressive strengths were obtained with a 100:20 mix ratio, it was decided to execute additional DSC tests on the SR128/ Ancamine[®] 2442 epoxy system at mix ratio 100:20. The used test setup, methodology and data post-processing procedure is entirely similar as previously explained in Chapter 4. Additionally, the step-by-step isothermal DSC test procedure can be found in Appendix A. The new experimental DSC results will be presented and discussed in Section 8.4.1. Subsequently, the corresponding autocatalytic model cure kinetic results will be discussed in Section 8.4.2.

8.4.1. Experimental DSC results from isothermal DSC scans

Three new sets of isothermal DSC tests were performed on the SR 1280/Ancamine[®] 2442 epoxy mixed at ratio 100:20. An overview of these DSC sets, including the given reference label is presented in Table 8.4. Note that all their experimental DSC (and autocatalytic model) cure kinetic plots/results can be found in Appendix B.6.

Table 8.4: Overview of DSC test reference number, used mix ratio (by weight) and isothermal DSC test temperatures.

DSC test ref. nr.	Type of resin	Type of hardener	Mix ratio	Iso. DSC temp.
5	SR 1280	Ancamine [®] 2442	100:60	90°C to 110°C
5.2	SR 1280	Ancamine [®] 2442	100:20	90°C to 110°C
5.2-MidTemp	SR 1280	Ancamine [®] 2442	100:20	115°C to 135°C
5.2-HighTemp	SR 1280	Ancamine [®] 2442	100:20	140°C to 160°C
5.2-AllTemp ¹	SR 1280	Ancamine [®] 2442	100:20	90°C to 160°C

¹ Collection of DSC test data from 5.2, 5.2-MidTemp and 5.2-HighTemp

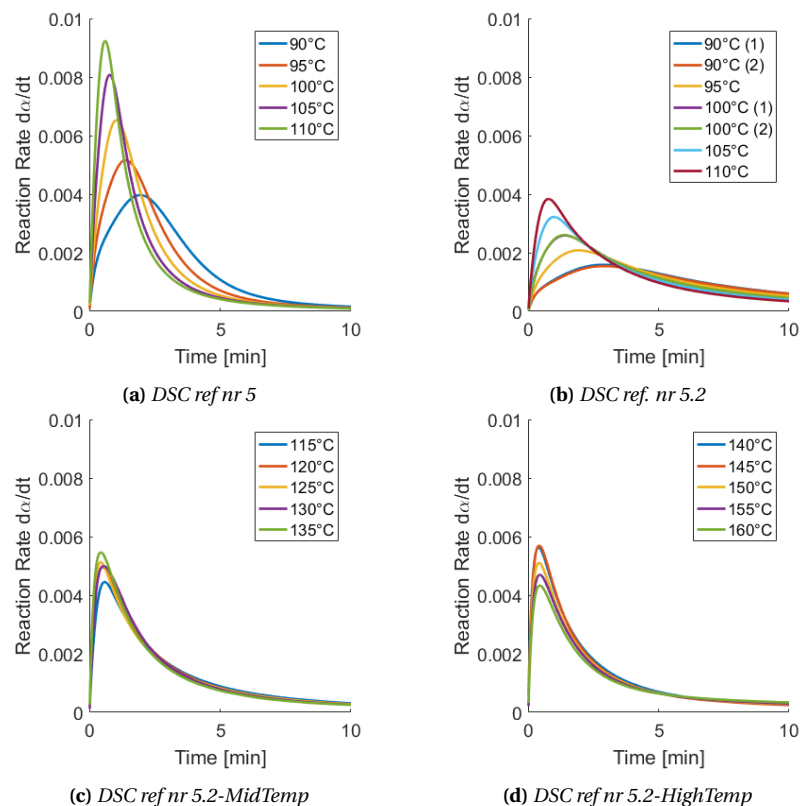


Figure 8.16: Measured reaction rate da/dt plotted as a function of time for different isothermal DSC tests. Tested resin SR1280 & hardener Ancamine[®] 2442 at mix ratio a) 100:60 and b,c,d) 100:20

The first new set of DSC scans (ref. nr. 5.2) were performed at isothermal temperatures 90°C, 95°C, 100°C, 105°C & 110°C, similar as was done for the previous 100:60 epoxy mix ratio DSC test (ref. nr. 5). The resulting reaction rates $d\alpha/dt$ for the first 10 minutes of the tests can be seen in Figure 8.16b. As expected, the reaction rates are lower than the ones previously obtained for the 100:60 epoxy ratio DSC scans (ref. nr. 5). These reaction rates are given as reference in Figure 8.16a. Also as expected, the reaction rates increase with increasing isothermal cure temperature.

Since several promising R3 and R4 series samples have been manufactured at a cure temperature of 160°C it was decided to perform an additional set of DSC scans at higher temperatures. This with as goal to verify and/or obtain a more accurate autocatalytic cure kinetic model at higher temperatures. Therefore 5 additional DSC scans were performed at isothermal temperatures ranging from 140°C to 160°C, referred to as "5.2-HighTemp". Some remarkable results were obtained; As can be seen in Figure 8.16d, the reaction rate dropped when isothermal cure temperature increased. This odd behavior could not directly be explained. It was decided to perform 5 extra DSC scans at the intermediate temperature range of 115 to 135°C. This test set is referred to as "5.2-MidTemp". The resulting reaction rates are plotted in Figure 8.16c. It can be seen in the figure that the reaction plots are all very close together, with the highest peak obtained for the 135°C test.

For ease of comparison all the specific heat flow curves are combined into one plot, shown in Figure 8.17. In this plot at the right, a close-up of the heat flow peaks is given. It can be observed that the heat flow peaks consequently increase with increasing cure temperatures until 120°C-135°C, with the highest peak obtained for the 135°C scan. Below this temperature the reaction peaks drop with increasing cure temperature.

In Figure 8.18, the total specific heat of reaction (H_{Tspec}) values for all the isothermal DSC scans ranging from 90 to 160°C are listed. For the first 6 DSC scans until 115°C, the H_{Tspec} values lie close together in the range of 213-218J/g. However, from the 120°C, 125°C, 130°C scans onwards H_{Tspec} starts to decrease to 204J/g, 186J/g and 178J/g respectively. For the 150°C DSC scan even a value as low as 166J/g had been obtained. These results are remarkable since under normal circumstances when the reaction is completed and the epoxy is fully cured, approximately the same total amount of energy should have been released for similar epoxy mixtures regardless if they are cured at a different temperature. Only the specific heat flow progress should be different.

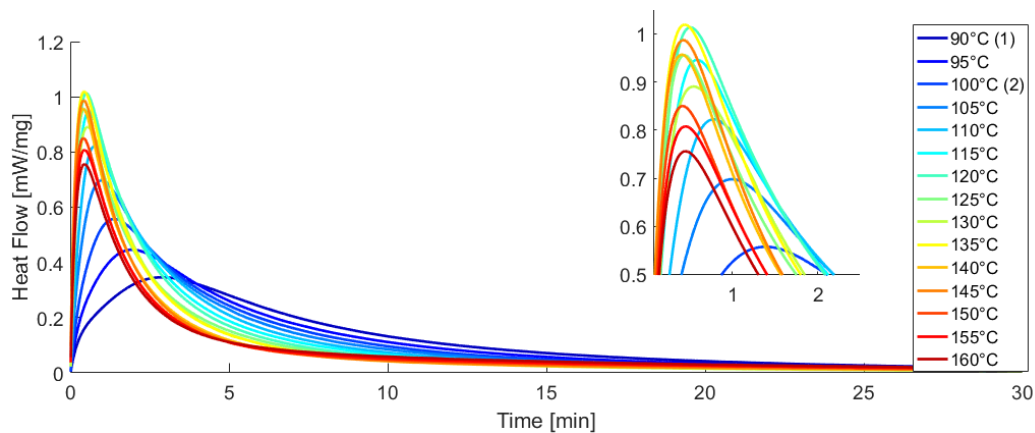


Figure 8.17: Specific heat flow ϕ_{spec} vs time at different isothermal DSC tests (5.2-AllTemp). Tested resin SR1280 & hardener Ancamine[®] 2442 at mix ratio 100:20. Close-up shown.

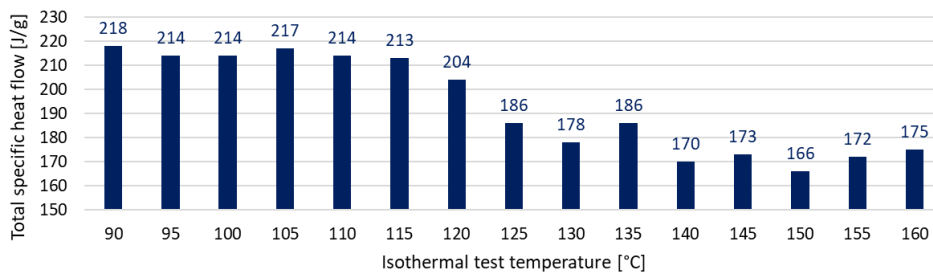


Figure 8.18: Bar chart of total specific total heat of reaction H_{Tspec} for isothermal DSC tests from 90°C to 160°C. Tested resin SR1280 & hardener Ancamine[®] 2442 at mix ratio 100:20.

The decrease in reaction rate when cured above 120°C-135°C is most probably related to the decrease in the total specific heat of reaction of the epoxy at these temperatures. This indicates that at higher cure temperatures for some reason less reaction takes place. Evonik came up with a possible explanation for this which is discussed in the following paragraph.

Possible clarifications cure kinetic behavior at elevated cure temperatures

Evonik, the manufacturer of the Ancamine[®] 2442 hardener was contacted with the question whether they could explain the decrease in reaction rate and total specific heat at cure temperatures above 120°C-135°C. They also found this behavior strange and initially could not come up with an explanation for this. They performed similar DSC tests with Ancamine[®] 2442 in combination with a diglycidyl ether of bisphenol A (DGEBA) epoxy resin. They obtained similar DSC results and also observed a decrease in reaction rate and total specific heat of reaction at higher cure temperatures. They decided to perform several additional tests in their lab to investigate the cause for this behavior. Ultimately, they came up with possible clarifications: First of all, the product acts as an accelerator for a pure epoxy-epoxy reaction and secondly, the OH groups that are formed during the reaction will further react at higher temperatures. So the theory is that at higher temperatures another cross-linked network is formed that leads to a less exothermic reaction and lower T_g. They also comment that it cannot be avoided that the product behaves like this, and so the performance is limited at higher temperatures. Additionally, they mentioned that Ancamine[®] 2442 is stable until ~170°C.

8.4.2. Modified-autocatalytic model cure kinetic parameters

The cure kinetic parameters of the new modified-autocatalytic model for the 100:20 SR 1280/ Ancamine[®] 2442 epoxy system as implemented in the numerical thermal model were calculated using only the DSC data from scans 90°C to 110°C (so DSC test ref. nr. 5.2). Due to the deviating behavior at higher cure temperatures, higher temperature scans were not included. The resulting cure kinetic parameters are given in Table 8.5. Note that intermediate post-processing and other autocatalytic model plots can be found in Appendix B.6.2.

The times to obtain 98% degree of cure at various cure temperatures are presented in Table 8.6. As reference the results of the 100:60 epoxy mix ratio tests (ref. nr. 5) are also given. It can be seen that the cure times more than doubled, for example from 7.2min to 18.8min when cured at 110°C. Nonetheless, this increase in cure time is justified since the measured specific compressive strength with the 100:20 mix ratio became more than 4 times higher (3.28kNm/kg vs 13.7kNm/kg) when cured at 110°C (see Section 8.3.2).

Table 8.5: Overview of the autocatalytic-model cure kinetic fit parameters and specific total heat of reaction for resin SR1280 & hardener Ancamine[®] 2442 at mix ratio 100:60 (ref. nr. 5) and mix ratio 100:20 (ref. nr. 5.2)

DSC test ref. nr.	Cure kinetic fit parameters						H _{Tspec} [J/g]
	n [-]	m [-]	E1 [kJ/mol]	E2 [kJ/mol]	A1 [1/s]	A2 [1/s]	
5	1.437	0.498	60.73	48.73	6.098E+04	1.210E+05	169
5.2	1.249	0.305	83.85	32.90	2.631E+07	1.967E+02	215

Table 8.6: Time to obtain 98% cure at 5 isothermal temperatures for resin SR1280 & hardener Ancamine[®] 2442 at mix ratio 100:60 (ref. nr. 5) and mix ratio 100:20 (ref. nr. 5.2). Determined with the modified autocatalytic model.

DSC test Ref. nr.	Time required for 98% cure [min]				
	90°C	95°C	100°C	105°C	110°C
5	16.8	13.5	10.9	8.8	7.2
5.2	33.5	28.8	24.9	21.6	18.8

Next, in Figure 8.19 the reaction rate $d\alpha/dt$ is plotted as a function of time for both the experimental DSC measurements (dashed curves) and modified-autocatalytic model results (solid curves). When comparing both results it can be seen that at 90°C, the model overestimated the reaction rate, while from 100°C onwards the model underestimates the reaction rates. This also has as an effect that the predicted degree of cure α deviates from the experimentally determined values, as visualized in Figure 8.20. These deviations are more pronounced than for example obtained for the 100:60 mix ratio (see Figures 4.13 and 4.13) but the reason

why this happens is unknown. It is thus important to take this into account in the validation of the EX-CORE numerical model discussed in Chapter 9.

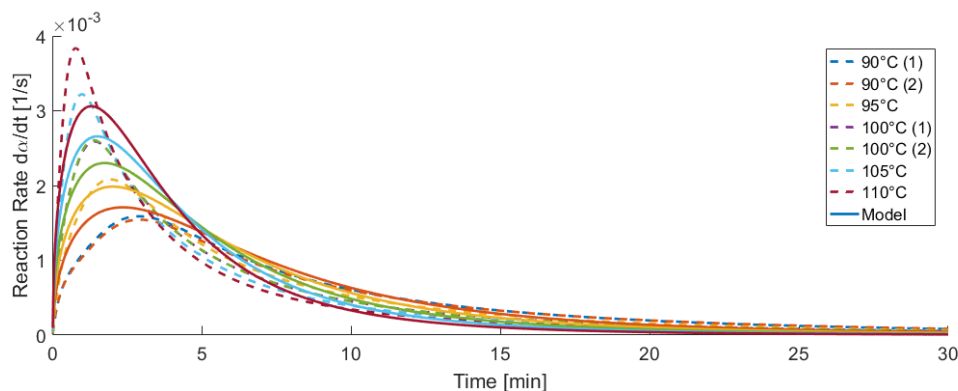


Figure 8.19: Reaction rate $\frac{d\alpha}{dt}$ vs time for both the experimental DSC tests (dashed line) and autocatalytic model (solid lines) when implementing the cure kinetic fit parameters (ref. nr. 5.2) shown in Table 8.5. Tested resin SR 1280 & hardener Ancamine® 2442 at mix ratio 100:20.

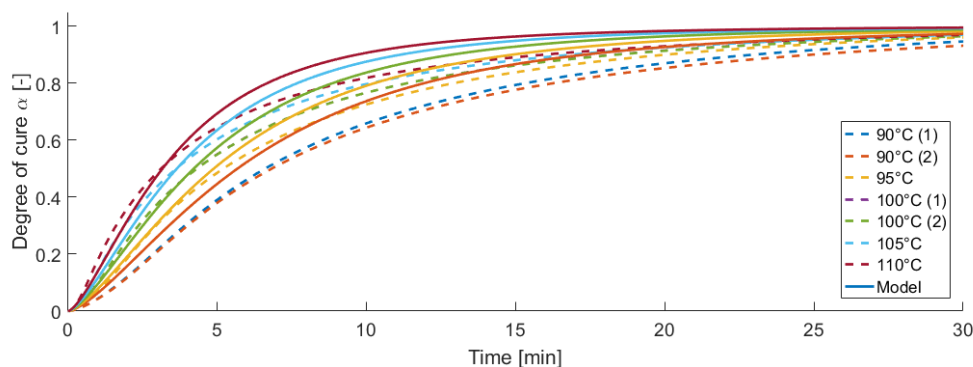


Figure 8.20: Degree of cure vs time for both the experimental DSC isothermal tests (dashed line) and autocatalytic model (solid lines) when implementing the cure kinetic fit parameters shown in Table 8.5. Tested resin SR 1280 & hardener Ancamine® 2442 at mix ratio 100:20.

8.5. Test series R5: Different EX-CORE mix formulation & increased DU content

In test series R5, three different samples were created with the 100:20 epoxy ratio; one sample with a new 80kg/m^3 mix formulation (see Table 8.9) and two 270-optimal mix samples with an increased Expancel® 043 DU 80 content of 7.5vol.%. An overview of the manufactured samples and their test results is given in Tables 8.7 and 8.8, respectively. Each of the samples is discussed in more detail in the following paragraphs.

Table 8.7: Overview of R5 series manufactured samples.

Sample label	Sample height	Mix	Resin type	Hardener type	Epoxy ratio r	043 DU 80 vol.%	Cure temp	Cure time
R5-TM1-1	55mm	80	SR 1280	Ancamine®2442	100:20	4%	110°C	43min
R5-TM1-2	30mm	270-opt	SR 1280	Ancamine®2442	100:20	7.5%	110°C	27min
R5-TM1-3	30mm	270-opt	SR 1280	Ancamine®2442	100:20	7.5%	110°C	27min

Table 8.8: Overview of R5 sample results, pressure and temperature measurements & rating of sample curing and expansion

Sample label	Room temp.	Sample mass	Max. surf. pressure	Time to reach 0.5bar (avg.)	Temp. at 0.5bar	Max. core. temp.	Sample curing ¹	Sample expansion ²
R5-TM1-1	24°C	146g	/	/	/	128°C	2	2
R5-TM1-2	24°C	267g	5.9bar	8.9min	103°C	146°C	5	5
R5-TM1-3	35°C	272g	5.9bar	9.0min	106°C	149°C	5	5

¹ On a scale from 1 to 5, with 5 being fully cured.

² On a scale from 1 to 5, with 5 being excellent expansion.

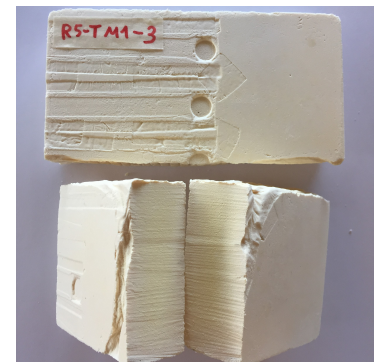
In previous research performed at Donkervoort some experiments were performed with an EX-CORE mix composition resulting in EX-CORE samples with an extremely low density around 80kg/m³. The composition of this mix, referred to as the "80" mix, is given in Table 8.9. The 80 mix does not contain any Q-Cel and as much as 95% Expancel[®] DE.

Table 8.9: Pseudo component volume percentages of the low density 80 (kg/m³) mix

Mix	Resin	DE	Q-cel
80	5%	95%	0%

To explore the effect of this mix composition with the new SR 1280/Ancamine[®] 2442 epoxy system, at the request of Donkervoort such an 80 mix sample was created with the new epoxy system at mix ratio of 100:20. The manufactured sample, labeled **R5-TM1-1** was 55m thick and contained 4vol.% of Expancel[®] 043 DU 80. When cured at 110°C it was estimated with the numerical model that the sample should be cured for 43min to obtain 98% cure. When taking the hot sample out of the mold after 43min the sample was not rigid. It was very loose in nature and easily crumbled. It also did not seem sufficiently expanded and the contours of the M8 nut imprint were still clearly visual. From this it could be hypothesized that in 80-mix EX-CORE samples (no matter which resin matrix used) there was simply not enough resin binder to form an epoxy network.

In previous research, promising looking and rigid 80-mix EX-CORE samples were obtained. However, it was hypothesized by the author that this was essentially caused due to the melting of the thermoplastic shells of the microspheres at elevated temperature & pressure and not by the formation of an epoxy network. To test this theory, rigid EX-CORE 80-mix samples available at Donkervoort were reheated in an oven at 110°C. It became clear that without any mold restriction, the samples re-expanded and burst open at elevated temperatures, confirming the hypothesis. The author therefore does not recommend any further testing with the 80-mix formulation. Instead more research is recommended to find the lower boundary of resin volume content (somewhere between 5-14vol.%) that will result in a rigid epoxy network that can withstand the Expancel[®] DU re-expansion at elevated temperatures. This and other recommendations are explained in more detail in Chapter 12.

**Figure 8.21:** Sample R5-TM1-1**Figure 8.22:** Sample R5-TM1-2**Figure 8.23:** Sample R5-TM1-3

From sample series R4 it became clear that a 4vol.% content of Expancel[®] 043 DU 80 in 270-optimal mix samples cured at 110°C did not result in sufficient pressure generation to obtain well expanded EX-CORE samples. Therefore it was decided to increase the content of 043 DU 80 in subsequent produced samples.

Sample **R5-TM1-2** was similar to sample R4-TM1-4 but instead of 4vol.%, now 7.5vol.% of 043 DU 80 was used. It was again 30mm high and was also cured for 26min at 110°C. This time when the upper mold lid was released, the cured sample could clearly not withstand the internal pressure generated by the 043 DU 80 microspheres at elevated temperatures. The top surface of the sample became convex and a large crack occurred in the cross section of the sample. This crack is indicated in Figure 8.22. Right before mold opening, the Flexiforce[®] sensors recorded pressures up to 5.5bar at the surface of the sample, while the NTC sensors recorded temperatures up to 136°C in the core (see plot R5-TM1-2 in Appendix H).

To verify that the large crack in the cross-section of sample R5-TM1-2 (and other previously cracked samples) occurred at the moment when the mold was opened while the sample was still hot, sample **R5-TM1-3** was created. This sample was entirely similar to R5-TM1-2 but it was left to cool-down to room temperature in the tile mold for an additional 200min before opening the mold. At that moment the maximum temperature measured in the core of the sample was 35°C. Note that it was an extremely hot day so the room temperature was 35°C! As expected, when the mold was opened the sample was dimensionally stable; it did not expand nor could a crack be observed in the cross-section of the sample. Sample R5-TM1-3 is shown in Figure 8.23.

8.6. Discussion on crack initiation

Since the non-cracked sample R5-TM1-3 (Figure 8.23) was similar to the cracked sample R5-TM1-2 (Figure 8.22), except that it was allowed to cool to room temperature before opening the mold, it was confirmed that cracks in the foam core occurred when the mold is opened directly after curing while the sample is still hot. At that moment the temperature in the center of the core can be up to 20-40°C higher than the surrounding mold temperatures due to the exothermic reaction of the epoxy resin and the insulation properties of EX-CORE. Due to the high internal core temperatures (above the onset expansion temperature of Expancel[®] DU) high internal pressures are present since the blowing agent in Expancel[®] DU microspheres still wants to expand. This expansion is initially restricted by the enclosed mold. Although ultimately a rigid cured epoxy network is formed around the DU microspheres, when the mold is opened the epoxy network cannot withstand the internal pressure caused by the blowing agent in the DU microspheres at high core temperatures. Consequently, the hot sample becomes convex and cracks when the upper mold lid is lifted.

The hypothesis is that when the core is allowed to cool below the onset expansion temperature of the Expancel[®] DU microspheres, cracking can be eliminated and a dimensionally stable sample would be obtained. This would however unfortunately mean that the required in-mold cycle times will drastically increase. This hypothesis will be tested and discussed in Section 10.1. Note that samples also have been obtained that did not show any cracks, although that the mold was directly opened after curing. In that case, the samples were simply not sufficiently expanded. This for example because of a low amount of DU content and/or a low core temperature which both result in less internal pressure built up.

8.7. Summary & chapter conclusions

In the third test phase covered in this chapter, several additional EX-CORE samples (test series R4) containing the SR 1280/ Ancamine[®] 2442 curing agent were manufactured with various epoxy mix ratios (100:20, 100:30, 100:60) cured at different isothermal temperatures. These and some previously manufactured R3 series samples were compression tested on Donkervoort's compression jack to investigate the effect of cure temperature, cure time and epoxy mix ratio on the compressive strength of EX-CORE samples. A summary of the compressive strength results is given here:

- Compressive strength of EX-CORE samples increased when the epoxy mix ratio lowered as follows: 100:60 < 100:30 < 100:20. EX-CORE samples created with 100:60 epoxy mix ratios only had marginal compressive strength, more than 4 times lower than similar cured 100:20 mix samples.
- Epoxy mix ratios below 100:20 (for example 100:10) are not recommended since it was observed in a simple test that in that case there is not sufficient hardener for the amount of resin. So resin will be left unreacted.
- Compressive strength of EX-CORE samples increased with cure temperature: 110°C < 140°C < 160°C. This effect is much more pronounced between similar 110° and 140° cured samples than between 140°C and 160°C cured samples.
- 5min extra cure time at 160°C slightly increased the average specific compressive strength by only 6% (sample R4-TM1-1).

- An additional 19min post-cure at 160°C on sample R3-TM1-6 originally cured at 140°C for 19min, had negligible effect on the compressive strength. Postcuring was therefore not investigated any further.
- The highest compressive strength result was obtained for EX-CORE sample R4-TM1-3 that was cured for 21min at 160°C. It obtained an average compressive strength of 4.3MPa for a density of 255kg/m³. So it has a specific compressive strength of 16.85kNm/kg, which is close to the 17.63kNm/kg value for the original 270-optimal mix formulation obtained in previous research [63, 64].

Remind that in the current research all EX-CORE samples were tested on the compression jack available at Donkervoort which is not conform ASTM standards. It was known from previous research performed at Donkervoort [64] that this jack is adequate in determining the compressive strength values within 10%. When in future research more accurate compressive strength values are required or datasheets needs to be set-up it is recommended to determine compressive strength properties according to ASTM standard D1621 [146] for example on the Zwick 250kN test bench available at the Delft University of Technology.

Additionally due to the limited time frame of the thesis research, only EX-CORE samples with one specific mix formulation were compression tested, namely the 270-optimal mix (see Table 6.1). The 270-optimal mix was formulated with a mathematical model in the research of Vial [63], which i.a. predicted the highest compressive strength properties for a 270kg/m³ foam with this specific formulation. It is however important to note that this mathematical model is based on compressive strength results from EX-CORE samples that were manufactured with the former epoxy resin and DU grade. It is therefore not guaranteed that this mix composition is also "optimal" for EX-CORE samples produced with the new SR 1280/ Ancamine[®] 2442 epoxy matrix and Expancel[®] 043 DU 80 grade. Additionally, the samples produced in this research are also cured under different conditions. The author therefore recommends further research to investigate the optimal mix compositions for a range of EX-CORE foam densities created with the new epoxy matrix and DU grade. To limit the amount of samples that have to be produced and tested, a designed experiment and mathematical model can be set up similar than the one previously developed in the Master's Thesis of Vial [63] (see also Section 3.2.5). This and other recommendations are explained in Chapter 12.

The higher compressive strength results of EX-CORE samples cured at higher temperatures do not necessarily imply that a high cure temperature results in a better/higher cross-linked epoxy network. It could for example also be possible that the resulting higher pressure due to the bigger expansion of the blowing agent at increased cure temperatures leads to a better compaction/melting of the thermoplastic shells of the microspheres. Indications that this later might be the cause for the higher compressive strength are the following: First of all the samples cured at 160°C show a yellow discoloration, which could occur due to degradation of the epoxy resin at high temperatures. The manufacturer also mentioned that the Ancamine[®] 2442 epoxy system is stable up to ~170°C. Since temperature peaks up to 190°C were measured in the core of the 160°C cured samples, degradation of the epoxy resin cannot be excluded. Secondly, it became clear from the additional DSC scans with the 100:20 epoxy ratio that at cure temperatures above 120-135°C the exothermic reaction of the Ancamine[®] 2442 epoxy system decreases. Evonik also mentioned that at higher cure temperatures another cross-linked network is formed due to the formation of OH groups that further react.

From the experimental DSC results performed with the 100:20 epoxy ratio new cure kinetic parameters were determined for the modified-autocatalytic cure kinetic model, which in turn are implemented in the numerical EX-CORE thermal model. From the DSC results it became clear that the times required to reach 98% degree of cure more then double compared to the 100:60 epoxy mix ratios. Nonetheless, this increase in cure time is justified since specific compressive strengths of EX-CORE samples became more than 4 times higher when using the 100:20 mix ratio (when cured at 110°C).

Finally, three additional EX-CORE samples were produced in test series R5 discussed in this chapter, one with a different 80kg/m³ mix formulation and two with the 270-optimal mix formulation but with an increased 043 DU 80 content of 7.5vol.%. The author does not recommend further research with the 80-mix formulation since it contains an insufficient amount of epoxy matrix which causes cured EX-CORE samples to re-expand at elevated temperatures. Instead more research is recommended to find the lower boundary of resin volume content (somewhere between 5-14vol.%) that will result in a rigid epoxy network that can withstand the Expancel[®] DU re-expansion at elevated operational temperatures. More details on this and other recommendations can be found in Chapter 12.

The cause for the large cracks visual in several samples manufactured throughout the research became also clear. Namely, it was verified that the cracks occurred when the mold lid was relieved and the hot samples were taken out of the mold directly after curing. Even if the EX-CORE foam is sufficiently cured when the mold is opened, the rigid epoxy network cannot withstand the high internal pressure caused by the blowing agent in the DU microspheres at elevated temperatures. So the EX-CORE foam becomes convex, dimensionally unstable and cracks when the mold is opened while the sample is hot. It was hypothesized that when the core is allowed to cool below the onset expansion temperature of the Expancel[®] DU microspheres, cracking can be eliminated. However, this would unfortunately mean that the required cycle times will drastically increase. In Section 10.1 this hypothesis will be tested and elaborated upon.

9

Validation of numerical EX-CORE thermal model

In this chapter the numerical EX-CORE thermal model, which was extensively discussed in Chapter 5, is validated with experimental temperature measurements obtained from various EX-CORE samples manufactured during this research. The general method of validation is explained in Section 9.1. The validation of the numerical model was performed in three different phases. In the first validation phase, discussed in Section 9.2, the simulated data is compared with experimental temperatures that were obtained using the metal NTC sensor grid. Since large discrepancies were found, the onset reaction temperature of the Ancamine[®] 2442 was verified with DSC measurements and updated in the numerical model, after which a new comparison of the experimental and simulated data was done. This is all covered in Section 9.3. Although the discrepancies reduced, there was reason to believe that the temperature measurements were affected by the conducting metal grid that was used. Therefore a new poor-conducting NTC sensor grid was constructed and new samples had to be produced. Finally, a third comparison of the results and final validation of the numerical model was performed, as discussed in Section 9.4. At the end of this chapter, in Section 9.5, a chapter summary and conclusions are given w.r.t. the validation of the numerical thermal EX-CORE model.

9.1. Validation methodology

Before discussing the general validation method, it is important to recall that the goal of the numerical thermal model was to predict the temperature and cure behavior of variable EX-CORE foam compositions during various cure cycles. This first off all to aid the development of EX-CORE products at Donkervoort and secondly, more specifically for the current study, the research towards reducing the cure cycle times of EX-CORE sandwich products. The temperature at various locations along the mid plane of EX-CORE tile samples was measured during curing with 15 NTC sensors that were positioned on a grid schematically shown in Figure 7.6. These measurements were compared with the simulated temperature distribution to validate the numerical model with experimental data. The most important data points that are used to validate/compare the model are:

- **Maximum temperature at the center (T_{center}) and at the top edge (T_{top})**

The maximum temperature at the center of the core is used to evaluate temperature peaks resulting from the exothermic reaction and insulating behavior of EX-CORE. High temperature overshoots could lead to issues with EX-CORE degradation and/or pressure generation. Additionally, the temperature near the top edge of the sample, more specifically at 90% of the sample height is compared. For both data points a maximum deviation of 10°C is considered acceptable to give the user a good notion of the temperature range occurring in the foam for the chosen set of parameters.

- **Time to peak temperature (t_{peak})**

This is the time after mold closure when the peak temperature is reached in the center of the sample. This will give an indication when the cure reaction is leveling off (see example in Figure 5.17). A maximal deviation of 5min is deemed acceptable for the 25-40min total cure times occurring in the current research.

- **Time to reach 95°C in the center ($t_{center@95C}$) and at the top edge ($t_{top@95C}$)**

The time to reach 95°C at the center and near the top edge (90% of height) of the sample refers to the onset expansion temperature of Expancel[®] 043 DU 80 (see Figure 7.1). Hence the user will get a good idea when EX-CORE will start to expand. Again a window of 5min is considered acceptable.

- **Transition temperature (T_{trans})**

This is the temperature at which the core temperature exceeds the edge temperature. When Expancel[®] 043 DU 80 is used, a transition below 95°C indicates that the onset expansion temperature is reached first in the center of the core. This results in beneficial density gradients with lower density in the core. This data point was considered in previous research by Eversdijk [64], where the effect of cure cycle dwells was investigated to tune the density gradients. Since in the current research an isothermal cure cycle is used, this datapoint is not directly relevant for this research. Nonetheless, it is still considered relevant for the current EX-CORE production at Donkervoort. In that case, a maximum deviation of 5°C is deemed adequate since transition points just exceeding the DU onset expansion temperature can lead to non-desirable density gradients [64].

For all validation simulations performed with the numerical model the verified time step and mesh size determined in Section 5.8.2 were used, being $\Delta x = \Delta y = 1.25\text{mm}$ and $\Delta t = \frac{1}{16} \frac{\Delta t}{\Delta t_{crit}}$. In the simulation, the initial temperature of EX-CORE was set to the average of the NTC sensor temperatures measured right before sample curing. In the model analysis the mold temperature was set to the predefined isothermal cure temperature. Note that in the numerical model the top edge temperature was taken from the node which was located closest to 90% of the sample height. It should also be noted that any experimental values listed in the tables presented in the next sections are values that were extracted from actual NTC sensor measurements. They were not obtained through data fitting.

Possibility of in-situ monitoring the degree of cure of EX-CORE using dielectrometry

It is important to note that during the research it was not possible to directly validate the degree of cure predictions of EX-CORE in the numerical model since they could not be experimentally measured. There is however a possibility that dielectric sensors could be used to monitor the cure progress of EX-CORE products during manufacturing. In essence dielectrometry is a technique that can be used to monitor the cure process of fiber reinforced polymer (FRP) composites during production molding operations. It makes use of conductor probes/electrodes that induce an alternating electric field in the part and consequently measure the changing dielectric loss factor that can be related to the degree of cure. Next to FRP composites it is also possible to monitor the cure and foaming behavior of foams with dielectrometric measurements. For example in a study by Vandebossche et al. [147] dielectrometry was successfully used to monitor polyurethane foams. For more background information on dielectrometry the reader is referred to the literature report [10]. Unfortunately, relatively expensive instruments, sensors and hardware/software are required, which are not readily available at Donkervoort.

To get an idea of the cure monitoring possibilities with EX-CORE, trial dielectric measurements were performed by Twenco CME B.V. on cured EX-CORE samples with and without prepreg facings. They concluded that it would be possible to monitor the curing process of EX-CORE when placed in between carbon prepreg layers. However, they observed many disturbances due to the lack of a good/stable test-setup and such could not reproduce the measurements within a small bandwidth. They proposed to perform more experiments to determine the most optimal measuring setup. Unfortunately, these additional tests were not yet performed when this report was finished.

9.2. Phase 1: Validation of numerical EX-CORE model using metal NTC sensor grid

In the first validation phase, it was tried to validate the numerical model with the temperature measurements that were obtained during curing of various EX-CORE samples with the metal NTC sensor grid in place. This setup was previously explained in Section 7.2.1. Both the 30mm and 55mm high metal grids were used (see Figures 7.7 and 8.7), corresponding with the sample heights. A comparison of the experimental measurements with the corresponding simulation results is discussed in the subsequent section. Note that in this first validation phase, in the numerical model the onset reaction temperature of the Ancamine[®] 2442 curing agent was set to 93°C as originally provided on the datasheet [99].

9.2.1. Comparison of numerical model simulation with experimental results (phase 1)

The initial validation data is retrieved from various R3 and R4 series samples which were previously discussed in Sections 7.3 and 8.1, respectively. Experimental measurements from 5 different samples were used. All samples contained the selected SR 1280/ Ancamine[®] 2442 epoxy system and 4vol.% of the Expancel[®] 043 DU 80 grade. The samples vary in height (30mm or 55mm), epoxy mix ratio (100:20) and cure temperature (110°C or 160°C). In Figure 9.1 the experimental temperatures are compared with the simulated temperatures for all 5 samples. Note that the given temperature curves do not all initiate at room temperature. This is because during R3 and R4 samples production sensor data recording was initiated after the mold was closed and tightened with glue claps. So approximately one minute after the sample casing was inserted in between the hot mold lids. During that time interval the temperature in EX-CORE already started to rise. To correct for this, the simulated curves are shifted in time such that the top edge temperature curves intersect at $t=0$.

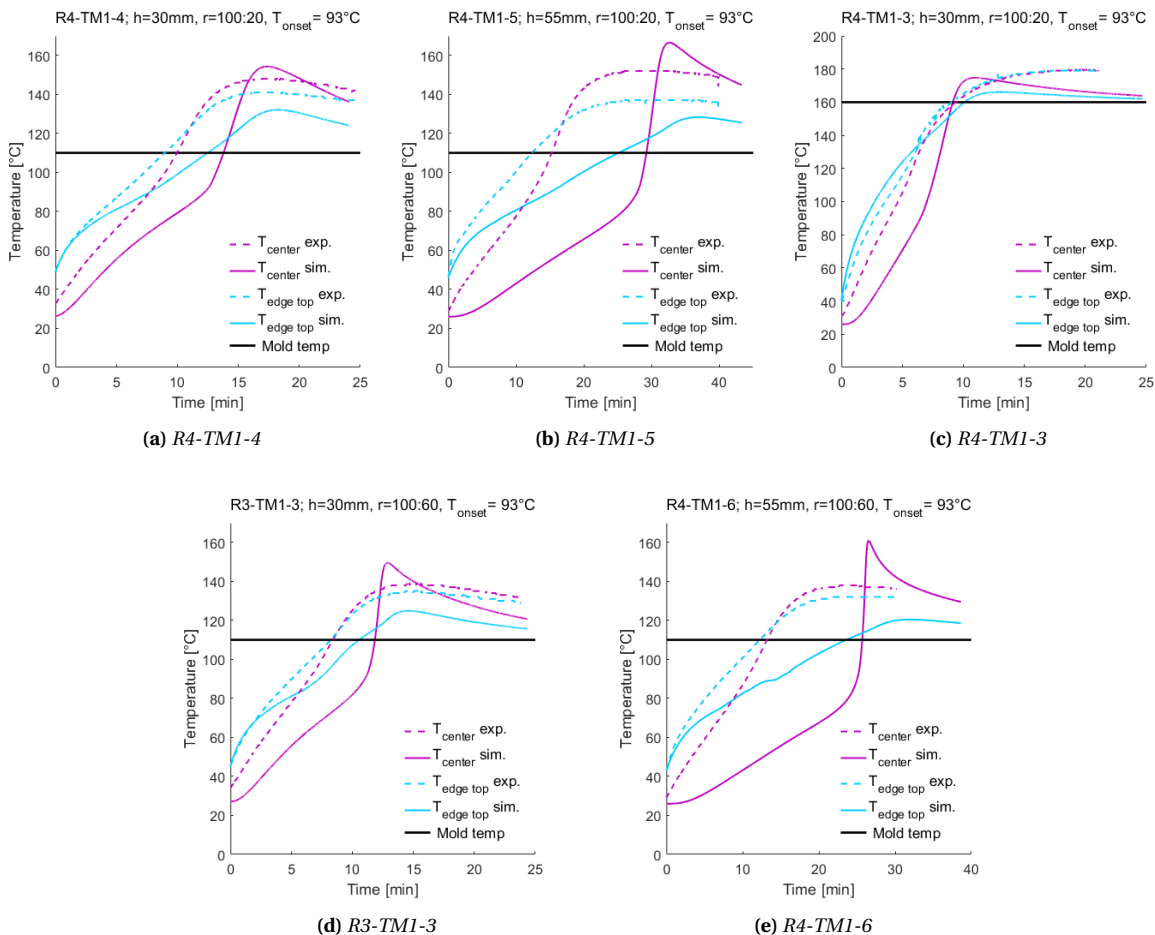


Figure 9.1: Comparison of experimental data with numerical simulation data at the center and top edge of tile mold samples R4-TM1-3 to R4-TM1-6 and R3-TM1-3. T_{onset} set to 93°C for all num. simulations.

In Table 9.1 an overview of the sample parameters (epoxy ratio r , height h and cure temperature T_{cure}) and comparison of important temperature points is given. Namely, the maximum temperature at the center (T_{center}) and the top edge (T_{edge}) of the sample and additionally, the transition temperature (T_{trans}). Next, in Table 9.2 the three important time points are compared, namely the time to peak temperature (t_{peak}) and the times to reach the 95°C onset expansion temperature of 043 DU 80 at the center ($t_{center@95C}$) and top ($t_{top@95C}$) of the sample.

From the results it can be seen that large discrepancies exist between the experimental and simulated data, which are way above the allowable discrepancy bounds stated in Section 9.1. The largest difference can be observed for the center temperature curves for the 55mm thick samples R4-TM1-5 (Figure 9.1b) and R4-TM1-6 (Figure 9.1e) resulting in a 14min and 15min discrepancy of $t_{center@95C}$ and $t_{top@95C}$, respectively. For sample R4-TM1-6 the model overestimates the maximum temperature in the core by 23°C, while for sample R4-TM1-3 the model underestimates the core temperature by 15°C.

Table 9.1: Comparison of the experimental and numerical simulation results for samples R4-TM1-3 to R4-TM1-6 and R3-TM1-3 at 3 important temperature points. T_{onset} set to 93°C for all num. simulations.

Sample	Sample parameters			Max. T_{center} [°C]			Max. T_{top} [°C]			T_{trans} [°C]		
	r [-]	h [mm]	T_{cure} [°C]	Exp.	Sim.	Error	Exp.	Sim.	Error	Exp.	Sim.	Error
R4-TM1-4	100:20	30	110	148	154	-6	141	132	9	123	118	5
R4-TM1-5	100:20	55	110	152	166	-14	137	128	9	125	118	7
R4-TM1-3	100:20	30	160	190	175	15	189	166	23	181	151	30
R3-TM1-3	100:60	30	110	139	150	-11	135	125	10	114	116	-2
R4-TM1-6	100:60	55	110	138	161	-23	132	120	12	118	114	4

Table 9.2: Comparison of the experimental and numerical simulation results for samples R4-TM1-3 to R4-TM1-6 and R3-TM1-3 at 3 important time points. T_{onset} set to 93°C for all num. simulations.

Sample	Sample parameters			t_{peak} [min]			$t_{center@95C}$ [min]			$t_{top@95C}$ [min]		
	r [-]	h [mm]	T_{cure} [°C]	Exp.	Sim.	Error	Exp.	Sim.	Error	Exp.	Sim.	Error
R4-TM1-4	100:20	30	110	16.2	17.4	-1.1	8.4	12.8	-4.5	6.4	9.0	-2.7
R4-TM1-5	100:20	55	110	25.7	32.6	-7.0	13.2	28.4	-15.2	8.6	17.4	-8.9
R4-TM1-3	100:20	30	160	21.2	11.0	10.2	5.1	6.8	-1.7	4.2	2.3	1.9
R3-TM1-3	100:60	30	110	14.5	12.8	1.7	6.9	11.3	-4.3	5.8	8.1	-2.3
R4-TM1-6	100:60	55	110	22.6	26.5	-3.9	11.2	25.3	-14.1	8.5	16.6	-8.1

9.3. Phase 2: Updating the reaction onset temperature of Ancamine® 2442 in the numerical model

It was thought that one possible reason for the large discrepancies found between the experimental and simulated data in the previous section was related to the onset reaction temperature implemented in the numerical model (see Section 5.6). On the datasheet of the Ancamine® 2442 curing agent an onset reaction temperature (T_{onset}) of 93°C is stated which was measured with a 10°C/min DSC scan [99]. It was decided to verify this onset reaction temperature and also investigate the effect of a different heat-up rate. This was done by performing several DSC measurements as discussed in the subsequent section.

9.3.1. Determining the reaction onset temperature of Ancamine® 2442 with DSC

To determine at which temperature the epoxy reaction starts to initiate and evaluate the effect of heat-up rate, four dynamic DSC scans were performed on the SR 1280/Ancamine® 2442 epoxy system mixed at 100:20 ratio. The DSC scans were again performed on the *Seiko Instruments Exstar 6000* heat flux DSC at the Delft University of Technology. The specimens were prepared similarly as explained in Appendix A. However, instead of preheating the DSC test chamber, the specimens were inserted at room temperature and then subsequently heated at either 0.5, 2, 10 or 15°C/min. The baseline corrected specific heat flow curves (solid lines/right axis) combined with the sample temperature (dashed lines/left axis) are shown in Figure 9.2.

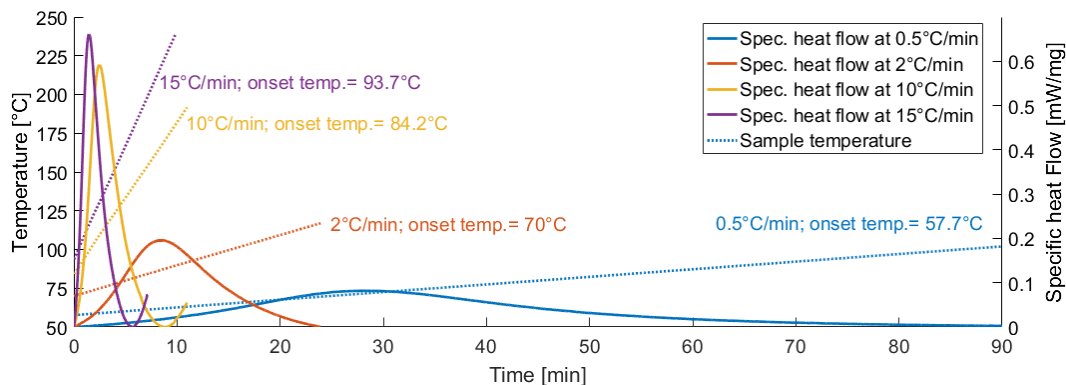


Figure 9.2: Specific heat flows (baselined) and sample temperatures for different DSC heat-up rates. Tested resin SR 1280 & hardener 2442 at mix ratio $r=100:20$.

The first initiation of heat release at $t=0$ in Figure 9.2 thus corresponds to the exothermic reaction onset. At this moment the sample temperature is noted, which is the corresponding onset reaction temperature (T_{onset}) for that specific heat-up rate. The obtained values are noted in Figure 9.2. For a heat-up rate of $10^{\circ}\text{C}/\text{min}$ a T_{onset} value of 84.2°C was obtained, while the datasheet mentioned for this heat-up rate a value of 93°C . Additionally, a T_{onset} value of 93.7°C was obtained for the $15^{\circ}\text{C}/\text{min}$ scan.

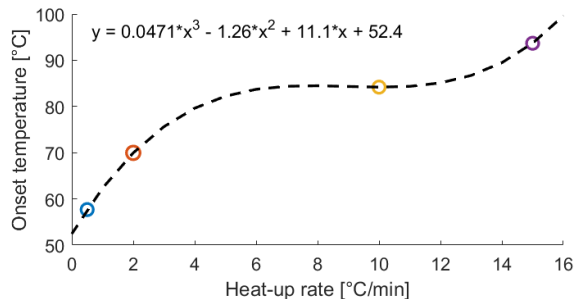


Figure 9.3: Onset reaction temperature vs heat-up rate: cubic fit result

Table 9.3: Measured heat-up rates for 110°C cured samples with corresponding estimated onset reaction temperature using cubic fit equation from Figure 9.3.

Sample	Heat-up rate x [$^{\circ}\text{C}/\text{min}$]	Onset temp $f(x)$ [$^{\circ}\text{C}$]
R3-TM1-3 ¹	7.93	84.5
R4-TM1-4	6.73	84.3
R4-TM1-5	4.41	80.8
R4-TM1-6 ¹	5.25	82.7
	Avg. ¹ :	82.6

¹ Samples with mix ratio $r=100:60$ not included.

The four T_{onset} values are plotted as function of the heat-up rate in Figure 9.3. A cubic polynomial is fitted through the datapoints. The resulting equation is used to estimate the reaction onset temperature for various heat-up rates occurring in EX-CORE samples. Note that due to the limited amount of time only 4 dynamic DSC tests were performed. In future research it is however strongly recommended to perform additional DSC scans at different heat-up rates to obtain more data points and such achieve an improved relation between heat-up rate and T_{onset} . This and other recommendations are discussed in more detail in Chapter 12.

Depending on the sample thickness, mold- & room temperatures and the location in the sample, the heat up rates in EX-CORE can vary. It was decided to determine the average heat-up rates measured in the samples. More specifically, the average heat-up rates were determined from the straight line constructed through the y-axis cross-sections and the cross-section of the experimental T_{center} and T_{top} curves in the plots in Figure 9.1. The resulting average heat-up rates and corresponding onset reaction temperatures for the 110°C cured samples are listed in Table 9.3. From the results it can be concluded that an onset reaction temperature of 83°C would be more realistic for the 110°C isothermally cured samples, than the previously used value of 93°C . In a similar manner for the 160°C cured sample R4-TM1-3 an average heat-up rate of $13^{\circ}\text{C}/\text{min}$ was obtained which resulted in a slightly higher onset reaction temperature of 87°C .

9.3.2. Comparison of numerical model simulation with experimental results (phase 2)

In the numerical model the onset reaction temperature of the Ancamine® 2442 hardener was updated from 93°C to 83°C for the 110°C isothermally cured samples and to 87°C for the 160°C cured sample. Then similarly as before a new comparison of the experimental results with the updated simulation results was performed for the same samples. The comparison of the important temperature and time points is given in Tables 9.4 and 9.5. The comparative temperature plots are given in Figure 9.4.

Table 9.4: Comparison of the experimental and numerical simulation results for samples R4-TM1-3 to R4-TM1-6 and R3-TM1-3 at 3 important temp points. T_{onset} set to 83°C for all num. simulations, except for 160°C cured sample R4-TM1-4, set to 87°C .

Sample	Sample parameters			Max. T_{center} [$^{\circ}\text{C}$]			Max. T_{top} [$^{\circ}\text{C}$]			T_{trans} [$^{\circ}\text{C}$]		
	r [-]	h [mm]	T_{cure} [$^{\circ}\text{C}$]	Exp.	Sim.	Error	Exp.	Sim.	Error	Exp.	Sim.	Error
R4-TM1-4	100:20	30	110	148	148	0	141	129	12	123	115	8
R4-TM1-5	100:20	55	110	152	154	-2	137	125	12	125	112	13
R4-TM1-3	100:20	30	160	190	173	17	189	165	24	181	151	30
R3-TM1-3	100:60	30	110	139	141	-2	135	122	13	114	111	3
R4-TM1-6	100:60	55	110	138	144	-6	132	117	15	118	107	11

Table 9.5: Comparison of the experimental and numerical simulation results for samples R4-TM1-3 to R4-TM1-6 and R3-TM1-3 at 3 important time points. T_{onset} set to 83°C for all num. simulations, except for 160°C cured sample R4-TM1-4, set to 87°C.

Sample	Sample parameters			t_{peak} [min]			$t_{center@95C}$ [min]			$t_{top@95C}$ [min]		
	r [-]	h [mm]	T_{cure} [°C]	Exp.	Sim.	Error	Exp.	Sim.	Error	Exp.	Sim.	Error
R4-TM1-4	100:20	30	110	16.2	15.4	0.8	8.4	10.6	-2.3	6.4	7.6	-1.2
R4-TM1-5	100:20	55	110	25.7	28.3	-2.6	13.2	23.2	-10.1	8.6	13.5	-4.9
R4-TM1-3	100:20	30	160	21.2	10.9	10.2	5.1	6.5	-1.4	4.2	2.3	1.9
R3-TM1-3	100:60	30	110	14.5	11.1	3.4	6.9	9.4	-2.5	5.8	6.6	-0.8
R4-TM1-6	100:60	55	110	22.6	22.7	-0.1	11.2	21.1	-9.9	8.5	12.7	-4.3

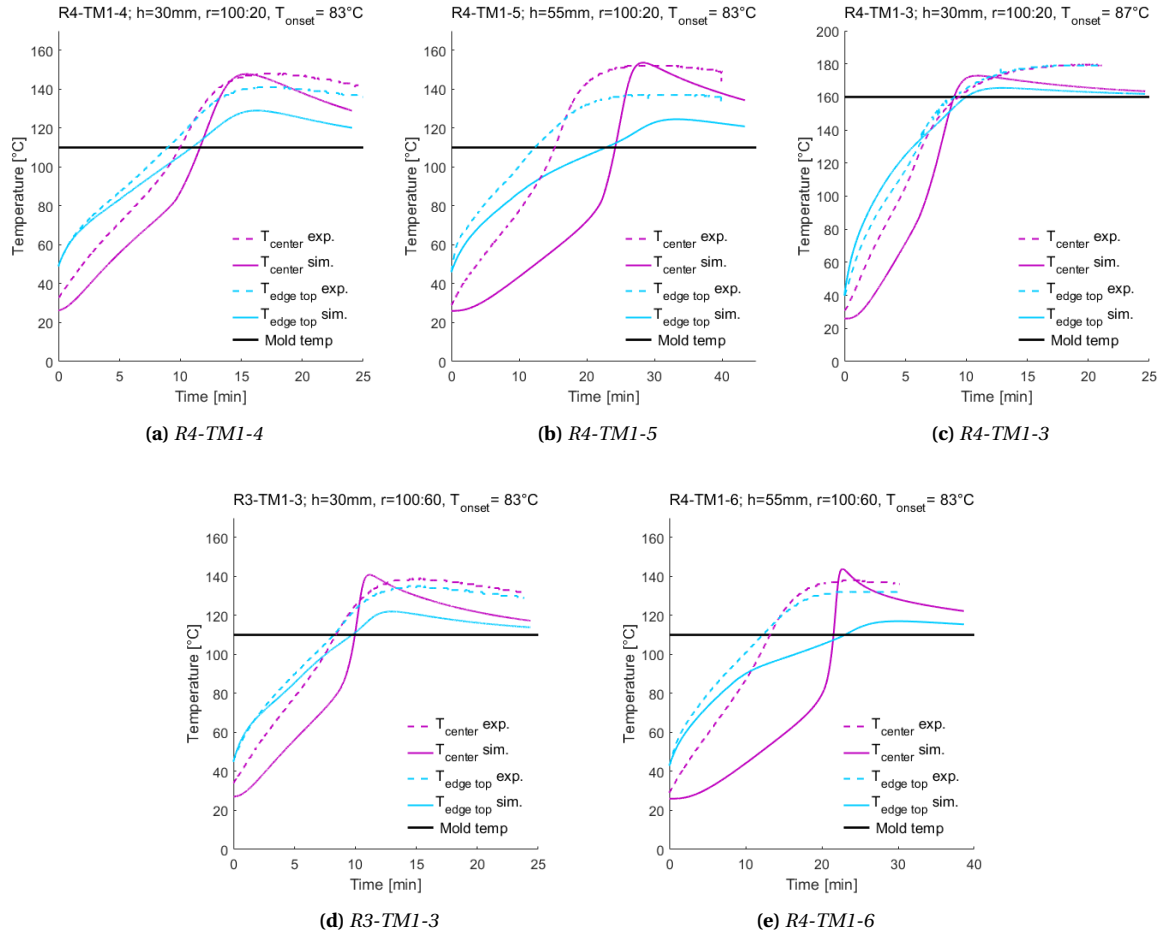


Figure 9.4: Comparison of experimental data with numerical simulation data at the center and top top of tile mold samples R4-TM1-3 to R4-TM1-6 and R3-TM1-3. T_{onset} set to 83°C for all num. simulations, except for 160°C cured sample R4-TM1-4, set to 87°C.

In general it can be observed that the updated reaction onset temperatures caused the simulated curves, and especially the T_{center} ones, to shift downwards and to the left (this will be more clearly illustrated in Section 9.3.3). This had the following effect on the important data point discrepancies:

- Overall the absolute T_{center} errors reduced. For all but one sample (R4-TM1-3), the model overestimated the maximum temperature with a maximum error of 6°C, which is acceptable according to the criteria defined in Section 9.1. For sample R4-TM1-3 however, the model underestimated the experimental value with 17°C.
- For each sample the T_{top} error increased. All discrepancies are also larger than the acceptable deviation of 10°C, namely the model underestimates the edge temperature by 12°C to 24°C.

- The T_{trans} error increased for almost all samples. A maximum deviation of 30°C is again observed for the 160°C cured sample R4-TM1-3.
- Overall the absolute t_{peak} error reduced. All deviations except for sample R4-TM1-3 are within the acceptable error range of 5°C.
- In all cases, the $t_{center@95C}$ errors reduced. The model consistently overestimated $t_{center@95C}$. Only for the 55mm thick samples the errors were outside the acceptable criteria of 5min.
- The $t_{top@95C}$ errors reduced for each sample. A maximum deviation of 4.9min was obtained which meets the set 5min criteria.

9.3.3. Effect of tuning onset reaction temperature on numerical model results

In Figure 9.5 the effect of lowering the onset reaction temperature on the numerical model results is illustrated for the example of sample R4-TM1-5. In this figure the center (T_{center}) and edge (T_{top}) temperatures are plotted and compared for the cases when the onset reaction temperature (T_{onset}) in the numerical model was set to 0°C, 83°C and 93°C. It can be seen that when T_{onset} is lowered, the T_{center} and T_{top} peaks drop and also the time to peak reduces. It can also be seen that tuning of T_{onset} has a more pronounced effect on T_{center} than on T_{top} . This is logical because the edges are much earlier effected by the heat of the mold and so experience less onset reaction delay. Lastly, in Figure 9.5a a deflection in the T_{center} curves can be observed when the 83°C and 93°C onset reaction temperatures are reached for the corresponding curves. This because at that point the exothermic reaction is initiated in the center of the sample and so the temperature more quickly rises.

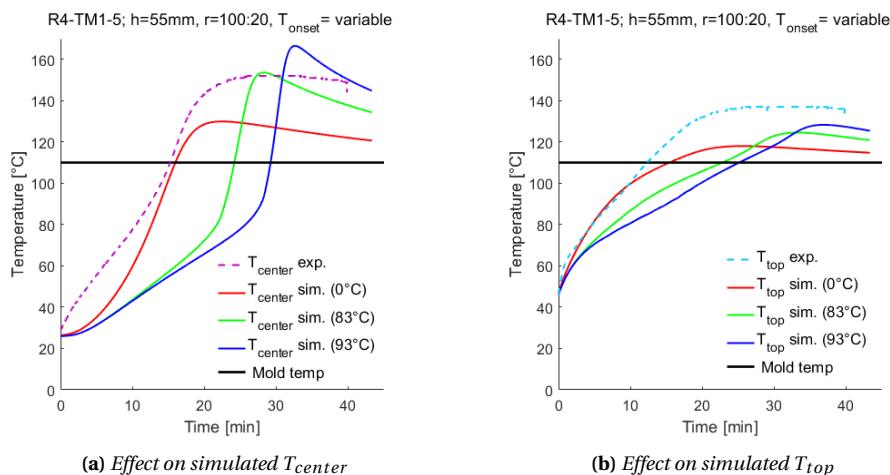


Figure 9.5: Effect of changing the onset reaction temperature T_{onset} on the numerical model results for sample R4-TM1-5. Curves shown for T_{onset} set to 0°C, 83°C and 93°C.

9.4. Phase 3: Validation of numerical EX-CORE model using bamboo NTC sensor grid

During the final phase of the research it was reasoned that the metal grid to which the NTC sensors are attached might influence the temperature measurements since metal is a much better thermal conductor than EX-CORE, this by more than a factor 1000. The heat of the mold could therefore be more quickly transferred throughout the sample compared to when the metal grid was not in place. Since a grid is necessary to keep the NTC sensors at the correct position, the idea came up to replace the original metal grid by a less conductive variant. The new sensor grid constructions were made from bamboo skewers as discussed in Section 9.4.1. New 30mm, 55mm and 75mm thick samples (R6 and R7 series) were manufactured with the new sensor grid in place. The R6 series samples are covered in Section 9.4.2, while the R7 series samples will be discussed in more detail later on in Section 10.2.2. A new result comparison and final validation of the numerical model is performed in Section 9.4.3. Additionally, a visualization and comparison of the temperature distribution inside an EX-CORE sample is presented in Section 9.4.4.

9.4.1. Poorly-conductive bamboo NTC sensor grid set-up

It was decided to construct new 30mm and 55mm high NTC sensor grids from bamboo skewers. The bamboo skewers were chosen because of their low thermal conductivity value $<0.59 \text{ W/mK}$ [148], small size, relatively high stiffness and low cost. The bamboo skewers were cut to the required size and connected to each other using 6mm wide kapton/polyimide tape by Pro-Power, which is heat resistant up to 280°C [149]. An example of the 30mm bamboo grid is shown in Figure 9.6. Next, the 15 NTC sensors were positioned along the same pattern previously illustrated in Figure 7.6. The resulting 30mm high NTC sensor grid setup is shown in Figure 9.7. Again the entire setup was covered in vacuum film before usage.

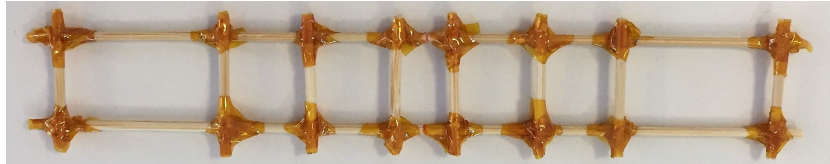


Figure 9.6: 30mm high bamboo grid constructed with kapton tape

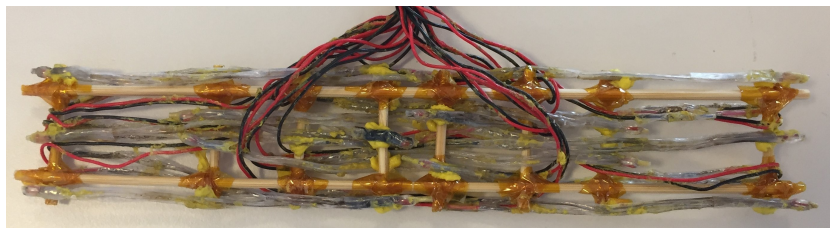


Figure 9.7: 15 NTC sensors attached to 30mm high bamboo grid

9.4.2. Test series R6: EX-CORE samples monitored with non-conducting NTC sensor grid

Two samples R6-TM1-1 and R6-TM1-2 were created that were entirely similar in composition and cure cycle than samples R4-TM1-5 and R4-TM1-4 (see Section 8.1), respectively. The only difference was that instead of the metal NTC sensor grid the new bamboo NTC sensor grid was used to monitor their temperature distribution progress in the core. Similarly as done for all other produced samples an overview of their formulation and measurement results is given in Tables 9.6 and 9.7.

Table 9.6: Overview of R6 series manufactured samples.

Sample label	Sample height	Mix	Resin type	Hardener type	Epoxy ratio r	043DU80 vol.%	Cure temp	Cure time
R6-TM1-1	55mm	270-opt	SR 1280	Ancamine [®] 2442	100:20	4%	110°C	40min
R6-TM1-2	30mm	270-opt	SR 1280	Ancamine [®] 2442	100:20	4%	110°C	26min

Table 9.7: Overview of R6 sample results, pressure and temperature measurements & rating of sample curing and expansion

Sample label	Room temp.	Sample mass	Max. surf. pressure	Time to reach 0.5bar (avg.)	Temp. at 0.5bar	Max. core. temp.	Sample curing ¹	Sample expansion ²
R6-TM1-1	21	441g	6.0bar	16.7min	102°C	169°C	5	3
R6-TM1-2	20	264g	4.6bar	10.2min	102°C	157°C	5	3

¹ On a scale from 1 to 5, with 5 being fully cured.

² On a scale from 1 to 5, with 5 being excellent expansion.

Compared with the maximum core temperatures measured with the metal NTC grid, the new measured core temperature with the bamboo grid increased from 152°C to 169°C and from 151°C to 157°C , respectively. Also again a crack originated in the 55mm thick sample R6-TM1-1 as indicated in Figure 9.8, while no crack could be observed in sample R6-TM1-2, shown in Figure 9.9. The experimental temperatures of both samples were compared with the numerical model prediction, this is discussed in more detail the next section.

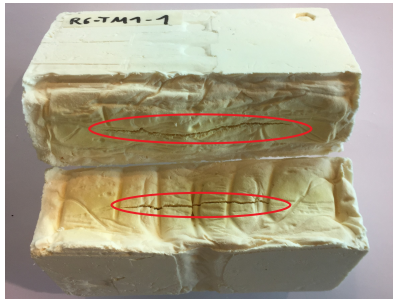


Figure 9.8: Sample R6-TM1-1, crack indicated.

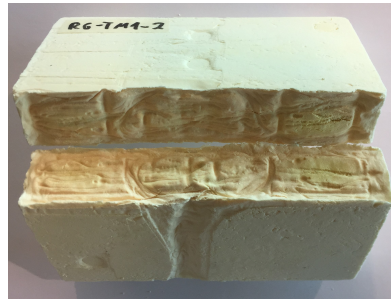


Figure 9.9: Sample R6-TM1-2

9.4.3. Comparison of numerical model simulation with experimental results (phase 3)

Next to samples R6-TM1-1 and R6-TM1-2 two additional R7 series samples were used in the last validation phase of the numerical model. These R7 series samples were originally produced to investigate the dimensional stability of cured EX-CORE samples when they are cooled to a certain temperature before mold opening. They are therefore discussed in more detail in Section 10.1.1. Nonetheless their temperature distribution was also monitored with the bamboo NTC grid. The data obtained from sample R7-TM1-2 was used which was similar to sample R6-TM1-2 except that 7.5vol.% instead of 4vol.% of 043 DU 80 was used. To validate the model results for thicker sample thicknesses, sample R7-TM1-4 was produced that was 75mm thick. Note that samples thinner than 30mm could not be experimentally validated due to the limited spacing for the NTC sensors.

Next to the bamboo grid, another improvement was done w.r.t. phase 1 and phase 2 experimental temperature measurements. This time the data recording was already initiated before the sample casing was inserted in between the preheated mold lids. Hence both the experimental T_{center} and T_{top} temperature curves initiated at room temperature. The same room temperature value was also used in the numerical simulation. Note that the onset expansion temperatures in the numerical model were again set to 83°C, similarly as done in phase 2. The new comparison of the experimental and numerical model results for the most important temperature and time data point is given in Tables 9.8 and 9.9, respectively. The experimental and simulated temperature curves are compared in Figure 9.10. Remember that all four samples used for validation were cured at 110°C.

Table 9.8: Comparison of the experimental and numerical simulation results for samples R6-TM1-1, R6-TM1-2, R7-TM1-2 and R7-TM1-4 (all cured at 110°C) at 3 important temperature points. T_{onset} set to 83°C for all num. simulations.

Sample	Sample parameters			Max. T_{center} [°C]			Max. T_{top} [°C]			T_{trans} [°C]		
	r [-]	h [mm]	043DU [vol.%]	Exp.	Sim.	Error	Exp.	Sim.	Error	Exp.	Sim.	Error
R6-TM1-1	100:20	55	4	170	154	16	141	125	16	128	112	16
R6-TM1-2	100:20	30	4	153	148	5	138	129	9	121	115	6
R7-TM1-2	100:20	30	7.5	155	144	10	136	127	9	122	114	8
R7-TM1-4	100:20	75	4	174	162	12	150	123	27	129	112	17

Table 9.9: Comparison of the experimental and numerical simulation results for samples R6-TM1-1, R6-TM1-2, R7-TM1-2 and R7-TM1-4 (all cured at 110°C) at 3 important time points. T_{onset} set to 83°C for all num. simulations.

Sample	Sample parameters			t_{peak} [min]			$t_{center@95C}$ [min]			$t_{top@95C}$ [min]		
	r [-]	h [mm]	043DU [vol.%]	Exp.	Sim.	Error	Exp.	Sim.	Error	Exp.	Sim.	Error
R6-TM1-1	100:20	55	4	31.3	29.7	1.6	19.1	24.6	-5.5	11.5	14.9	-3.4
R6-TM1-2	100:20	30	4	18.4	16.4	2.1	11.3	11.5	-0.3	7.6	8.5	-0.9
R7-TM1-2	100:20	30	7.5	19.8	16.8	3.0	11.6	11.8	-0.2	11.6	8.7	2.9
R7-TM1-4	100:20	75	4	48.6	40.0	8.6	26.4	35.8	-9.4	15.6	20.5	-4.9

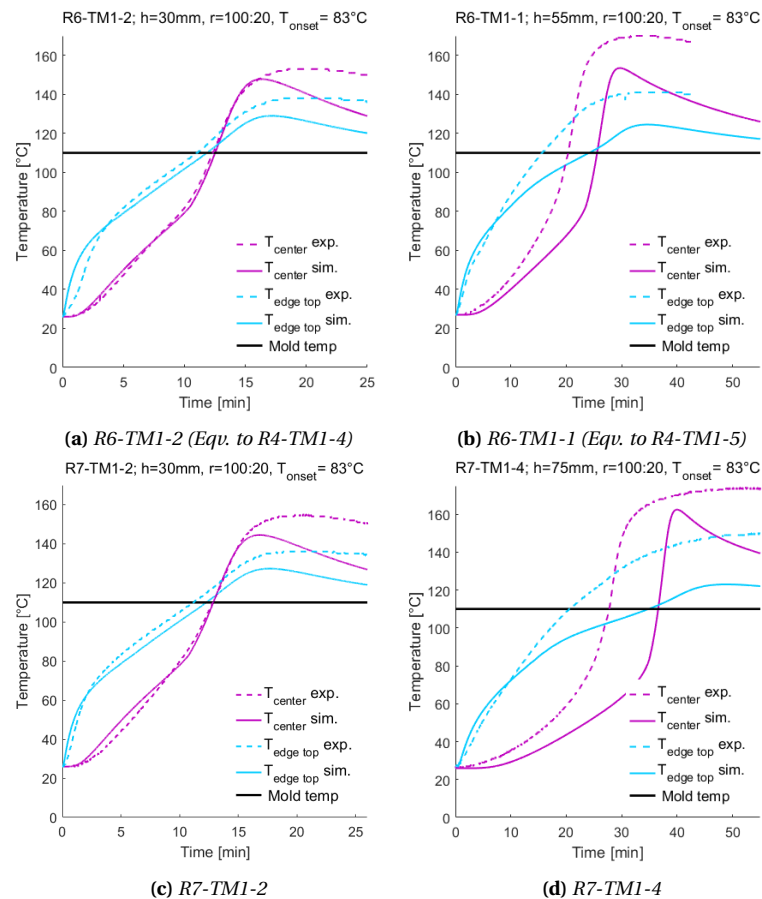


Figure 9.10: Comparison of experimental data with numerical simulation data at the center and top edge of tile mold samples R6-TM1-1, R6-TM1-2, R7-TM1-2 and R7-TM1-4. Difference with given equivalent samples is that temperature is monitored with wood sensor grid! T_{onset} set to 83°C for all num. simulations.

When inspecting plots a) and b) in Figure 9.10 and comparing them with the corresponding sample plots a) and b) in Figure 9.4, a way better fit with the simulated data curves can be observed. As can be seen in Figure 9.10a, until the peak temperature an almost perfect fit is obtained for the 30mm thick sample R6-TM1-2. A similar good fit is achieved for the 30mm thick sample R7-TM1-2, shown in Figure 9.10b. Although that the discrepancies reduced for the 55mm thick sample R6-TM1-1, shown in Figure 9.10b (compared to R4-TM1-5), the deviations are still relatively large. They are even more pronounced for the 75mm thick sample shown in Figure 9.10d. When reviewing the comparison of the experimental vs. simulation data for the important temperature and time datapoints in Tables 9.8 and 9.9 the following outcomes can be noted:

- Only for the 30mm samples, the T_{center} errors fell within the acceptable 10°C bound. A maximum deviation of 16°C is obtained for the 55mm sample R6-TM1-1. In all cases the model underestimates the experimental data by 5°C or more. The discrepancies also increase with sample thickness.
- Similarly, only for the 30mm samples the T_{top} deviations meet the acceptable 10°C error criteria. Again the model underestimates the experimental results, this by at least 9°C for the 30mm thick samples to even 27°C for the 75mm thick sample R7-TM1-4.
- Overall, the T_{trans} errors reduced (when comparing samples R6-TM1-1 vs R4-TM1-5 and R6-TM1-1 vs R4-TM1-4). However, the obtained errors all exceed the 5°C error criteria. The smallest errors 6°C and 8°C were obtained for the 30mm thick samples. Again, the error increases with sample thickness.
- In all cases, the model underestimates t_{peak} . Nonetheless for the 30mm and 55mm thick samples the errors are within the acceptable bound of 5min. Only for the 75mm thick sample, the set criteria was exceeded since an error of 8.6min was obtained.
- Compared to the phase 2 results, the errors of $t_{center@95C}$ reduced. For the 30mm samples, $t_{center@95C}$ was predicted within 18s of the experimental results. However, for the 55mm and 75mm samples the model overestimated the times by 5.5min to 9.4min, hence exceeding the acceptable bound of 5min.

- All obtained errors for $t_{top@95C}$ are within the acceptable 5 min error criteria. Again a trend can be observed that the $t_{top@95C}$ discrepancies increase with samples thickness

Possible causes of discrepancies between experimental and numerical results

There are a few possible explanations for the discrepancies observed during the third validation phase. Two of them are related to the assumptions made in the numerical model (see Section 5.1.1):

Firstly, since an almost perfect fit was obtained for the 30mm samples until the peak temperature, after which the simulated temperature curves more quickly reduced than the experimental ones did, it was reasoned that this could be caused due to the assumption of constant mold temperature in the numerical model. In reality, due to the exothermic reaction of the epoxy resin, it could be possible that part of the mold lids and aluminum plates/casing also became hotter than the predefined isothermal mold temperature. This hypothesis could however not be confirmed; The recordings of the type-J thermocouples built inside the mold lids were investigated but no temperature overshoots higher than 114°C could be observed. It should however be noted that these thermocouples are not directly located near the surface of the mold lids.

Secondly, another source for the observed discrepancies could be the assumption of constant onset reaction temperature, which is independent of heat up rate. The onset reaction rate of Ancamine® 2442 was experimentally tested with DSC scans performed at various heat-up rates (see Section 9.3). T_{onset} values of 57.7°C to 93.7°C were obtained for heat-up rates from 0.5°C/min to 15°C/min. Additionally, changing the T_{onset} parameter value in the numerical model was shown to have a large effect on the temperature curves (see Section 9.3.3). Since the heat-up rates in EX-CORE are not constant in time nor with location in the sample the assumption of constant onset reaction temperature could contribute to the observed discrepancies. It is logical that this effect is more pronounced in thicker samples since there larger variations in temperature distributions and so also larger variations in heat-up rates occur.

Another possible contribution to the observed discrepancies could be related to the modified-autocatalytic model implemented in the numerical thermal model to simulate the heat release of the exothermic reaction. The cure kinetic model results of the SR 1280/Ancamine® 2442 at 100:20 epoxy mix ratio were presented in Section 8.4.2. There both the reaction rate and degree of cure of the DSC measurements were compared with the modified-autocatalytic model fits. When comparing both results it can be seen that at 90°C, the cure kinetic model overestimated the reaction rate, while from 100°C onwards the model underestimates the reaction rates. However, for temperatures below 90°C this would mean that the predicted EX-CORE temperatures would increase faster than in reality. This is however not what can be observed in Figures 9.10b and 9.10d. On the contrary, for temperatures below 90°C, T_{center} exp. progresses faster than T_{center} sim. Similarly, for EX-CORE temperatures higher than 100°C this means the predicted EX-CORE temperatures would increase (or decrease due to faster reaction completion) slower than in reality. This however is also not what can generally be observed in the plots in Figure 9.10.

Note that recommendations on how the numerical model could be further improved and validated are given in Chapter 12.

9.4.4. Visualization of temperature distribution

In Figures 9.11 and 9.11 a comparison of the experimental vs. simulated mid plane temperature distribution of EX-CORE sample R6-TM1-2 is given at two different points in time. Namely, the moment when $t_{center@95C}$ and t_{peak} is reached in the numerical model. The experimental temperatures were obtained from the 15 NTC sensors which locations are indicated in the plots by the black dots. The temperature distributions were created by interpolating over the 15 datapoints using the "griddata" function in MATLAB with the "v4" bi-harmonic spline interpolation method. The fitted data is solely used for visualization of the temperature distribution. No conclusions can be made based on the fitted temperature values between the actual sensor locations. Although variations in experimental vs simulated temperature distributions can be observed, overall the experimental temperatures are close to the predicted temperature distribution. As expected from plot 9.10a, the largest discrepancies are obtained at t_{peak} .

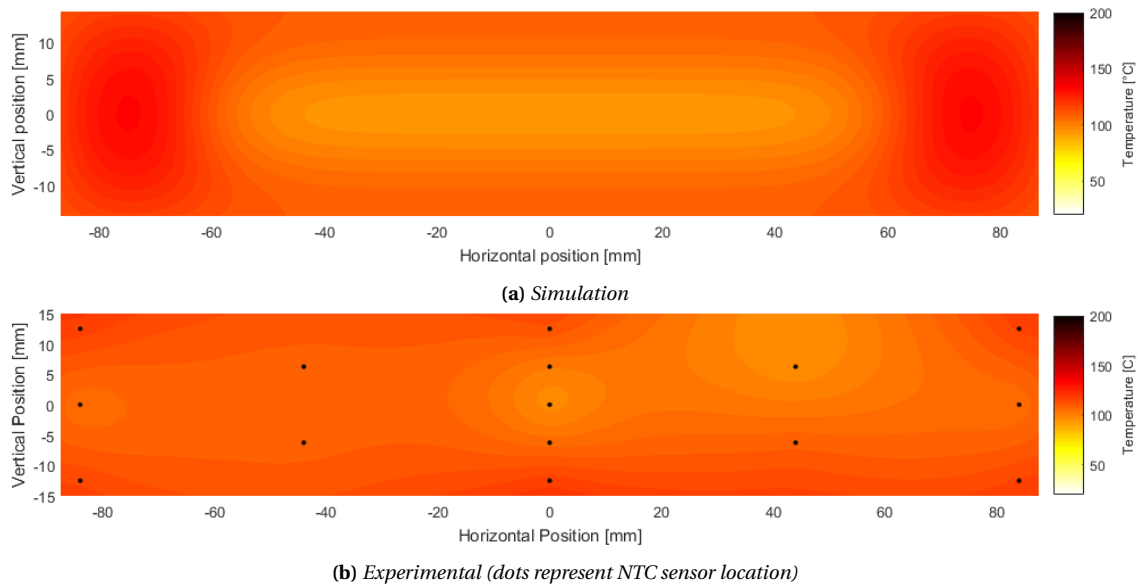


Figure 9.11: Comparison of mid plane temperature distribution of experimental and simulated data for 30mm thick sample R6-TM1-2, snapshot taken at 11.5min ($=t_{center@95C}$ sim.)

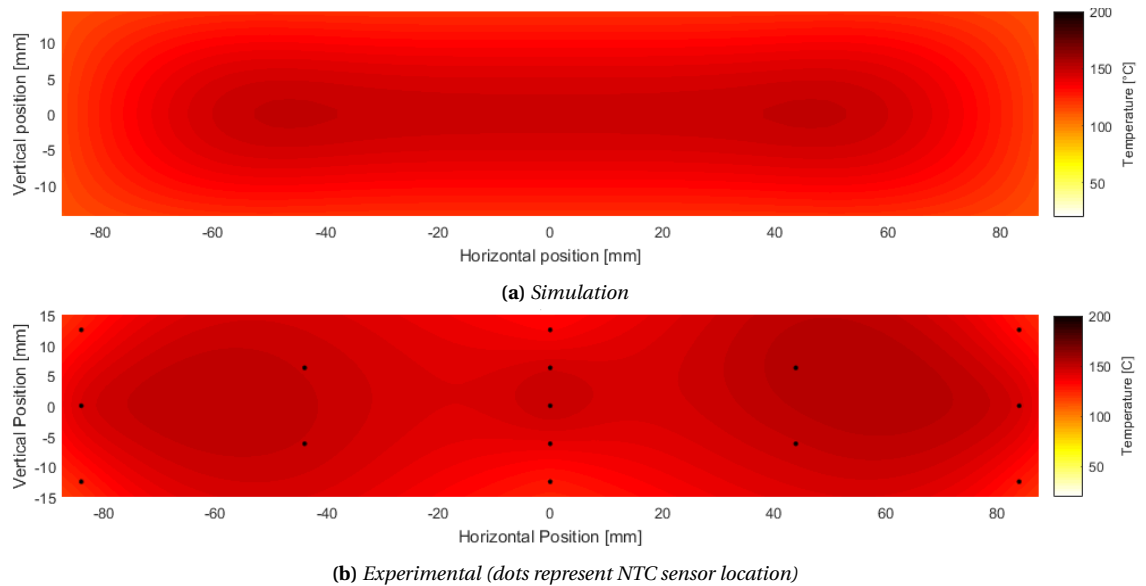


Figure 9.12: Comparison of mid plane temperature distribution of experimental and simulated data for 30mm thick sample R6-TM1-2, snapshot taken at 16.4min ($=t_{peak}$ sim.)

9.5. Summary & chapter conclusions

To validate the numerical model discussed in Chapter 5, simulated temperature predictions were compared with experimental data obtained from various 270-optimal mix EX-CORE samples produced with the SR 1280/Ancamine[®] 2442 epoxy system and the new Expancel 043 DU 80 grade. During curing the temperature distribution along the mid plane of the samples was monitored with 15 NTC sensors that were initially positioned on a metal grid.

Since large discrepancies were found for the first set of comparisons, the originally implemented 93°C onset reaction temperature (T_{onset}) given on the datasheet [99] of the Ancamine[®] 2442 curing agent was verified with DSC experiments. It was found that the onset temperature of the exothermic reaction was highly dependent on the heat-up rate. Namely, for dynamic DSC scans performed at 0.5, 2, 10 and 15°C/min, onset reaction temperatures of 58, 70, 84 and 94°C respectively were recorded. By fitting a cubic polynomial through the datapoints, T_{onset} values were obtained that corresponded better to the average heat-up rates measured

in the EX-CORE samples. More specifically, T_{onset} values between 83°C and 87°C, were obtained for 110°C and 160°C cured samples. Note however that for future research it is recommended to perform additional DSC scans at different heat-up rates to obtain more datapoints.

Next, the numerical model was updated with these new T_{onset} values and the resulting simulated data was again compared with the experimental results. Although that discrepancies reduced, there was a suspicion that the experimental measurements themselves were affected by the conductive metal sensor grid that was used. New 30, 55 and 75mm NTC sensor grids were constructed from poor-conductive bamboo skewers and new EX-CORE samples were manufactured to monitor their temperature distribution in the core. For the 30mm samples almost perfect fits with the predicted model curves were obtained until the point when the maximum temperatures were reached in the core. Then the simulated results dropped more drastically than the experimental data did. For the 55mm and 75mm thick samples larger discrepancies were observed, also before the peak temperature. These discrepancies increased with sample thickness. Two most probable causes for the obtained discrepancies are related to the assumptions made for the numerical model. First of all, the assumption of constant mold temperature and secondly the assumption of constant onset reaction temperature of the Ancamine[®] 2442 curing agent.

In conclusion, the updated numerical model could only be validated for 30mm thick 270-optimal mix EX-CORE samples that were isothermally cured at 110°C, because the predictions of thicker 55mm and 75mm samples fell outside the acceptable error criteria defined at the start of this chapter. Due to time constraints other mix formulations and cure cycles could not be investigated. It is also important to note that the EX-CORE degree of cure predictions could not be directly validated. There is however a possibility that in the future the cure process of EX-CORE could be monitored in-situ during production using dielectrometry. Some first promising dielectric measurements were performed at Twenco CME B.V., but more research is required. Recommendations on how the model could be further improved and validated are given in Chapter 12.

10

Discussion on achievable cure & cycle times of EX-CORE prepreg sandwich panels

It was explained in Chapter 8 that the large cracks observed in several EX-CORE samples produced throughout the research originated when the mold was opened directly after curing when the sample was still hot. Crack formation was prevented when samples were left to cool to room temperature before the mold was opened. It was however hypothesized that it would probably be sufficient that the temperature in the core drops just below the onset expansion temperature of the DU microspheres. This hypothesis is tested in Section 10.1. Next, in Section 10.2 EX-CORE sandwich panel samples produced with carbon fiber prepreg facings are discussed and their effect on the temperature distribution in the EX-CORE core is investigated. Then, in Section 10.3 achievable cure and in-mold cycle times of EX-CORE products with a range of core thicknesses, cured at various temperatures are explored. Additionally, in Section 10.4 a case study w.r.t. cure cycle time reductions is performed for the example of the floor panels of the Donkervoort D8 GTO-RS. Next, in Section 10.5 a discussion is given on remaining questions and challenges w.r.t. the future development of EX-CORE towards large series production. Finally in Section 10.6, a chapter summary and conclusions are given.

10.1. Investigating required EX-CORE cool-down

It was verified in Section 8.6 that when the mold is opened directly after EX-CORE curing, the rigid cured epoxy network cannot withstand the high internal pressure caused by the blowing agent in the DU microspheres that wants to expand at elevated temperatures. To investigate until which temperature the core temperature in EX-CORE should drop before the mold can be safely opened without the risk of sample expansion/cracking, sample series R7 was produced, as explained in the subsequent paragraphs.

10.1.1. Test series R7: EX-CORE samples cooled before mold opening

The first three samples produced in test series R7 were all equal in formulation to samples R5-TM1-2 and R5-TM1-3 (see Section 8.5). They were 30mm thick and were also cured at 110°C for 27min. Additionally, a thicker 75mm sample (R7-TM1-4) was produced, this to verify the obtained results and also to 'validate' the numerical model for thicker samples, as was discussed in Chapter 9. This time, the mold was opened when the measured core temperatures dropped below either 95°C, 115°C or 125°C. This because the hypothesis was that around the 95-115°C onset expansion temperature of the Expancel[®] 043 DU 80 microspheres the sample would be thermally stable and could be taken out of the mold [56]. During sample production the temperature values from the 15 NTC sensors located in the mid plane of the mold were live-monitored through serial connection between the Arduino[®] Mega and a computer. After a 27min cure at 110°C the power was shut down and the insulation blankets were removed from the tile mold. Finally, when all 15 temperatures dropped below the predefined temperature, the sample was taken out of the mold. An overview of the manufactured R7 series samples is given in Table 10.1 where the specific cool-down temperatures are also listed. In Table 10.2 an overview of the cured sample, pressure and temperature results is given, similarly as was done for all other samples series produced in this research. Remark the similarity of the results of samples R7-TM1-1 to R7-TM1-3 listed in Table 10.2, indicating good repeatability of the results. For example, the obtained maximum core temperatures were all between 154°C and 158°C. Note also that with 7.5vol.% of 043 DU 80, pressures over 6bar were obtained, which is a typical pressure used in autoclave processes.

Table 10.1: Overview of R7 series manufactured samples. All produced with the 270-optimal mix formulation.

Sample label	Sample height	Resin type	Hardener type	Epoxy ratio r	043 DU 80 vol.%	Cure temp	Cure time	Core cooled to
R7-TM1-1	30mm	SR 1280	Ancamine [®] 2442	100:20	7.5%	110°C	27min	95°C
R7-TM1-2	30mm	SR 1280	Ancamine [®] 2442	100:20	7.5%	110°C	27min	115°C
R7-TM1-3	30mm	SR 1280	Ancamine [®] 2442	100:20	7.5%	110°C	27min	125°C
R7-TM1-4	75mm	SR 1280	Ancamine [®] 2442	100:20	4%	110°C	53min	115°C

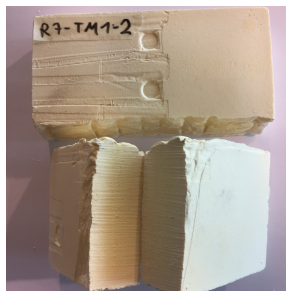
Table 10.2: Overview of R7 sample results, pressure and temperature measurements & rating of sample curing and expansion.

Sample label	Room temp.	Sample mass	Max. surf. pressure	Time to reach 0.5bar (avg.)	Temp. at 0.5bar	Max. core. temp.	Sample curing ¹	Sample expansion ²
R7-TM1-1	20°C	273g	/	/	/	154°C	5	5
R7-TM1-2	20°C	275g	6.2bar	11min	99°C	155°C	5	5
R7-TM1-3	20°C	272g	6.9bar	11min	105°C	158°C	5	5
R7-TM1-4	20°C	610g	4.4bar	22min	99°C	174°C	5	2

¹ On a scale from 1 to 5, with 5 being fully cured.

² On a scale from 1 to 5, with 5 being excellent expansion.

Sample **R7-TM1-1** was taken out of the tile mold when the maximum temperature in the core dropped below 95°C (the lower boundary of the onset expansion range of 043 DU 80). This took 43 extra minutes on top of the 27min predicted 98% cure time. The cool-down rate in the center of the sample was calculated to be around 1.22°C/min (see also Table 10.3 where they are listed for all samples). As expected, the sample was dimensionally stable and no cracks were observed in the cross-section of the sample, as shown in Figure 10.1. The next similar sample **R7-TM1-2** was already taken out of the mold when the core temperatures dropped below 115°C (the upper boundary of the onset expansion range of 043 DU 80). This was after 26min of extra cool down time. Again, as can be seen in Figure 10.2, no cracks were observed in the cured sample. The third sample **R7-TM1-3** which was cooled until only 124°C was reached in the core, was taken out of the mold after 20min of extra cool down time. This time cracks occurred through the cross-section as indicated in Figure 10.3. This indicates that in order to obtain dimensionally stable EX-CORE products, they should be cooled for such an extend that the temperature in the core is allowed to drop below the onset expansion temperature of Expancel[®] DU. The last sample **R7-TM1-4** was 75mm thick and contained only 4vol.% of DU. Its core temperature was also allowed to cool below 115°C. This took 70 additional minutes! Again no cracks originated. The sample is shown in Figure 10.4.

**Figure 10.1:** Sample R7-TM1-1**Figure 10.2:** Sample R7-TM1-2**Figure 10.3:** Sample R7-TM1-3**Figure 10.4:** Sample R7-TM1-4**Table 10.3:** Overview of additional cool-down time and cool-down rates measured in the center of R7 series samples.

Sample label	Core cooled to	Cool-down rate (center)	Extra time to cool
R7-TM1-1	95°C	1.22°C/min	43min
R7-TM1-2	115°C	1.38°C/min	26min
R7-TM1-3	125°C	1.04°C/min	20min
R7-TM1-4	115°C	0.86°C/min	70min

10.1.2. Discussion on maximum allowable core temperature before mold opening

From the R7 samples it became clear that no cracks originated when the maximum temperature in the core was allowed to drop just below 115°C, while a similar sample that was cooled only to 125°C was dimensionally unstable when taken out of the mold and cracked. This 115°C was the upper boundary of the onset expansion temperature range (95-115°C) of Expancel[®] 043 DU 80 as mentioned on the datasheet [56]. However, later it became clear from sample series R8 (see Section 10.2.2), that samples should be cooled below the lower boundary of the onset expansion temperature range, so 95°C in case of 043 DU 80. This because for example the R8-TM1-1 sample, which was cooled to 115°C still cracked (see Figure 10.5). In contrary, not a single sample cooled to 95°C showed cracking behavior and/or thermal instabilities.

In conclusion, to obtain dimensionally stable EX-CORE products without cracks they should be left to cool for such an extend that the temperature in the core is allowed to drop below the lower boundary of the onset expansion temperature of Expancel[®] DU. Unfortunately, this has as a consequence that the total required "in-mold cycle times" (curing & cooling) significantly increases. For example, for sample R7-TM1-1 which was cured for 27min at 110°C, an additional extra cool-down of 43min was required, leading to a total in-mold cycle time of 70min! It is hereby important to mention that the tile mold assembly was simply left to cool at room temperature (~20°C) without insulation blankets since it was not possible to cool the mold more quickly. Although that for large scale production it would be desirable to use molds that are always kept at the same temperature and do not have to be cooled, the effect of quicker mold cool down rates on the required cool-down time is explored using the numerical model. This is discussed in Section 10.3. It was expected that, even if it was possible to achieve high mold cool-down rates, this would not necessarily mean that the inner core would cool down proportionally, especially because of the insulating properties of the EX-CORE foam.

10.2. EX-CORE samples with prepreg facings and their effect on core temperature

Since the new "fast-curing" EX-CORE will ultimately be used in combination with CFRP facings to obtain sandwich structures, the effect of prepreg facesheets on the core temperature was investigated. Since non of the available prepregs at Donkervoort were "snap-cure" prepreg systems, a prepreg had to be ordered which resin system was compatible with the fast curing EX-CORE process. The prepreg selection criteria and final obtained prepreg are discussed in Section 10.2.1. Next, in Section 10.2.2 the manufactured samples with prepreg facings (R8 series) are reviewed. Finally, in Section 10.2.3, the effect of the CFRP prepreg facings on the temperature distribution inside the EX-CORE foam is evaluated.

10.2.1. Selection of snap-cure prepreg

Due to the long delivery times, the search for a new prepreg was already started during the first stage of the thesis in parallel with the search for a new epoxy system. The selection criteria for the prepreg resin were therefore similar to the ones defined for the epoxy matrix in EX-CORE discussed in Section 4.1.1. Most importantly, the prepreg resin also had to obtain a *98% cure in less than 10minutes, this at a cure temperature above 80° C but preferably below 120° C*. Additionally, as recommended in the research of Berckmoes [57] (see Section 3.2.6), the prepreg should be *fully impregnated*, so no semi-impregnated VBO prepregs can be used. For more background on the different prepreg types see also Section 2.1.2.

With respect to the carbon fiber fabric, a *3K 2x2 twill weave with a density around 200-250g/m²* was opted for. This was based on the good surface finish results with these type of prepregs obtained in the research of Berckmoes [57]. He investigated that the amount of surface porosity decreases when the out-of-plane permeability of the laminate increases.

Finding a compatible prepreg proved to be a difficult task since most snap-cure prepreg system are only purchasable when ordered in large quantities (>50-100m²). In the end a sample batch of snapcure prepreg was offered by TenCate which they had left in stock. It contained the snap-cure resin system "E732" which according to the datasheet [150] cures in 4 minutes at 160°C such that a Tg of 170°C is achieved. When cured at 140°C or 120°C it takes 10 or 20 minutes, respectively. It was originally developed for hot-in hot-out compression molding prepreg applications, and so this would make it suitable for medium to high production rate EX-CORE applications. With this snap-cure resin system TenCate only had 12K 2x2 twill weave prepreg in stock with a density of 650g/m². Since this was the best compatible prepreg that was available, this prepreg was used in the current research. Throughout the rest of this report, it be referred to as "TenCate E732 prepreg".

10.2.2. Test series R8: EX-CORE samples with CFRP prepreg facings

In total four EX-CORE sandwich panel samples with the TenCate E732 prepreg as facings were manufactured. The EX-CORE foams were in formulations entirely similar to samples R7-TM1-1,-2 & -3, all containing 7.5vol.% of 043 DU 80. An overview of the sample formulations, cure & cool down times and used prepreg facings can be found in Table 10.4. The sample results are listed in Table 10.5. Note that with the last two R8 samples the temperature and pressure was not monitored. This was done to obtain presentable samples with prepreg facings on both sides without imprints of sensors.

Table 10.4: Overview of R8 series manufactured samples. All produced with the 270-optimal mix formulation.

Sample label	Sample height	Resin type	Hardener type	Epoxy ratio r	043 DU 80 vol.%	Cure temp	Cure time	Core cooled to	Prepreg layers
R8-TM1-1	30mm	SR 1280	Ancamine [®] 2442	100:20	7.5%	110°C	27min	115°C	1 at bottom
R8-TM1-2	30mm	SR 1280	Ancamine [®] 2442	100:20	7.5%	110°C	27min	95°C	3 at bottom
R8-TM1-3	30mm	SR 1280	Ancamine [®] 2442	100:20	7.5%	110°C	27min	~95°C	2 each side
R8-TM1-4	10mm	SR 1280	Ancamine [®] 2442	100:20	7.5%	110°C	19min	~95°C	2 each side

Table 10.5: Overview of R8 sample results, pressure and temperature measurements & rating of sample curing and expansion.

Sample label	Room temp.	Sample mass	Max. surf. pressure	Time to reach 0.5bar (avg.)	Temp. at 0.5bar	Max. core. temp.	Sample curing ¹	Sample expansion ²
R8-TM1-1	20°C	299g	6.3bar	11min	100 °C	153°C	5	5
R8-TM1-2	20°C	346g	3.5bar	13min	103°C	165°C	5	5
R8-TM1-3	20°C	393g	/	/	/	/	5	5
R8-TM1-4	20°C	185g	/	/	/	/	5	5

¹ On a scale from 1 to 5, with 5 being fully cured.

² On a scale from 1 to 5, with 5 being excellent expansion.

The first 30mm thick sample **R8-TM1-1** was produced with 1 layer of TenCate E732 prepreg which was placed at the bottom of the sample casing before the EX-CORE paste was applied. The bamboo NTC sensor grid was again placed in the mid plane of the sample. The pressure generation was monitored with the Flexiforce sensors attached to the top metal plate. Similarly as done for R7-TM1-2, the sample was cured for 27min at 110°C after which the current was shut down and the sample was left to cool in the mold until the monitored temperature in the core dropped below 115°C. This took 25 additional minutes with an average cool-down rate of 1.32°C/min (see Table 10.6). As mentioned already in Section 10.1.2, a crack occurred in the sample when the mold was opened. The crack is indicated in Figure 10.5. The cured prepreg surface is shown in Figure 10.6. Although that a dry area with a relatively high amount of surface porosity/pinholes was present, the overall surface finish of the prepreg facing was very promising.

The 30mm thick sample **R8-TM1-2** was similar the previous one except that 3 layers of TenCate E732 prepreg were used and that it was left to cool until the temperature in the core dropped below 95°C. This took 47 additional minutes on top of the 27min cure time. When taken out of the mold the sample was dimensionally stable and no cracks could be observed. The top surface of the sample is shown in Figure 10.7. Again some pinholes were present but no dry areas could be observed on the prepreg surface. The temperature measurements of both samples R8-TM1-1 and R8-TM1-2 will be discussed in Section 10.2.3.

Table 10.6: Overview of additional cool-down time and cool-down rates measured in the center of R7 series samples.

Sample label	Core cooled to	Cool-down rate (center)	Extra time to cool
R8-TM1-1	115°C	1.32°C/min	25min
R8-TM1-2	95°C	1.19°C/min	47min
R8-TM1-3	~95°C	\	47min
R8-TM1-4	~95°C	\	35min

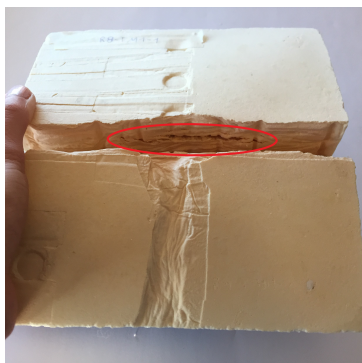


Figure 10.5: Sample R8-TM1-1 (top surface), crack indicated



Figure 10.6: Sample R8-TM1-1 (bottom surface), dry area with rel. large amount of surface porosity indicated

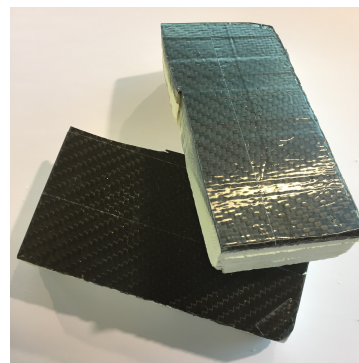


Figure 10.7: Sample R8-TM1-2



Figure 10.8: Sample R8-TM1-3 (top surface)



Figure 10.9: Sample R8-TM1-4 (top surface)

To obtain a representable prepreg EX-CORE sandwich panel, sample **R8-TM1-3** was produced with 2 layers of prepreg on both the top and bottom surface. To achieve a glossy surface, the aluminum top plate was polished beforehand. Because the temperature could not be monitored in the core, the sample was taken out of the mold after 47 additional minutes, similar to sample R8-TM1-2. The resulting cured sample was dimensionally stable and got a smooth surface finish but some surface porosity was present as can be seen in Figure 10.8.

Sample **R8-TM1-4** was similar to the previous one except that it was only 10mm thick. The required 98% cure time of the EX-CORE foam core was predicted using the numerical model to be 19min (see Figure 10.10). Additionally, since there was no reference for the required cool down time and because the core temperature was not monitored, the predicted maximum temperature of 130°C in the core in combination with a conservative 1°C/min cool down rate in the core was used to calculate a cool-down time of 35min to reach 95°C. Note that this is conservative because the peak temperature in the core already drops before the 19min cure time is finished (see Figure 10.10). The resulting sample is shown in Figure 10.9. An even better surface quality than sample R8-TM1-4 was obtained with less pinholes.

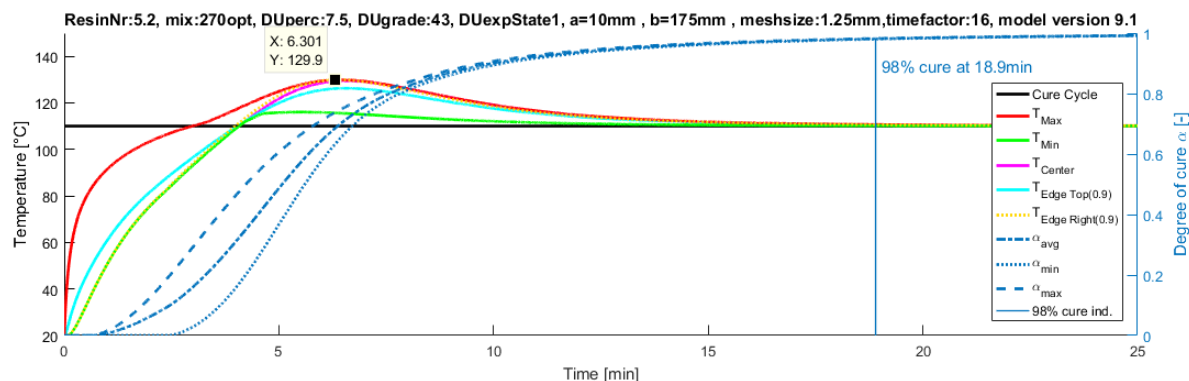


Figure 10.10: Numerical model simulation of the EX-CORE foam core in sample R8-TM1-4

10.2.3. Effect of CFRP prepreg facings on EX-CORE foam core temperature distribution

To investigate the effect of the prepreg facings on the temperature distribution in the EX-CORE foam core, the temperature measurements of the similar samples R7-TM1-2, R8-TM1-1 and R8-TM1-2 are compared. All three samples were 30mm thick, contained the same EX-CORE formulations and were all isothermally cured at 110°C for 27min. The difference was that sample R7-TM1-2 was manufactured without any prepreg layers, while samples R8-TM1-1 and R8-TM1-2 were produced with 1 and 3 prepreg layers at the bottom surface, respectively. The bottom edge, center and top edge temperatures of these samples as measured by NTC sensors nr. 10, 8 and 6 respectively (see Figure 7.6) are plotted in Figure 10.11. A comparison of important temperature and time data points is also given in Table 10.7.

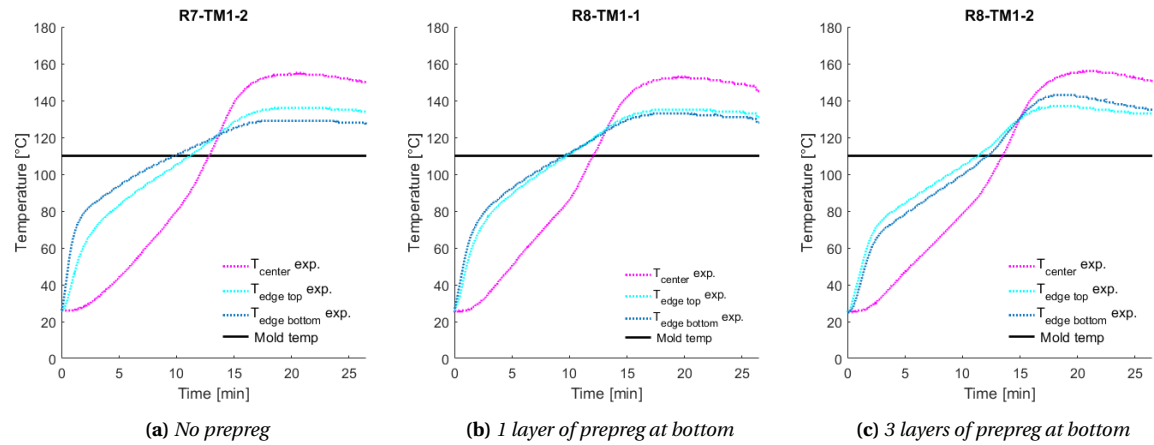


Figure 10.11: Temperature plots for samples R7-TM1-2, R8-TM1-1 and R8-TM1-2 (all: 270mix, 7.5%DU, 110C cured for 26.5min) with 0, 1 and 3 layers of prepreg at bottom, respectively.

Table 10.7: Comparison of experimental data from samples R7-TM1-2, R8-TM1-1 and R8-TM1-2 (all: 270mix, 7.5%DU, 110C cured for 26.5min) with 0, 1 and 3 layers of prepreg at bottom, respectively.

Sample Nr.	Max. T_{center} [C°]	Max. T_{top} [C°]	Max. T_{bottom} [C°]	Max. T_{trans} [C°]	t_{peak} [min]	$t_{center@95C}$ [min]	$t_{top@95C}$ [min]
R7-TM1-2	155	136	129	122	19.8	11.6	7.4
R8-TM1-1	153	135	133	125	19.1	10.8	6.1
R8-TM1-2	156	137	143	130	20.1	12.1	7.5

Before discussing the results, it should be remembered that the discrepancy/non-symmetry between the T_{top} and T_{bottom} curves in plot 10.11a of the non-prepregged EX-CORE sample is the result of the fact that the bottom surface is heated several seconds before the top surface. This because the sample (-casing) is placed on the preheated bottom mold lid after which the heated top lid is placed on top. When comparing the three sample results, several conclusions can be made:

- The maximum center (T_{center}) and top (T_{top}) temperatures are not influenced by the extra layer(s) of prepreg because the obtained temperatures all fall within a narrow range of 153-156°C and 135-137°C, respectively. These deviations can be related to experimental variations and sensor accuracy. Remember that the NTC sensors have an accuracy range of 3.4°C at 110°C (see Section 6.1.2).
- When compared to sample R7-TM1-2, the "discrepancy" between T_{top} and T_{bottom} reduces with sample R8-TM1-1, while with sample R8-TM1-2 T_{top} even transcends T_{bottom} . So this implies that the prepreg facings slightly delays the moment that T_{bottom} temperature starts to increase. Due to the conductive properties of the carbon fiber fabric this effect is however minimal.
- The maximum bottom temperature (T_{bottom}) is influenced by the presence of 1 or 3 prepreg layers. It increases with 4 and 14°C w.r.t. to the plain EX-CORE sample. This most probably due to the high exothermic heat release of the nearby prepreg resin.

- The transition temperature T_{trans} is slightly effected with the presence of 1 or 3 layers of prepreg. Namely it increases with 3°C and 8°C. This is most probably a side effect of the previous two points listed. Remember that, as explained in Section 9.1, that T_{trans} is not directly relevant for the current research.
- Since no rising/declining trend can be observed for any of the three time data points comparisons, the differences are most probably related to test variations.

Overall it can be concluded that the CFRP prepreg facings have marginal effect on the temperature distribution occurring in the EX-CORE. Only locally, near the prepreg surface, the core temperature is affected. This implies that the temperature distributions predicted by the EX-CORE numerical model should give "good" indications (within validated bounds as discussed in Chapter 9) of the temperature distributions of EX-CORE prepreg sandwich panels. Due to the marginal effect on the measured core temperature distribution, detailed modeling and incorporation of the CFRP prepreg facings in the numerical model should not be given the highest priority in future research.

10.3. Exploring achievable cure and in-mold cycle times of EX-CORE products with a range of core thicknesses and cure temperatures

To get a better impression on achievable cure and in-mold cycle times of sandwich panels with the re-designed EX-CORE composition, the predicted 98% cure time, additional cool-down time and resulting total in-mold cycles times are explored using the numerical model for a range of core thicknesses and isothermal cure temperatures. All graphs presented in this section are predictions obtained for the example of a "270-optimal" EX-CORE mix formulation with the SR 2180/Ancamine[®] 2442 epoxy matrix at 100:20 mix ratio. For all simulations the onset reaction temperature of the curing agent was set to 83°C. A 7.5vol.% of 043 DU 80 was chosen because successful samples were produced with this volume fraction. The sample width was set to 175mm (similar to the tile mold samples) and thickness was varied from 5mm to 100mm. It is hereby important to note that the model could not be validated for sample thickness higher then 30mm as discussed in Chapter 9. So the results for core thicknesses higher then 30mm should be treated with care.

The graph shown in Figure 10.12 compares the required time to reach at least 98% degree of cure everywhere throughout the sample when cured at 100°C, 110°C and 120°C. Results are plotted as a function of core thickness. As expected the required cure time increases both with thicker core thickness and lower cure temperature. It can be seen that even for a 5mm thin sample cured at 120°C the 10min part cycle time driver defined in Section 3.5.4 cannot be achieved. More specifically in that case a cure time of 14.4min is predicted to which the required cool time should be added on top (see later in Figure 10.16).

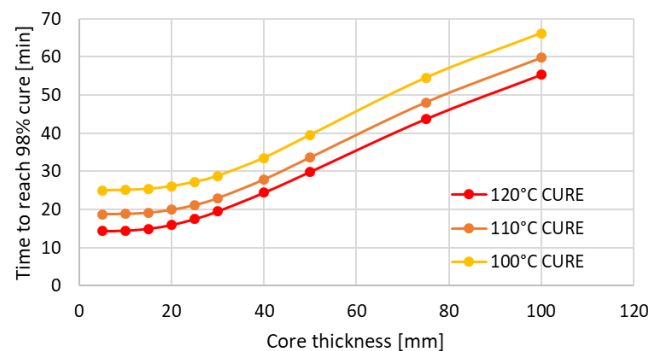


Figure 10.12: Time to reach 98% degree of cure for various EX-CORE core thicknesses cured at 100°C, 110°C or 120°C

Next, in Figure 10.13 the maximum peak temperatures occurring in EX-CORE are plotted as a function of core thickness when cured at 100°C, 110°C and 120°C. High temperature peaks could degrade the epoxy matrix (see Section 8.4.1) and could cause the DU microspheres to deflate when their maximum temperature is reached. For 043 DU 80 this is around 147-167°C [56]. This is especially detrimental when the epoxy network is not yet sufficiently cured since then the blowing agent can escape and the EX-CORE mixture could shrink. As expected, the peak temperatures increase with core thickness, as can be seen in Figure 10.13. Until a core thickness of ~50mm, peak temperatures are higher when EX-CORE is cured at higher temperatures. However, after ~50mm the 100°C, 110°C and 120°C curves approach each other.

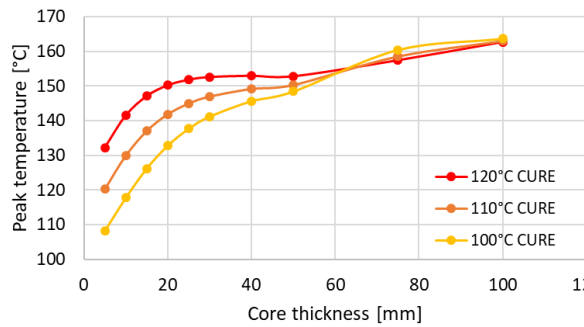


Figure 10.13: Peak temperature (T_{peak}) for various core thicknesses when cured at 100°C, 110°C or 120°C

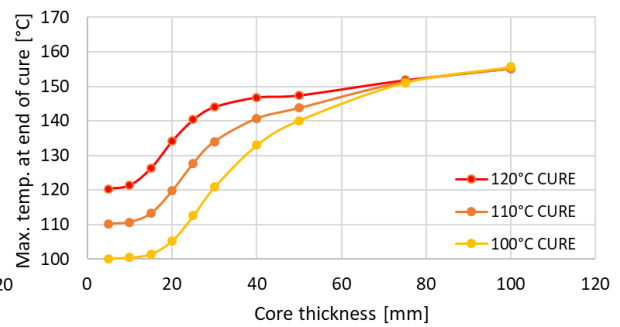


Figure 10.14: Maximum temperature at the end of cure (@ 98% degree of cure) for various core thicknesses when cured at 100°C, 110°C or 120°C

In Figure 10.14 the maximum temperatures at the end of the required cure cycle (so at the predicted moment when 98% is reached) are plotted as a function of core thickness and cure temperature. These values give an indication from which temperature the core should cool back to 95°C before the mold can be opened. As expected, the resulting temperatures increase with core thickness. They are also higher when cured at higher temperature. Again the curves approach each other when the core thickness becomes higher than ~50mm. So even though that with higher cure temperatures shorter cure cycle times can be achieved, the required cool-down time becomes larger because higher peak temperatures occur in the core. The net effect on the total required in-mold cycle times becomes clear in the following paragraphs.

Another important aspect to consider is that, with the insulating properties of the EX-CORE foam, it does not necessarily imply that high mold cool down rates result in equally fast cool down rates in the center of the EX-CORE core. This is illustrated in Figure 10.15 for the example of a 30mm thick EX-CORE sample isothermally cured at 120°C until 98% cure is reached. Then the mold is cooled with a rate of 5°C/min to room temperature of 20°C. It is indicated that at 19.5min, 98% cure is reached and at that moment the maximum temperature in the core is 144°C. 15 minutes later (at 34.5min) this center core temperature dropped to 95°C. So this means that the temperature in the center of the core dropped with a rate of 3.27°C/min, so slower than the predefined 5°C/min rate of the mold.

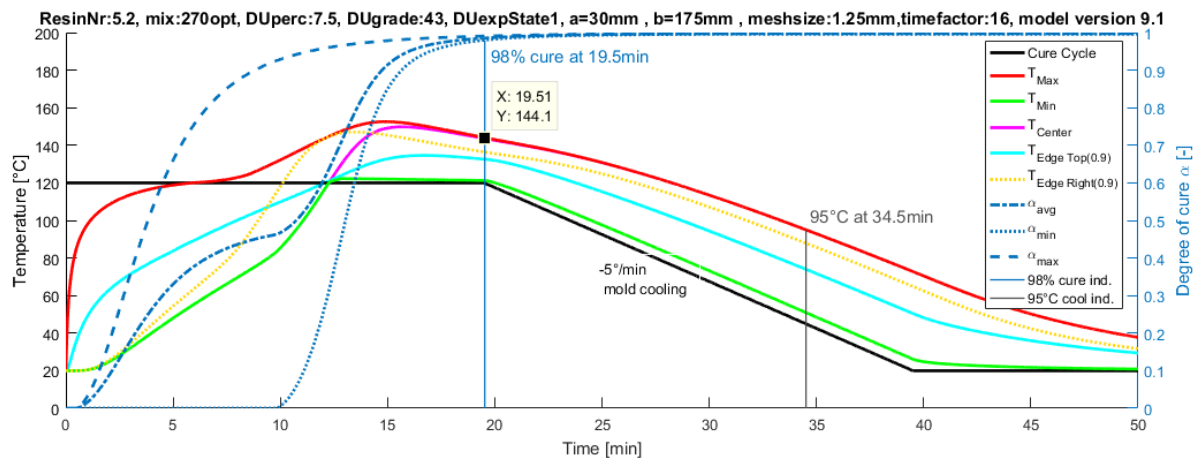


Figure 10.15: Example of simulated temperature and degree of cure plotted as a function of time for a 30mm thick EX-CORE sample cured at 120°C until 98% degree of cure is reached after which the mold is cooled at 5°C/min.

The additional cool down time required to drop from the maximum temperature in the core at the end of cure (which values were plotted in Figure 10.14) to the required 95°C before the mold can be opened are plotted in Figure 10.16 as a function of core thickness. Results are given in case the mold is cooled at either 1, 2 or 5°C/min. A comparison is also given for the 110°C and 120°C cured sample results. Note that curing at temperatures below 110°C is not recommended since it could not be verified that sufficient pressure can be generated by the 043 DU 80 microspheres, which have their onset expansion temperature in the range of 95°C to 115°C [56]. As expected, the additional in-mold cool time increases with core thickness, cure temperature and slower mold cool down rate. The shortest extra time to cool is 3.8min, this for the example of a 5mm thick samples cured at 110°C and mold cooling of 5°C/min. The longest plotted extra time to cool is 93min obtained for the example of a 100mm core thickness heated at 120°C and which mold is cooled at 1°C/min.

Finally, the resulting total in-mold cycle times combining the 98% cure time (Figure 10.12) and the additional required cool down time (Figure 10.16) are plotted in Figure 10.17 as a function of core thickness for the three different mold cool down rates. Again results of the 110°C and 120°C cured samples are compared. Interestingly, when cooled at 1°C/min, shorter cycle times are obtained for the 110°C cured samples than for the 120°C cured samples. When cooled at 2°C/min both 110°C or 120°C results curves approach each other. In that case only slightly shorter cycle times are obtained when cured at 120°C, with a maximum difference of 1.4min. In contrary, when cooled at 5°C/min slightly shorter cure cycle times are obtained for the 120°C cured samples when compared to the 110°C cured ones. However, this difference is at most 2.4min for the 5mm thick sample (22.6min vs 20.2min when cured at 110°C or 120°C respectively). In conclusions, the graph in Figure 10.17 gives a good impression of the in-mold cycles times that can be achieved for various EX-CORE core thicknesses.

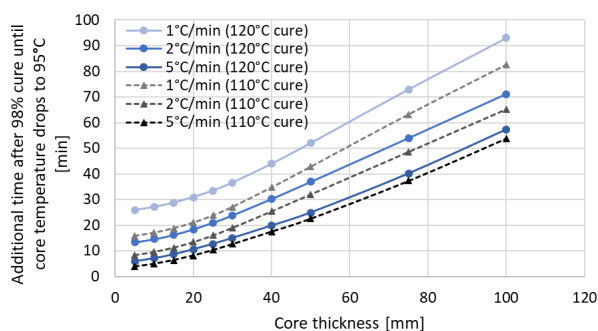


Figure 10.16: Additional time to cool from $T_{@98\%cure}$ (see graph 10.13) to 95°C, for various core thicknesses when cured at 110°C or 120°C and when the mold is cooled either at 1, 2 or 5°C/min.

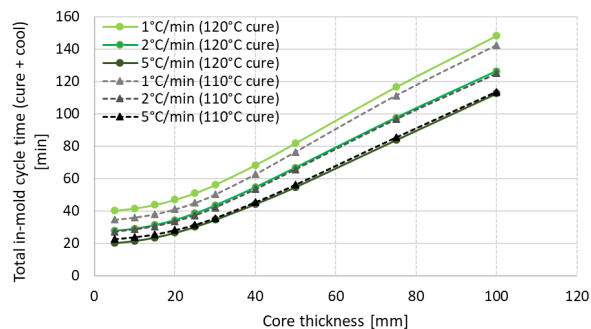


Figure 10.17: Total in-mold time for various core thicknesses, when cured both at 110°C and 120°C

10.4. Case study: cycle time reduction of floor panels

A case study was performed to investigate the possible in-mold cycle time reduction with the new fast curing EX-CORE for the floor panels of the Donkervoort D8 GTO-RS. A technical CAD drawing and picture of the floor panels can be seen in Figures 10.18 and 10.19. Currently, at Donkervoort these floor panels are produced according to the process guidelines formulated in the research of Berckmoes [57], as discussed in Section 3.2.6. The 270-optimal mix formulation is used with the original epoxy matrix system (Ancarez[®] RZ4010/Ancamide[™] 3399) and 1.5vol.% of the original Expancel[®] 031 DU 40 grade. The standard cure cycle of the panels is as follows: first a 1.5°C/min ramp up from room temperature (20°C) to 110°C, followed by a dwell at 110°C for 120min. Currently, the total cure time thus takes 3 hours (see also the recommended cure cycle window in Figure 3.16). It is important to note that after this 3 hour cure cycle the mold assembly is left to cool to room temperature for approximately 1 hour before the panels are taken out of the mold. Hence for the current floor panel production, the total in-mold cycle time adds up to 4 hours.

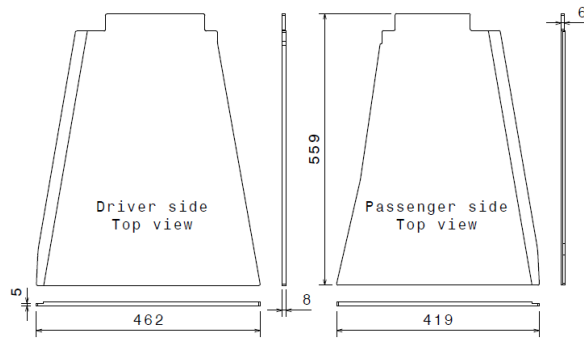


Figure 10.18: CAD drawing of floor panels [57]

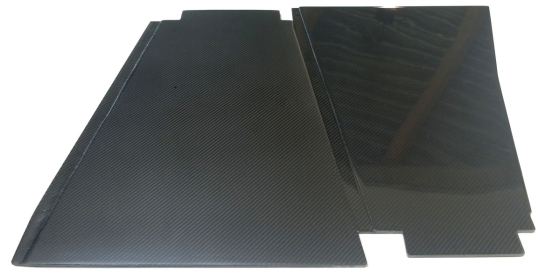


Figure 10.19: Picture of floor panels [57]

Due to time constraints and required mold adaptations, floor panels could not be manufactured with the new EX-CORE formulation containing the new SR 1280/Ancamine[®] 2442 epoxy system and Expancel[®] 043 DU 80 grade in the current research. Nonetheless, the numerical model could be used to predict the required cure time to reach 98% cure and determine the cure temperature that would result in the shortest in-mold cycle time. As input parameters, the 270-optimal mix formulation was selected with 1.5vol.% of 043 DU 80. The epoxy mix ratio of SR 1280/Ancamine[®] 2442 was set at 100:20 and the onset reaction temperature at 83°C. The initial EX-CORE temperature was set to 20°C. Since the model is two-dimensional (with infinite depth in 3rd dimension), the width (rounded to 460mm) and thickness (8mm) of the driver side panel were implemented, while the longest side of the panel could be considered infinitely long.

The model was used to determine and compare the total in-mold cycle times for an isothermal cure cycle of 120°C and 110°C when assuming a conservative mold cool down rate of 1°C/min. Ultimately, it became clear that curing at 110°C resulted in the shortest in-mold cycle time of 35.1min (18.7min cure + 16.4min cool down time) while a slightly larger in-mold cycle time of 39.7min (14.3min cure + 25.4min cool down time) was predicted when cured at 120°C. Remember again that curing at temperatures below 110°C is not recommended since it could not be verified that sufficient pressure can be generated by the 043 DU 80 microspheres, which have their onset expansion temperature in the range of 95 to 115°C [56].

The temperature and degree of cure prediction plotted vs time for the floor panels when isothermally cured at 110°C can be seen in Figure 10.20. As indicated in this figure, a maximum temperature of 127.1°C is reached after 4.9min. After 18.7min 98% degree of cure is reached, at that moment the core temperature leveled off to ~110°C everywhere throughout the cross-section. So this case study illustrates that with the new epoxy matrix, and if the floor panels are isothermally cured in a preheated mold at 110°C, the required cure time reduces from 3hours to 18.7min which is a cure time reduction of 89.6%. If we then take a conservative cool down rate of 1°C/min in the center of the core, it would take 16.4 additional minutes to cool from 110°C to 95°C. Hence the total required in-mold cycle time becomes 35 minutes. Compared to the current floor panel production in-mold cycle time of 4 hours this is a reduction of 85.4%.

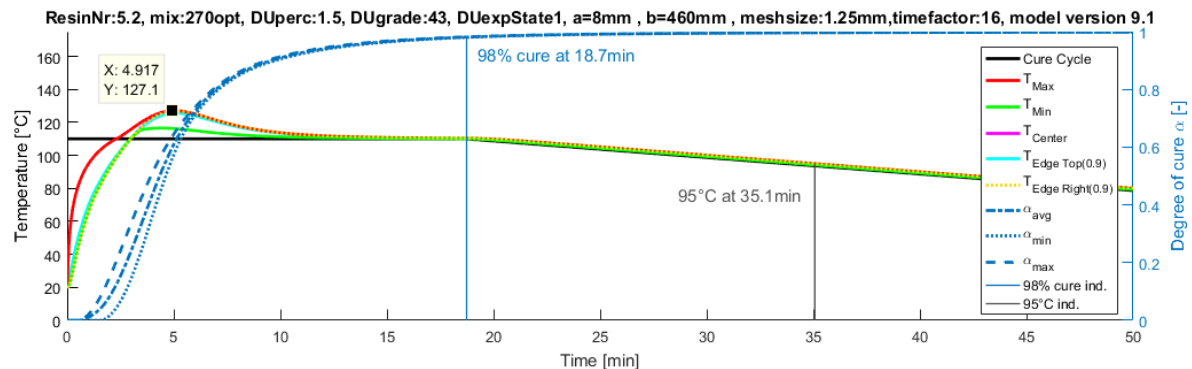


Figure 10.20: Temperature and degree of cure vs time predicted by the numerical model for the floor panels with the new "fast-curing" EX-CORE formulation at 110°C isothermal cure followed by a mold cool-down at 1°C/min

10.5. Remaining questions and challenges w.r.t. EX-CORE development towards large scale automotive manufacturing

It is without doubt that there are still a lot of things left to investigate w.r.t to the future development of EX-CORE towards large series automotive manufacturing. For example, the question remains whether or not for future larger series EX-CORE production it is beneficial to use preheated molds and an isothermal cure cycle. This because in this study it became clear that the mold should be cooled afterwards to allow the core temperature of the cured product to drop below 95°C to ensure that the product is dimensionally stable when the mold is opened. Then the mold should be heated again for the next product etc. Another possibility could be to apply the prepreg and EX-CORE on a mold that is preheated below the onset expansion temperature of Expancel DU and preferably also below the onset reaction temperature of the epoxy system. This would prevent curing and/or expansion initiation during lay-up. It would also limit the required ramp-up and eliminate the additional time, energy and hence cost that would otherwise be required to heat-up/cool-down from/to room temperature.

Another aspect that should be investigated is the type of mold and heating/cool-down system that would be suitable for large scale EX-CORE manufacturing. For large series production it would probably be more economic to replace the integrally heated hand lay-up composite molds by milled aluminum/metal molds that are less prone to degradation, especially when multiple products have to be produced every day. Then the higher expense of the milled metal molds also pays off. With respect to quickly heating and cooling the molds it could for example be an option to use a system of hot and cold water pipes that run through the conductive metal molds.

Another challenge which has to be tackled is how the CFRP prepreg facings and more importantly the EX-CORE paste can be quickly and automatically applied in the mold. Prepreg preforms/lay-ups could for example be produced with automatic tape layup (ATL) or automated fiber placement (AFP) which respectively place prepreg tapes or individual prepreg tows on a mold using a robotic placement head. More research is however required to explore the possibilities whether or not the EX-CORE paste can be automatically applied. It could for example be investigated if it is possible to inject the EX-CORE paste in an enclosed mold (with prepreg lay-up in place). As explained in Section 3.2, research w.r.t. automatically dosing and mixing of EX-CORE components was initiated by Mattheus [66] during her internship at Donkervoort. A proof-of-concept dosing and mixing setup was developed from which promising results were obtained. This project was continued by Ten Hoeve [67] who ultimately proposed a prototype "EX-CORE production machine". For more information see Section 3.2.9. Nevertheless, there still a lot of development required w.r.t. production automation in order to make the EX-CORE technology suitable for larger series automotive manufacturing.

10.6. Summary & chapter conclusions

In order to obtain dimensionally/thermally stable EX-CORE products without cracks, it was verified that they should be left to cool for such an extend that the temperature in the core is allowed to drop below the lower boundary of the onset expansion temperature of Expancel® DU. So in case of the new 043 DU 80 grade this is 95°C. Unfortunately, this has as a consequence that the total required "in-mold cycle times" (curing & cooling) significantly increase. The 98% cure cycle times, peak temperatures, cool times and resulting total in-mold cycles times were explored using the numerical model for a range of core thicknesses, mold cool-down rates and cure temperatures. Interestingly, it became clear that higher cure temperatures do not necessarily imply shorter in-mold cycle times. The reason is that higher maximum core temperature are obtained which increase the required cool time to let the core temperature drop below 95°C.

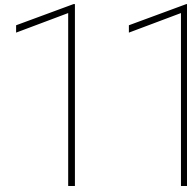
Successful sandwich panel samples with good surface quality were created with the re-designed EX-CORE formulation and the snap-cure TenCate E732 prepreg. The effect of the CFRP prepreg facings on the temperature distribution in the EX-CORE core was also investigated. Overall it can be concluded that the CFRP prepreg facings only have marginal effect on the temperature distribution occurring in EX-CORE. The influence of the prepreg facing concentrated near the prepreg facings. For example, the maximum core temperature is not affected. This implies that the temperature distributions predicted by the EX-CORE numerical model (within the validated bounds) should give good indications of the temperature distributions of EX-CORE prepreg sandwich panels. Detailed modeling and incorporation of the CFRP prepreg facings in the numerical model should therefore not be given the highest priority in future research.

The numerical thermal EX-CORE model can be used as a design tool to explore which cure cycle might be most beneficial. It is hereby important to note that the model could only be validated for cores not thicker than 30mm (see Chapter 9). Care should therefore be taken when using the model to explore thicker core

thicknesses. From the simulated results it became clear that with the new EX-CORE composition it is impossible to obtain in-mold or even cure cycle times below 10 minutes. The poor conductive properties of the microspheres DU, DE and Q-Cel, that characterize the EX-CORE foam, form the largest limitation to obtain fast cure- and cool-down times and hence short total in-mold cycle times. For example, for a 5mm thin core cured at 110°C a total 27.1min in-mold cycle time is predicted which consists of a 18.8min cure and 8.3min cool-down time (with mold cool-down rate of 2°C/min). For a 30mm thick sample the predicted in-mold cycle times becomes 42min, consisting of 23min cure time and 19min cool down time. Even when it is possible to quickly cool down the surrounding mold, the poor conductive properties of the EX-CORE foam limit the rate at which the center of the core can be cooled.

Additionally, a case study was performed for the floor panels of the Donkervoort D8 GTO-RS. It became clear that with an isothermal cure at 110°C, the shortest in-mold cycle times can be achieved when assuming a conservative mold cool down rate of 1°C/min. Namely, a total in-mold cycle time of 35.1min was predicted which consisted out of 18.7min cure followed by 16.4min cool time in the mold, in case the mold temperature drops with 1°C/min. When compared to the current 3hour cure cycle and total 4 hour in-mold cycle time of the floor panels produced at Donkervoort, the cure cycle time is reduced by 89.6% while the total in-mold cycle time is reduced by 85.4%.

Although that the EX-CORE foam material has been redesigned to facilitate cure cycle time reductions it was discussed that there is still a lot of research and development required w.r.t. production automation, mold tooling, EX-CORE application etc. in order to make the EX-CORE technology suitable for larger series automotive manufacturing.



Conclusion

The objective of this study was to contribute to the development of the one-shot manufacturing of EX-CORE CFRP sandwich structures for large scale automotive manufacturing. EX-CORE, can be classified as a syntactic foam since it contains microspheres embedded in a binder matrix, more specifically an epoxy resin. It is unique in the sense that it contains the expandable microspheres Expancel[®] DU which increase in volume under elevated temperature. When enclosed in a heated mold, this expansion is restricted which generates an internal pressure that is used to consolidate the CFRP facesheets. When cooled back to room temperature, the cured epoxy matrix ensures that the product remains in its expanded state. Next to its function as a lightweight core material, the EX-CORE technology can offer several unique advantages compared to other CFRP composite manufacturing processes. Complexly shaped sandwich structures can be produced in a one-shot process while allowing to obtain a high surface finish on all sides of the product. This significantly reduces the amount of processing steps and hence, production- and labor cost. Furthermore, no external pressure tooling such as an autoclave or vacuum bag is required, resulting in a reduced amount of tooling and consumables.

Currently, one of the main limitations for commercialization of EX-CORE towards large scale automotive manufacturing is the relatively long part cycle time of the current EX-CORE process. For example, the cure cycle alone takes 3 hours or more, which leads to a total in-mold cycle time of over 4 hours. In order to become competitive with other CFRP manufacturing technologies suitable for large series applications, such as HP-RTM and WCM, the cycle times should be drastically reduced to several minutes. The research presented in this report therefore focused on reducing the cure cycle times by re-engineering the EX-CORE material.

As a first important step, several fast-curing epoxy systems were selected that could replace the currently used Ancarez[®] RZ4010/Ancamide[™] 3399 epoxy binder. More specifically, the low viscous resin SR 1280 was acquired and three new types of hardeners; one liquid hardener SZ 8525 and two powder hardeners Ancamine[®] 2337s and Ancamine[®] 2442. The latter two have a physical thermal block that result in an onset reaction temperature (T_{onset}) around 71°C and 93°C according to the datasheets [97, 99]. The cure kinetics of the new epoxy systems were experimentally determined using Differential Scanning Calorimetry (DSC). The experimental data could be fitted with a modified autocatalytic cure kinetic model such that the reaction rate and degree of cure of the epoxies could be simulated. The required time to obtain 98% degree of cure for the pure epoxy systems could be determined at various cure temperatures. For example, when cured at 110°C, the time to obtain 98% cure ranged from 13.9min for SR 1280/SZ 8525 to as low as 7.2min for SR 1280/Ancamine[®] 2442. For the original Ancarez[®] RZ4010/Ancamide[™] 3399 epoxy system this was 46min and thus the cure time reduced between 70% and 84%, respectively. Note however that when the epoxy resins are used in combination with the poor conductive microspheres in EX-CORE, the required cure times increase. Especially for thicker cores it can take several minutes before the heat of the mold reaches the center of the core.

To be able to predict the heat transfer, temperature and degree of cure distribution over time inside EX-CORE, an existing numerical heat conduction based model was used and updated. It should hereby be noted that the EX-CORE foam is highly tailorable since the volume fractions of the components can be changed. The model is however capable of simulating the thermal behavior of a wide variety of EX-CORE mixtures

with various core dimensions under specified cure cycles. The two-dimensional transient finite difference model was built upon in MATLAB. The energy balance method was used to establish the governing equation with internal heat generation caused by the exothermic reaction of the epoxy resin. Again, an explicit solution strategy was used. The autocatalytic cure kinetic models were implemented to simulate the heat release of the selected epoxy systems. Additionally, theoretical models were used to predict the effective thermal conductivity and specific heat capacity of the chosen EX-CORE formulation. They were based on the thermal properties of the various material constituents and volume/mass fractions. The simplified numerical model was verified with an analytical solution; when using a mesh size of at least 1.25mm in combination with a time step of $1/16 t_{crit}$, a converged numerical solution was obtained with an error of less than 2% compared to the analytical solution. Additionally, a sensitivity study was performed to evaluate how accurately the effective thermal conductivity and specific heat capacity have to be obtained. It was concluded that to obtain an accuracy of $\pm 5^{\circ}\text{C}$, they should be determined within 0.092W/mk and 152J/kgK, respectively.

To limit the amount of variables during the research, all samples were produced with the same base EX-CORE mix composition. More specifically, the "270-optimal" mix was selected based on previous research. All samples were isothermally cured inside a preheated integrally heated tile mold in which square EX-CORE samples could be produced with variable thickness. Initially the samples were taken out of the mold when the predicted 98% cure time was reached. Along the mid plane of the samples the temperature of the core could be measured with NTC thermistor sensors. Additionally, the generated pressure on the surface of the sample could be monitored with Flexiforce[®] HT201 force sensitive sensors.

During the first test phase, various EX-CORE samples were produced with the new epoxy matrices to explore their compatibility. Both the SZ 8525 and the Ancamine[®] 2442 curing agent, in combination with the SR 1280 resin, gave promising results when used as binder matrix in EX-CORE. However, none of the samples created with the Ancamine[®] 2773s hardener were sufficiently cured or dimensionally stable. Hence, this hardener was eliminated from further testing.

In the second test phase, the current Expancel[®] 031 DU 40 grade was replaced with the more solvent resistant 043 DU 80 grade that also has a higher onset expansion temperature range (95-115 $^{\circ}\text{C}$ instead of 80-95 $^{\circ}\text{C}$) and higher maximum temperature range (147-167 $^{\circ}\text{C}$ instead 120-130 $^{\circ}\text{C}$). Multiple EX-CORE samples were produced with this new DU grade and the SR 1280 resin in combination with either the SZ 8525 or Ancamine[®] 2442 hardener. At the end of this test phase the Ancamine[®] 2442 was selected as the most suitable curing agent to continue the research with for the following reasons: First of all, the SZ 8528 does not have a physical thermal block. Thus once mixed, the exothermic reaction is initiated at room temperature which would make it difficult to pre-mix and store large batches of EX-CORE paste. Additionally, consistent results cannot be guaranteed due to variations in initial degree of cure. Secondly, due to the higher specific heat of reaction of SZ8525 (287J/g vs 169J/g) high temperature overshoots occur in EX-CORE. For example when cured at 110 $^{\circ}\text{C}$, temperature peaks up to 182 $^{\circ}\text{C}$ were measured in the core of 30mm EX-CORE samples containing the SZ 8528 hardener. For a similar sample containing Ancamine[®] 2442, the maximum temperature became not higher than 141 $^{\circ}\text{C}$.

In the third test phase, compression tests were performed on various EX-CORE samples containing the SR 1280/Ancamine[®] 2442 epoxy matrix to investigate the effect of cure temperature, cure time and epoxy mix ratio on compressive strength. Based on these results, several interesting conclusion could be made:

First of all, the compressive strength was found to increase when lowering the epoxy mix ratio as follows; 100:60<100:30<100:20. Since mix ratios lower than 100:20 did not contain sufficient hardener, the 100:20 epoxy ratio was selected. New DSC scans had to be performed to determine the corresponding cure kinetics. Although the time required to reach 98% cure more than doubled compared to the 100:60 ratio, the compressive strength was 4 times higher, coming close to specific strength values obtained for EX-CORE in previous research, hence justifying the choice.

Secondly, the compressive strength of EX-CORE samples increased with cure temperature: 110 $^{\circ}\text{C}$ <140 $^{\circ}\text{C}$ <160 $^{\circ}\text{C}$. However, there were several indications that the higher cure temperatures did not directly result in a stronger/more cross-linked epoxy network. It could, for example, be possible that the resulting higher pressure due to the higher expansion of the blowing agent at increased cure temperatures led to a better compaction/melting of the thermoplastic microspheres. From the DSC tests performed at 100:20 ratio, it became clear that cure temperatures above 120-135 $^{\circ}\text{C}$ caused the exothermic reaction of the Ancamine[®] 2442 epoxy system to decrease. Evonik also mentioned that at higher cure temperatures, another cross-linked

network is formed due to the reaction of OH groups and that Ancamine[®] 2442 is only stable until ~170°C.

Thirdly, 5min extra cure time or post curing at higher temperature only had a marginal effect on the compressive strength. This was therefore not investigated any further.

To validate the numerical model, experimental temperature data gathered from various 270-opt mix samples produced throughout the research with the SR 1280/Ancamine[®] 2442 epoxy matrix and Expancel[®] 043 DU 80 was used and compared with model predictions. Since large discrepancies were found for the first set of comparisons, the originally implemented 93°C onset reaction temperature (T_{onset}) given on the datasheet [99] of the Ancamine[®] 2442 curing agent was verified. Dynamic DSC scans were performed at 0.5, 2, 10 and 15°C/min, for which onset reaction temperatures of 58, 70, 84 and 94°C respectively were recorded. Consequently, T_{onset} was updated to 83°C in the numerical model since this corresponded better to the average heat-up rate measured in 110°C isothermally cured samples.

Although discrepancies reduced, there was a suspicion that the temperature measurements themselves were affected by the conductive metal grid to which the 15 NTC temperature sensors were attached. The grid was therefore replaced by a poorly conducting grid constructed from bamboo skewers with which new 30, 55 and 75mm samples were manufactured. For the 30mm samples, almost perfect fits with the model predictions were obtained until the point when the maximum temperature was reached in the core. Then the simulated results dropped more drastically than the experimental data did. For the 55mm and 75mm thick samples increasingly larger discrepancies were observed across the whole cure cycle. Two probable causes for the observed discrepancies are related to the assumptions made for the numerical model. First of all, the assumption of constant mold temperature and secondly the assumption of constant onset reaction temperature of the Ancamine[®] 2442 curing agent.

In the end the updated numerical model could only be validated for 30mm thick 270-opt mix samples that were isothermally cured at 110°C since thicker samples fell outside the acceptable discrepancy bounds. Due to time constraints, other mix formulations and/or cure cycles could not be tested. It is also important to note that the EX-CORE degree of cure predictions could not be experimentally validated. In the future however a possibility could be to use dielectrometry to monitor the cure process during production of EX-CORE sandwich structures (see recommendations in Chapter 12).

It was verified that the large cracks observed in several EX-CORE samples produced throughout the research originated when the mold was opened directly after curing when the sample was still hot. Even if the EX-CORE foam is sufficiently cured, the epoxy network cannot withstand the high internal pressure caused by the blowing agent in the DU microspheres that wants to expand at elevated temperatures. It was investigated that, to obtain dimensionally stable EX-CORE products without crack formation, the mold cannot be opened before the maximum temperature in the core is allowed to drop below the lower boundary of the onset expansion temperature of Expancel[®] DU. So in case 043 DU 80 is used, this is 95°C. Unfortunately, the consequence is that the total required "in-mold cycle time" (curing & cooling) increases. Even when it is possible to quickly cool down the surrounding mold, the poorly conductive EX-CORE foam limits the rate at which the center of the core can cool down.

The 98% cure-, extra cool- and resulting in-mold cycle times were explored with the numerical model for a range of core thicknesses, mold cool-down rates and cure temperatures. Interestingly, it was found that higher cure temperatures do not necessarily imply shorter in-mold cycle times. The reason is that higher maximum core temperatures are obtained which increase the cool time to let the core temperature drop below 95°C. From the simulations it became clear that, even with the new EX-CORE formulation containing the fast curing SR 1280/Ancamine[®] 2442 epoxy (at mix ratio 100:20), it is not possible to obtain in-mold or even cure cycle times below 10 minutes. The poorly conductive properties of the microspheres DU, DE and Q-Cel form the largest limitation to obtain fast cure- and cool-down times.

Promising sandwich panels with good surface quality were created with the re-designed EX-CORE foam and TenCate E732 prepreg facesheets. It can be concluded that CFRP prepreg facings had marginal effect on the temperature distribution occurring in the core. Only locally, near the prepreg facings, the temperature was influenced. Temperature distributions predicted by the EX-CORE numerical model should therefore provide a good indication of the temperature distributions of EX-CORE prepreg sandwich panels (within validated bounds). Hence, it can be used as a design tool to explore which cure cycle might be most beneficial for a specific product.

A case study was worked out for the floor panels of the D8 GTO-RS. With a conservative mold cool-down rate of 1°C/min, the shortest in-mold cycle time can be achieved if the panels are isothermally cured at 110°C. Then a total in-mold cycle time of 35.1min was predicted, which consisted out of 18.7min cure followed by

16.4min cool-down time. When compared to the 3hour cure cycle and total in-mold cycle time of 4hour as currently applied at Donkervoort, the cure cycle time would be reduced by 89.6% while the in-mold cycle time would be reduced by 85.4%. Curing at temperatures below 110°C is not recommended since it could not be verified that sufficient pressure can be generated by the 043 DU 80 microspheres, which have their onset expansion temperature in the range of 95°C to 115°C [56].

The knowledge obtained throughout the present research provided more insight into the possibilities and limitations of fast-curing EX-CORE, which will guide its future development towards larger series applications. Nonetheless, there is still a lot of research and development required w.r.t. commercialization, production automation, mold tooling, EX-CORE application etc.

Recommendations

Although that the EX-CORE technology can offer several unique advantages, not only from a material but also from a production point of view, it should be realized that the commercialization and development of EX-CORE w.r.t high volume applications is still in its early stages. In the current research the EX-CORE foam material has been redesigned to facilitate cure cycle time reductions but there is still a lot of research and development required to make the EX-CORE technology suitable for large scale automotive manufacturing. In this chapter recommendations for future research are discussed that came to mind during the performed thesis research.

12.1. EX-CORE

The recommendations given in this section are related to the formulation of the EX-CORE foam material.

Conductive fillers

In the current research major cure cycle reductions had been achieved by replacing the former epoxy matrix with the fast curing epoxy system SR 1280/Ancamine[®] 2442 which according to the modified autocatalytic cure kinetic model achieves 98% cure in 7.5min when isothermally cured at 110°C. However, in combination with the poor conductive microspheres DU, DE and Q-Cel, it was not possible to obtain 98% cure times below 10min, not even for 5mm thin EX-CORE samples. Additionally, even when the surrounding mold is rapidly cooled, the poorly conductive foam limits the rate at which the temperature in the core cools-down below the required 95°C before the mold can be safely opened.

To further reduce the in-mold cycle times it should be investigated whether the thermal conductivity of the EX-CORE foam can be increased, while simultaneously limiting the increase in density of the foam. Since the use of a thermosetting binder matrix and Expancel[®] DU is essential for the working principle of EX-CORE, the most straight forward solution would be to replace the hollow glass microspheres Q-Cel by highly conductive microspheres. Q-Cel 5028 microspheres were initially added to increase the compressive strength properties of EX-CORE and so they could be replaced with microspheres of comparable or even higher specific compressive strength.

One type of conductive lightweight microspheres commercially available are hollow or solid glass microspheres that are coated with a highly conductive layer of metal, typically silver or nickel. They are available in a wide range of particle sizes and densities [151]. *Microsphere Technology* produces silver/nickel coated hollow microspheres under the name of CONDUCTOSPHERES[™]. Two grades in particular are most comparable to Q-Cel, namely CONDUCTOSPHERES[™] M-45 and M-60, which are hollow glass microspheres coated with 50nm of silver. Their properties are listed and compared with Q-Cel 5028 in Table 12.1. From the table it can be seen that the M-60 grade has the same mean particle size, but compressive strength and density values are lower than those of Q-Cel. On the other hand, the compressive strength of M-45 is more than twice as high as but the density is higher and the particle size lower. Nevertheless, the highest strength over weight ratio is obtained for the M-45 grade (43.13kNm²/kg vs 12.94kNm²/kg for M-60 and 23.79 kNm²/kg for Q-Cel) and such it might be more beneficial to opt for the M-45 grade. Unfortunately, a major downside of these microspheres is that they are relatively expensive. A quotation was received with a cost price of 780euro for 5L of 60µm CONDUCTOSPHERES[™] coated with 50-50nm of silver.

Table 12.1: Properties of Q-Cel[®] 5028 and CONDUCTOSPHERES[™] M-45 & M-60 [69, 70, 152]

	Particle size (mean) [μm]	True density ¹ [kg/m^3]	Bulk density [kg/m^3]	Compr. Strength [Mpa]
Q-Cel 5028	<75	290	160	6.9
CONDUCTOSPHERES M-45	43	320	200	13.8
CONDUCTOSPHERES M-60	74	160	100	2.07

¹ Density of a single microsphere

As covered in Section 5.4.1, the Maxwell-Garnett model was implemented in the numerical model to determine the effective thermal conductivity of the EX-CORE foam. Zhu et. all. [134] experimentally determined this model to be valid for hollow glass microspheres up to 60vol.% in an epoxy matrix. However, care should be taken when using the Maxwell-Garnett model (and hence numerical model) to determine the effective thermal conductivity of EX-CORE formulations containing high volume contents (>50%) of highly conducting microspheres (w.r.t. low conductive binder) such as CONDUCTOSPHERES embedded in an epoxy matrix. At a certain volume fraction, referred as the percolation threshold, conductivity paths/networks are formed which suddenly cause the effective conductivity of the mixture to increase. As said, this effect is mainly prominent when the thermal conductivity of the filler widely differs from that of the matrix. This is relatively close between epoxy (0.363W/mK) and the borosilicate wall of Q-Cel (1.14W/mK) (see properties in Table 5.1) but largely deviates from that of pure silver (407W/mK) [153].

Due to the potential incompatibility of the Maxwell Garnett model, comments on the predicted increase in effective thermal conductivity of EX-CORE when incorporating highly conductive fillers could therefore not be made. Nor could comments be given on the potential cure/in-mold cycle times reductions. A literature study is first of all recommended to investigate which theoretical thermal conductivity models are most suitable for the chosen type of conductive fillers. Several thermal models for particle filled composites are discussed in the following suggested papers: [118, 132–136, 140, 154–156].

Lower boundary of epoxy volume fraction to ensure thermal stability

As discussed in Section 8.5, the author does not recommend further testing with the 80kg/m³ "80-mix" EX-CORE formulation since it contains an insufficient amount of epoxy matrix (<5vol%). Due to the lack of a rigid thermally stable epoxy network, "cured" 80mix EX-CORE samples re-expanded and torn open when re-heated at 110°C without mold restriction. Instead, research is recommended to find the lower boundary of resin volume content (somewhere between 5- 14vol.%) that will result in thermally stable samples which have a rigid epoxy network that can withstand the re-expansion of Expancel[®] DU microspheres at elevated operational temperatures. This could be done by manufacturing several EX-CORE samples that vary in epoxy volume fraction and explore if the cured samples re-expand when re-heated. The resulting volume fraction will also provide more insight into the lower boundary of foam density that can still be safely applied.

Designed experiment and mathematical model to identify optimal mix formulations for range of foam densities

The 270-optimal mix composition was selected in the current research (see Section 6.1.1) as basis for the manufactured samples. In the research of Vial [63], the 270-optimal mix had been formulated with a mathematical model, which i.a. predicted the highest compressive strength properties for a 270kg/m³ foam with this specific formulation. It is however important to note that this mathematical model is based on compressive strength results from EX-CORE samples that were manufactured with the former epoxy resin and DU grade. It is therefore not guaranteed that this mix composition is also "optimal" for EX-CORE samples produced with the new SR 1280/Ancamine[®] 2442 epoxy matrix and Expancel[®] 043 DU 80 grade. Additionally, the samples produced in this research were also cured under different conditions. The author therefore recommends further research to investigate the optimal mix compositions for a range of EX-CORE foam densities created with the new epoxy matrix and DU grade. To limit the amount of samples that have to be produced and tested, a designed experiment and mathematical model can be set up similar than the one previously developed in the Master's Thesis of Vial [63] (see also Section 3.2.5).

Remind also that in the current research all EX-CORE samples were tested on the compression jack available at Donkervoort which is not conform ASTM standards. It was known from previous research performed at Donkervoort [64] that this jack is adequate in determining the compressive strength values within 10%.

However, when setting up the mathematical model, it is recommended to determine compressive strength properties according to ASTM standard D1621 [146] for example on the Zwick 250kN test bench available at the Delft University of Technology.

12.2. Prepreg

Although that promising EX-CORE sandwich panel samples with good overall surface quality were manufactured with the snap-cure E732 prepreg, additional research is recommended to explore which type of prepreg might be best compatible with the new EX-CORE formulation and fast curing process. This way the amount of surface porosity could be reduced. With respect to this, the research performed by Berckmoes [57] on surface defects (see Section 3.2.6) forms a good starting point and gave already some interesting insight w.r.t. suitable prepreps. His recommendations might also be valid for the fast curing EX-CORE process; For example in combination with the pressure generated with EX-CORE, fully impregnated (no semi-impregnated VBO) prepreps are recommended. With respect to the top (visual) carbon fiber fabric layer, a 3K 2x2 twill weave with a density around 200-250g/m² is recommended [57]. For larger series production and so when ordered in larger batches, custom made prepreps can be produced with almost any type of carbon fiber fabric and compatible epoxy binder. It might even be possible to customize prepreps with the same epoxy binder used as matrix in EX-CORE.

12.3. Further improvement and validation of numerical model

In the end, the updated numerical thermal model could only be validated for 30mm thick 270-opt mix samples that were isothermally cured at 110°C, because thicker samples fell outside the expectable discrepancy bounds. Due to time constraints, other mix formulations and/or cure cycles could not be tested. Comments on the validity for different EX-CORE mix formulations and/or different cure cycles cannot be made since no experimental data had been generated. Nevertheless, the same mold and sensor tooling can be used to generate additional validation data. It is also important to note that the EX-CORE degree of cure predictions could not be experimentally validated due to the lack of suitable equipment. Additional recommendations to further validate and improve the numerical model are presented in the following paragraphs.

Onset reaction temperature

As discussed in Chapter 9, one probable cause for the observed discrepancies between the simulated and experimental temperature data for EX-CORE samples thicker than 30mm is related to the assumption of constant onset reaction temperature, implemented in the numerical model. As said, the Ancamine[®] 2442 curing agent has a physical thermal block which prevents it from reacting with the epoxy resin until a certain "onset reaction" temperature (T_{onset}) has been reached. It was confirmed with dynamic DSC scans that the onset reaction temperature of the Ancamine[®] 2442 is however not constant but varies with heat-up rate. Four dynamic DSC scans were performed at 0.5, 2, 10 and 15°C/min, for which onset reaction temperatures of 58, 70, 84 and 94°C respectively were recorded. Based on these results, the T_{onset} value in the numerical model was updated to 83°C which corresponded to the average heat-up rate recorded in 30mm thick EX-CORE samples cured at 110°C. This reduced the observed discrepancies.

It is important to realize that the heat-up rate in EX-CORE not only varies in time but also with cross-sectional location. Especially for thicker samples, the heat-up rates and such onset reaction temperatures in the core can vary more widely. In addition, in Section 9.3.3 it was clearly visualized that tuning the (constant) T_{onset} in the numerical has a major effect on the simulation results. It is therefore strongly recommended to perform additional DSC scans at different heat-up rates to obtain more data points and such obtain an improved relation between heat-up rate and T_{onset} .

Due to its strong effect on the simulated results, it would even be better to find a way to implement a variable T_{onset} in the numerical model. However, due to its unknown physical nature and interdependence with heat-up rate that is simultaneously predicted with the numerical model this is not straightforward. It could be investigated (i.a. from literature) whether or not it is possible to model this phenomenon using a different cure kinetic model that for example is based on dynamic DSC experimental data.

Thermal conductivity of EX-CORE

As explained in Section 5.4.4, experimental validation of the theoretical conductivity model could not be performed due to the un-availability of required test setups. However, a sensitivity study was performed in Section 5.9 which showed that, within the expected foam densities ranging from 230 to 330 kg/m³ (containing the new SR 1280/Ancamine[®] 2442 and Expancel[®] 043 DU 80), the effective thermal conductivity (k_{eff}) varies only from 0.098 to 0.145 W/mK. This leads to a maximum deviation in T_{center} and T_{top} of only 0.3°C and 2.6°C, respectively. Consequentially, to limit the temperature deviations within the required 5°C accuracy, the effective thermal conductivity should be determined within 0.092 W/mK.

Although less critical for the low conductive microspheres and epoxy used in EX-CORE, experimental validation of the thermal conductivity model is strongly recommended if high conductive fillers are implemented in EX-CORE in the future research. This is because they will have a large effect on the temperature distribution/progress, especially when the percolation threshold is reached. A suitable method is the Guarded Heat Flow meter technique which is described in ASTM standard E1225 [138] and which was also used by Zhu et al. [134]. Another possibility is to use the Laser-Flash method as covered in ASTM standard E1461 [139]. Either of both methods are recommended but the required test equipment should be available.

Specific heat capacity of EX-CORE

Similarly as for the thermal conductivity, a sensitivity study was performed for the effective specific heat capacity $C_{p_{eff}}$ of EX-CORE (see Section 5.9). For the EX-CORE foam density range of 230 to 330 kg/m³, $C_{p_{eff}}$ varied from 1753.5 to 1747.3 J/kgK which caused T_{center} and T_{top} to vary only 0.2°C and 0.1°C, respectively. Hence to obtain a temperature accuracy of 5°C, the effective specific heat capacity of EX-CORE should be known within 152 J/kgK. Similarly as concluded by Eversdijk [64], highly accurate experimental validation of $C_{p_{eff}}$ should therefore be given less priority, especially when compared to k_{eff} .

Nonetheless, if it is chosen to do so, it is advised to experimentally determine the specific heat capacity of the separate components first, since the theoretical model of the effective specific heat capacity of EX-CORE relies on the simple (adjusted) rule of mixtures using the specific heat capacities of the separate components. The test standard E1269 [141] is recommended. However, as became clear from earlier tests performed by Eversdijk [64] (see also Section 5.5.4), care should be taken to assure that the thermal resistance between the calibration standard and EX-CORE constituents is comparable. He also recommended to let the tests perform by an experienced lab technician and to use hermetically sealed sample crucibles to allow better surface contact between the crucible and powder.

Thermal interface resistance between EX-CORE and mold surface

In the numerical model the thermal interface resistance R_{int} between EX-CORE and the aluminum mold surface was set to 0.03 m²K/W. This value was selected in the study of Eversdijk [64] based on the best fit obtained through varying R_{int} between upper- (0.37 m²K/W) and lower- ($1.6 \cdot 10^{-5}$ m²K/W) boundaries found in literature (see Section 5.2.2). As became clear from his study, tuning the thermal interface resistance had a large impact on the temperature distribution, especially for core thicknesses less than 30 mm. R_{int} was however not experimentally validated. It would be useful to do this in future research. Multiple test methods are explained in ASTM standard D5470 [157]. The reader is also recommended to read the following paper, which compares different test methods: [158]. Note that when different mold surface materials are used in the future, the corresponding R_{int} should be determined and updated in the numerical model.

Implementation of CFRP prepreg

As discussed in Section 10.2.3, detailed modeling and incorporation of CFRP prepreg facings in the numerical model should not be given the highest priority in consecutive research. This is because the influence of the prepreg facings on the core temperature is limited and mainly concentrates near the prepreg facings. This implies that the temperature distribution predicted by the EX-CORE numerical model should give a good indication of the temperature distributions of EX-CORE prepreg sandwich panels (within validated bounds). If deemed necessary, it is however possible to implement CFRP prepreg facings into the numerical model by adding a range of nodes between the EX-CORE boundary and the aluminum mold surface. Thermal properties such as thermal conductivity and specific heat are widely available in literature for carbon/glass- epoxy composites. It is hereby important to include the thermal interface resistance between the mold/facesheet which should be attained from literature or experimentally determined. To account for the small thickness of the facesheets, the mesh can locally be refined.

Cure monitoring using dielectrometry

The possibility of using dielectrometry for monitoring the cure process of EX-CORE products was already discussed in Section 9.1. This would not only be useful to validate the cure predictions of the numerical model but could also be used for live-monitoring the cure produces of EX-CORE products by implementing dielectric sensors in the surface of the mold. This allows to ensure sufficient curing with the minimal amount of cure time. With the eye on large series applications it is therefore highly recommended to further research and develop this technology for EX-CORE cure monitoring.

12.4. EX-CORE commercialization and further development towards large scale applications

Although that the EX-CORE foam material had been redesigned to facilitate cure cycle time reductions it was already discussed in Section 10.5 that there are still many remaining questions and challenges to be tackled in order to make the EX-CORE technology suitable for larger series automotive manufacturing. Resulting recommendations and suggestions were already proposed in more detail in Section 10.5. In summary, more research and development is required on the following topics:

- Mold tooling and type of heating/cooling system
- Type of cure cycle/ preheated mold temperature
- Production automation, i.a.:
 - Further development/automation of EX-CORE mixing, dosing and process-ability
 - Automation of EX-CORE (& prepreg) application/injection in enclosed mold and/or ontop of prepregged mold surface
- Process monitoring, such as dielectromerty to monitor and verify degree of cure during production

Additional recommendations are discussed in the next paragraphs:

Lower boundary of degree of cure < 98%

Throughout the entire research the predicted 98% degree of cure in the numerical model was taken as baseline to define when EX-CORE samples would be sufficiently cured. It is however possible that lower degree of cure values could be used without compromising on resulting product quality or mechanical properties. Hence shorter cure cycle times can be achieved. However, to get insight into the lower boundary of degree of cure that is applicable, extensive experimental testing would be required for various samples that are cured until various degree of cures. In the first place the time to obtain a certain % degree of cure could be predicted with the numerical model, or live cure monitoring using dielectrometry could be used. The resulting samples in turn have to be inspected and tested on compression etc.

Nitrogen application in opened resin and hardener drums

To prevent degradation/aging of the epoxy resin and curing agents due to moisture absorption, it is recommended to saturate opened drums of epoxy resins and hardeners with nitrogen. This will prevent moisture (from the air entrapped in the drum) interaction at the surface of the resin/hardener. Since nitrogen is heavier than air, nitrogen will cover the surface of the resin. According to Evonik, this is common practice. Hence it is strongly recommended to do so for every opened resin and hardener drum at Donkervoort. The procedure is relatively simple; only a hose is required that is connected to the nitrogen bottle. Every time some material is taken out of the drum, the hose should be hold into the drum (not into the product) such that the atmosphere in the drum becomes saturated with nitrogen.

Remember that in the current research additional DSC tests were performed on the former Ancarez® RZ4010/Ancamide™ 3399 epoxy system, which had already been tested in previous research by Eversdijk [64]. His DSC tests were performed approximately one year earlier, using the same DSC apparatus, with resin and curing agent out of the same drums. It became clear that the epoxy had already significantly degraded because the measured total specific heat of reaction decreased from 312J/g to 189J/g. This is most probably caused due to moisture interaction (see Section 4.4.1), indicating the importance of proper storage over time.

Bibliography

- [1] L. A. Khan and A. H. Mehmood, *Lightweight Composite Structures in Transport*, book section 5 - Cost-effective composites manufacturing processes for automotive applications, pp. 93–119. Woodhead Publishing, 2016.
- [2] P. K. Mallick, *Fiber-reinforced composites: materials, manufacturing, and design*. Boca Raton: CRC press, 2007.
- [3] S. Mazumdar, “Opportunity and challenges in automotive composite industry.” Lucintel, December 2013. <http://www.lucintel.com/lucintelbrief/lucintel-brief-opportunity-and-challenges-in-automotive-composites-industry.pdf>, accessed 20/2/2018.
- [4] R. Brooks, S. M. Shanmuga Ramanan, and S. Arun, *Reference Module in Materials Science and Materials Engineering*, book section Composites in Automotive Applications: Design. Elsevier, 2017.
- [5] A. Wilson, “Vehicle weight is the key driver for automotive composites,” *Reinforced Plastics*, vol. 61, no. 2, pp. 100–102, 2017.
- [6] “Forecast of Global Demand of CFRP for Automobile Manufacturing: Key Research Findings 2016 .” Yano Research institute, November 2016. <https://www.yanoresearch.com/press/pdf/1610.pdf>, accessed 20/20/2018.
- [7] S. Das, J. A. Warren, D. West, and S. M. Schexnayder, “Global carbon fiber composites. supply chain competitiveness analysis,” report, Oak Ridge National Laboratory (ORNL), Oak Ridge, TN (United States), 2016.
- [8] T. Ishikawa, K. Amaoka, Y. Masubuchi, T. Yamamoto, A. Yamanaka, M. Arai, and J. Takahashi, “Overview of automotive structural composites technology developments in japan,” *Composites Science and Technology*, vol. 155, no. Supplement C, pp. 221–246, 2018.
- [9] M. Holmes, “High volume composites for the automotive challenge,” *Reinforced Plastics*, vol. 61, no. 5, pp. 294–298, 2017.
- [10] K. J. M. Mattheus, “Exploring EX-CORE, a novel core material for one-shot manufacturing of sandwich structures..” Literature Study, Delft University of Technology, 2018.
- [11] A. Petras, *Design of sandwich structures*. Phd thesis, University of Cambridge, 1999.
- [12] “HexWeb Honeycomb sandwich design technology.” HEXCEL composites, December 2000. https://www.hexcel.com/user_area/content_media/raw/Honeycomb_Sandwich_Design_Technology.pdf, accessed 20/9/2018.
- [13] S. Mazumdar, *Composites manufacturing: materials, product, and process engineering*. Boca Raton: CRC press, 2002.
- [14] Committee, A. S. M. International. Handbook, *ASM handbook : Composites Vol. 21*. Ohio: ASM International, 2001.
- [15] L. Merad, P. Bourson, Y. Guedra, F. Jochem, and B. Benyoucef, “Kinetic study of the RTM6/TiO₂ by DSC/TGA for improved hardness of resin,” *Journal of the Association of Arab Universities for Basic and Applied Sciences*, vol. 11, no. 1, pp. 37–44, 2012.
- [16] I. M. Daniel and O. Ishai, *Engineering mechanics of composite materials*. New York: Oxford University Press, 2nd ed., 2006.
- [17] W.D.Callister and D.G.Retwisch, *Material Science and Engineering SI version*. Wiley, eight ed., 2011.

- [18] P. Hubert, T. Centea, L. Grunefelder, S. Nutt, J. Kratz, and A. Levy, *Comprehensive Composite Materials II*, book section 2.4 Out-of-Autoclave Prepreg Processing, pp. 63–94. Oxford: Elsevier, 2018.
- [19] M. F. Ashby and R. M. Medalist, “The mechanical properties of cellular solids,” *Metallurgical Transactions A*, vol. 14, no. 9, pp. 1755–1769, 1983.
- [20] A. F. Volker Altstädt, *Multifunctionality of Polymer Composites*, book section Chapter 8 - Mechanical properties of multifunctional foam core materials, pp. 262–301. Oxford: William Andrew Publishing, 2015.
- [21] “Airex T10 the industrialised structural PET foam core datasheet.” AirexBaltekBanova, 2017. <http://www.airexbaltekbanova.com/en/airex-t10-pet-foam.html>, accessed 26/1/2018.
- [22] “Divinycell P technical data sheet.” Divinycell, February 2017. <http://www.diabgroup.com/en-GB/Products-and-services/Core-Material/Divinycell-P>, accessed 26/1/2018.
- [23] “Armaform pet-gr and pet-ft foams datasheets.” ArmaCell, 2017. <http://www.airexbaltekbanova.com/en/airex-t10-pet-foam.html>, accessed 26/1/2018.
- [24] “Divinycell H technical data sheet.” Divinycell, 2017. <http://www.diabgroup.com/en-GB/Products-and-services/Core-Material/Divinycell-H>, accessed 26/1/2018.
- [25] “Airex C70 universal structural foam datasheet.” AirexBaltekBanova, 2017. <http://www.airexbaltekbanova.com/airex-c70-pvc-foam.html>, accessed 26/1/2018.
- [26] “GURIT PVC HT structural foam core General data sheet.” GURIT, 2017. <http://www.gurit.com/Our-Business/Composite-Materials/Structural-Core-Materials/Gurit-PVC-HT>, accessed 26/1/2018.
- [27] “Genuine lightweight construction.” Evonik, 2018. <https://www.rohacell.com/product/rohacell/en/>, accessed 26/1/2018.
- [28] “ROHACELL Triple F technical information datasheet.” Evonik, March 2015. <http://www.rohacell.com/sites/lists/RE/DocumentsHP/PI-ROHACELL-Triple-F-EN.pdf>, accessed 26/1/2018.
- [29] S. Black, “Getting to the core of composite laminates.” CompositesWorld Online Article, 2003. <https://www.compositesworld.com/articles/getting-to-the-core-of-composite-laminates>, accessed 25/1/2018.
- [30] “Structural Core Materials.” Gurit, 2018. <http://www.gurit.com/Our-Business/Composite-Materials/Structural-Core-Materials>, accessed 26/1/2018.
- [31] B. John and C. P. Reghunadhan Nair, *Handbook of Thermoset Plastics (Third Edition)*, book section 13 - Syntactic Foams, pp. 511–554. Boston: William Andrew Publishing, 2014.
- [32] “Researchers show how syntactic foams can be produced for cars and consumer goods.” NYU Tandon School of Engineering, Polytechnic institute, September 2017. <http://archive.engineering.nyu.edu/news/2017/09/08/researchers-show-how-syntactic-foams-can-be-produced-cars-consumer-goods>, accessed 20/9/2018.
- [33] S. Sankaran, B. N. Ravishankar, K. Ravi Sekhar, S. Dasgupta, and M. N. Jagdish Kumar, *Composite Materials: Processing, Applications, Characterizations*, book section Syntactic Foams for Multifunctional Applications, pp. 281–314. Springer, 2017.
- [34] N. Gupta and E. Woldesenbet, “Characterization of flexural properties of syntactic foam core sandwich composites and effect of density variation,” *Journal of Composite Materials*, vol. 39, no. 24, pp. 2197–2212, 2005.
- [35] D. Pinisetty, V. C. Shunmugasamy, and N. Gupta, *Hollow Glass Microspheres for Plastics, Elastomers, and Adhesives Compounds*, book section 6 - Hollow Glass Microspheres in Thermosets—Epoxy Syntactic Foams, pp. 147–174. Oxford: William Andrew Publishing, 2015.

- [36] G. Kister and E. Dossi, "Cure monitoring of CFRP composites by dynamic mechanical analyser," *Polymer Testing*, vol. 47, pp. 71–78, 2015.
- [37] F. C. Campbell, *Manufacturing Processes for Advanced Composites*. Elsevier, 2004.
- [38] D. Kim, T. Centea, and S. R. Nutt, "In-situ cure monitoring of an out-of-autoclave prepreg: Effects of out-time on viscosity, gelation and vitrification," *Composites Science and Technology*, vol. 102, pp. 132–138, 2014.
- [39] T. A. Bogetti and J. W. Gillespie, "Process-induced stress and deformation in thick-section thermoset composite laminates," *Journal of Composite Materials*, vol. 26, no. 5, pp. 626–660, 1992.
- [40] T. A. Bogetti and J. W. Gillespie, "Two-dimensional cure simulation of thick thermosetting composites," *Journal of Composite Materials*, vol. 25, no. 3, pp. 239–273, 1991.
- [41] L. J. Lee and C. W. Macosko, "Heat transfer in polymer reaction molding," *International Journal of Heat and Mass Transfer*, vol. 23, no. 11, pp. 1479–1492, 1980.
- [42] A. Cheung, Y. Yu, and K. Pochiraju, "Three-dimensional finite element simulation of curing of polymer composites," *Finite Elements in Analysis and Design*, vol. 40, no. 8, pp. 895–912, 2004.
- [43] Z.-S. Guo, S. Du, and B. Zhang, "Temperature field of thick thermoset composite laminates during cure process," *Composites Science and Technology*, vol. 65, no. 3, pp. 517–523, 2005.
- [44] J. H. Oh, "Prediction of temperature distribution during curing thick thermoset composite laminates," *Materials Science Forum*, vol. 544/545, pp. 427–430, 2007.
- [45] L. Shi, "Heat transfer in the thick thermoset composites." PhD Thesis, Delft University of Technology, 2016.
- [46] L. Ma, S. R. Athreya, R. Mehta, D. Barpanda, and A. Shafi, "Numerical modeling and experimental validation of nonisothermal resin infusion and cure processes in large composites," *Journal of Reinforced Plastics and Composites*, vol. 36, no. 10, pp. 780–794, 2017.
- [47] J. M. Kenny, "Determination of autocatalytic kinetic model parameters describing thermoset cure," *Journal of Applied Polymer Science*, vol. 51, no. 4, pp. 761–764, 1994.
- [48] B. Bilyeu, W. Brostow, and K. P. Menard, "Epoxy thermosets and their applications. iii. kinetic equations and models," *Journal of materials education*, vol. 23, no. 4-6, pp. 189–204, 2001.
- [49] M. Ghaemy, M. Barghamadi, and H. Behmadi, "Cure kinetics of epoxy resin and aromatic diamines," *Journal of Applied Polymer Science*, vol. 94, no. 3, pp. 1049–1056, 2004.
- [50] J. Clark, "Rate constants and the Arrhenius equation," 2002. <https://www.chenguide.co.uk/physical/basicrates/arrhenius.html>, accessed 27/7/2018.
- [51] "A Review of DSC Kinetics Methods." TA Instruments, 2017. <http://www.tainstruments.com/pdf/literature/TA073.pdf>, accessed 21/5/2018.
- [52] M. E. Ryan and A. Dutta, "Kinetics of epoxy cure: a rapid technique for kinetic parameter estimation," *Polymer*, vol. 20, no. 2, pp. 203–206, 1979.
- [53] P. I. Karkanis and I. K. Partridge, "Cure modeling and monitoring of epoxy/amine resin systems. i. cure kinetics modeling," *Journal of Applied Polymer Science*, vol. 77, no. 7, pp. 1419–1431, 2000.
- [54] "Expancel microspheres, the world's favorite secret ingredient." AkzoNobel, 2016. <https://expancel.nouryon.com/siteassets/brochure-expancel-overview-english.pdf>, accessed 1/2/2018.
- [55] M. Jonsson, O. Nordin, and E. Malmström, "Increased onset temperature of expansion in thermally expandable microspheres through combination of crosslinking agents," *Journal of Applied Polymer Science*, vol. 121, no. 1, pp. 369–375, 2011.

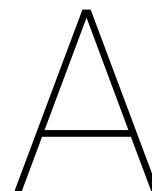
- [56] "Product specification for Expancel DU Microspheres." AkzoNobel, February 2018. https://expancel.akzonobel.com/siteassets/expancel_prod-spec-du_201802_en_m.pdf, accessed 17/2/2018.
- [57] D.O.Berckmoes, "The effect of x-core foam processing on the surface defects in carbon fiber-epoxy sandwich composites,," Master's thesis, Delft University of Technology, 2017.
- [58] J. Houwers, "Expanderende sandwichkernen." Internship report, Academie Life Science, engineering & design, Saxion Enschede, 2013.
- [59] L. Vaikhanski and S. R. Nutt, "Synthesis of composite foam from thermoplastic microspheres and 3d long fibers," *Composites Part A: Applied Science and Manufacturing*, vol. 34, no. 8, pp. 755–763, 2003.
- [60] F. Minde, "One shot manufacturing of complex sandwich structures," Master's thesis, Delft University of Technology, 2014.
- [61] Q. Boegem, "Van laboratorium opstelling naar serieproductie bij Donkervoort Automobielen B.V.," Graduation report, Haagse Hogeschool, 2016.
- [62] D. O. Berkmoes, "Integrally heated tooling for composite manufacturing at donkervoort automobielen b.v.," Internship report, Delft University of Technology, 2016.
- [63] S. Vial, "Development of a novel core material for one-shot manufacturing," Master's thesis, Delft University of Technology, 2016.
- [64] M. P. J. Eversdijk, "Relating process parameters to X-core properties through experimental testing and modeling," Master's thesis, Delft University of Technology, 2017.
- [65] "Flexiforce sensors users manual." Tekscan, 2010. <https://www.tekscan.com/resources/product-guide/flexiforce-user-manual>, accessed 21/5/2018.
- [66] K. J. M. Matheus, "One shot core material for OEM applications at Donkervoort Automobielen B.V.," Internship report, Delft University of Technology, 2017.
- [67] B. ten Hoeve, "EX-CORE Productiemachine." Graduation report, Haagse Hogeschool, 2018.
- [68] "Product specification for Expancel DE Microspheres ." AkzoNobel, May 2017. https://expancel.akzonobel.com/siteassets/expancel_prod_spec_de_201709_en_m.pdf, accessed 17/2/2018.
- [69] "Potters Industries Q-Cel[®] 5028 ." Potters, 2017. <http://www.matweb.com/search/datasheet.aspx?matguid=f4b39f9c7c344de2a2303dd7f079bd35&ckck=1>, accessed 17/2/2018.
- [70] "Q-Cel[®] 5028 Hollow Microspheres Typical Properties ." Potters, 2014.
- [71] D. Roquette, F. Meyer, and L. Herbeck, "High volume manufacturing of carbon fiber reinforced plastics for body in white." Audi, Voith, Materialien des Karosseriebaus, Bad Nauheim, May 2017. http://voith.com/composites-en/20170516_Bad-Nauheim_Audi_Voith_Online.pdf, accessed 20/2/2018.
- [72] J. Starke, "Carbon composites in automotive structural applications." EuCIA: composites and sustainability, Brussels, March 2016. <http://www.eucia.eu/userfiles/files/Starke-Eucia%202016-V4-Druck%20b.pdf>, accessed 5/2/2018.
- [73] M. A. Siddiqui, H. Koelman, and P. S. Shembekar, "High Pressure RTM Process Modeling for Automotive Composite Product Development," sae technical paper, Symposium on International Automotive Technology, January 2017.
- [74] C. Fais, "Lightweight automotive design with HP-RTM," *Reinforced Plastics*, vol. 55, no. 5, pp. 29–31, 2011.
- [75] G. Gardiner, "HP-RTM on the rise." CompositesWorld Online Article, 2015. <https://www.compositesworld.com/articles/hp-rtm-on-the-rise>, accessed 31/3/2018.

- [76] A. Wettach, "The wet molding method, an economical alternative for the mass production of carbon fiber-reinforced plastics," *Plastics engineering*, April 2015.
- [77] G. Gardiner, "Wet compression molding." CompositesWorld Online Article, February 2016. <https://www.compositesworld.com/blog/post/wet-compression-molding>, accessed 31/3/2018.
- [78] J. A. Schroeder, T. Ahmed, B. Chaudhry, and S. Shepard, "Non-destructive testing of structural composites and adhesively bonded composite joints: pulsed thermography," *Composites Part A: Applied Science and Manufacturing*, vol. 33, no. 11, pp. 1511–1517, 2002.
- [79] A. Lutz, "Structural bonding in automotive body shop," *Adhesion Adhesives & sealants*, vol. 14, no. 1, pp. 14–21, 2017.
- [80] "SME Instruments Phase 1 final report." Donkervoort Automobielen B.V., March 2017.
- [81] "Syncore design guide, an aerospace technology." Henkel, March 2011. http://www.loctite.co.th/tht/content_data/LT3729_TT_Aerospace_Syncore_Design_Guide.pdf, accessed 24/2/2018.
- [82] "Horizon 2020-grant agreement-number 823331-XCORE." European Commission EASME & Donkervoort Automobielen, August 2018.
- [83] "Q-Cel[®] Hollow Microspheres Safety Data Sheet ." Potters, 2010.
- [84] "Borosilicate Glass Properties." Schott Algea Brochure. <https://www.schott.com/d/tubing/9a0f5126-6e35-43bd-bf2a-349912caf9f2/1.0/schott-algae-brochure-borosilicate.pdf>, accessed 8/8/2018.
- [85] "Ancarez[™] RZ4010 Epoxy Resin." Technical Data Sheet, AIR PRODUCTS, August 2010.
- [86] K. P. Menard, *Dynamic mechanical analysis: a practical introduction*. CRC Press, 2008.
- [87] A. Franck, "Understanding rheology of thermosets." TA Instruments, 2004. http://www.tainstruments.com/pdf/literature/AAN015_V1c_U_Thermoset.pdf, accessed 27/2/2018.
- [88] "Voraforce epoxy systems product data sheet." DOW, 2018. <https://www.dow.com/en-us/products/voraforceepoxyresinsystems>, accessed 5/3/2018.
- [89] J. Sloan, "JEC world 2017: show report, part 1." CompositesWorld Online Article, March 2017. <https://www.compositesworld.com/blog/post/jec-world-2017-show-report-part-1>, accessed 5/3/2018.
- [90] S. Black, "Automotive composites: Thermosets for the fast zone." CompositesWorld Online Article, 2015. <https://www.compositesworld.com/articles/automotive-composites-thermosets-for-the-fast-zone>, accessed 6/3/2018.
- [91] "Epoxy systems for automotive structural components." Hexion, 2018. <http://www.hexion.com/en-us/applications/composites/automotive/structural>, accessed 6/3/2018.
- [92] "Huntsman develops new compression molding process," *Reinforced Plastics*, vol. 60, no. 3, p. 132, 2016.
- [93] "Dynamic fluid compression molding, a new process for composite mass-production." Huntsman, March 2016. [http://www.huntsman.com/advanced_materials/a/Your%20Industry/Auto/Dynamic%20Fluid%20Compression%20Molding%20\(DFCM\)](http://www.huntsman.com/advanced_materials/a/Your%20Industry/Auto/Dynamic%20Fluid%20Compression%20Molding%20(DFCM)), accessed 5/2/2018.
- [94] "EPODIL 750 Reactive Diluent." Technical Data Sheet, Evonik Industries, January 2016.
- [95] "Sicomin SR1280 ." Safety Data Sheet, Sicomin, January 2016.
- [96] "Sicomin SR1280/SZ8525 Epoxy resin systems." Technical Data Sheet, Sicomin, September 2014.
- [97] "ANCAMINE[®] 2337S Curing Agent. Epoxy agents and modifiers." Technical Data Sheet European Version, Evonik Corporation, June 2017.

- [98] “ANCAMINE[®] 2337S Curing Agent.” Safety Data Sheet, Evonik Industries, January 2017.
- [99] “ANCAMINE[®] 2442 Curing Agent. Epoxy agents and modifiers .” Technical Data Sheet European Version, Evonik Corporation, March 2018.
- [100] “ANCAMINE[®] 2442 Curing Agent.” Safety Data Sheet, Evonik Industries, January 2017.
- [101] R. J. Young and P. A. Lovell, *Introduction to polymers*. Boca Raton: CRC Press, 3rd ed., 2011.
- [102] ASTM E2070-13, *Standard test method for kinetic parameters by differential scanning calorimetry using isothermal methods*. Standard, ASTM International, West Conshohocken, USA, 2013.
- [103] J.-D. Nam and J. C. Seferis, “Application of the kinetic composite methodology to autocatalytic-type thermoset prepreg cures,” *Journal of Applied Polymer Science*, vol. 50, no. 9, pp. 1555–1564, 1993.
- [104] D. J. O’Brien and S. R. White, “Cure kinetics, gelation, and glass transition of a bisphenol f epoxide,” *Polymer Engineering & Science*, vol. 43, no. 4, pp. 863–874, 2003.
- [105] J. McHugh, P. Fideu, A. Herrmann, and W. Stark, “Determination and review of specific heat capacity measurements during isothermal cure of an epoxy using TM-DSC and standard DSC techniques,” *Polymer Testing*, vol. 29, no. 6, pp. 759–765, 2010.
- [106] Y. A. Cengel, *Heat transfer : a practical approach*. McGraw-Hill series in mechanical engineering, Boston: McGraw-Hill, 3rd ed. ed., 2007.
- [107] M. N. Özisik, *Heat conduction*. John Wiley & Sons, 1993.
- [108] T. Blomberg, “Heat conduction in two and three dimensions. Computer modelling of building physics applications.” Report TVBH-1008, Lund University Department of Building Physics, May 1996.
- [109] T. L. Bergman, F. P. Incropera, D. P. DeWitt, and A. S. Lavine, *Fundamentals of heat and mass transfer*. John Wiley & Sons, 7th ed., 2011.
- [110] “6060-t6 aluminum properties.” MakeItFrom, August 2018. <https://www.makeitfrom.com/material-properties/6060-T6-Aluminum>, accessed 6/9/2018.
- [111] E. Chapelle, B. Garnier, and B. Bourouga, “Interfacial thermal resistance measurement between metallic wire and polymer in polymer matrix composites,” *International Journal of Thermal Sciences*, vol. 48, no. 12, pp. 2221–2227, 2009.
- [112] M. A. Stubblefield, S.-S. Pang, and V. A. Cundy, “Heat loss in insulated pipe the influence of thermal contact resistance: A case study,” *Composites Part B: Engineering*, vol. 27, no. 1, pp. 85–93, 1996.
- [113] “Safety Data Sheet Expancel 920 DE 80 d30.” AkzoNobel. Rev. date 05/12/17.
- [114] “Safety Data Sheet Expancel 920 DE 80 d30.” AkzoNobel. Rev. date 23/08/10.
- [115] “Safety Data Sheet Expancel 031 DU 40.” AkzoNobel. Rev. date 06/12/17.
- [116] “Safety Data Sheet Expancel 043 DU 80.” AkzoNobel. Rev. date 06/12/17.
- [117] D. Mishra, *A study on thermal and dielectric characteristics of solid glass microsphere filled epoxy composites*. Phd thesis, National Institute of Technology, Rourkela,, 2014.
- [118] F. Lin, G. S. Bhatia, and J. D. Ford, “Thermal conductivities of powder-filled epoxy resins,” *Journal of Applied Polymer Science*, vol. 49, no. 11, pp. 1901–1908, 1993.
- [119] Y. Yang, *Physical properties of polymers handbook*, book section Thermal conductivity, pp. 155–163. Springer, 2007.
- [120] G. Van Assche, A. Van Hemelrijck, H. Rahier, and B. Van Mele, “Modulated differential scanning calorimetry: isothermal cure and vitrification of thermosetting systems,” *Thermochimica Acta*, vol. 268, pp. 121–142, 1995.

- [121] M. Reading and D. J. Hourston, *Modulated temperature differential scanning calorimetry : theoretical and practical applications in polymer characterisation*, book section The application of modulated temperature differential scanning calorimetry for the characterisation of curing systems., pp. 83–160. Springer, 2006.
- [122] “Glass properties: Borosilicate glass.” Cambridge Glassblowing. <http://www.camglassblowing.co.uk/glass-properties/>, accessed 8/8/2018.
- [123] T. L. Bergman, F. P. Incropera, D. P. DeWitt, and A. S. Lavine, *Fundamentals of heat and mass transfer*. John Wiley & Sons, 6th ed., 2007.
- [124] D. Annaratone, *Engineering heat transfer*. Springer Science & Business Media, 2010.
- [125] “Poly(acrylonitrile).” Polymerdatabase, 2015. <http://polymerdatabase.com/polymers/polyacrylonitrile.html>, accessed 8/8/2018.
- [126] “Properties of Polyacrylonitrill.” IGTPAN, 2016. <http://www.igtpan.com/Ingles/propriedade-poli.asp>, accessed 8/8/2018.
- [127] “Isopentane Physical Properties.” Air Liquide Group. <https://encyclopedia.airliquide.com/isopentane>, accessed 8/8/2018.
- [128] “Liquefied Natural Gas.” Material Data Sheet, Linde. <http://www.lngbunkering.org/sites/default/files/Linde%20LNG%20Material%20Safety%20Datasheet.pdf>, accessed 8/8/2018.
- [129] I. Martinez, “Properties of Gases,” 2018. <http://webserver.dmt.upm.es/~isidoro/dat1/eGAS.pdf>, accessed 8/8/2018.
- [130] “Isobutane Physical Properties.” Air Liquide Group. <https://encyclopedia.airliquide.com/isobutane>, accessed 8/8/2018.
- [131] “Ancamide™3399.” Technical Data Sheet, AIR PRODUCTS, March 2010.
- [132] Y. P. Mamunya, V. V. Davydenko, P. Pissis, and E. V. Lebedev, “Electrical and thermal conductivity of polymers filled with metal powders,” *European Polymer Journal*, vol. 38, no. 9, pp. 1887–1897, 2002.
- [133] V. S. Shabde, K. A. Hoo, and G. M. Gladysz, “Experimental determination of the thermal conductivity of three-phase syntactic foams,” *Journal of Materials Science*, vol. 41, no. 13, pp. 4061–4073, 2006.
- [134] P. Dongsheng, W. Jian, W. Jun, M. Jing, and Z. Bailin, “Thermal, dielectric and compressive properties of hollow glass microsphere filled epoxy-matrix composites,” *Journal of Reinforced Plastics and Composites*, vol. 31, no. 19, pp. 1311–1326, 2012.
- [135] A. G. Leach, “The thermal conductivity of foams. i. models for heat conduction,” *Journal of Physics D: Applied Physics*, vol. 26, no. 5, pp. 733–739, 1993.
- [136] K. Pietrak and T. S. Wisniewski, “A review of models for effective thermal conductivity of composite materials,” *Journal of Power Technologies*, vol. 95, no. 1, pp. 14–24, 2014.
- [137] Z. Hashin, “Assessment of the self consistent scheme approximation: conductivity of particulate composites,” *Journal of Composite Materials*, vol. 2, no. 3, pp. 284–300, 1968.
- [138] ASTM E1125-13, *Standard test method for thermal conductivity of solids using the guarded comparative-longitudinal heat flow technique*. Standard, ASTM International, West Conshohocken, USA, 2013.
- [139] ASTM 1461-13, *Standard test method for thermal diffusivity by the flash method*. Standard, ASTM International, West Conshohocken, USA, 2013.
- [140] K. H. Kate, R. K. Enneti, S.-J. Park, R. M. German, and S. V. Atre, “Predicting Powder-Polymer Mixture Properties for PIM Design,” *Critical Reviews in Solid State and Materials Sciences*, vol. 39, no. 3, pp. 197–214, 2014.
- [141] ASTM E1269-11, *Standard test method for determining specific heat capacity by differential scanning calorimetry*. Standard, ASTM International, West Conshohocken, USA, 2011.

- [142] "NTC thermistors for temperature measurements. Glass-encapsulated sensors, standard type." EPCOS, February 2009. <https://docs-emea.rs-online.com/webdocs/0e29/0900766b80e2933f.pdf>, accessed 14/5/2018.
- [143] "EPCOS NTC R/T Online Calculation tool." TDK, 2018. <https://en.tdk-electronics.tdk.com/web/designtools/ntc/dist/index.html>, accessed 1/6/2018.
- [144] "PTFE Series 4:1 High temperature heat shrink tubing." Pro-power, August 2016. http://www.farnell.com/datasheets/2119767.pdf?_ga=2.9527093.1095983868.1538648475-1263621097.1525532874&_gac=1.241459894.1538725442.EAIaIQobChMI98Cw9-bu3QIVKpPtCh2DDQ-7EAAAYASAAEgJMcvD_BwE, accessed 1/6/2018.
- [145] "DS18B20 Programmable Resolution 1-wire digital thermometer." Maxim integrated, 2015. <https://datasheets.maximintegrated.com/en/ds/DS18B20.pdf>, accessed 29/2/2018.
- [146] ASTM D1621-16, *Standard Method for Compressive Properties of Rigid Cellular Plastics. Standard*. ASTM international, West Conshohocken, USA, November 2016.
- [147] L. Vandenbossche, L. Dupré, and J. Melkebeek, "On-line cure monitoring of polyurethane foams by dielectrometric viscosity measurements," *International Journal of Applied Electromagnetics and Mechanics*, vol. 25, no. 1-4, pp. 589–593, 2007.
- [148] D. U. Shah, M. C. D. Bock, H. Mulligan, and M. H. Ramage, "Thermal conductivity of engineered bamboo composites," *Journal of Materials Science*, vol. 51, no. 6, pp. 2991–3002, 2016.
- [149] "KPT-238 Kapton tape." Pro-power, October 2011. <http://www.farnell.com/datasheets/1492217.pdf>, accessed 24/10/2018.
- [150] "TenCate E732 Snap cure prepreg Product Data Sheet." TenCate Advanced Composites, December 2016.
- [151] "Conductive Microspheres." Cospheric, 2018. https://www.cospheric.com/conductive_microspheres_beads_powders.html, accessed 8/11/2018.
- [152] "CONDUCTOSPHERES." Microsphere Technology, 2018. <http://microspheretechnology.com/microsphere/products/conductospheres/>, accessed 8/11/2018.
- [153] "Thermal conductivity of metals." The Engineering Toolbox, 2018. https://www.engineeringtoolbox.com/thermal-conductivity-metals-d_858.html, accessed 8/11/2018.
- [154] E.-S. Lee, S.-M. Lee, D. J. Shanefield, and W. R. Cannon, "Enhanced thermal conductivity of polymer matrix composite via high solids loading of aluminum nitride in epoxy resin," *Journal of the American Ceramic Society*, vol. 91, no. 4, pp. 1169–1174, 2008.
- [155] Y. K. Park, J.-G. Kim, and J.-K. Lee, "Prediction of thermal conductivity of composites with spherical microballoons," *Materials Transactions*, vol. 49, no. 12, pp. 2781–2785, 2008.
- [156] N. Gupta and D. Pinisetty, "A review of thermal conductivity of polymer matrix syntactic foams-effect of hollow particle wall thickness and volume fraction," *JOM*, vol. 65, no. 2, pp. 234–245, 2013.
- [157] ASTM D5470-17, *Standard test method for thermal transmission properties of thermally conductive electrical insulation materials*. Standard, ASTM International, West Conshohocken, USA, 2017.
- [158] R. N. Jarrett, C. K. Merritt, J. P. Ross, J. Hisert, and rd Annual, *Twenty-Third Annual IEEE Semiconductor Thermal Measurement and Management Symposium*, book section Comparison of Test Methods for High Performance Thermal Interface Materials, pp. 83–86. IEEE, 2007.
- [159] ASTM E537-12, *Standard test method for the thermal stability of chemicals by differential scanning calorimetry*. Standard, ASTM International, West Conshohocken, USA, 2012.
- [160] "FlexiForce HT201 High-temperature force & load sensor." Tekscan, 2011. http://ubsenthoff.de/wp/wp-content/uploads/2011/10/HT201_Data_Sheet.pdf, accessed 21/5/2018.



Procedure isothermal DSC

The cure kinetics of the epoxy systems were analyzed using a Differential Scanning Calorimetry (DSC) apparatus. A *Seiko Instruments Exstar 6000* heat flux DSC was used to measure the heat flows of the exothermic reaction under isothermal conditions in accordance to ASTM standard E2070-13 [102]. The DSC setup is shown in Figure A.1. For each isothermal DSC test the experimental methodology as listed in this appendix was performed. Note that this methodology is similar to the procedure suggested in the research of Eversdijk [64]. The main difference is that in contrary to Eversdijk, data collection was started immediately after sample insertion (see step 10). Eversdijk suggested to start data collection approximately 15-20s after sample insertion when the isothermal temperature was reached within $\pm 1K$. However, for the new fast curing epoxy resin systems, it became clear that the exothermic reaction already started before the isothermal temperature was reached within $\pm 1K$. In all new DSC tests, exothermic heat flows were already observed when the isothermal temperature was reached with a maximum of -3K difference.

1. Pre-heat the DSC test chamber to the required isothermal temperature.

In previous research by Eversdijk [64] several DSC scans were initially performed using a 20K/min heat-up rate. It became clear that the exothermic reaction peaks (for the former epoxy system Ancarez[®] RZ4010 & Ancamide[™] 3399) already occurred during the ramp-up phase of the DSC. For example, the ramp-up to 100°C took around 3.5 min, while the exothermic peaks occurred around 1-2min. This resulted in un-usable data. It was therefore decided to pre-heat the DSC chamber for all subsequent tests. This approach was also followed in the current research. Especially because the new epoxy resins react even faster than the former EX-CORE epoxy system.

2. Insert a small pinhole (approx. 50-100 μ m) in the lid of the crucible. This can be done with a needle.

This is done to ensure that at elevated temperatures the pressure in the crucible is in equilibrium with the ambient pressure inside the DSC chamber [159].

3. Weigh the aluminum crucible sample pan and lid to the nearest 0.1mg.

According to ASTM E2070 a scale with an accuracy of 1 μ g should be used [102]. However, the scales that were available for this research had a maximum accuracy of 0.1mg.

4. Weight approx. 15 \pm 0.01g of epoxy resin in a plastic measuring cup.

5. Add the required amount of hardener to the resin at the prescribed mix ratio. Weigh to the nearest 0.01g.

The mixing ratios used in this research are listed in Table 4.1.

6. Mix the resin and hardener with a wooden mixing stick for 3 minutes. Make sure that the mix is homogeneous and that non of the resin/hardener is left on the edges or bottom of the cup.

7. Let the mixture degas slightly for approx. 1 minute.

8. Use a small spatula or glass capillary pipette to extract a small amount of epoxy mix from the bottom of the measuring cup. Carefully place approx. 10mg of the mix in the crucible pan. Make sure that the mix is not sticking to the edges of the crucible. Weight the sample to the nearest 0.1mg.
9. Carefully place the lid on the crucible pan and press very lightly. The crucibles should not be hermetically sealed since this will cause the viscous resin to flow out.
10. Quickly open the DSC chamber and place the sample crucible next to the reference empty crucible. Close the DSC and immediately start data recording.
After sample insertion the DSC chamber temperature typically dropped around 10K, which took around 15-20s to correct.
11. Continue the DSC scan at the isothermal temperature for at least 60 minutes. The experiment can then be terminated when the resin is fully cured. This is the case when an horizontal asymptote of the heat flow curve can be observed.
12. Terminate the DSC experiment and collect the sample from the chamber.
13. Re-weight the sample with 0.1mg accuracy and compare with the sample mass before DSC testing.
If a mass deviation larger than 0.1mg is detected, the DSC experiment has to be critically evaluated since weight loss can influence the data.



(a) Seiko Instruments Exstar 6000 DSC and computer used for data collection



(b) DSC test chamber and furnace of the Seiko Instruments Exstar 6000 DSC

Figure A.1: DSC setup used for isothermal heat flow data collection

B

Experimental DSC & autocatalytic model cure kinetic results

In this appendix, for each of the epoxy systems on which isothermal DSC tests were performed, the specific heat flow vs time, specific total heat of reaction, convergence of fit parameters n , m & $\ln(K_2)$ and lastly, the Arrhenius plots as required for the determination of the cure kinetic parameters as discussed in Chapter 4 are presented. In addition, the reaction rate and degree of cure vs time for both the experimental isothermal DSC data and autocatalytic model fits are plotted for each epoxy system.

B.1. Former resin: Ancarez[®] RZ4010 & hardener: Ancamide[™] 3399

The former resin system (Ancarez[®] RZ4010 & hardener: Ancamide[™] 3399) as currently used for EX-CORE production at Donkervoort had been tested once again to verify the DSC results obtained by Eversdijk [64] in 2017. Both are included in this section.

B.1.1. Previous results by Eversdijk ; May 2017 (Ref. nr: 0a)

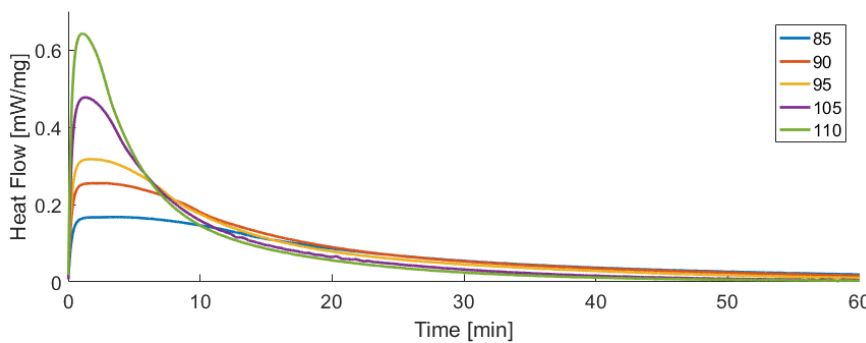


Table B.1: Specific total heat of reaction. Tested resin Ancarez[®] RZ4010 & hardener Ancamide[™] 3399 at mix ratio 100:60. (Original data by Eversdijk [64].)

T_{iso} [°C]	$H_{T_{spec}}$ [J/g]
85	290.42
90	331.41
95	317.04
105	307.01
110	314.00
Avg.	311.98

Figure B.1: Specific heat flow ϕ_{spec} vs time at different isothermal DSC tests. Tested resin Ancarez[®] RZ4010 & hardener Ancamide[™] 3399 at mix ratio 100:60. (Plot generated using original data from Eversdijk [64].)

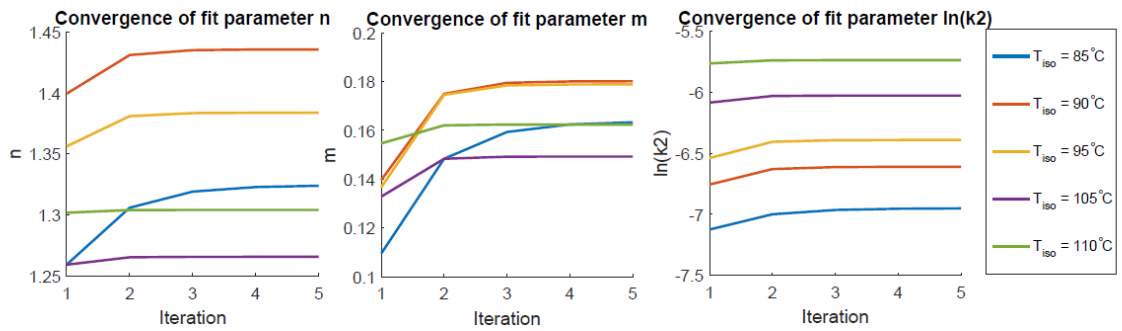


Figure B.2: Convergence plots of cure kinetics fit parameters n , m and $\ln(k_2)$ for 5 iterations at different isothermal DSC temperatures. Tested resin Ancarez[®] RZ4010 & hardener Ancamide[™] 3399 at mix ratio 100:60. (Original plot from Eversdijk [64].)

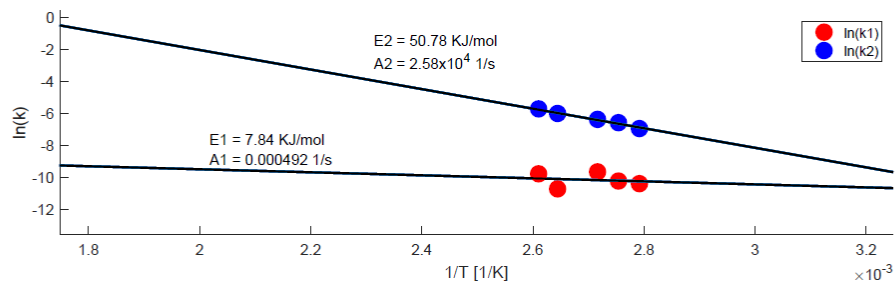


Figure B.3: Arrhenius plots relating temperature with rate constants k_1 and k_2 . Indicated values for the activation energies (E) and pre-exponential factors (A) obtained from a linear regression slope fit and y-axis intercept respectively. Tested resin Ancarez[®] RZ4010 & hardener Ancamide[™] 3399 at mix ratio 100:60. (Original plot from Eversdijk [64].)

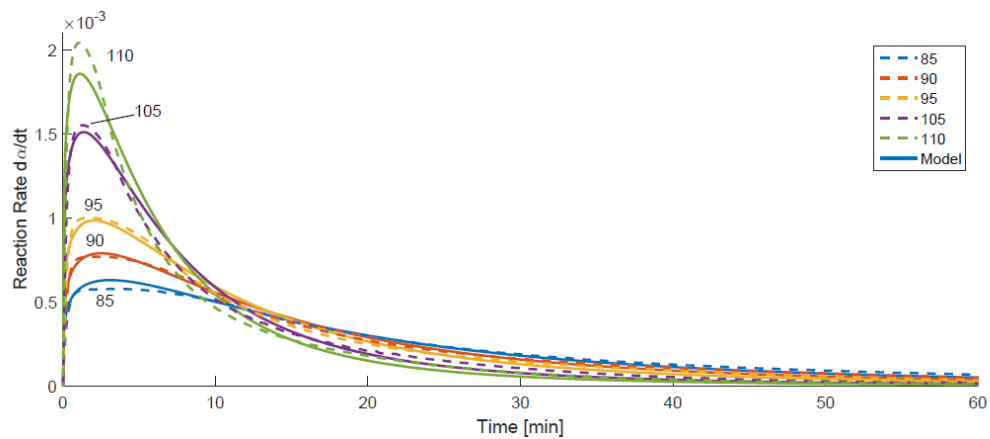


Figure B.4: Reaction rate $\frac{d\alpha}{dt}$ vs time for both the experimental DSC isothermal tests (dashed line) and autocatalytic model (solid lines) when implementing the cure kinetic fit parameters shown in Table 4.3. Tested resin Ancarez[®] RZ4010 & hardener Ancamide[™] 3399 at mix ratio 100:60. (Original plot from Eversdijk [64].)

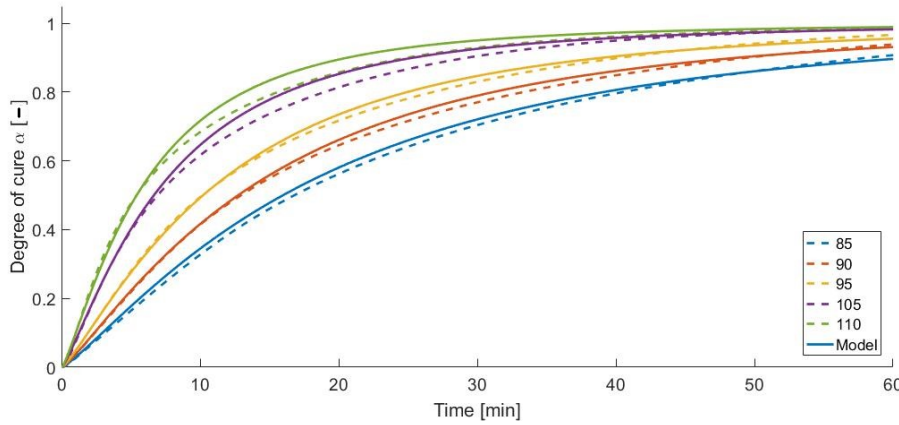


Figure B.5: Degree of cure vs time for both the experimental DSC isothermal tests (dashed line) and autocatalytic model (solid lines) when implementing the cure kinetic fit parameters shown in Table 4.3. Tested resin Ancarez[®] RZ4010 & hardener Ancamide[™] 3399 at mix ratio 100:60. (Plot generated using original data from Eversdijk [64].)

B.1.2. Re-do by Mattheus; April 2018 (Ref. nr.: 0b)

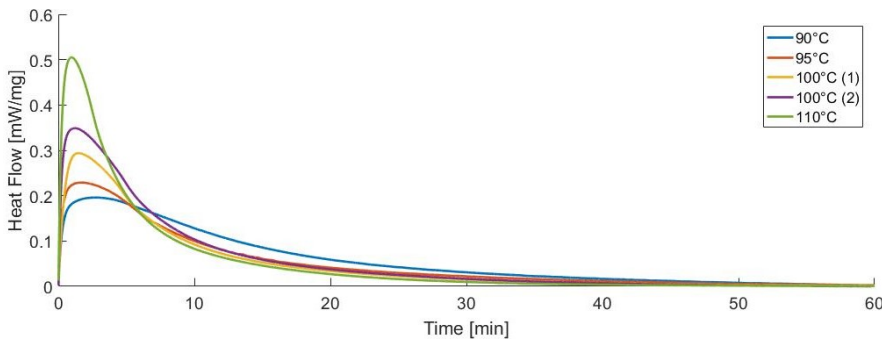


Table B.2: Specific total heat of reaction. Tested resin Ancarez[®] RZ4010 & hardener Ancamide[™] 3399 at mix ratio 100:60.

T_{iso} [°C]	$H_{T_{spec}}$ [J/g]
90	203.76
95	177.63
100 (1)	173.10
100 (2)	197.23
110	190.97
Avg.	188.54

Figure B.6: Specific heat flow ϕ_{spec} vs time at different isothermal DSC tests. Tested resin Ancarez[®] RZ4010 & hardener Ancamide[™] 3399 at mix ratio 100:60.

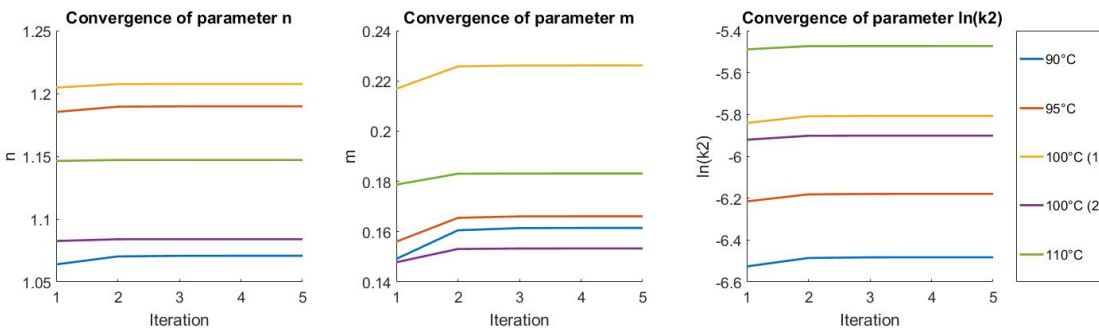


Figure B.7: Convergence plots of cure kinetics fit parameters n , m and $\ln(k_2)$ for 5 iterations at different isothermal DSC temperatures. Tested resin Ancarez[®] RZ4010 & hardener Ancamide[™] 3399 at mix ratio 100:60.

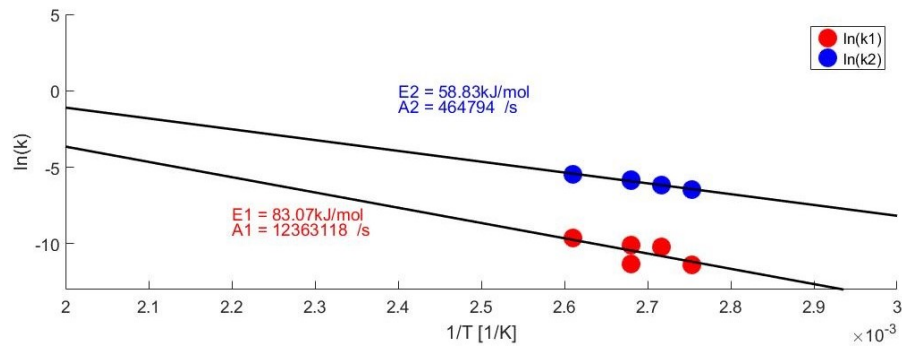


Figure B.8: Arrhenius plots relating temperature with rate constants k_1 and k_2 . Indicated values for the activation energies (E) and pre-exponential factors (A) obtained from a linear regression slope fit and y-axis intercept respectively. Tested resin Ancarez[®] RZ4010 & hardener Ancamide[™] 3399 at mix ratio 100:60.

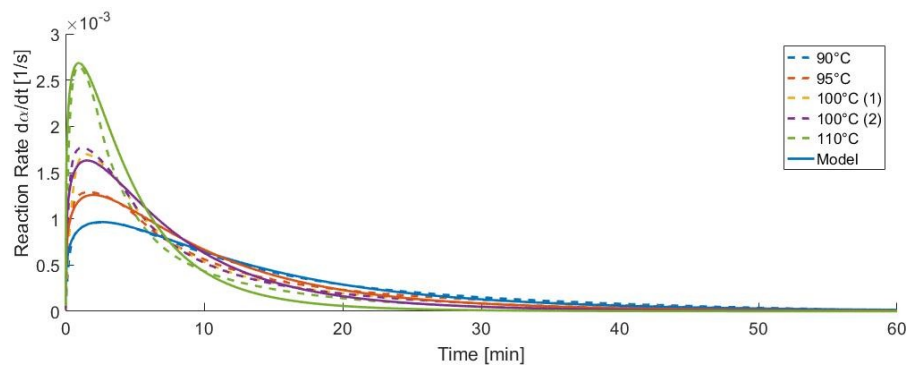


Figure B.9: Reaction rate $\frac{da}{dt}$ vs time for both the experimental DSC isothermal tests (dashed line) and autocatalytic model (solid lines) when implementing the cure kinetic fit parameters shown in Table 4.3. Tested resin Ancarez[®] RZ4010 & hardener Ancamide[™] 3399 at mix ratio 100:60.

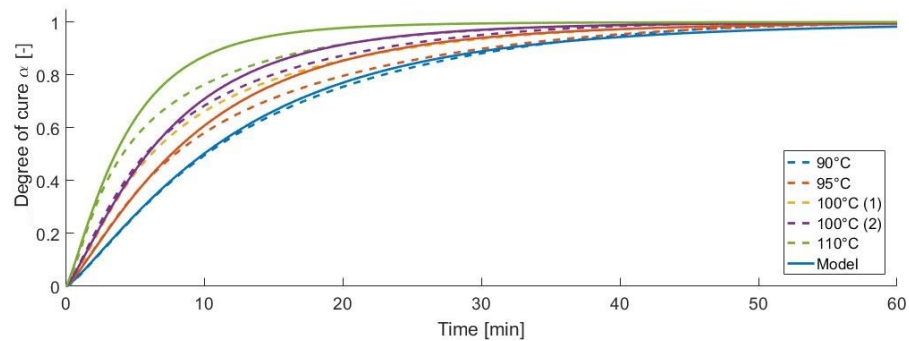


Figure B.10: Degree of cure vs time for both the experimental DSC isothermal tests (dashed line) and autocatalytic model (solid lines) when implementing the cure kinetic fit parameters shown in Table 4.3. Tested resin Ancarez[®] RZ4010 & hardener Ancamide[™] 3399 at mix ratio 100:60.

B.2. Resin: SR 1280 & Hardener: SZ 8525 (Ref. nr.: 1)

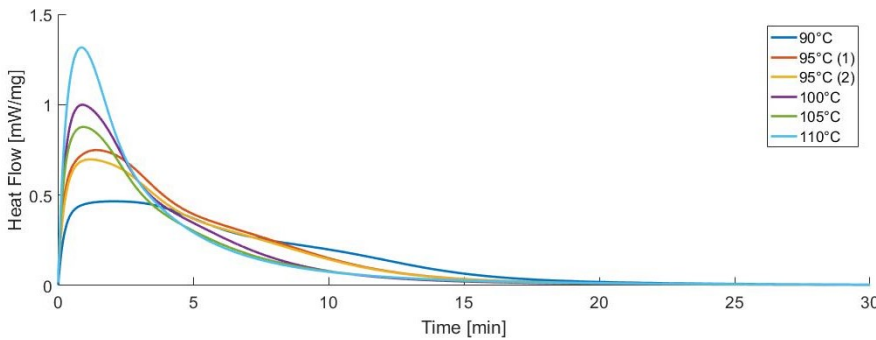


Table B.3: Specific total heat of reaction. Tested resin SR 1280 & hardener SZ 8525 at mix ratio 100:24.

T_{iso} [°C]	$H_{T_{spec}}$ [J/g]
90	265.85
95 (1)	296.90
95 (2)	278.08
100	277.59
105	252.62
110	295.74
Avg.	274.21

Figure B.11: Specific heat flow ϕ_{spec} vs time at different isothermal DSC tests. Tested resin SR 1280 & hardener SZ 8525 at mix ratio 100:24.

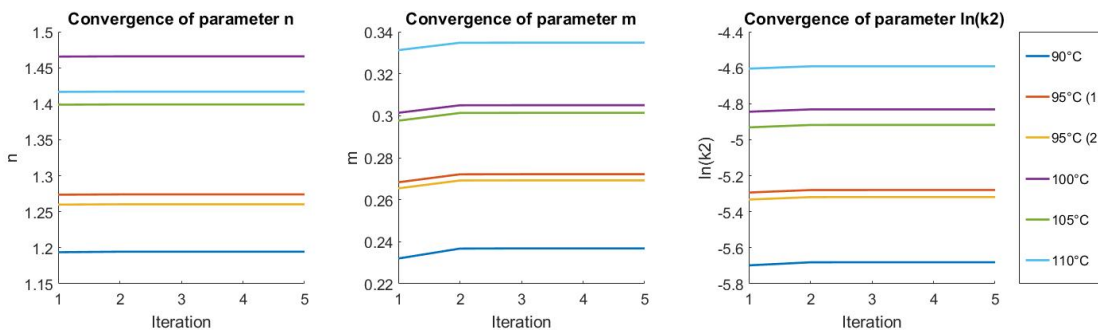


Figure B.12: Convergence plots of cure kinetics fit parameters n , m and $\ln(k_2)$ for 5 iterations at different isothermal DSC temperatures. Tested resin SR 1280 & hardener SZ 8525 at mix ratio 100:24.

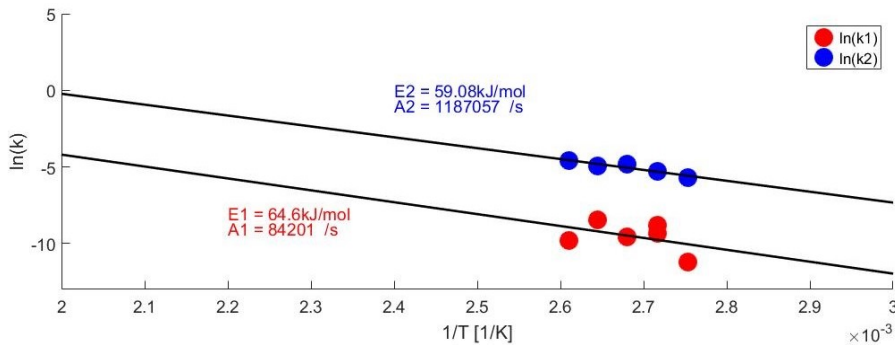


Figure B.13: Arrhenius plots relating temperature with rate constants k_1 and k_2 . Indicated values for the activation energies (E) and pre-exponential factors (A) obtained from a linear regression slope fit and y-axis intercept respectively. Tested resin SR 1280 & hardener SZ 8525 at mix ratio 100:24.

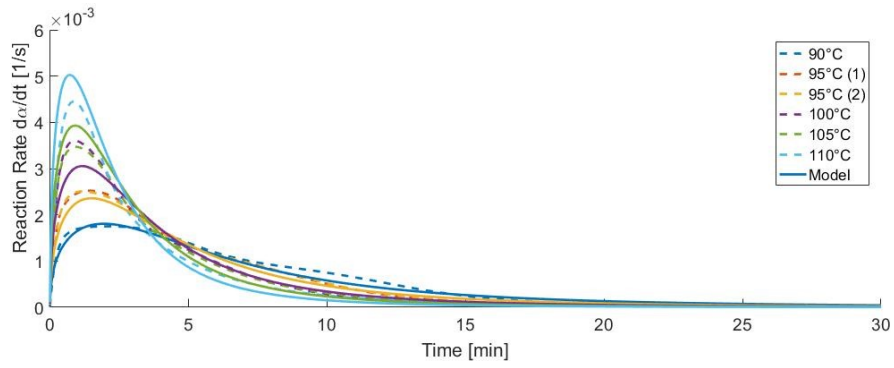


Figure B.14: Reaction rate $\frac{d\alpha}{dt}$ vs time for both the experimental DSC isothermal tests (dashed line) and autocatalytic model (solid lines) when implementing the cure kinetic fit parameters shown in Table 4.3. Tested resin SR 1280 & hardener SZ 8525 at mix ratio 100:24.

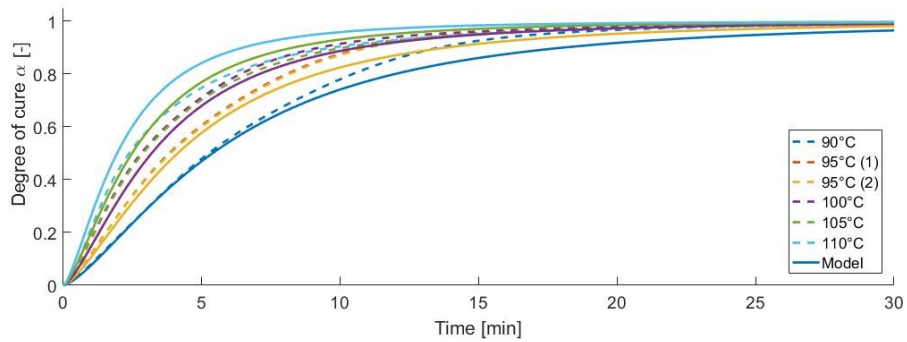


Figure B.15: Degree of cure α vs time for both the experimental DSC isothermal tests (dashed line) and autocatalytic model (solid lines) when implementing the cure kinetic fit parameters shown in Table 4.3. Tested resin SR 1280 & hardener SZ 8525 at mix ratio 100:24.

B.3. Resin: Ancarez[®] RZ4010 & hardener: Ancamine[™] 2337s (Ref. nr.: 2)

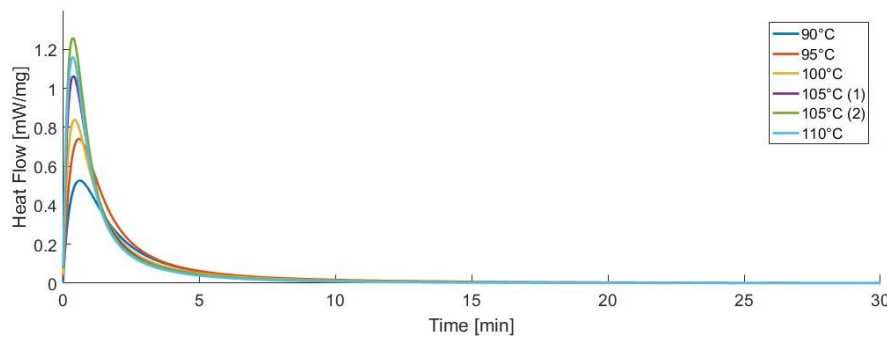


Figure B.16: Specific heat flow ϕ_{spec} vs time at different isothermal DSC tests. Tested resin Ancarez[®] RZ4010 & hardener Ancamine[®] 2337s at mix ratio 100:60.

Table B.4: Specific total heat of reaction. Tested resin Ancarez[®] RZ4010 & hardener Ancamine[®] 2337s at mix ratio 100:60.

T_{iso} [°C]	$H_{T_{spec}}$ [J/g]
90	86.97
95	103.36
100	95.71
105 (1)	100.50
105 (2)	108.01
110	98.99
Avg.	98.91

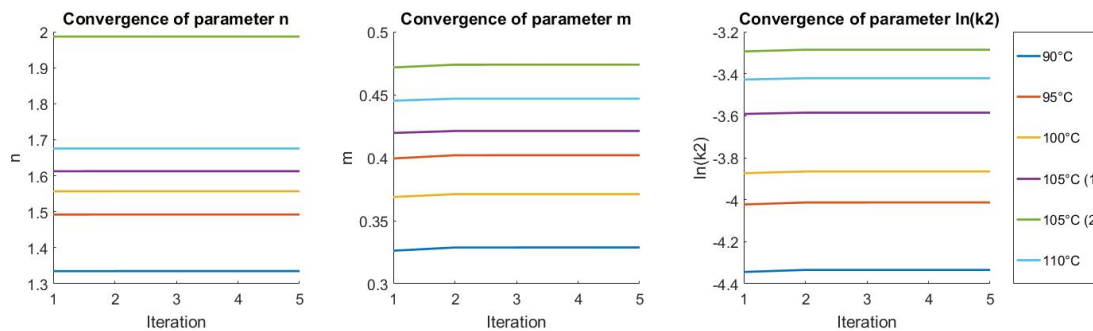


Figure B.17: Convergence plots of cure kinetics fit parameters n , m and $\ln(k_2)$ for 5 iterations at different isothermal DSC temperatures. Tested resin Ancarez[®] RZ4010 & hardener Ancamine[®] 2337s at mix ratio 100:60.

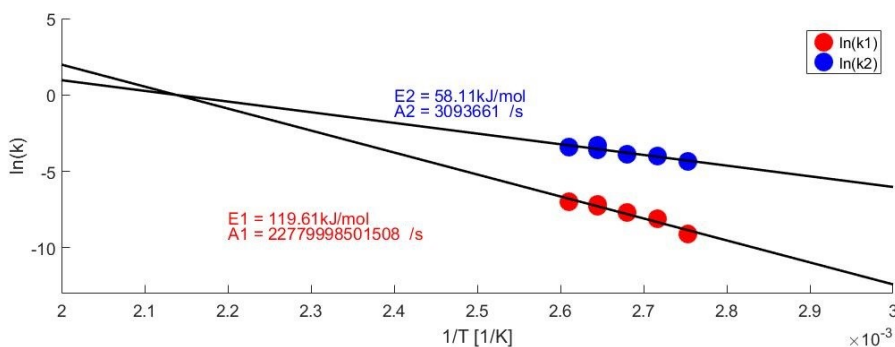


Figure B.18: Arrhenius plots relating temperature with rate constants k_1 and k_2 . Indicated values for the activation energies (E) and pre-exponential factors (A) obtained from a linear regression slope fit and y-axis intercept respectively. Tested resin Ancarez[®] RZ4010 & hardener Ancamine[®] 2337s at mix ratio 100:60.

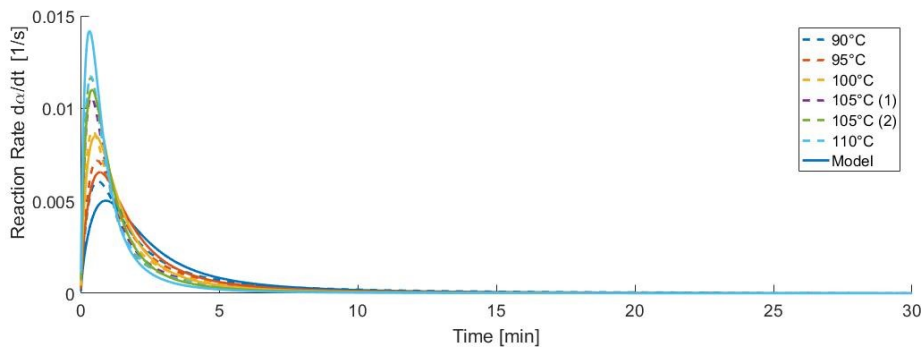


Figure B.19: Reaction rate $\frac{da}{dt}$ vs time for both the experimental DSC isothermal tests (dashed line) and autocatalytic model (solid lines) when implementing the cure kinetic fit parameters shown in Table 4.3. Tested resin Ancarez[®] RZ4010 & hardener Ancamine[®] 2337s at mix ratio 100:60.

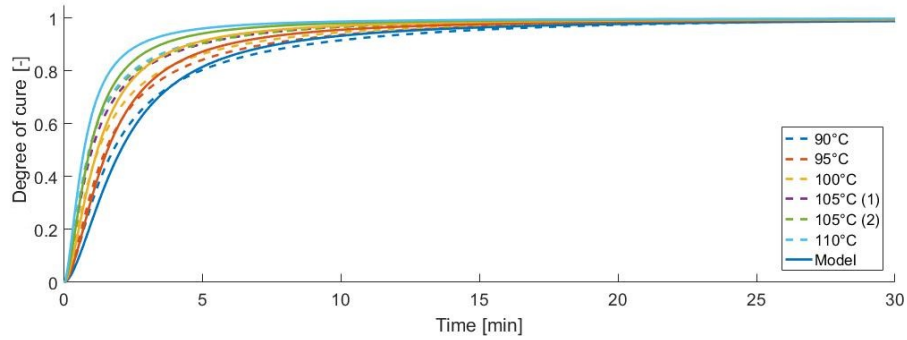


Figure B.20: Degree of cure vs time for both the experimental DSC isothermal tests (dashed line) and autocatalytic model (solid lines) when implementing the cure kinetic fit parameters shown in Table 4.3. Tested resin Ancarez® RZ4010 & hardener Ancamine® 2337s at mix ratio 100:60..

B.4. Resin: Ancarez® RZ4010 & hardener: Ancamine™ 2442 (Ref. nr.: 3)

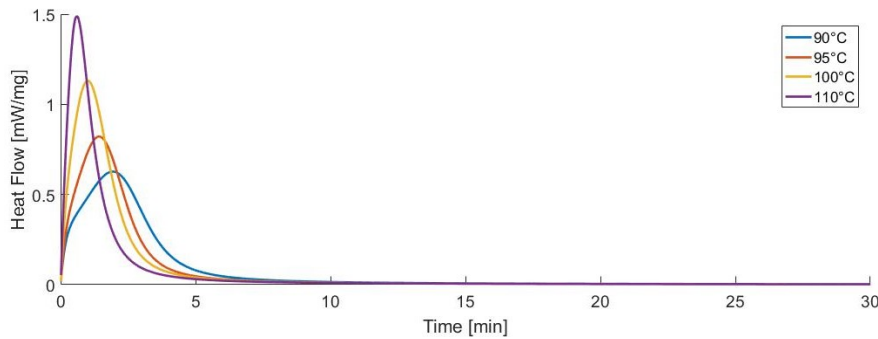


Table B.5: Specific total heat of reaction. Tested resin Ancarez® RZ4010 & hardener Ancamine® 2442 at mix ratio 100:60..

T_{iso} [°C]	$H_{T_{spec}}$ [J/g]
90	130.00
95	127.05
100	140.20
110	129.30
Avg.	131.64

Figure B.21: Specific heat flow ϕ_{spec} vs time at different isothermal DSC tests. Tested resin Ancarez® RZ4010 & hardener Ancamine® 2442 at mix ratio 100:60..

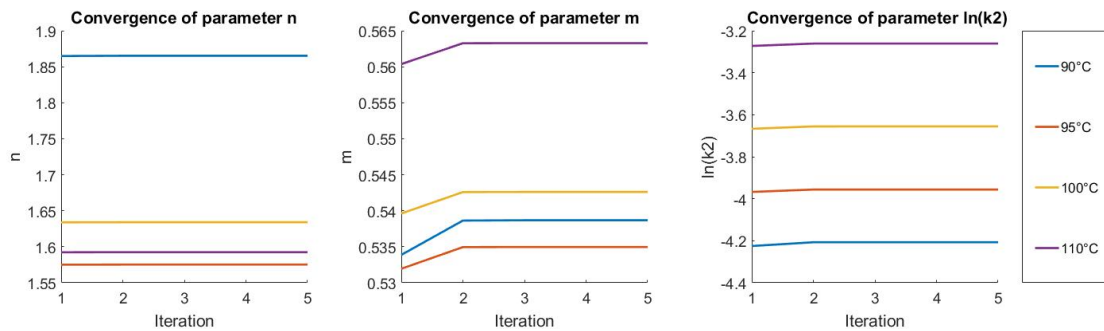


Figure B.22: Convergence plots of cure kinetics fit parameters n , m and $\ln(k_2)$ for 5 iterations at different isothermal DSC temperatures. Tested resin Ancarez® RZ4010 & hardener Ancamine® 2442 at mix ratio 100:60..

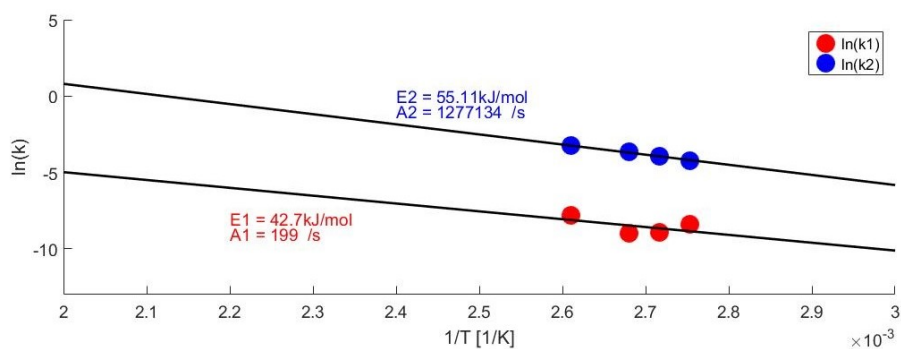


Figure B.23: Arrhenius plots relating temperature with rate constants k_1 and k_2 . Indicated values for the activation energies (E) and pre-exponential factors (A) obtained from a linear regression slope fit and y-axis intercept respectively. Tested resin Ancarez[®] RZ4010 & hardener Ancamine[®] 2442 at mix ratio 100:60.

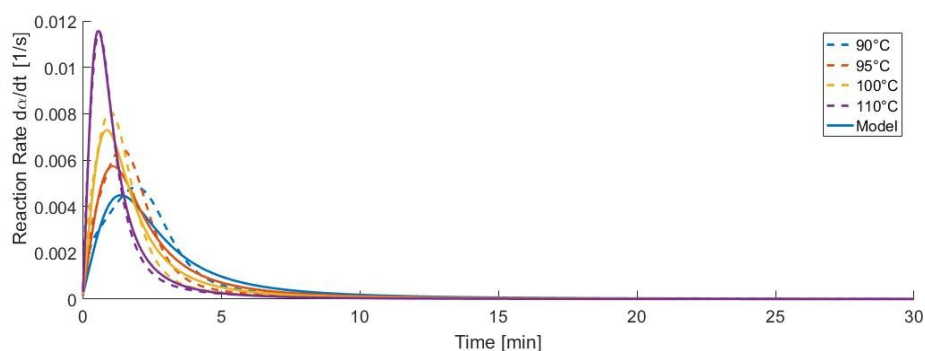


Figure B.24: Reaction rate $\frac{d\alpha}{dt}$ vs time for both the experimental DSC isothermal tests (dashed line) and autocatalytic model (solid lines) when implementing the cure kinetic fit parameters shown in Table 4.3. Tested resin Ancarez[®] RZ4010 & hardener Ancamine[®] 2442 at mix ratio 100:60.

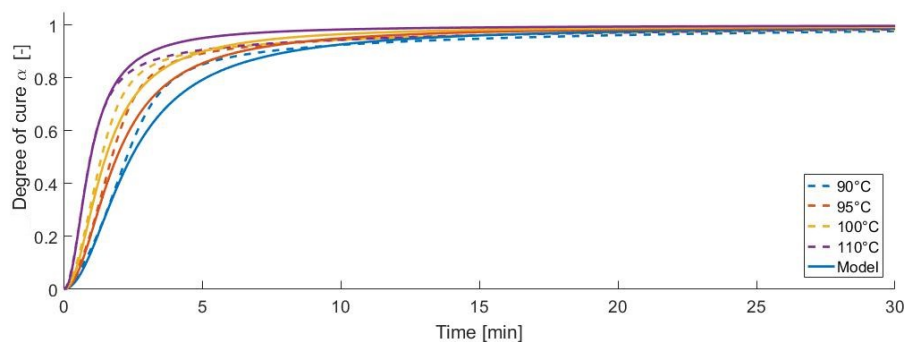


Figure B.25: Degree of cure α vs time for both the experimental DSC isothermal tests (dashed line) and autocatalytic model (solid lines) when implementing the cure kinetic fit parameters shown in Table 4.3. Tested resin Ancarez[®] RZ4010 & hardener Ancamine[®] 2442 at mix ratio 100:60.

B.5. Resin: SR 1280 & hardener: Ancamine[®] 2337s (Ref. nr.: 4)

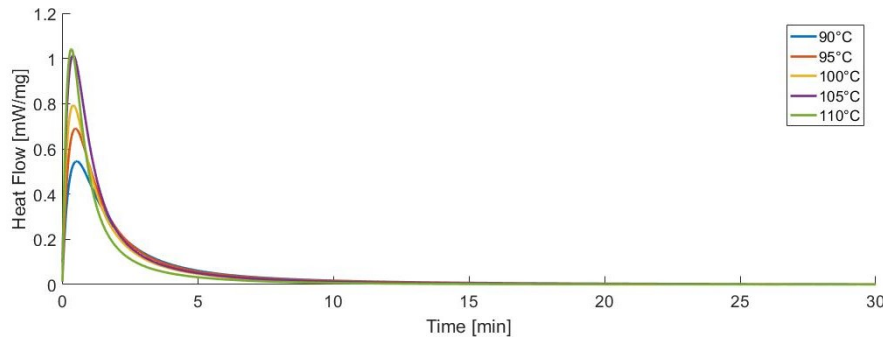


Table B.6: Specific total heat of reaction. Tested resin SR 1280 & hardener Ancamine[®] 2337s at mix ratio 100:60.

T_{iso} [°C]	$H_{T_{spec}}$ [J/g]
90	86.54
95	92.40
100	89.10
105	103.62
110	82.71
Avg.	90.87

Figure B.26: Specific heat flow ϕ_{spec} vs time at different isothermal DSC tests. Tested resin SR 1280 & hardener Ancamine[®] 2337s at mix ratio 100:60.

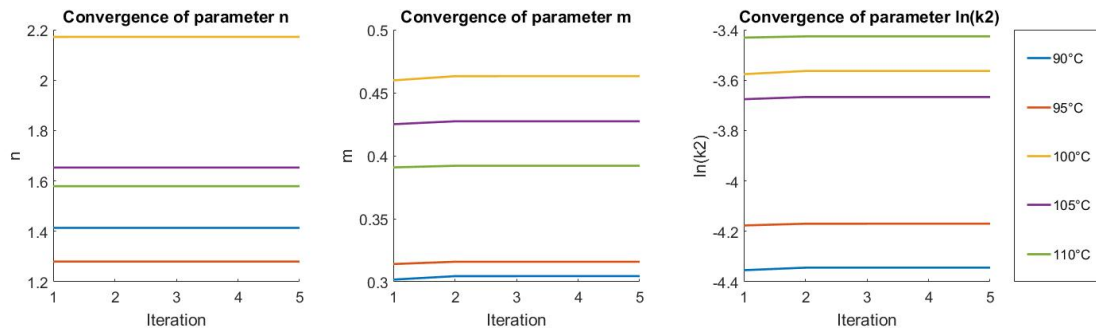


Figure B.27: Convergence plots of cure kinetics fit parameters n , m and $\ln(k_2)$ for 5 iterations at different isothermal DSC temperatures. Tested resin SR 1280 & hardener Ancamine[®] 2337s at mix ratio 100:60.

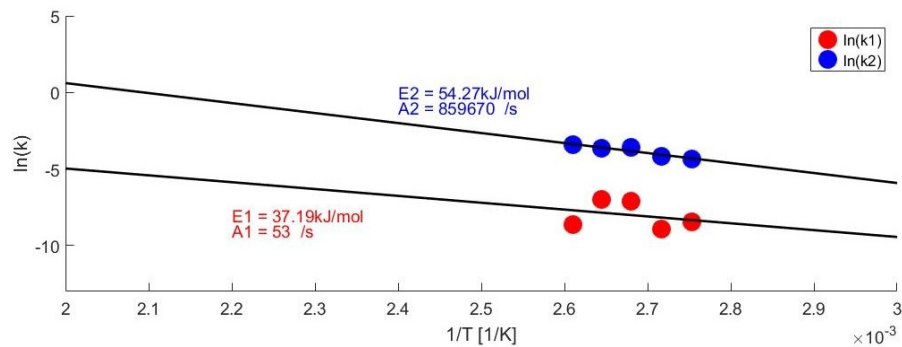


Figure B.28: Arrhenius plots relating temperature with rate constants k_1 and k_2 . Indicated values for the activation energies (E) and pre-exponential factors (A) obtained from a linear regression slope fit and y-axis intercept respectively. Tested resin SR 1280 & hardener Ancamine[®] 2337s at mix ratio 100:60.

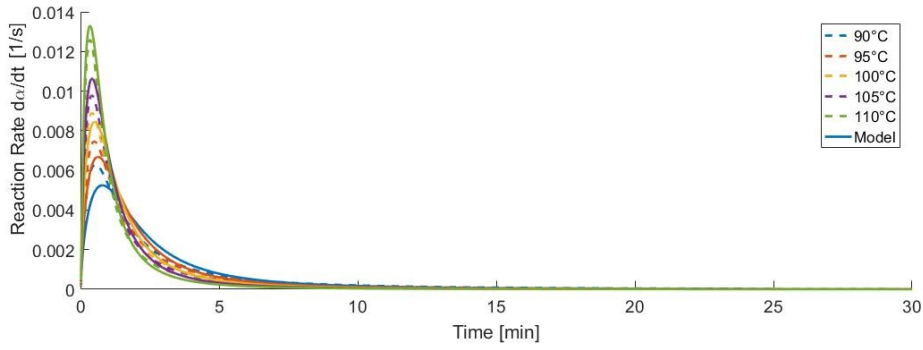


Figure B.29: Reaction rate $\frac{d\alpha}{dt}$ vs time for both the experimental DSC isothermal tests (dashed line) and autocatalytic model (solid lines) when implementing the cure kinetic fit parameters shown in Table 4.3. Tested resin SR 1280 & hardener Ancamine® 2337s at mix ratio 100:60.

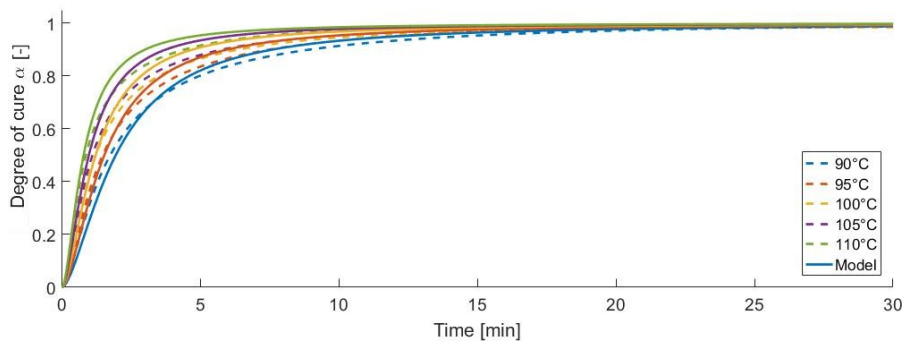


Figure B.30: Degree of cure α vs time for both the experimental DSC isothermal tests (dashed line) and autocatalytic model (solid lines) when implementing the cure kinetic fit parameters shown in Table 4.3. Tested resin SR 1280 & hardener Ancamine® 2337s at mix ratio 100:60.

B.6. Resin: SR 1280 & hardener: Ancamine® 2442

B.6.1. Test series 1: epoxy mix ratio: 100/60 (Ref. nr.: 5)

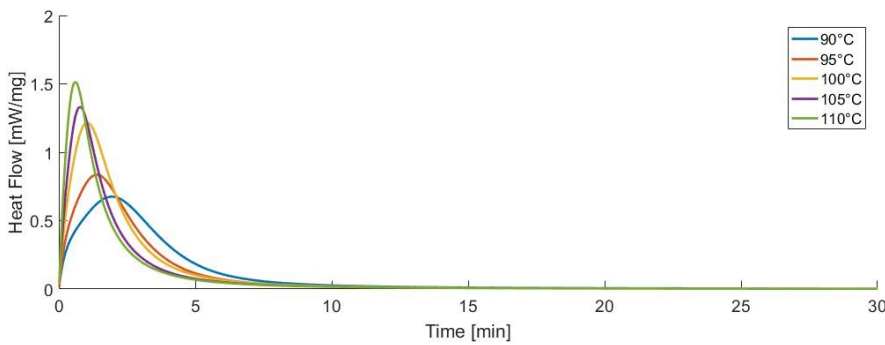


Table B.7: Specific total heat of reaction. Tested resin SR 1280 & hardener Ancamine® 2442 at mix ratio 100:60.

T_{iso} [°C]	$H_{T_{spec}}$ [J/g]
90	170.04
95	161.94
100	186.46
105	164.86
110	163.99
Avg.	169.46

Figure B.31: Specific heat flow ϕ_{spec} vs time at different isothermal DSC tests. Tested resin SR 1280 & hardener Ancamine® 2442 at mix ratio 100:60.

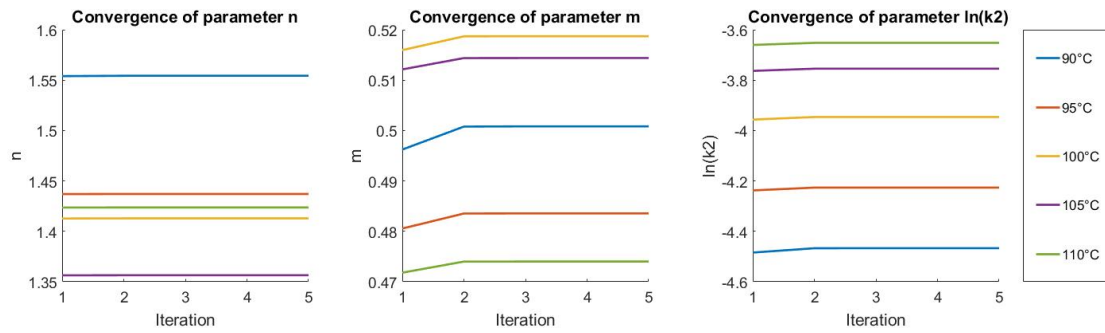


Figure B.32: Convergence plots of cure kinetics fit parameters n , m and $\ln(k_2)$ for 5 iterations at different isothermal DSC temperatures. Tested resin SR 1280 & hardener Ancamine[®] 2442 at mix ratio 100:60.

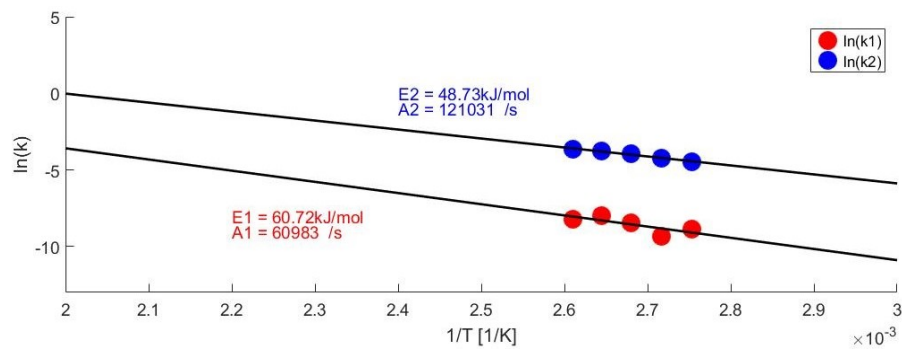


Figure B.33: Arrhenius plots relating temperature with rate constants k_1 and k_2 . Indicated values for the activation energies (E) and pre-exponential factors (A) obtained from a linear regression slope fit and y-axis intercept respectively. Tested resin SR 1280 & hardener Ancamine[®] 2442 at mix ratio 100:60.

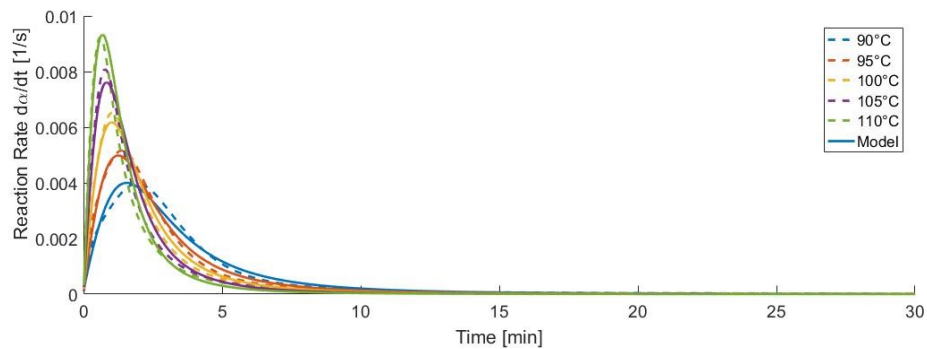


Figure B.34: Reaction rate $\frac{d\alpha}{dt}$ vs time for both the experimental DSC isothermal tests (dashed line) and autocatalytic model (solid lines) when implementing the cure kinetic fit parameters shown in Table 4.3. Tested resin SR 1280 & hardener Ancamine[®] 2442 at mix ratio 100:60.

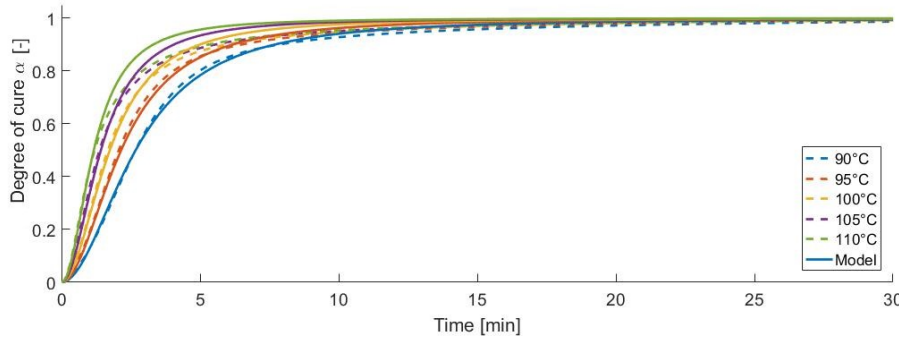


Figure B.35: Degree of cure vs time for both the experimental DSC isothermal tests (dashed line) and autocatalytic model (solid lines) when implementing the cure kinetic fit parameters shown in Table 4.3. Tested resin SR 1280 & hardener Ancamine® 2442 at mix ratio 100:60.

B.6.2. Test series 2: epoxy mix ratio: 100/20 at temperatures 90°C to 110°C (Ref. nr.: 5.2)

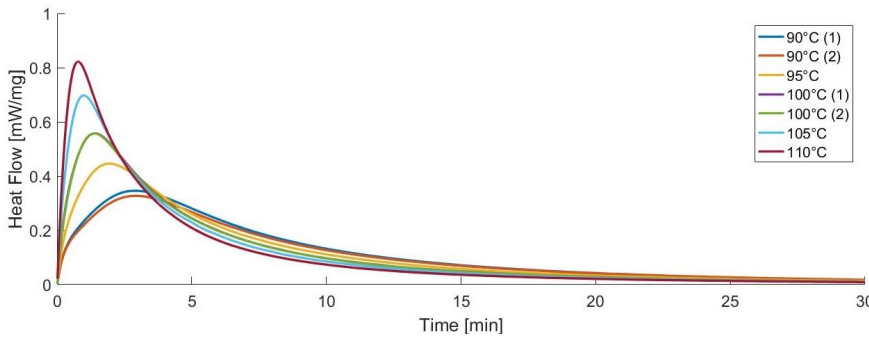


Table B.8: Specific total heat of reaction. Tested resin SR 1280 & hardener Ancamine® 2442 at mix ratio 100:20.

T_{iso} [°C]	$H_{T_{spec}}$ [J/g]
90 (1)	218
90 (2)	212
95	214
100 (1)	215
100 (2)	214
105	217
110	214
Avg.	215

Figure B.36: Specific heat flow ϕ_{spec} vs time at different isothermal DSC tests. Tested resin SR 1280 & hardener Ancamine® 2442 at mix ratio 100:20.

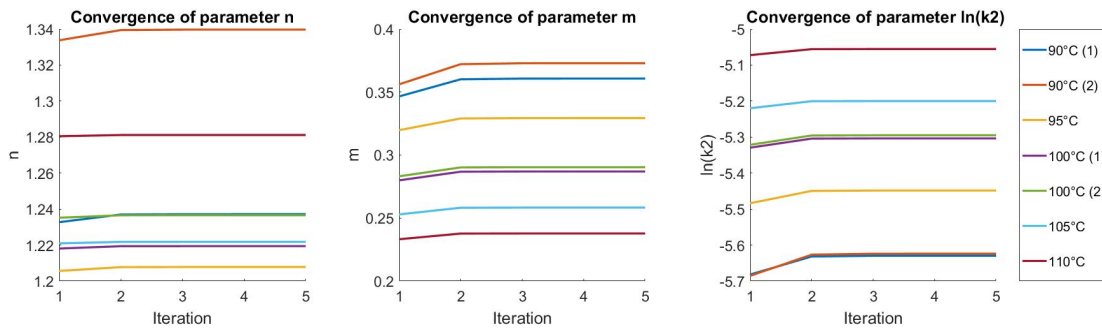


Figure B.37: Convergence plots of cure kinetics fit parameters n , m and $\ln(k_2)$ for 5 iterations at different isothermal DSC temperatures. Tested resin SR 1280 & hardener Ancamine® 2442 at mix ratio 100:20.

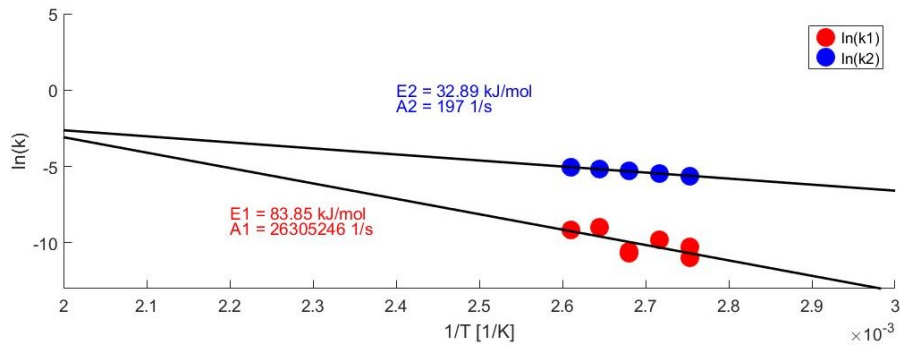


Figure B.38: Arrhenius plots relating temperature with rate constants k_1 and k_2 . Indicated values for the activation energies (E) and pre-exponential factors (A) obtained from a linear regression slope fit and y-axis intercept respectively. Tested resin SR 1280 & hardener Ancamine[®] 2442 at mix ratio 100:20.

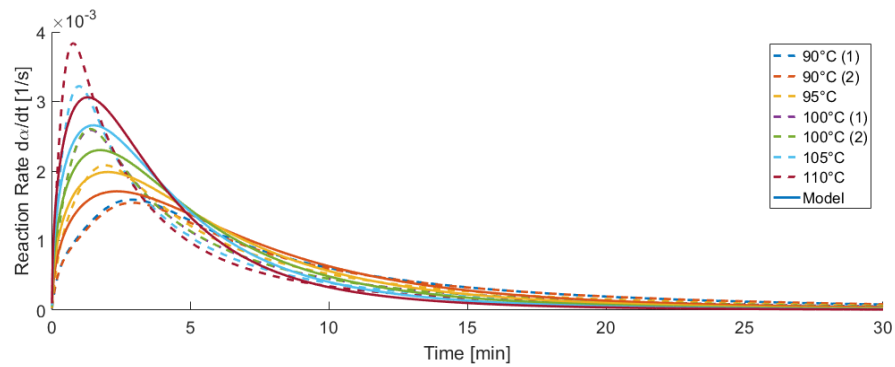


Figure B.39: Reaction rate $\frac{d\alpha}{dt}$ vs time for both the experimental DSC isothermal tests (dashed line) and autocatalytic model (solid lines) when implementing the cure kinetic fit parameters shown in Table 8.5. Tested resin SR 1280 & hardener Ancamine[®] 2442 at mix ratio 100:20.

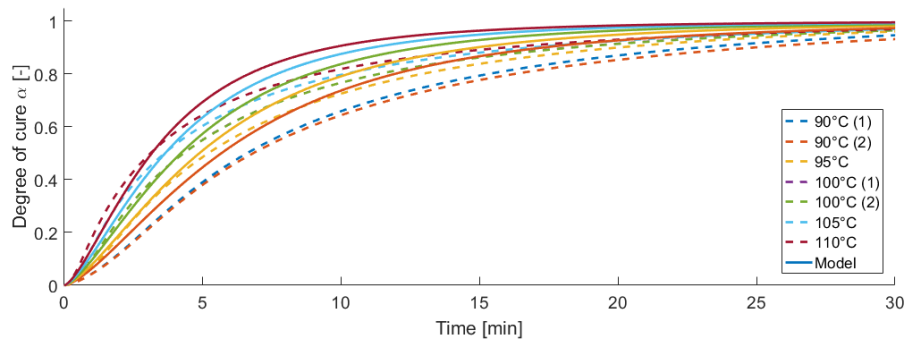


Figure B.40: Degree of cure vs time for both the experimental DSC isothermal tests (dashed line) and autocatalytic model (solid lines) when implementing the cure kinetic fit parameters shown in Table 8.5. Tested resin SR 1280 & hardener Ancamine[®] 2442 at mix ratio 100:20.

B.6.3. Test series 3: epoxy mix ratio: 100/20 at temperatures 140°C to 160°C (Ref. nr.: 5.2-HighTemp)

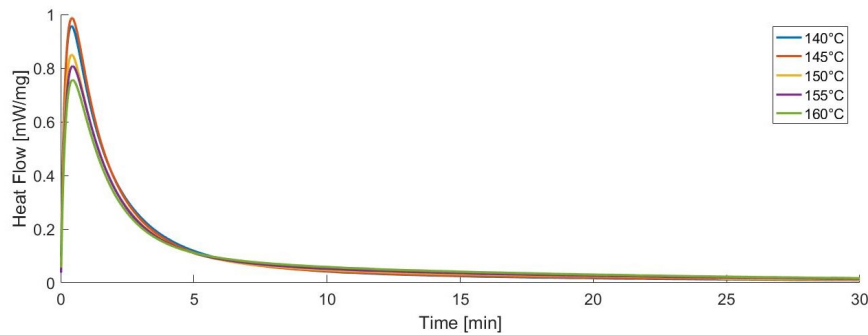


Figure B.41: Specific heat flow ϕ_{spec} vs time at different isothermal DSC tests. Tested resin SR 1280 & hardener Ancamine® 2442 at mix ratio 100:20.

Table B.9: Specific total heat of reaction. Tested resin SR 1280 & hardener Ancamine® 2442 at mix ratio 100:20.

T_{iso} [°C]	$H_{T_{spec}}$ [J/g]
140	170
145	173
150	166
155	172
160	175
Avg.	171

B.6.4. Test series 4: epoxy mix ratio: 100/20 at temperatures 115°C to 135°C (Ref. nr.: 5.2-MidTemp)

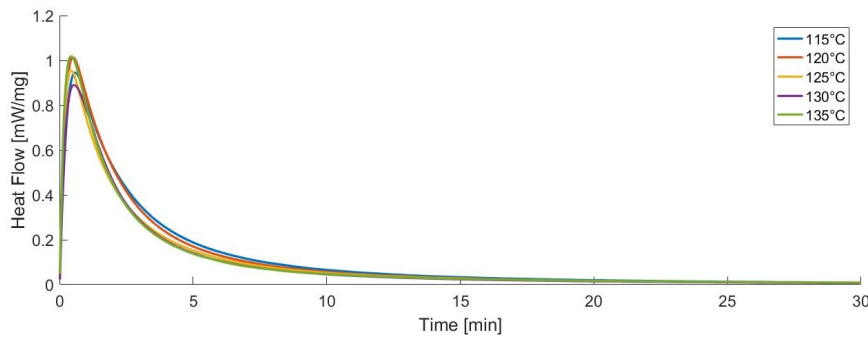


Figure B.42: Specific heat flow ϕ_{spec} vs time at different isothermal DSC tests. Tested resin SR 1280 & hardener Ancamine® 2442 at mix ratio 100:20.

Table B.10: Specific total heat of reaction. Tested resin SR 1280 & hardener Ancamine® 2442 at mix ratio 100:20.

T_{iso} [°C]	$H_{T_{spec}}$ [J/g]
115	213
120	204
125	186
130	178
135	186
Avg.	193

B.6.5. Combined test series 2, 3 and 4: epoxy mix ratio: 100/20. Temperatures 90°C to 160°C (Ref. nr.: 5.2-AllTemp)

Table B.11: Specific total heat of reaction. Tested resin SR 1280 & hardener Ancamine® 2442 at mix ratio 100:20.

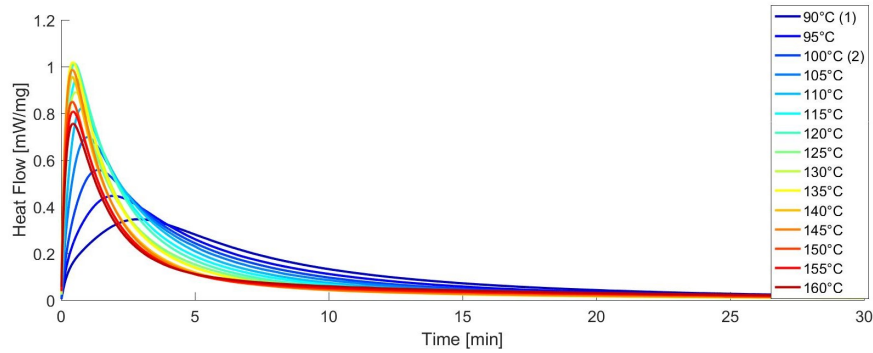
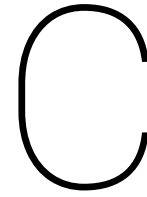


Figure B.43: Specific heat flow ϕ_{spec} vs time at different isothermal DSC tests. Tested resin SR 1280 & hardener Ancamine® 2442 at mix ratio 100:20.

T_{iso} [°C]	$H_{T_{spec}}$ [J/g]
90 (1)	218
95	214
100 (2)	214
105	217
110	214
115	213
120	204
125	186
130	178
135	186
140	170
145	173
150	166
155	172
160	175
Avg.	193



Effect of isothermal aluminum edge assumption in numerical model

As explained in Section 5.1.1, one of the assumptions of the thermal model was that "*all mold edges maintain the prescribed (isothermal) cure temperature.*" This implies that in the model analysis all the mold edges (and thus boundary nodes) are assumed to be at the prescribed cure temperature from the beginning of the analysis. However, in reality only the top and bottom lids of the mold are preheated, after which the aluminum sample casing is inserted in between both lids. So this means that in practice not only the EX-CORE sample but also the aluminum casing is heated from room temperature.

To investigate the effect of this assumption, the 2D numerical model had been rewritten to simulate the heat-up of the left & right aluminum edges as well. The resulting adapted numerical model that takes the heat-up effect of the aluminum nodes into account will be further referred to as version v10, while the latest version of the numerical modal as used in the current research is referred by v9. Note that the bottom edge of the casing was made from 2 layers of aluminum, with a thickness of 0.075mm per layer, in direct contact with the pre-heated aluminum bottom mold plate. The time delay caused by the heat-up of the aluminum tape can therefore be considered negligible.

In the numerical model, the side edges of the aluminum casing are represented by the left and right boundary nodes. In the model v9, these nodes were assigned the constant isothermal cure/mold temperature. However, in version v10 the heat flow between the aluminum nodes is simulated in a similar way as explained in Chapter 5 for EX-CORE. The properties of 6060-T6 grade Aluminum were assigned to these boundary nodes; namely thermal conductivity $k_{alu}=210\text{W/mK}$, specific heat capacity $C_{p_{alu}}=900\text{J/kgK}$ and density $\rho_{alu}=2710\text{kg/m}^3$ [110]. In addition, no heat-flow was allowed to the outside environment, since an insulated mold was assumed.

For both model versions, the temperature progress in a 55mm thick EX-CORE sample was tracked at different locations along the N/2 centerline (or mid thickness) of the sample, more specifically at 0, 2, 5, 10, 20% etc. from the right edge. These temperatures are plotted in Figure C.1, where the solid black lines represent the reference v9 model data, and the colored dashed lines the results from model v10. The mid-thickness temperature of the aluminum side as modeled in v10 is also shown (in red).

In Figure C.1 it can be seen that, in the v10 analysis, the aluminum edge quickly approaches the mold temperature of 110°C; reaching 108°C in less than one second. Due to this quick heat up, only a minimal temperature shift in time is caused between the v9 and v10 data. This shift in time also diminishes further with nodes away from the edge. In addition, no measurable effect on the maximum temperature reached in the core or time to reach 98% cure was obtained. From these results it can be concluded that the assumption of constant mold edge temperatures for the aluminum side edges is acceptable since it does not impair the model accuracy. Additionally, modeling the heat-up of the aluminum edges would significantly reduce the critical time step required for stability (see stability criteria Equation 5.10); from $\Delta t_{crit} \approx 1.5\text{sec}$ for typical EX-CORE mixtures to 0.0045sec for modeling the heat transfer in aluminum. In practice this means that the total computational time for a single simulation increases from $\pm 30\text{s}-3\text{min}$ to more than one hour. This would impair the functionality of the model as a quick analysis tool.

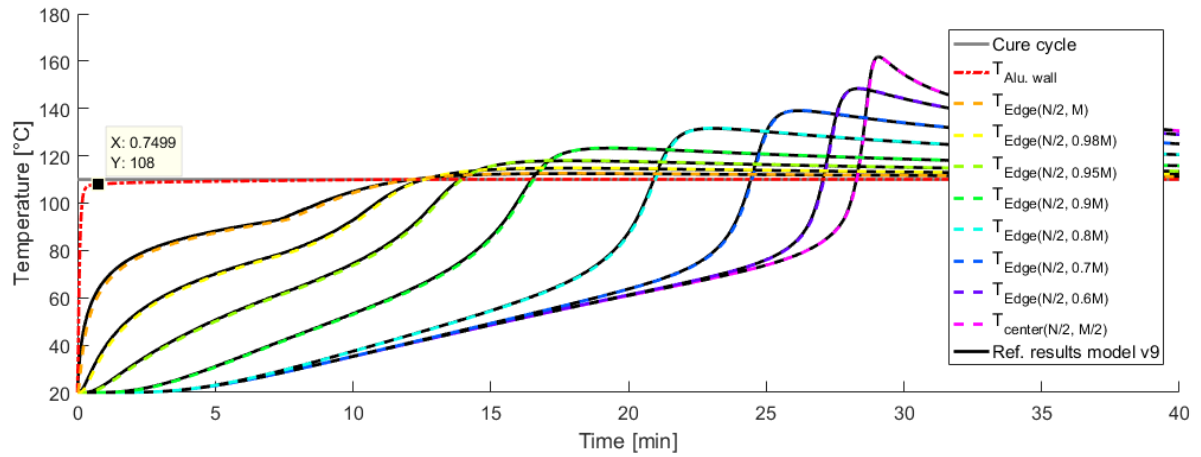


Figure C.1: Comparison of temperature results obtained from numerical model v10; including heat-transfer in aluminum edges (dashed colored lines) and reference model v9; with isothermal aluminum edges (solid black lines). (Chosen model settings; resinNr:5, mix:270opt: DUperc:4, DUgrade:43, DUexpState1, a=55mm, b=175mm, meshsize: 1.25mm, $\Delta t=0.0045$)

D

Verification Heisler charts

The charts given in this appendix form a graphical representation of the analytical solution of the one-dimensional transient conduction in a plane wall with thickness $2L$. They are used for the verification of the numerical heat transfer model as explained in Section 5.8

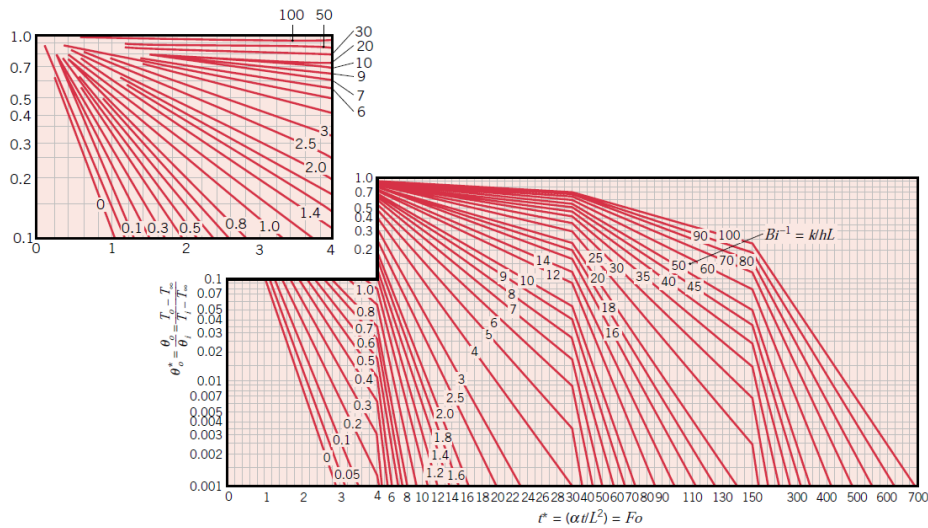


Figure D.1: Chart for determining the midplane temperature as a function of time for a plane wall with thickness $2L$. [123]

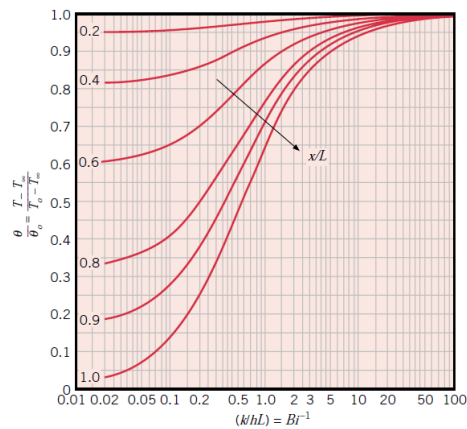
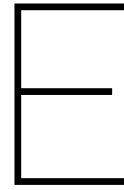


Figure D.2: Chart for determining the temperature distribution along the thickness of a plane wall with thickness $2L$. [123]



EX-CORE sample manufacturing procedures

In this appendix the procedure for the manufacturing of the EX-CORE samples made during this research is explained. Unless otherwise specified in this report, this is the standard procedure for manual EX-CORE sample preparation. The naming convention used for sample labeling is also described at the end of this appendix.

E.1. Steps for EX-CORE sample preparation

Required tooling

- Tile mold lids, aluminum (top & bottom) cover plates and aluminum stackable side edges.
- PI controller & software on Windows computer
- Aluminum tape
- Release agent Loctite® 700-NC™ Frekote™
- Digital balance with at least 0.1g precision
- Plastic mixing/measuring cups in different sizes, depending on the required mix volume
- Small spoon or spatula
- Wooden stirring sticks
- Plastic syringe
- 4 metal glue clamps

Safety equipment

It is recommended to wear protective nitril or vinyl disposable gloves when handling EX-CORE. Wearing a dust mask with gas filter is also advised for all steps involving non-cured EX-CORE because gases can escape from the epoxy (and mold release agent) and the lightweight microspheres tend to get airborne easily. When handling samples to or from the hot mold, heat-protective/welding gloves should be worn.

A) Step-by-step tile mold preparation

The following steps describe the preparation of the tile mold, sample casing and sensors (if required).

1. *If necessary, remove dirt or curing remains from the mold lids, aluminum- edges and cover plates with a wooden scraper and/or brake cleaner.*
2. *Attach aluminum top and bottom cover plates to the mold lids using aluminum tape (see Figure E.1)*
3. *If required, attach the FSR sensors to the top cover plate*
The FSR pressure sensors are attached to the top aluminum cover plate using aluminum tape (as shown in Figure E.1). Note that all sensors are wrapped in vacuum foil "Scabro Vacfilm 450V" to protect them from contamination.

4. *Prepare "sample-casing" using stackable aluminum side edges and aluminum tape*
Stack the required amount of aluminum edges (each ± 5 mm thick) on top of each other, such that the desired sample thickness is obtained. Attach all edges to each other using aluminum tape (see Figure E.2). The bottom of the sample casing should be made from 2 layers of aluminum tape.
5. *Apply at least 3 layers of release agent Loctite® 700-NC™ Frekote™ to the mold cover plates, sample casing edges and wrapped sensors.*
6. *Preheat mold lids at desired cure temperature*
Upload the required "recipe" in the PI controller software. For the samples produced in this research, this means a ramp-up from room temperature to the required cure temperature (for example to 110°C at 1.5°C/min), followed by an isothermal dwell at the cure temperature. Select a recorder file. Then turn on the switch on the PI-controller and press start.

Note that the top aluminum cover plate with NTC sensors is preheated with the NTC sensors already in place (if required). The aluminum "sample casing" is not preheated since it is used for sample molding (see part C)). This allows the quick transferral of the uncured sample mixture in between the preheated mold lids.

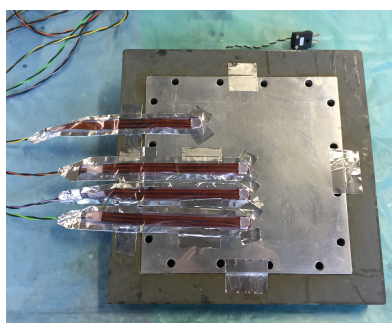


Figure E.1: Tile mold upper lid. Aluminum cover plate and 4 FRS sensors attached with aluminum tape.

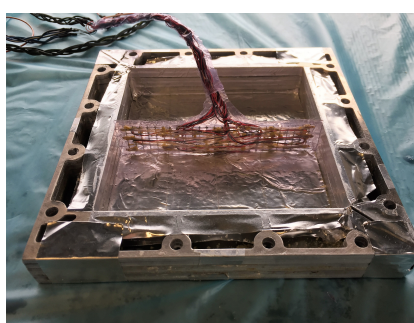


Figure E.2: "Sample casing": stackable aluminum mold edges connect with aluminum tape. Bottom of sample casing created using 2 layers of aluminum tape. NTC sensor grid put in place.



Figure E.3: Closed tile mold using 4 glue clasps.

B) Step-by-step EX-CORE constituent (manual) weighing & mixing

The steps below describe the procedure for manual mixing and dosing of the EX-CORE constituents. It is however also possible to mix and dose the components automatically using the dosing and mixing set-up developed by Mattheus [66] and Ten Hoeve [67]. For all samples produced during this research, the weighing/dosing and mixing of the constituents was done manually. This because different types of resin, hardener and DU are used in this research which could contaminate the setup used for production at Donkervoort. In addition, manual processing gave better insight into the viscosity and ease of mixing of the mixture.

1. *Determine the amount of constituents that are required.*
This is based on the required mix volume fractions, the total required mix volume (usually nominal mold volume \times 130% margin), the resin mix ratio and the density of the used constituents.
2. *Place a suitable size of plastic cup or bucket on the scale.*
For ease of mixing the cup/bucket should be larger than the total required mixing volume.
3. *Weigh and mix the correct amount of resin and hardener in the mixing cup to the nearest 0.1g.*
The correct resin-hardener weight fraction should be used. Depending on the type of epoxy system, resin mix ratio's ranging from 100:60 to as low as 100:20 are used throughout this report.
It is advised to first weigh the resin, zero the balance and then add the hardener to the plastic cup. Depending on the type of hardener; liquid or powdery, a small syringe or spoon/spatula can be used. This is done to prevent that too much hardener is added to the resin which is hard to remove afterwards.
Finally, mix for at least 2 minutes using a wooden stirring stick until a uniformly colored mixture is obtained.

4. *Add the required mass of DU to the mixing cup. Weigh to the nearest 0.1g.*
Zero the scale and use a small spoon to carefully add small amounts of DU ($\pm 0.2\text{g}$) at a time. This to prevent overfilling, since removing DU afterwards is challenging.
5. *Mix homogeneously.*
Start steering slowly, to prevent the DU from getting airborne. When the DU is dispersed, continue steering at a higher speed until it is homogeneously dispersed into the mixture. The DU may not stick together any more.
6. *Add the required mass of Q-Cel to the mixing cup and mix homogeneously. Weight to the nearest 0.01g.*
Zero the scale. A small plastic cup and stirring stick can be used to poor the Q-Cel in the mixture. Again, start mixing slowly to prevent the Q-Cel from releasing into the air. After some time the mixture becomes a kind of paste which can be kneaded by hand. Continue mixing/kneading until no white loose powder is visible anymore and a homogeneous viscous paste is obtained. Depending on the total amount of Q-Cel, addition and mixing can be split up into multiple smaller steps.
7. *Add the required mass of DE to the mixing cup and mix homogeneously. Weight to the nearest 0.01g.*
This again can best be done in multiple smaller steps. Slowly stir/knead the DE powder into the EX-CORE paste, to prevent that the DE microspheres evacuate into the air. Continue mixing until a homogeneous mixture is obtained. Depending on the mix composition, either a paste like or powdery like final mixture is obtained.

C) Step-by-step EX-CORE molding & curing in preheated tile mold

Now the EX-CORE mixture is ready to be placed inside the preheated mold and cure:

1. *If required; place the NTC sensor grid in the center of the square tile mold sample casing before mold filling. (See Figure E.2)*
2. *Put the required amount of EX-CORE paste in the aluminum sample casing.*
Based on the nominal mold volume and required mold filling percentage, the amount of EX-CORE paste to be put in the mold can be determined. Weigh this amount of paste and use it to fill up the mold cavity such that the required mold filling percentage is reached. This can easily be done by hand. The EX-CORE paste is knead-able, and so it can be easily deformed into the mold.
3. *Connect all sensors (if required) to the Arduino setup.*
Make sure an SD card is inserted into the SD card reader. Check if all sensors are functioning properly.
4. *Quickly open the preheated tile mold and remove the top (hot!) lid.*
Place the lid on some breather blankets or ask someone to help and hold the lid.
5. *Place the sample-casing containing the EX-CORE mixture (& NTC sensors) in between the two preheated mold lids.*
6. *Put the mold lid on top of the sample casing and use 4 metal glue clamps to ensure mold closure during sample expansion/curing.*
7. *Simultaneously; start sensor recording by pushing the Arduino reset button & start cure time timer*
The required cure time is usually estimated by making use of the numerical model, from which the time to reach at least 98% cure is obtained.

Make sure that the current to the Arduino sensors is not interrupted during curing. This will cause the Arduino to reset, which overwrites the stored data to the SD card!
8. *Wrap the entire tile mold in at least 6 layers of bleeder fabric/insulating blankets.*

When cure time has passed;

9. *Shut-off current to mold, retract SD card, remove insulation blankets and disconnect sensors.*
To prevent the Arduino from resetting (and so data file overwriting), retract the SD cards before disconnecting the USB and/or 5V power connection to the Arduino.
10. *If required; let the sample cool down in the mold for specified amount of time or until desired core temperature is reached.*
11. *Take the (hot) sample out of the (hot) mold*
Open the mold and take the sample casing out. Then take out the sample itself by folding away the aluminum corner edges.
12. *Let the EX-CORE sample (further) cool down at room temperature.*

E.2. Sample naming convention

In Figure E.4 the naming convention used for sample labeling during this research is explained.

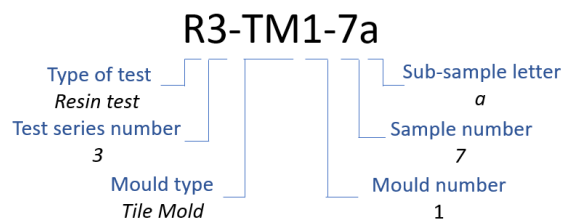


Figure E.4: Naming convention used for sample labeling

Flexiforce[®] HT201 FSR calibration

Each of the four Flexiforce[®] HT201 Force Sensing Resistor (FSRs) by Tekscan were calibrated separately using the calibration setup schematically represented in Figure E.1. This setup allows for introducing a predefined amount of weight on the sensor area using a puck. First, an initial zero-weight point was obtained. Next, the sensor was loaded with the bar-, bucket- and puck setup, followed by eight step-wise weight increments. For each increment an additional 1 liter of water was placed in the bucket. This represented a pressure range from 0 to 7bars, in line with the expected pressure generated by EX-CORE. Before each calibration step a "load break-in" as recommended by the user manual [65] was performed. This was done by manually applying around 1kg of additional load. Additionally, before each calibration step the puck and weights were repositioned on the sensor area.

The resistivity of the Flexiforce[®] sensor decreases under loading. The resulting changing sensor voltage was measured using an Arduino[®] that provides 5V to the Flexiforce[®] sensor. Therefore the measured sensor voltage will be in the range of 0 to 5V. The Arduino converts this voltage to a 10-bit integer value between 0 and 1023. For example, an integer value of 100 represents a measured voltage of $100 \cdot \frac{5}{1024} = 0.488V$. To increase the sensitivity of the sensor signal, a $10k\Omega \pm 1\%$ reference resistor was used. Therefore the following calibration data is only valid with these $10k\Omega \pm 1\%$ resistor. The sensor signal was live monitored using serial communication with a computer. After $\pm 20sec$ the sensor signal stabilized and was recorded. Calibration was done at a room temperature of 20°C. The obtained data curves for each sensor are shown in Figure E.2, together with the second order polynomials that could be fitted through the data. Note that according to the data sheet [160], a temperature correction factor of 0.16% output change per °C should be taken into account when the sensors are used at a different temperature than the calibration temperature.

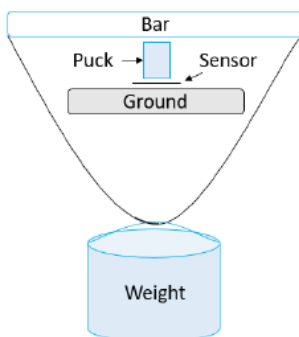


Figure E.1: Schematic of the setup used for calibration of the Flexiforce[®] HT201 FSRs [63]

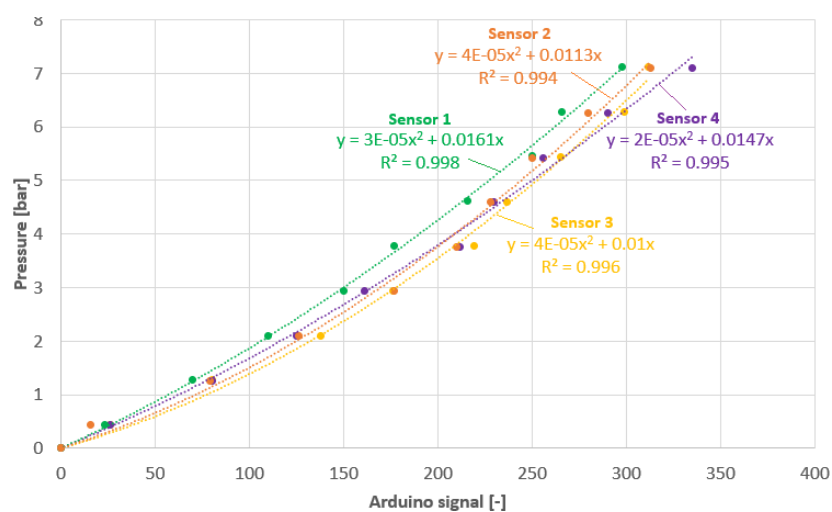


Figure E.2: Flexiforce[®] HT201 FSR calibration data and fitted second order polynomials (tested at 20° C and valid in combination with $10k\Omega \pm 1\%$ resistors)

G

NTC calibration

The fifteen NTC thermistors of the type EPCOS B5760 G104F were calibrated using a pre-calibrated PT100 sensor attached to an eltherm ELTC-14 temperature unit. This made it possible to monitor the PT100 temperature with 1K accuracy. The NTC's signals were recorded using an Arduino MEGA. The NTC sensors were attached to the PT100 sensor using aluminum tape to ensure equal temperature of all sensors. A small Tefal oven was used to stepwise increase the temperature from room temperature until 200°C. For each step, a 10 minute dwell time was used to allow temperature leveling, then the PT100's temperature and NTC signals were recorded. Note that $4.7\text{k}\Omega \pm 1\%$ resistors were used to give a linear behavior around the test temperature range of 100-170°C. Therefore the presented calibration data in Figure G.1 is only valid when the NTC sensors are used in combination with these resistors. A third order polynomial was fit through the test data, which gave an R^2 value of 0.998.

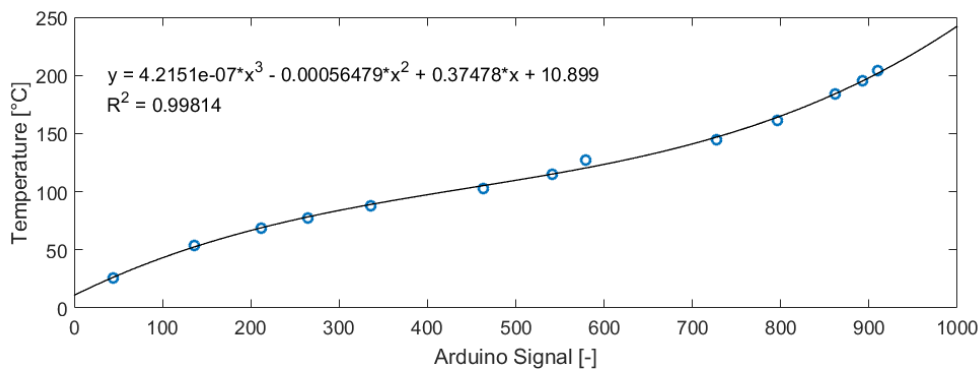
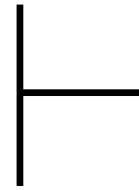


Figure G.1: NTC calibration data and fitted polynomial (valid in combination with $4.7\text{k}\Omega \pm 1\%$ resistor).



Pressure and temperature measurements

In this appendix the recorded pressures and temperatures using the Flexiforce® HT201 FSR pressure sensors and NTC temperature sensors respectively, are plotted for the various samples created during this research.

H.1. Measurements of samples R1-TM1-1 to R1-TM1-7

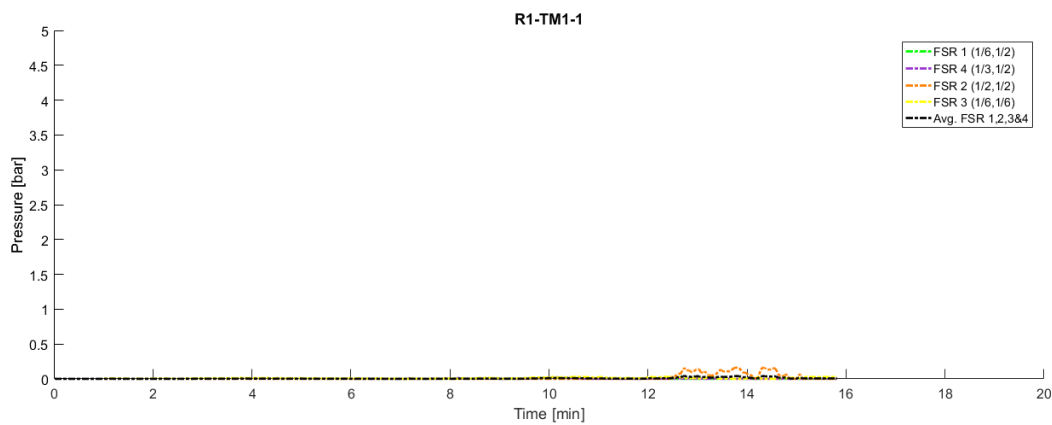


Figure H.1: Measured pressure of sample R1-TM1-1 during 15min cure in pre-heated 110° C mold.

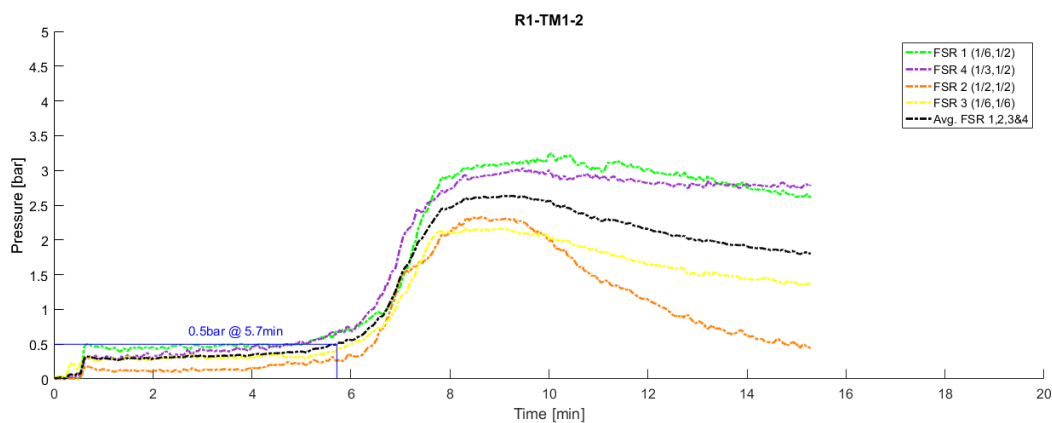


Figure H.2: Measured pressure of sample R1-TM1-2 during 15min cure in pre-heated 110° C mold.

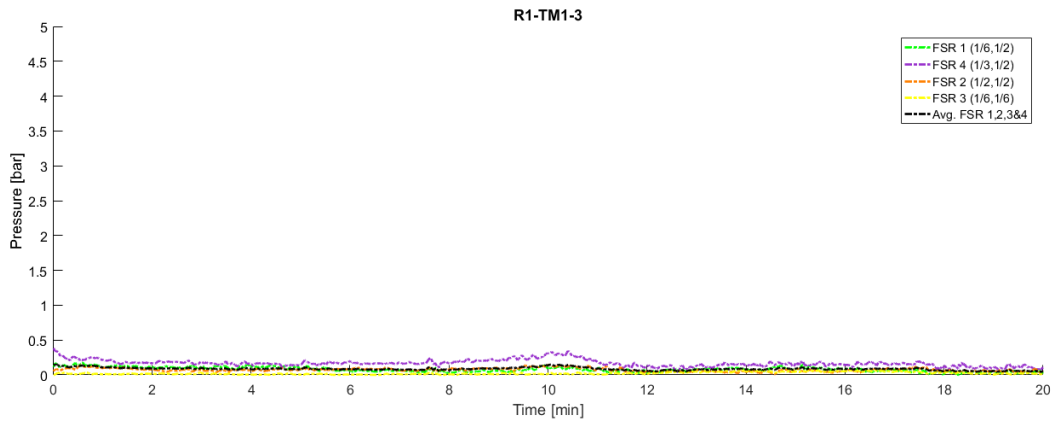


Figure H.3: Measured pressure of sample R1-TM1-3 during 20min cure in pre-heated 110°C mold.

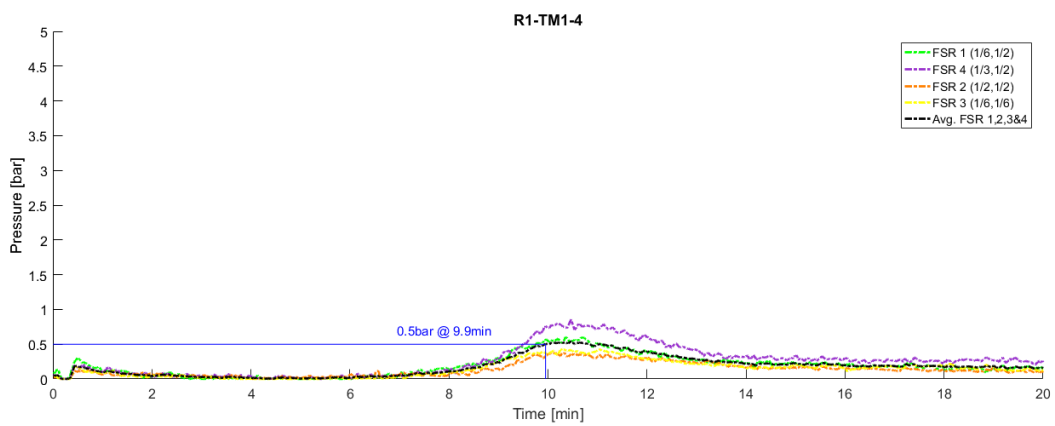


Figure H.4: Measured pressure of sample R1-TM1-4 during 20min cure in pre-heated 110°C mold.

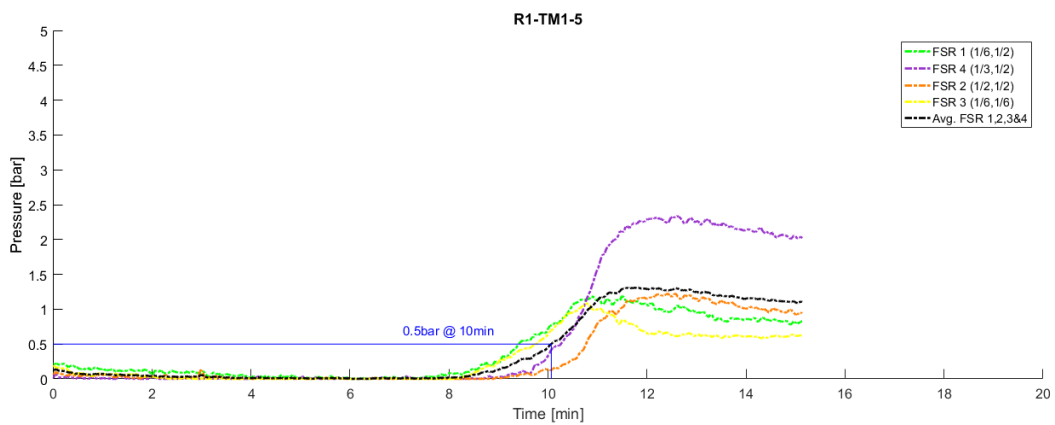


Figure H.5: Measured pressure of sample R1-TM1-5 during 15min cure in pre-heated 110°C mold.

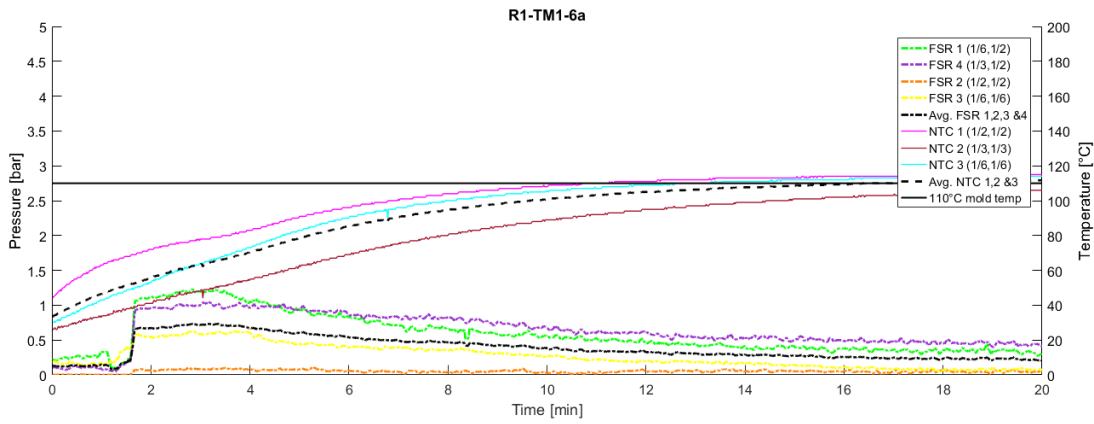


Figure H.6: Measured pressure and temperature of sample R1-TM1-6 during heating in pre-heated 110°C mold.

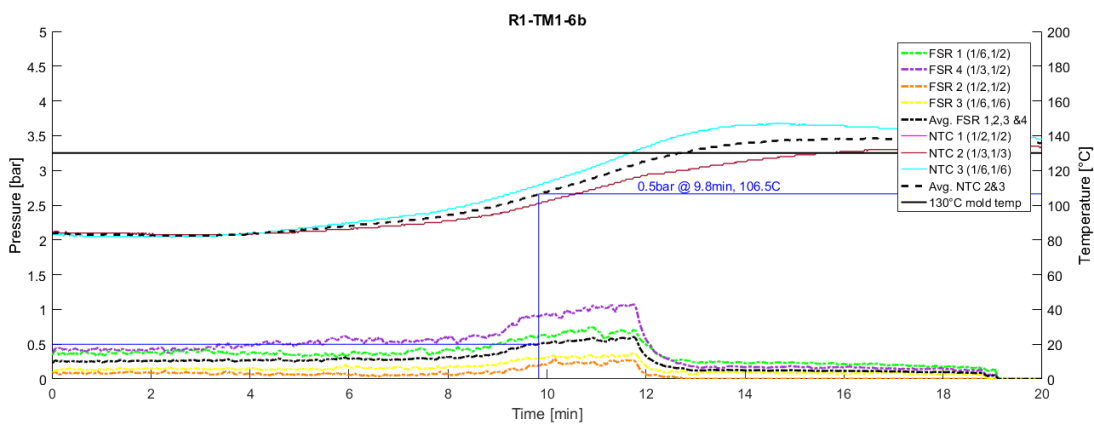


Figure H.7: Measured pressure and temperature of sample R1-TM1-6 during heating in 110°C mold ramped up to 130°C. (Continuation of Figure H.6.) (NTC1 temperature neglected due to erroneous/short-circuited signal.)

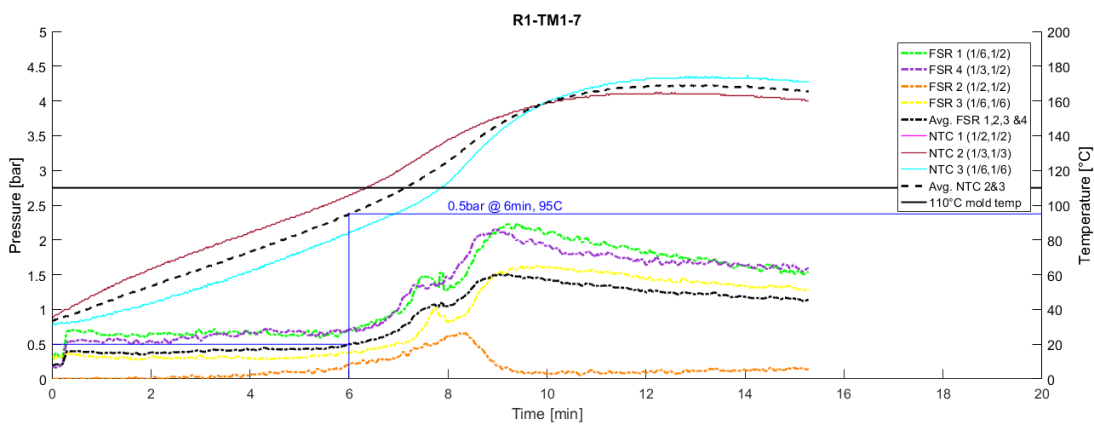


Figure H.8: Measured pressure and temperature of sample R1-TM1-7 during 15min cure in pre-heated 110°C mold. (NTC1 temperature neglected due to erroneous/short-circuited signal.)

H.2. Measurements of samples R2-TM1-1 to R2-TM1-2

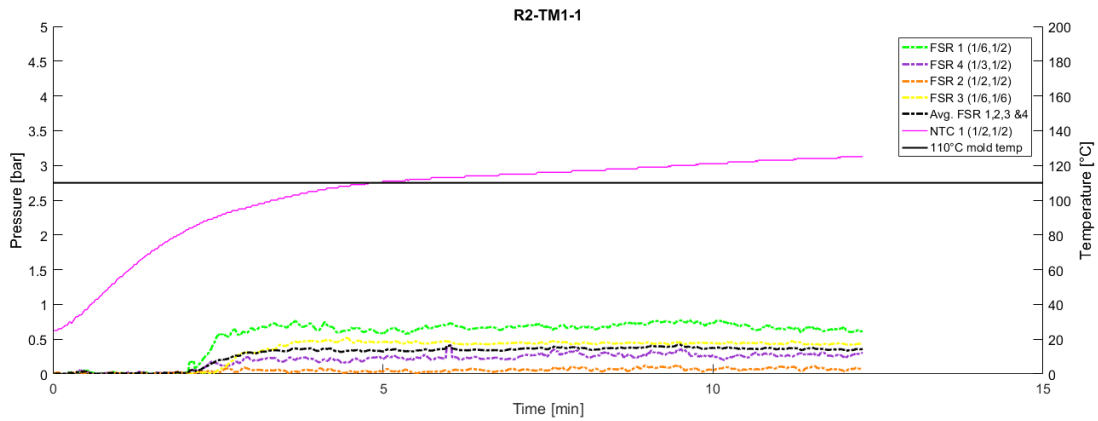


Figure H.9: Measured pressure and temperature of sample R2-TM1-1 during 12min cure in pre-heated 110°C mold.

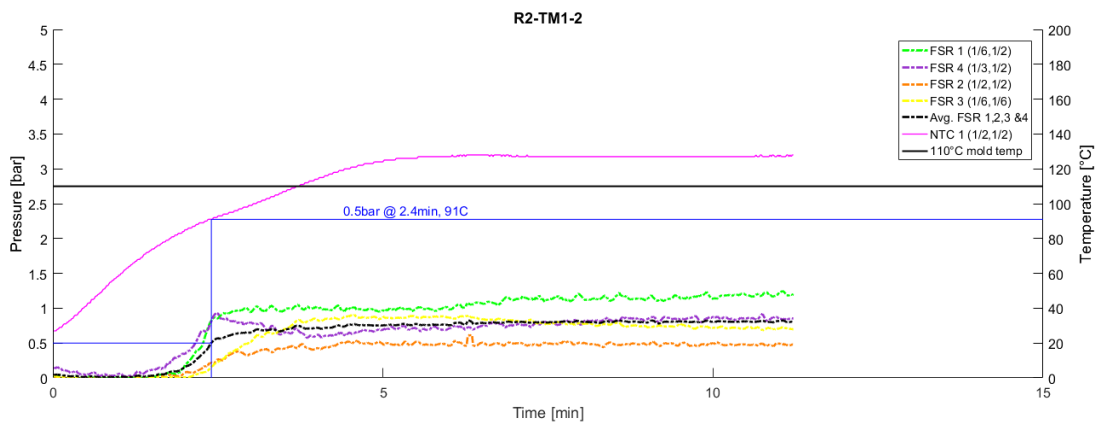


Figure H.10: Measured pressure and temperature of sample R2-TM1-2 during 11min cure in pre-heated 110°C mold.

H.3. Measurements of samples R3-TM1-1 to R3-TM1-7

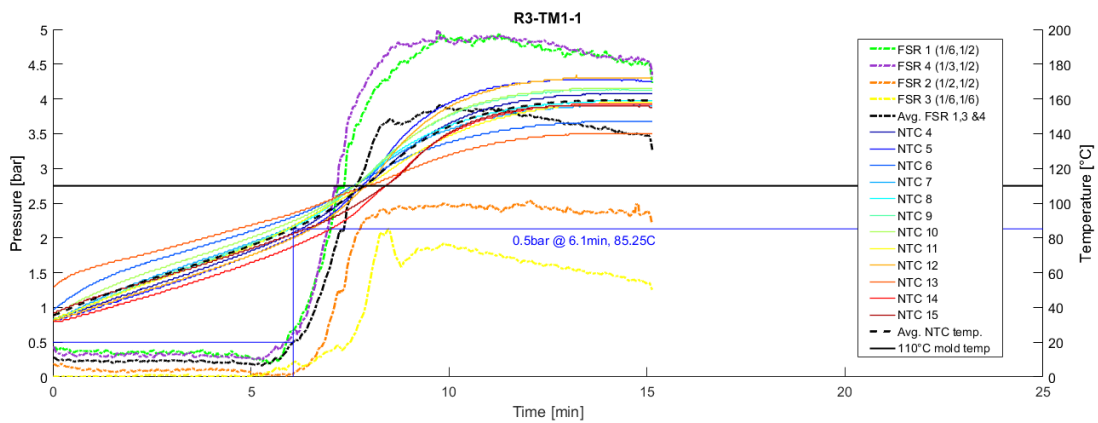


Figure H.11: Measured pressure and temperature of sample R3-TM1-1 during 15min cure in pre-heated 110°C mold.

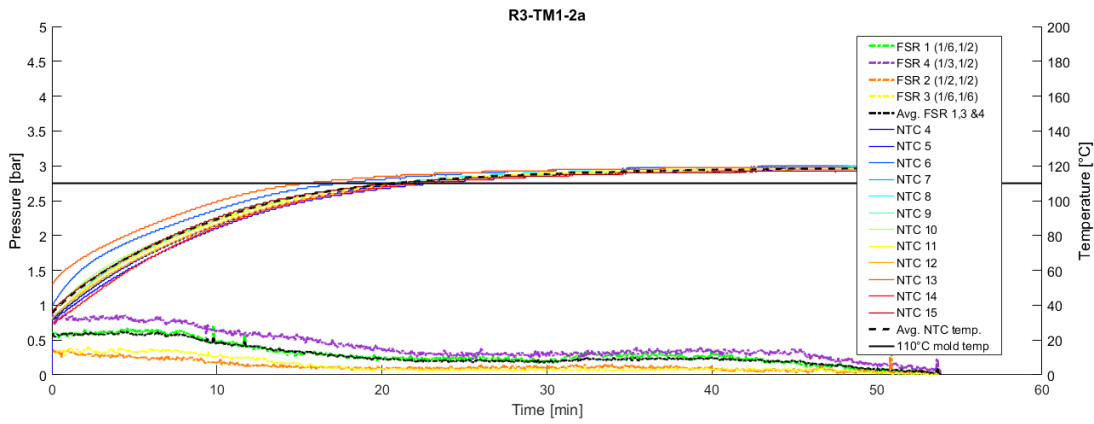


Figure H.12: Measured pressure and temperature of sample R3-TM1-2 during heating in pre-heated 110° C mold. (NTC7 and NTC9 temperature neglected due to erroneous/short-circuited signal.)

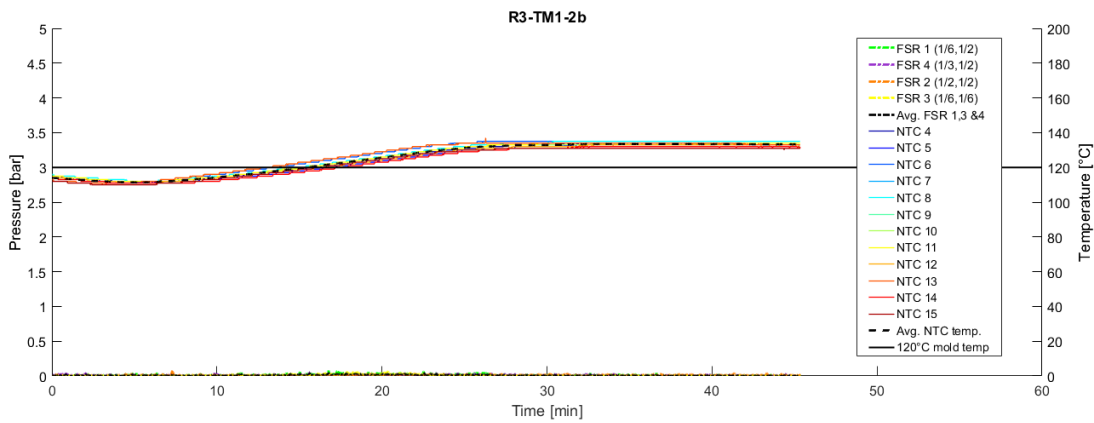


Figure H.13: Measured pressure and temperature of sample R3-TM1-2 during heating in 110° C mold ramped up to 120° C (Continuation Fig. H.12.) (NTC7 and NTC9 temperature neglected due to erroneous/short-circuited signal.)

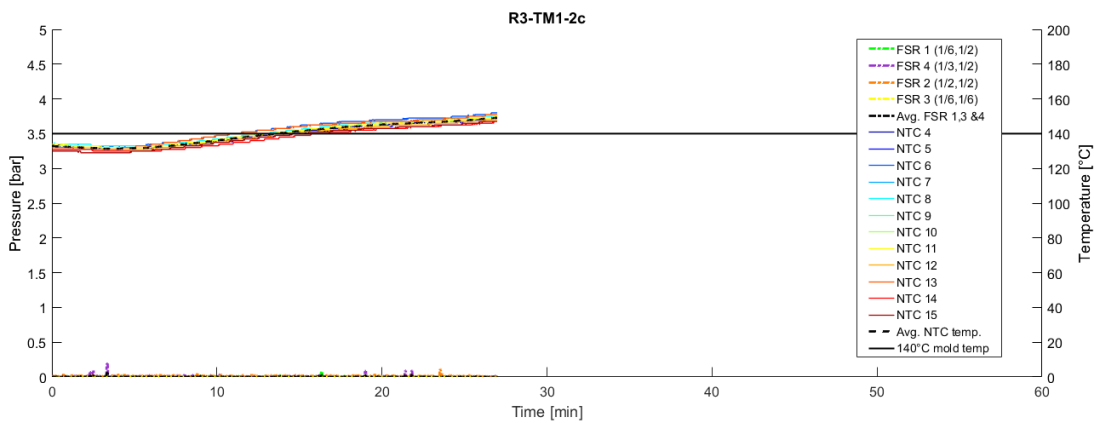


Figure H.14: Measured pressure and temperature of sample R3-TM1-2 during heating in 130° C mold ramped up to 140° C (Continuation Fig. H.13.) (NTC7 and NTC9 temperature neglected due to erroneous/short-circuited signal.)

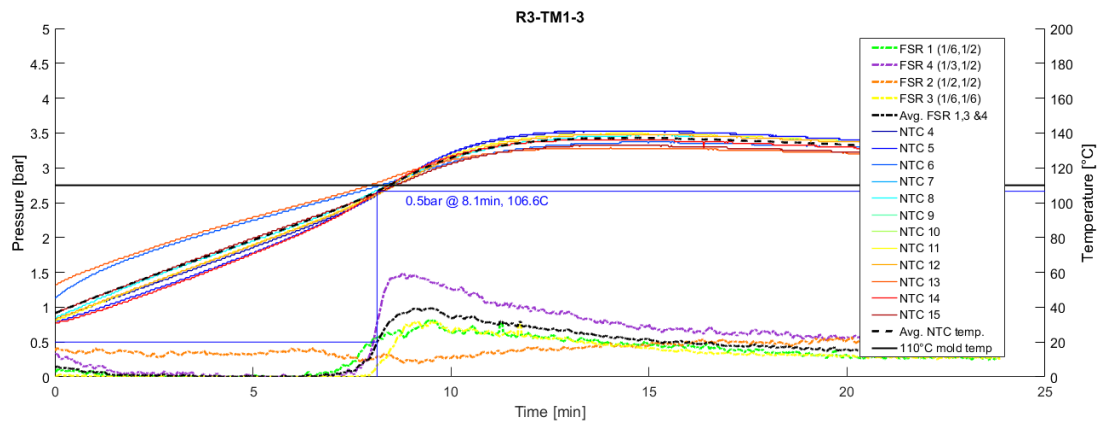


Figure H.15: Measured pressure and temperature of sample R3-TM1-3 during 24min cure in pre-heated 110° C mold. (NTC7, NTC9 and NTC10 temperature neglected due to erroneous/short-circuited signal.)

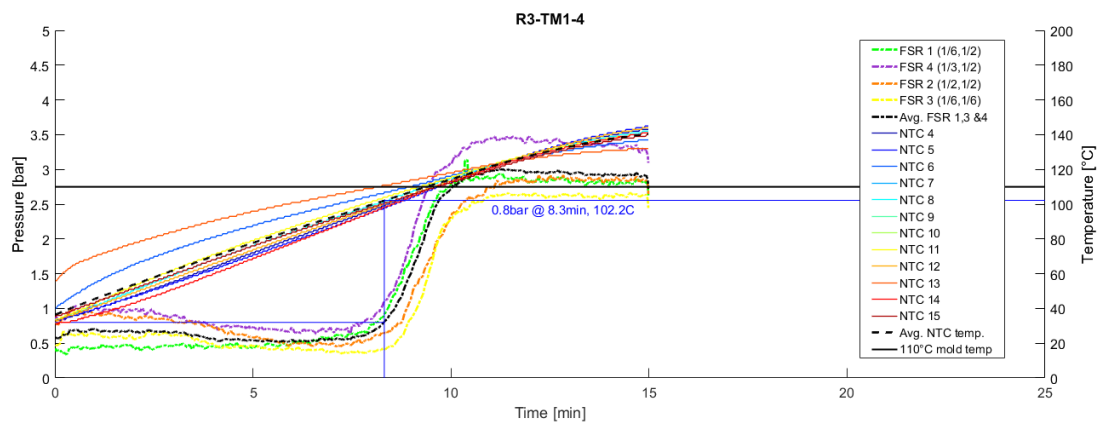


Figure H.16: Measured pressure and temperature of sample R3-TM1-4 during 15min cure in pre-heated 110° C mold. (NTC7, NTC9 and NTC10 temperature neglected due to erroneous/short-circuited signal.)

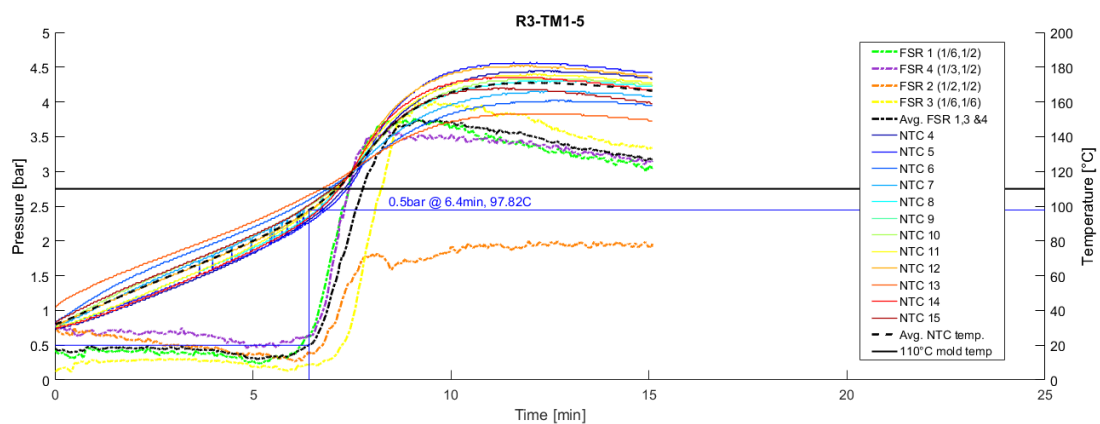


Figure H.17: Measured pressure and temperature of sample R3-TM1-5 during 15min cure in pre-heated 110° C mold. (NTC9 temperature neglected due to erroneous/short-circuited signal.)

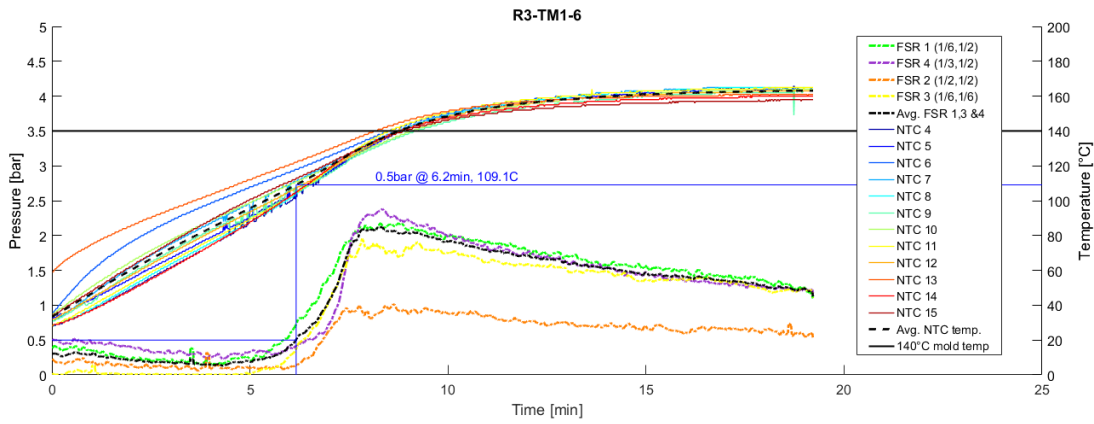


Figure H.18: Measured pressure and temperature of sample R3-TM1-6 during 19min cure in pre-heated 140° C mold.

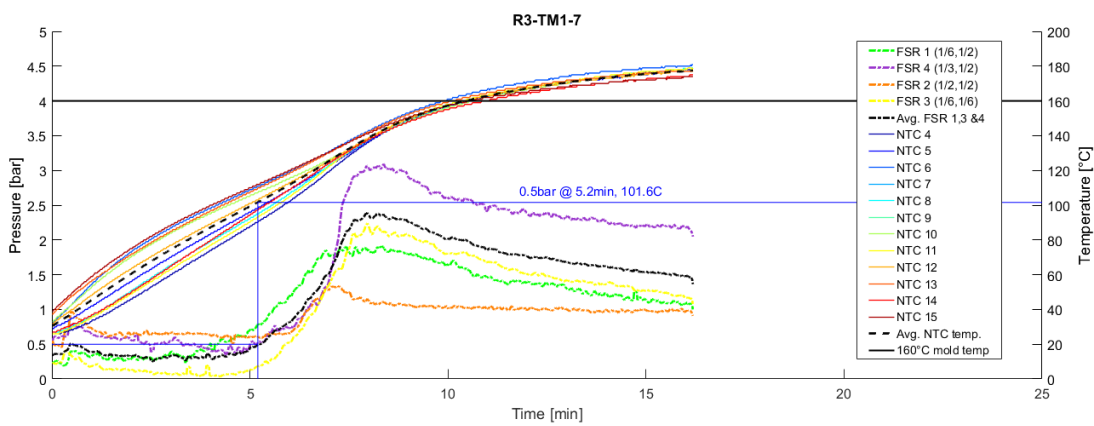


Figure H.19: Measured pressure and temperature of sample R3-TM1-7 during 16min cure in pre-heated 160° C mold. (NTC7 and NTC9 temperature neglected due to erroneous/short-circuited signal.)

H.4. Measurements of sample R4-TM1-1 to R4-TM1-6

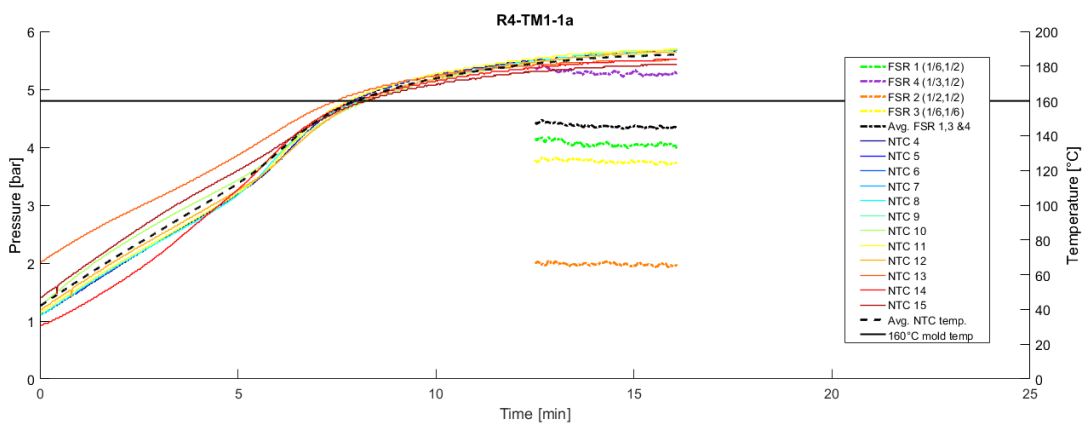


Figure H.20: Measured pressure and temperature of sample R4-TM1-1 during 16min cure in pre-heated 160° C mold. (NTC5, NTC6, NTC7 and NTC9 temperature neglected due to erroneous/short-circuited signal. Also pressure initially not recorded due to wrong data collection settings.)

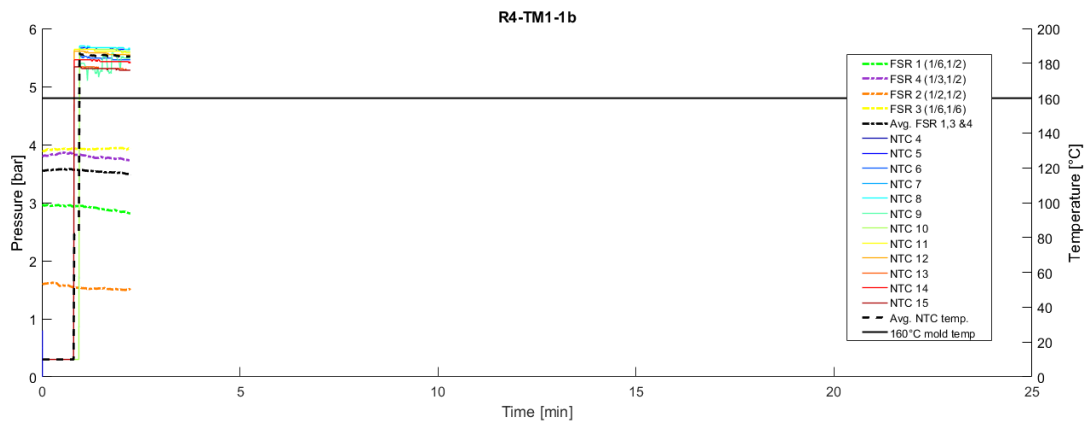


Figure H.21: Measured pressure and temperature of sample R4-TM1-1 during additional 5min cure in pre-heated 160° C mold. (Continuation Fig. H.20.)

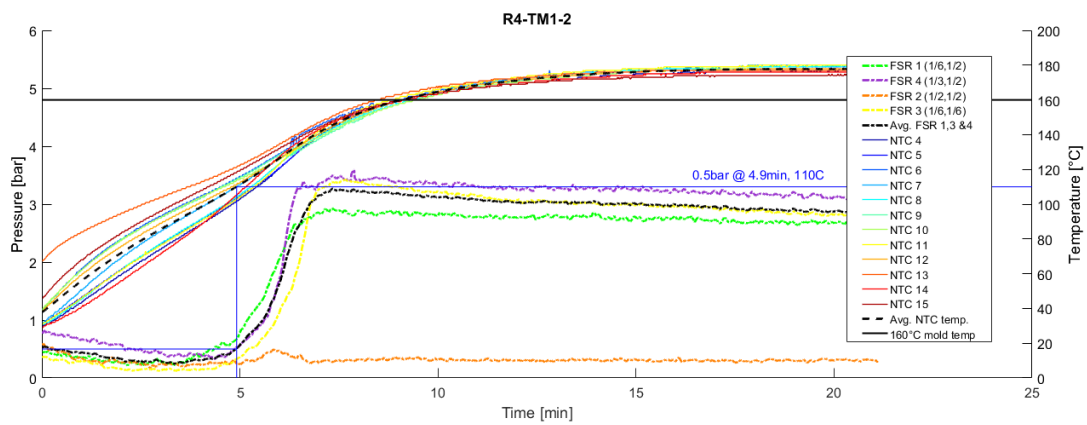


Figure H.22: Measured pressure and temperature of sample R4-TM1-2 during 21min cure in pre-heated 160° C mold.

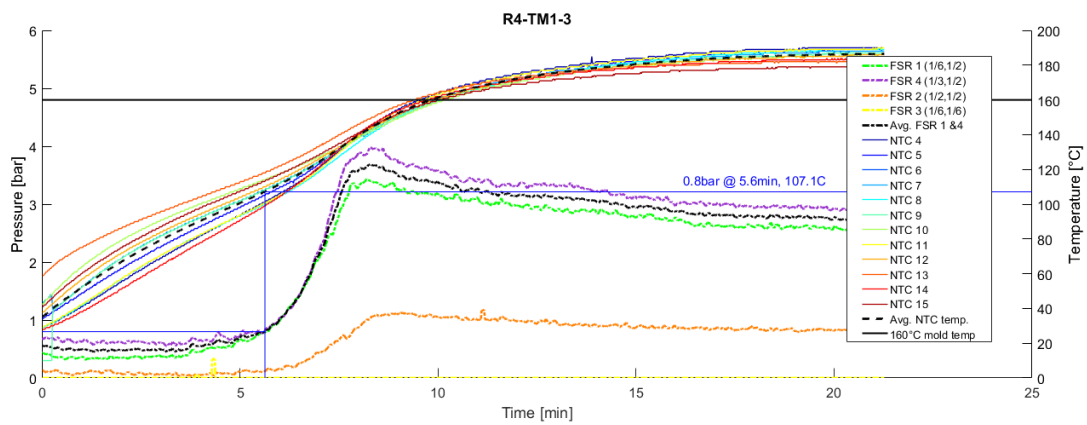


Figure H.23: Measured pressure and temperature of sample R4-TM1-3 during 21min cure in pre-heated 160° C mold.

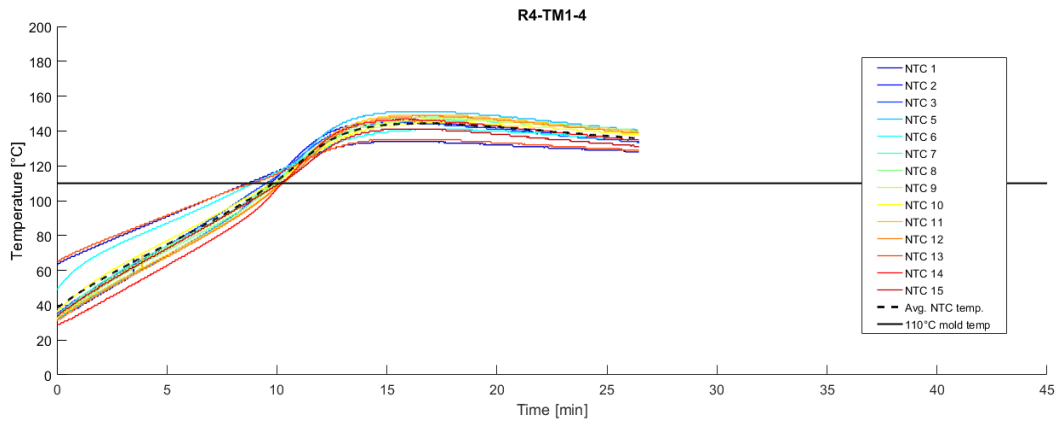


Figure H.24: Measured temperature of sample R4-TM1-4 during 26min cure in pre-heated 110° C mold. (NTC4 temperature neglected due to erroneous/short-circuited signal. Pressure data unavailable due to Arduino Nano malfunction.)

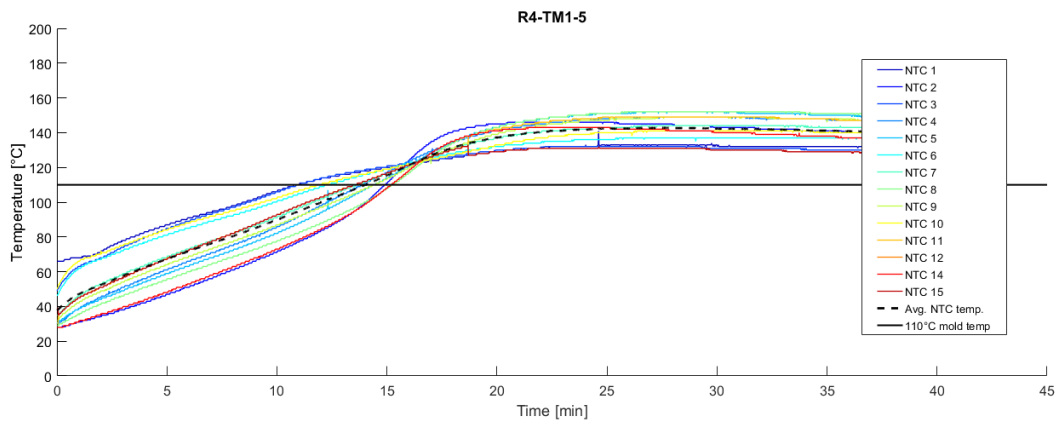


Figure H.25: Measured temperature of sample R4-TM1-5 during 40min cure in pre-heated 110° C mold. (NTC12 & 13 temperature neglected due to erroneous/short-circuited signal. Pressure data unavailable due to Arduino Nano malfunction.)

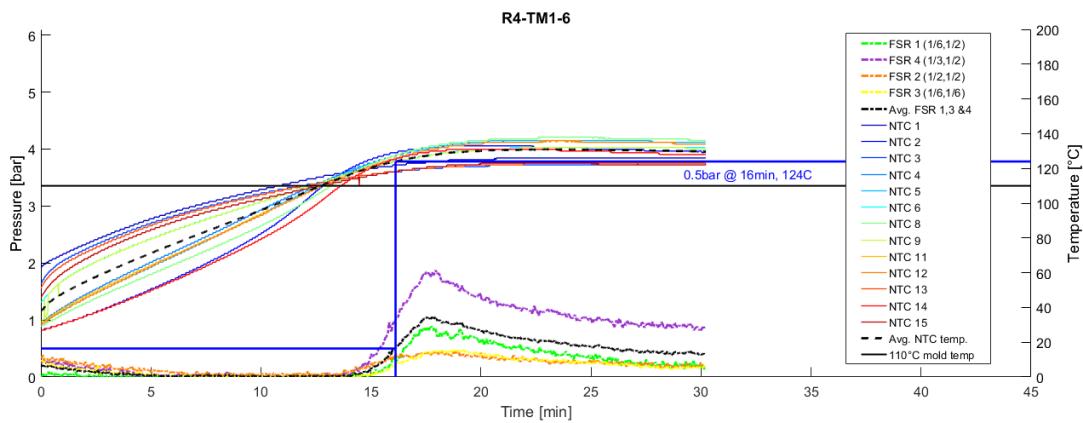


Figure H.26: Measured pressure and temperature of sample R4-TM1-6 during 30min cure in pre-heated 110° C mold. (NTC7 & 10 temperature neglected due to erroneous/short-circuited signal.)

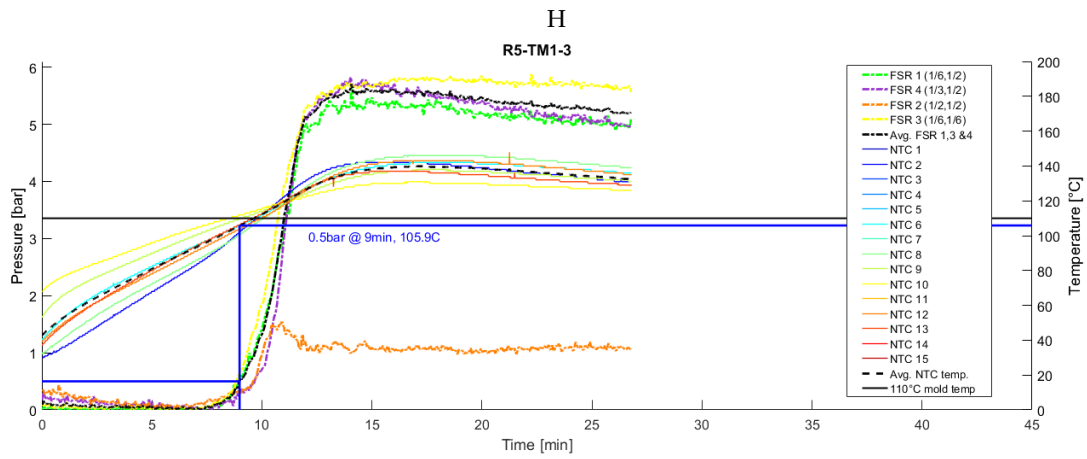


Figure H.29: Measured temperature of sample R5-TM1-3 during 26.5min cure in pre-heated 110° C mold. (NTC 1, 3, 4, 5, 7, 11, 14 & 15 temperature neglected due to erroneous/short-circuited signal.)

H.5. Measurements of sample R5-TM1-1 to R5-TM1-3

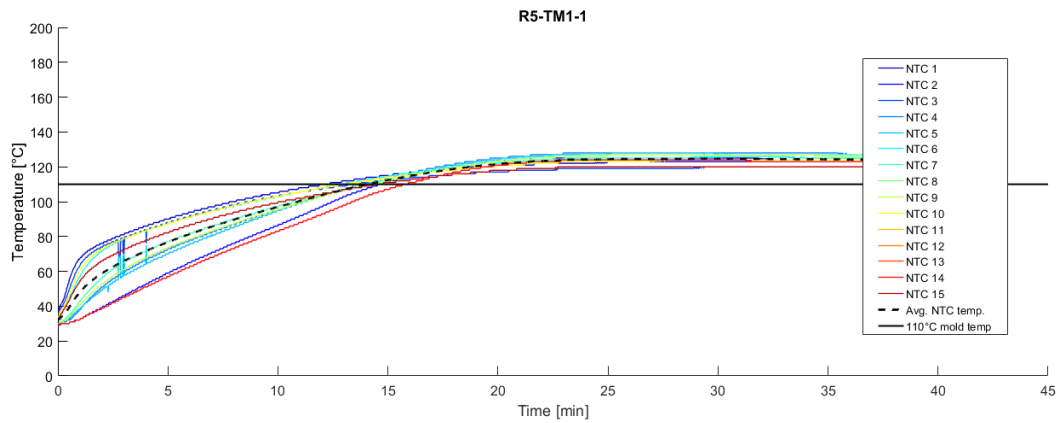


Figure H.27: Measured temperature of sample R5-TM1-1 during 41min cure in pre-heated 110° C mold. (NTC 8,11,12 &13 temperature neglected due to erroneous/short-circuited signal. Pressure data unavailable due to Arduino Nano malfunction.)

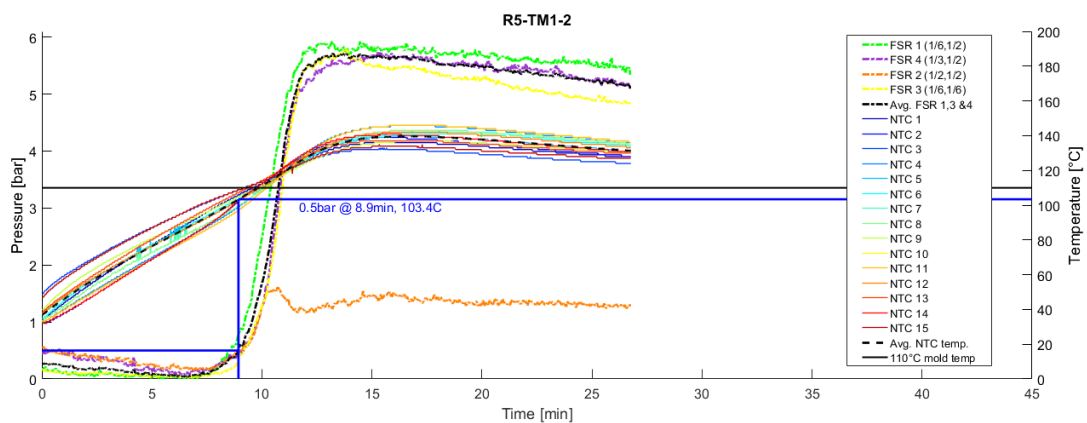


Figure H.28: Measured temperature of sample R5-TM1-2 during 26.5min cure in pre-heated 110° C mold. (NTC 10 temperature neglected due to erroneous/short-circuited signal.)

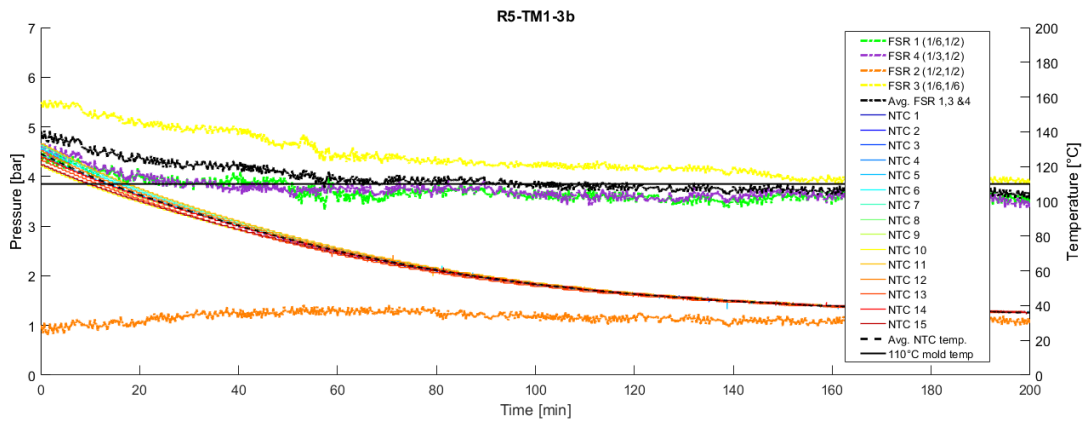


Figure H.30: Measured temperature of sample R5-TM1-3 during cool down to room temp. (Continuation fig. H.29) (NTC 1 temperature neglected due to erroneous/short-circuited signal.)

H.6. Measurements of sample R6-TM1-1 to R6-TM1-2

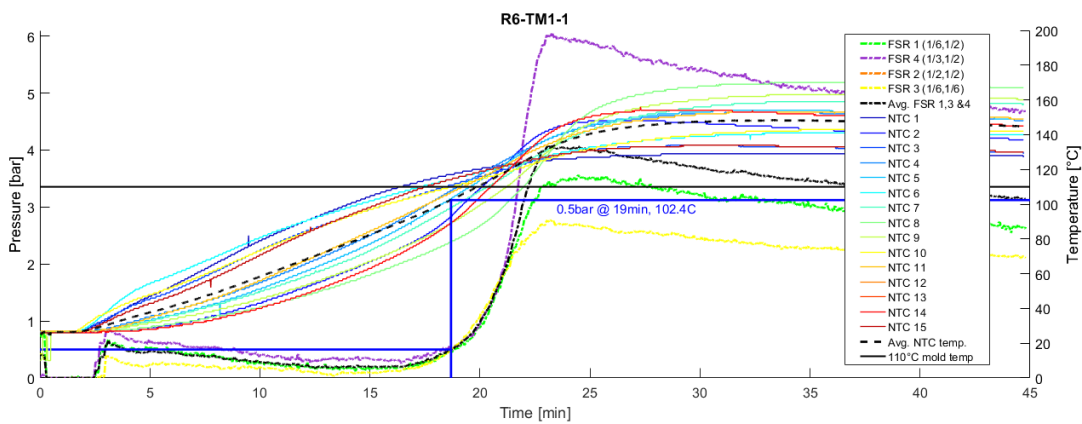


Figure H.31: Measured temperature of sample R6-TM1-1 during 40min cure in pre-heated 110°C mold. (NTC 12 & 13 temperature neglected due to erroneous/short-circuited signal.)

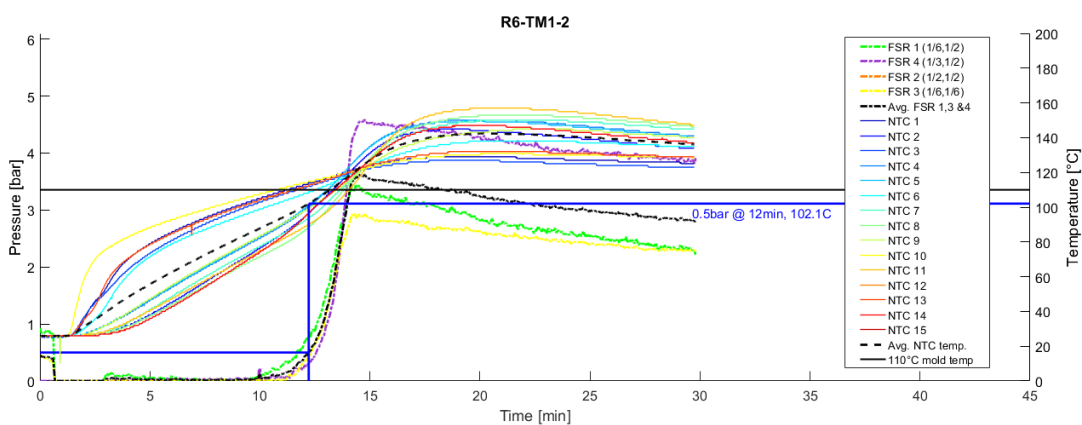


Figure H.32: Measured temperature of sample R6-TM1-2 during 26min cure in pre-heated 110°C mold. (NTC 12 & 15 temperature neglected due to erroneous/short-circuited signal.)

H.7. Measurements of sample R7-TM1-1 to R7-TM1-4

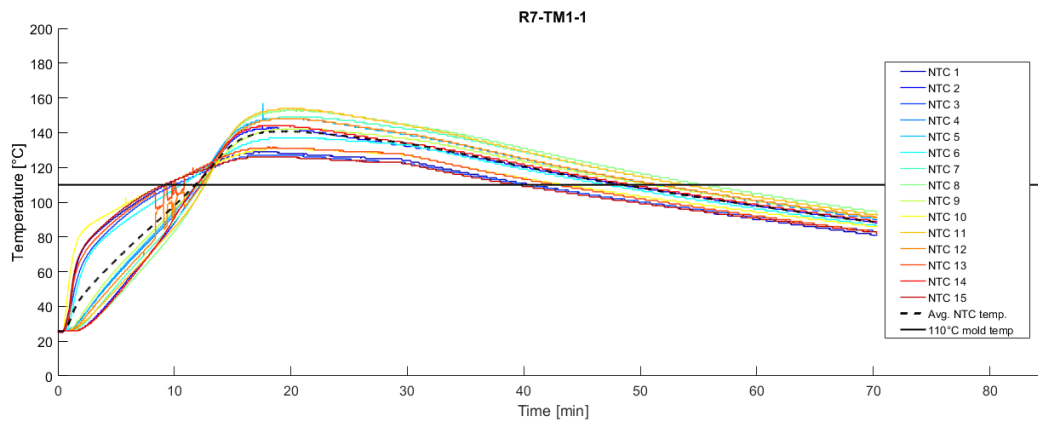


Figure H.33: Measured temperature of sample R7-TM1-1 during 26.5min cure in pre-heated 110° C mold, followed by cool down until 95° reached in core. (NTC 12 & 13 temperature neglected due to erroneous/short-circuited signal. Pressure data unavailable due to Arduino Nano malfunction.)

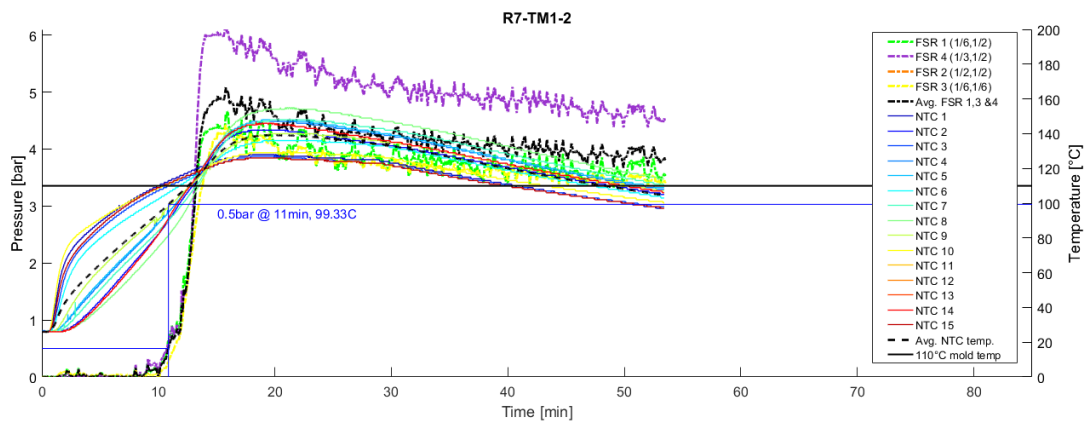


Figure H.34: Measured temperature of sample R7-TM1-2 during 26.5min cure in pre-heated 110° C mold, followed by cool down until 115° reached in core. (NTC 11, 12 & 15 temperature neglected due to erroneous/short-circuited signal.)

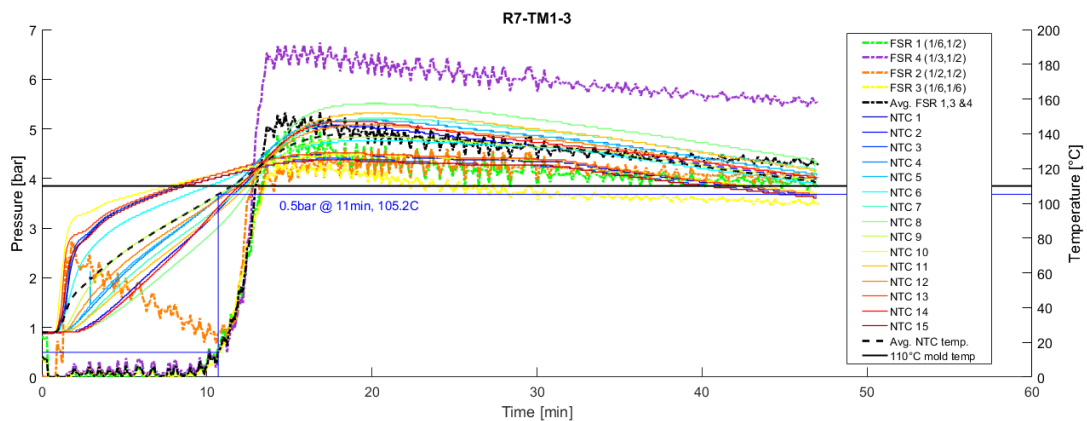


Figure H.35: Measured temperature of sample R7-TM1-3 during 26.5min cure in pre-heated 110° C mold, followed by cool down until 125° was reached in core.

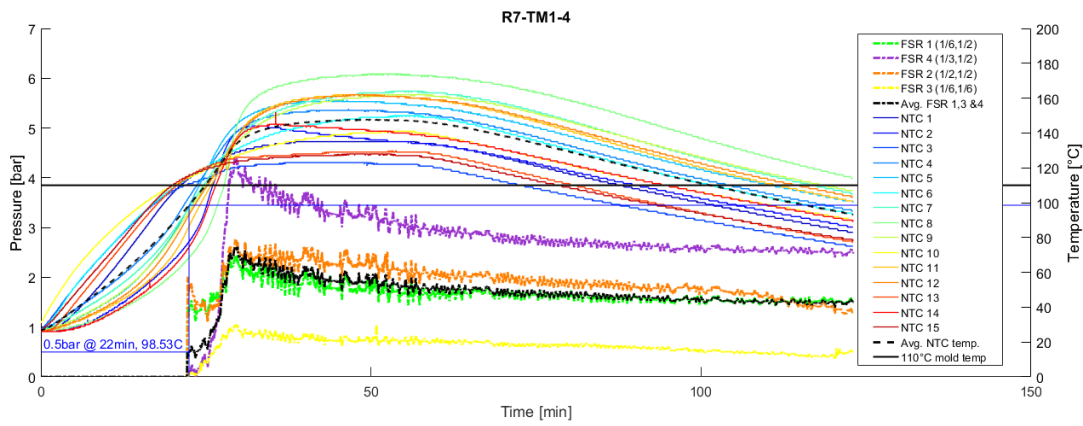


Figure H.36: Measured temperature of sample R7-TM1-4 during 53min cure in pre-heated 110° C mold, followed by cool down until 115° was reached in core.

H.8. Measurements of sample R8-TM1-1 to R8-TM1-2

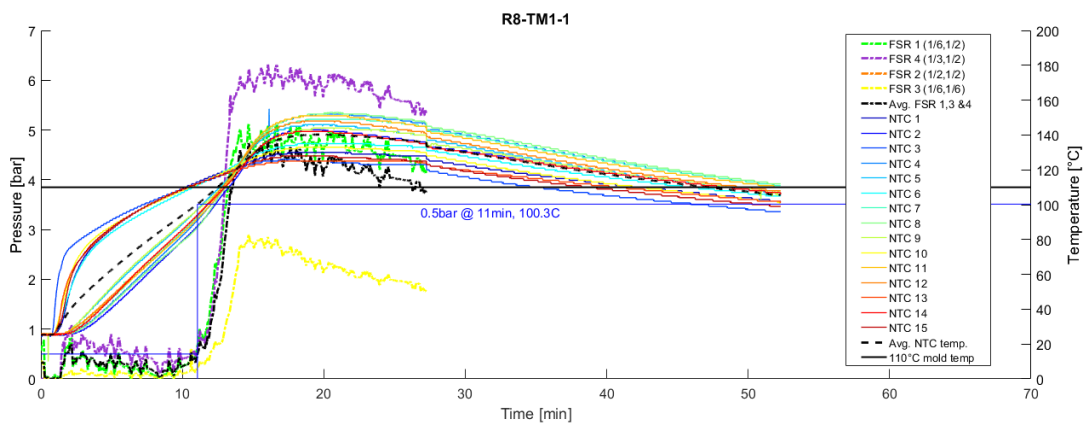


Figure H.37: Measured temperature of sample R8-TM1-1 during 26.5min cure in pre-heated 110° C mold, followed by cool down until 115° was reached in core.

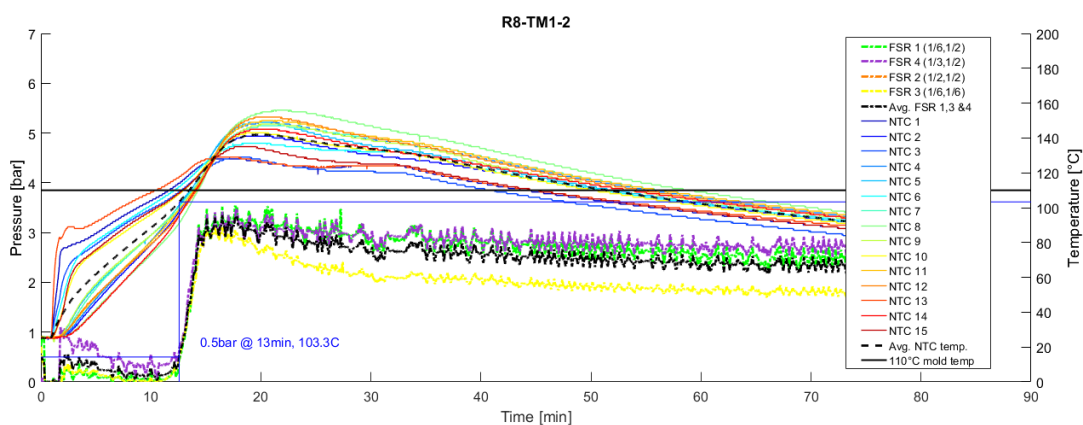


Figure H.38: Measured temperature of sample R8-TM1-2 during 26.5min cure in pre-heated 110° C mold, followed by cool down until 95° was reached in core.



Compression test results

On overview of the compression strength results, sample densities and specific compressive strength results of compression tested EX-CORE samples can be found in Table I.1 on the next page.

Table I.1: Compressive strength, density and specific compressive strength results for samples R3-TM1-3,-6,-7 and R4-TM1-1,-2, -3 & -4 tested on the Donkervoort pressure jack.

Sample nr	Compr. Strength		Density		Specific Compr. Strength		
	Per sample [MPa]	Average [Mpa]	Per sample [kg/m ³]	Average [kg/m ³]	Per sample [kN m/kg]	Average [kN m/kg]	St. dev. [kN m/kg]
R3-TM1-3a	0.52		214.96		2.42		
R3-TM1-3b	0.92		226.47		4.04		
R3-TM1-3c	0.89		235.70		3.78		
R3-TM1-3d	0.55	0.74	219.38	225.17	2.49	3.28	0.68
R3-TM1-3e	0.84		228.74		3.65		
R3-TM1-3f	0.74		225.78		3.26		
R3-TM1-6a	1.93		226.09		8.55		
R3-TM1-6b	2.63		265.10		9.90		
R3-TM1-6c	2.45		252.90		9.69		
R3-TM1-6d	1.40	1.98	221.38	237.14	6.35	8.27	1.47
R3-TM1-6e	1.55		229.59		6.75		
R3-TM1-6f	1.91		227.76		8.39		
R3-TM1-6g	2.41		254.91		9.46		
R3-TM1-6h	1.99		232.66		8.54		
R3-TM1-6i ¹	3.50		288.42		12.13		
R3-TM1-6j	2.14	2.06	246.51	244.48	8.67	8.40	0.77
R3-TM1-6k	1.99		253.58		7.85		
R3-TM1-6l	1.76		234.72		7.49		
R3-TM1-7a	2.03		236.71		8.56		
R3-TM1-7b	2.40		260.17		9.24		
R3-TM1-7c	2.37		253.69		9.33		
R3-TM1-7d	2.06	2.23	234.76	243.25	8.78	9.17	0.52
R3-TM1-7e	2.16		238.81		9.06		
R3-TM1-7f	2.36		235.34		10.05		
R4-TM1-1a	2.44		214.40		11.37		
R4-TM1-1b	2.74		226.95		12.08		
R4-TM1-1c	3.25		250.35		12.97		
R4-TM1-1d	3.13	2.86	215.72	226.41	14.53	12.59	1.18
R4-TM1-1e	2.37		205.52		11.54		
R4-TM1-1f	3.20		245.49		13.05		
R4-TM1-2a	1.88		218.45		8.62		
R4-TM1-2b	2.20		227.84		9.65		
R4-TM1-2c	2.16		228.71		9.45		
R4-TM1-2d	2.84	2.25	266.10	229.85	10.66	9.74	0.71
R4-TM1-2e	1.99		203.75		9.76		
R4-TM1-2f	2.42		234.23		10.31		
R4-TM1-3a	4.08		246.71		16.53		
R4-TM1-3b	4.35		256.10		16.99		
R4-TM1-3c	4.35		256.39		16.96		
R4-TM1-3d	4.40	4.30	261.86	255.01	16.80	16.85	0.20
R4-TM1-3e	4.21		246.69		17.07		
R4-TM1-3f	4.40		262.28		16.76		
R4-TM1-4a	3.63		262.48		13.82		
R4-TM1-4b	3.90		268.35		14.52		
R4-TM1-4c	3.57		261.85		13.63		
R4-TM1-4d	3.40	3.57	256.46	260.53	13.25	13.70	0.45
R4-TM1-4e	3.51		257.89		13.60		
R4-TM1-4f	3.42		256.14		13.35		

¹ Outlier R3-TM1-6i not included in averages.

